THE UNIVERSITY OF QUEENSLAND

AUSTRALIA

Holocene sea level and climate variability on the Great Barrier Reef, Australia

Nicole Deanne Leonard

Bachelor Marine Studies (Hons)

A thesis submitted for the degree of Doctor of Philosophy at

The University of Queensland in 2016

School of Earth Sciences

This page is intentionally left blank

Abstract

The Great Barrier Reef (GBR) is a natural, social and economic asset synonymous with Australia; however, there are concerns regarding both the frequency and extent of modern reef decline, especially in regions within close proximity to the coastline. With the future of coral reefs uncertain, elucidating the controls on reef growth and decline in the recent geological past prior to anthropogenic impacts is imperative to future management strategies. Numerous reef cores have revealed a substantial hiatus period or reef "turn-off" event during the mid-Holocene (~4600 years before present; yBP 1950) clearly prior to anthropogenic influence. Previously published research has suggested that changes in sea level, climate, and/or environmental conditions caused this reef "turn-off", but the exact cause is still tentative.

Whether sea level varied significantly during the Holocene has been debated for over half a century, with oscillations generally dismissed as dating artefacts due to large age errors or to the misinterpretation or inaccuracies of the sea level indicator. Coral microatolls, one of the most reliable sea level indicators, were used to test whether relative (RSL) oscillations could be detected during the Holocene. Elevation surveys of sub-fossil coral microatolls (n=32) and non-microatoll reef flat corals (n=10) were conducted on three separate sites in the Keppel Islands, southern GBR and dated using high precision uranium thorium (U-Th) techniques. The resultant palaeo-sea-level reconstruction revealed a rapid lowering of RSL of at least 0.4 m from 5500 to 5300 yBP following a RSL highstand of ~0.75 m above present from ~6500 to 5500 yBP. RSL then returned to higher levels before a 2000-yr hiatus in reef flat corals after 4600 yBP.

To determine if this was a local scale response, or part of a broader regional signal, the same methodology was applied to another 8 sites from a wide latitudinal range along the GBR (11˚S to 20˚S). The 94 U-Th dates of sub-fossil microatolls from this research adds support to the RSL lowering event at 5500 yBP, with microatolls close to present sea level found at ~5100 yBP. A second oscillation of ~ -0.3m at 4600 yBP was also detected in the northern GBR, with microatolls at three sites close to modern SL between 4600 – 4000 yBP. The RSL oscillations at 5500 yBP and 4600 yBP coincide with both substantial reduction in reef accretion and wide spread reef "turn-off", respectively, thereby suggesting that oscillating sea level was the primary driver of reef shut down on the GBR.

Understanding the coeval palaeo-climate and -environmental conditions may reveal both the cause of these sea level oscillations and further modes of stress placed on coral reefs prior to the mid-Holocene hiatus. In the first instance one of the simplest and most efficient methods of extracting information from the annual bands of massive Porites *sp.* coral cores is by using the growth characteristics (i.e. linear extension) and ultra violet (UV) luminescent intensity which are linked to

sea surface temperate and river discharge, respectively. As the El Niño Southern Oscillation (ENSO) is recognised as one of the main modulators of rainfall on the GBR, continuous wavelet transforms (CWT) of previously published modern coral luminescence index record was compared to sea surface temperature (SST) anomalies in the Niño 3 and Niño 3.4 regions (an indicator of ENSO). The transformed coral luminescence record matched well with the ENSO signal, so is therefore considered a viable tool for reconstructing ENSO in the Holocene. Continuous wavelet transforms were then applied to luminescence index data of three *Porites* corals U-Th dated to 5200 yBP, 4900 yBP and 4300 yBP. Results suggest less intense ENSO events during the mid-Holocene with a reduction in ENSO frequency in the 2-7 year band after 5200 y BP. Limited linear extension rates in the fossil corals ($<10 mm yr^{-1}$) compared to modern values (~15mmyr-1) also suggest SSTs were cooler than present between 5200 - 4300 yBP.

Although luminescent signals in corals can provide information on palaeoclimatic states, quantification of environmental conditions (e.g. sediment/turbidity levels) from geochemical signals in corals has proven to be more difficult. The ratio between barium and calcium (Ba/Ca) is one of the most commonly used proxies for river discharge reconstructions, yet as Ba is biologically mediated peaks in Ba/Ca decoupled from river discharge events are ubiquitous. The rare earth elements (REEs) and Yttrium (Y) offer potential as a proxy for terrestrial run-off as ~90% of coastal oceanic REE's are derived from fluvial sources, but few studies have evaluated this proxy at sub annual scales.

Four modern corals collected across a known water quality gradient were used to assess high resolution (monthly) REE and Y concentrations compared to rainfall and river discharge events, and with overall water quality conditions. Total REE (ΣREE) concentrations were found to be up to seven times higher at inshore locations (50-126 ppb) compared to the mid-shelf (17 ppb), with spatial interpolation of the data reflecting the known water quality gradient, suggesting utility in future palaeo-environmental reconstructions. Time series of monthly resolved ΣREE concentrations matched well with river discharge in some but not all of the corals, with resuspension of sediments interfering with the run-off signal. Time series of ΣREE however demonstrated an overall coherency with rainfall, indicating that early season (smaller) discharge peaks are associated more efficient removal of top soils following dry periods.

Overall it is demonstrated in this thesis that RSL oscillations centred at 5500 and 4600 yBP were the most likely cause of reduced reef accretion and reef hiatus in the mid-Holocene on the GBR respectively. Coral luminescence and linear extension signals suggest cooler SSTs, and less variable river discharge likely linked to reduced strength of ENSO after 5200 yBP. Furthermore it has been demonstrated that REE geochemical data from coral cores have the potential to reconstruct palaeo-water quality gradients.

Declaration by author

This thesis is composed of my original work, and contains no material previously published or written by another person except where due reference has been made in the text. I have clearly stated the contribution by others to jointly-authored works that I have included in my thesis.

I have clearly stated the contribution of others to my thesis as a whole, including statistical assistance, survey design, data analysis, significant technical procedures, professional editorial advice, and any other original research work used or reported in my thesis. The content of my thesis is the result of work I have carried out since the commencement of my research higher degree candidature and does not include a substantial part of work that has been submitted to qualify for the award of any other degree or diploma in any university or other tertiary institution. I have clearly stated which parts of my thesis, if any, have been submitted to qualify for another award.

I acknowledge that an electronic copy of my thesis must be lodged with the University Library and, subject to the policy and procedures of The University of Queensland, the thesis be made available for research and study in accordance with the Copyright Act 1968 unless a period of embargo has been approved by the Dean of the Graduate School.

I acknowledge that copyright of all material contained in my thesis resides with the copyright holder(s) of that material. Where appropriate I have obtained copyright permission from the copyright holder to reproduce material in this thesis.

Publications during candidature

1. **Leonard, N. D**., Welsh, K. J., Lough, J. M., Feng, Y. X., Pandolfi, J. M., Clark, T. R. & Zhao, J. X. 2016a. Evidence of reduced mid-Holocene ENSO variance on the Great Barrier Reef, Australia. *Paleoceanography* **31,** 1248-1260
2. **Leonard, N. D**., Zhao, J.-X., Welsh, K. J., Feng, Y.-X., Smithers, S. G., Pandolfi, J. M. & Clark, T. R. 2016b. Holocene sea level instability in the southern Great Barrier Reef, Australia: high-precision U–Th dating of fossil microatolls. *Coral Reefs* **35,** 625-639.
3. **Leonard, N.D**., Welsh, K. J., Zhao, J.-x., Nothdurft, L. D., Webb, G. E., Major, J., Feng, Y-x. & Price, G. J. 2013. Mid-Holocene sea-level and coral reef demise: U-Th dating of subfossil corals in Moreton Bay, Australia. The Holocene, 23, 1841-1852.
4. Sadler, J., Nguyen, A. D., **Leonard, N. D**., Webb, G. E. & Nothdurft, L. D. 2016. Acropora interbranch skeleton Sr/Ca ratios: Evaluation of a potential new high-resolution paleothermometer. *Paleoceanography* **31,** 505-517.
5. Sadler, J., Webb, G. E., **Leonard, N. D.,** Nothdurft, L. D. & Clark, T. R. 2016b. Reef core insights into mid-Holocene water temperatures of the southern Great Barrier Reef. *Paleoceanography* **(accepted – online first)**
6. Clark, T. R., **Leonard, N. D**., Zhao, J.-X., Brodie, J., Mccook, L. J., Wachenfeld, D. R., Duc Nguyen, A., Markham, H. L. & Pandolfi, J. M. 2016. Historical photographs revisited: A case study for dating and characterizing recent loss of coral cover on the inshore Great Barrier Reef. *Scientific Reports,* 6**,** 19285
7. Liu, E.T., Zhao, J.-x., Clark, T. R., Feng, Y.-x., **Leonard, N. D**., Markham, H. L. & Pandolfi, J. M. 2014. High-precision U–Th dating of storm-transported coral blocks on Frankland Islands, northern Great Barrier Reef, Australia. Palaeogeography, Palaeoclimatology, Palaeoecology, 414, 68-78.
8. Liu, E.T, Wang, H., Li, Y., Zhou, W., **Leonard, N. D**., Lin, Z. & Ma, Q. 2014. Sedimentary characteristics and tectonic setting of sublacustrine fans in a half-graben rift depression, Beibuwan Basin, South China Sea. Marine and Petroleum Geology, 52, 9-21.

Publications included in this thesis

1. **Leonard, N.D**, Zhao, J. X., Welsh, K. J., Feng, Y. X., Smithers, S. G., Pandolfi, J. M. & Clark, T. R. 2016. Holocene sea level instability in the southern Great Barrier Reef, Australia: high-precision U–Th dating of fossil microatolls. *Coral Reefs*, **35,** 625-639 - Incorporated as **Chapter 2**.

Contributor	Statement of Contribution
Nicole Leonard	**Study design 85%** **Fieldwork 80%** **Column Chemistry 100%** **Wrote the original manuscript 100%** **Manuscript editing 50%**
Jian-xin Zhao	**Calculated U-Th ages 100%** **Manuscript editing 5%** **Provided Funding 50%**
Yuexing Feng	**Ran samples on MC ICP MS 100%**
Scott Smithers	**Study design 5%** **Manuscript editing 10%**
John Pandolfi	**Manuscript editing 5%** **Provided funding 50%**
Tara Clark	**Study design 5%** **Fieldwork 20%** **Manuscript editing 10%**
Kevin Welsh	**Study design 5%** **Manuscript editing 20%**

2. Leonard, N. D., Welsh, K. J., Lough, J. M., Feng, Y. X., Pandolfi, J. M., Clark, T. R. & Zhao, J. X. 2016a. Evidence of reduced mid-Holocene ENSO variance on the Great Barrier Reef, Australia. *Paleoceanography* **31,** 1248-1260 –Incorporated in **Chapter 4**

Contributor	Statement of Contribution
Nicole Leonard	**Study design 80%** **Fieldwork 90%** **Column Chemistry 100%** **Wrote the original manuscript 100%** **Manuscript editing 50%**
Kevin Welsh	**Study design 10%** **Manuscript editing 20%**
Janice Lough	**Study design 10%** **Fieldwork 10%** **Manuscript editing 15%**
Yuexing Feng	**Ran samples on MC ICP MS 100%**
John Pandolfi	**Manuscript editing 5%** **Provided funding 50%**
Tara Clark	**Manuscript editing 10%**
Jian-xin Zhao	**Calculated U-Th ages 100%** **Provided Funding 50%**

Contribution by others to the Thesis

In **Leonard, N.D, Zhao, J. X., Welsh, K. J., Feng, Y. X., Smithers, S. G., Pandolfi, J. M. & Clark, T. R. 2015**. Holocene sea level instability in the southern Great Barrier Reef, Australia: high-precision U–Th dating of fossil microatolls. *Coral Reefs*, 1-15 – **(Chapter 2):**

NDL designed the study, selected the field sites, conducted sampling and elevation surveys prepared all samples for geochemistry, conducted column chemistry, interpreted results and composed the initial and final versions of the manuscript. NDL, J-xZ, KJW and JMP developed the concept of this study. SGS and TRC assisted in determining field sites and TRC assisted with sampling and elevation surveys. Y-xF ran the analysis of samples on the Multi-collector Inductively Coupled Mass Spectrometer (MC-ICP-MS) and J-xZ calculated U-Th ages. KJW assisted in data interpretation, and JMP and J-xZ provided funding. All authors commented on the original and revised versions of the manuscript prior to publication.

In **Leonard, N.D., Zhao, J-x., Welsh, K.J., Feng, Y-x, Pandolfi, J.M. & Clark, T.R.,** Holocene sea level oscillations on the Great Barrier Reef and links to climate (*in prep*) **- (Chapter 3):**

NDL designed the study, selected the field sites, conducted sampling and elevation surveys prepared all samples for geochemistry, conducted column chemistry, interpreted results and composed the initial and final versions of the manuscript. NDL, J-xZ, KJW and JMP developed the concept of this study. TRC assisted with field sampling and elevation surveys. Y-xF ran the analysis of samples on the Multi-collector Inductively Coupled Mass Spectrometer (MC-ICP-MS) and J-xZ calculated U-Th ages. KJW assisted in data interpretation, and all authors commented on the original and revised versions of the manuscript prior to submission.

In **Leonard, N.D., Welsh, K.J., Lough J.M., Pandolfi, J.M., Clark, T.R., & Zhao, J-x.,** Evidence for reduced ENSO variance in the mid-Holocene: wavelet analysis of modern and fossil coral luminescence indices from the Great Barrier **(***Paleoceanography***) - (Chapter 4):**

NDL designed the study, selected the corals for sampling, conducted sampling, prepared all samples for geochemistry and conducted column chemistry for U-Th dating, conducted luminescence analysis, statistical analysis, interpreted results and composed the initial and final versions of the manuscript. J.M Lough provided knowledge and assistance in accessing the fossil corals. All authors commented on the original and revised versions of the manuscript prior to submission.

In **Leonard, N.D., Welsh, K.J., Nguyen, A-D., Sadler, J., Pandolfi, J.M., Clark, T.R., Zhao, J-x. & Webb, G.E.** (*in prep*). High resolution geochemical analysis of massive Porites sp. corals from the Wet Tropics region, Great Barrier Reef; Rare Earth Elements and Yttrium as indicators of terrigenous input - **(Chapter 5):**

NDL designed the study, selected the corals for coring, conducted sampling, prepared all samples for geochemistry, conducted geochemical procedures, calibrated the data, conducted statistical analysis, interpreted results and composed the initial and final versions of the manuscript. NDL, J-xZ, KJW and JMP developed the concept of this study. TRC assisted with field sampling. A.D Nguyen ran samples on the Quadrupole ICP-MS and assisted with geochemical procedures and data calibration. J. Sadler assisted with sub sampling techniques for geochemistry. G.E. Webb assisted with data interpretation. All authors commented on the original and revised versions of the manuscript.

We are indebted to Eric Matson from the Australian Institute of Marine Science (AIMS) for technical assistance in obtaining the fossil coral cores used in Chapter 5 and to all the staff at Hard Rock Earth Works in Townsville for allowing access to the fossil corals and for bulldozing them around for us. We also sincerely thank Malcolm McCullough and Juan Pablo D'Olivo from the University of Western Australia for allowing use of their coral lab to cut the fossil coral cores and to Gang Xi for assistance with preparation of thin sections.

Statement of parts of the thesis submitted to qualify for the award of another degree

"None"

Acknowledgements

This project was funded by the National Environment Research Programme (NERP) Tropical Ecosystems Hub Project 1.3 to J-x. Zhao, J. Pandolfi, S. Smithers, T. Clark, Y-x. Feng and others, Australian Research Council Linkage, Infrastructure, Equipment and Facilities (LIEF) grant (LE0989067 for the MC-ICP-MS) to J-x. Zhao, J. Pandolfi, Y-x. Feng and others, and an Australian Postgraduate Award to N.D.Leonard. I am also grateful for funding for international conference attendance and travel provided by The University of Queensland School of Earth Sciences and K. J. Welsh.

I would firstly like to thank my supervisors Dr Kevin Welsh, Prof. John Pandolfi and Prof. Jian-xin Zhao for all the time and effort given to me throughout my PhD journey. Your individual expertise and passion for informative science has inspired me throughout, and this thesis would not have been possible without all of your support and advice. A very special thanks also goes out to Dr Tara Clark for her unwavering support (and fun in the field) and Dr Yuexing Feng and Dr Ai Duc Nguyen for their endless patience in the Radiogenic Isotope Facility. Thanks to Prof. Gregg Webb for always having an ear for my research ideas, and to Dr G. (Dr Gilbert Price) for the motivational pep talks. Thanks to Dr Janice Lough and Eric Matson from the Australian Institute of Marine Science for assistance in collecting the fossil coral cores in Townsville. Much gratitude to Ashleigh Paroz for trying to keep me on track throughout my candidature, and to the administration team in the School of Earth Sciences that have assisted with the all the details involved in my project. To all the staff and students, past and present, from the School of Earth Sciences who have helped keep me somewhat sane throughout, I thank you. To the "NERP" team (Hannah Markham, Martina Prazeres, Mauro Lapore, Beto Rodriguez-Ramirez, Juan-Pablo D'Olivo, Ian Butler and Entao Liu), the extra supporters (James "Buddy" Sadler, Jack Coates-Marnane, and all the volunteers), and to the boat operators involved in field work I thank you for all the hard work and fun times.

More personally I'd like to thank all my family and friends for supporting and encouraging me throughout this journey, and for feigning interest in 6000 year old corals. To my niece Olivia (aka bug-a-lugs) I'm sorry I didn't manage to include mermaids in my thesis, I ran out of time! Special thanks to Rodrigo Cardozo Ferreira for all the extra support, helping to load and unload field gear, suffering silently with a house full of stinking coral, and making sure that I ate at least some vegetables in the last few months of my candidature. *Nuestro pequeño mundo*!

Keywords

Holocene, sea level, Great Barrier Reef, reef hiatus, microatolls, U-Th dating, rare earth element geochemistry, coral luminescence, palaeoclimate

Australian and New Zealand Standard Research Classifications (ANZSRC)

040699 Physical Geography and Environmental Geoscience 40%

040303 Geochemistry 40%

040605 Palaeoclimatology 20%

Fields of Research (FoR) Classification

0406 Physical Geography and Environmental Geoscience 60%

0402 Geochemistry 40%

Table of Contents

List of Tables

List of Figures

This page is intentionally left blank

Chapter 1

Introduction

Background

The recent decline of coral reefs globally is of great concern, and is often labelled as unprecedented or more significant than in the past due to both increasing anthropogenic impacts and climate change (Pandolfi et al., 2003, Carpenter et al., 2008, Miller et al., 2009). The Great Barrier Reef (GBR) is no exception, with recent scrutiny by the United Nations Educational, Scientific and Cultural Organization (UNESCO) putting the health and management strategies of the GBR in the spotlight for all the wrong reasons (Brodie and Waterhouse, 2012, Hughes et al., 2015).

The largest contiguous reef system in the world, the GBR is a natural, social and economic asset synonymous with Australia (Fig. 1). Spanning two thirds of the Queensland coast, it contains over 3000 separate reefs covering an area of 345 000 km^2, with ~600 of these reefs being located in inshore environments (defined as inner-shelf, <20m bathymetry under the influence of terrigenous deposits; Larcombe et al., 2001, Lawrence, 2010). Increased anthropogenic pressures such as catchment clearing (Fabricius, 2005, Wooldridge, 2009, Risk and Edinger, 2011), overfishing (Bellwood et al., 2004) and agricultural nutrient input (Fabricius, 2005, De'ath and Fabricius, 2010, Kroon et al., 2012, Uthicke et al., 2012) are all contributing to the decline of reefs, especially in regions within close proximity to the coastline. Estimates suggest a ~50% reduction in coral cover since the 1960's (Bellwood et al., 2004, Bruno and Selig, 2007, Hughes et al., 2011) with hard coral cover declining from 27% to ~14% for the period 1985 – 2012 (De'ath et al., 2012). However, it is likely that the true magnitude of decline may be underestimated due to the "shifting baseline" (sensu Pauly, 1995) against which modern coral assemblages are assessed (Greenstein et al., 1998, Pandolfi et al., 2003, Knowlton and Jackson, 2008, Hughes et al., 2011, Roff et al., 2013). To enable improved management strategies on the GBR, an evaluation of natural versus anthropogenic drivers of change at relevant temporal resolutions is required, in conjunction with longer term archives of coral decline (or recovery) beyond historical scientific monitoring records (Pandolfi, 2015).

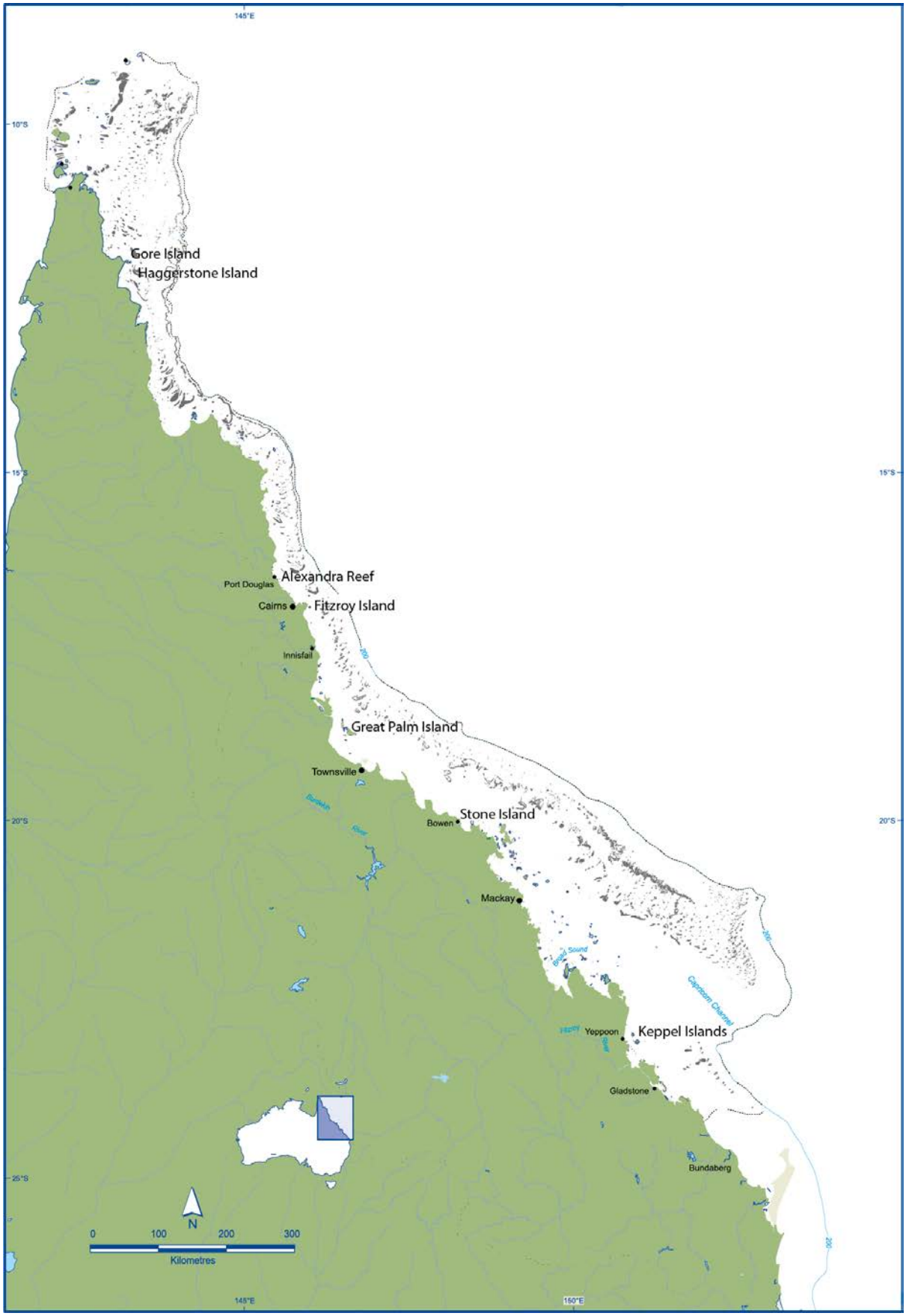

Figure 1: Queensland Coast and Great Barrier Reef, Australia. Labelled Islands and coral reefs are the main study sites within this Thesis.

Holocene reef growth on the Great Barrier Reef

Coral reef growth is constrained by a number of climatic and environmental factors such as light, sea surface temperature (SST), turbidity, salinity and sea level (Buddemeier and Hopley, 1988, Montaggioni, 2005, Montaggioni and Braithwaite, 2009). These factors have also determined the geographic location of reefs throughout the Holocene, and beyond into the deep geological past allowing for comparisons and analogues beyond the "shifting baseline" of anthropogenic reef decline (Knowlton and Jackson, 2008, Hughes et al., 2011, Pandolfi, 2011, Pandolfi, 2015).

The GBR as recognised today is a relatively young feature in geological terms. The oldest date obtained from a Holocene coral is ~9500 years before present (yBP- where present is defined as 1950; Hopley et al., 1978), with the most prolific accretion phase centred around ~7500 yBP (Smithers et al., 2006). Inshore reefs on the GBR demonstrate similarities in patterns of reef growth history, initiating soon after inundation of the shallow Pleistocene shelf during the post glacial marine transgression, and accreting rapidly in a either a "catch up" or "keep up" mode of growth to ~5500 yBP (McLean et al., 1978, Stoddart et al., 1978, Neumann and Macintyre, 1985, Kleypas and Hopley, 1992, Dullo, 2005, Montaggioni, 2005, Hopley, 2006, Smithers et al., 2006, Perry and Smithers, 2011). Yet, after 5500 yBP the growth history of the GBR becomes somewhat more complicated with a significant reef "turn-off" and hiatus period of up to ~2000 years identified on many inshore reefs(Smithers et al., 2006, Perry and Smithers, 2011).

Reef "turn-on" and "turn-off" events were initially defined by Buddemeier and Hopley (1988) to explain periods of optimal coral growth and non-accretion/net erosion, respectively, at significant spatial and temporal scales. On the GBR, Smithers et al. (2006) examined data from 21 inshore and fringing reefs and discovered that Holocene reef flat progradation reduced abruptly and significantly between 5500 and 4800 yBP. They attributed this slow down to a scarcity of suitable substrate for further reef expansion and reduced accommodation space due to a (smoothly) falling sea level following the mid-Holocene highstand. A subsequent study by Perry and Smithers (2011) examined 76 chronologically controlled reef cores from new and previously published data from 22 reefs along the GBR, and identified a distinct "turn off" or hiatus event occurring predominantly at inshore reefs, and specifically in the northern and southern GBR regions, between ~5500 to 2600 yBP, with no significant reef accretion after 4500 yBP (Fig. 2; Perry and Smithers, 2011). Clearly this

hiatus event precedes modern human development of the Queensland coast, and is therefore driven by natural perturbations however, the mechanism driving the collapse of coral reefs in the mid-Holocene remains uncertain. Perry and Smithers (2011) concluded that the hiatus on the GBR was likely the result of the synergistic effects of multiple factors including; a reduction in accommodation space due to a lowering of sea level, proximity of the reefs to the terrigenous sediment wedge (Larcombe and Woolfe, 1999) resulting in increased turbidity, and/or limited calcification due to decreasing sea surface temperatures (SST) and increased extremes in rainfall affecting sediment delivery to the GBR lagoon. Though, in addition to the homogeneity of reef decline on the GBR in the mid-Holocene, broadly synchronous decreases in accretion, and/or coral reef hiatus have been noted in the wider Indo-Pacific.

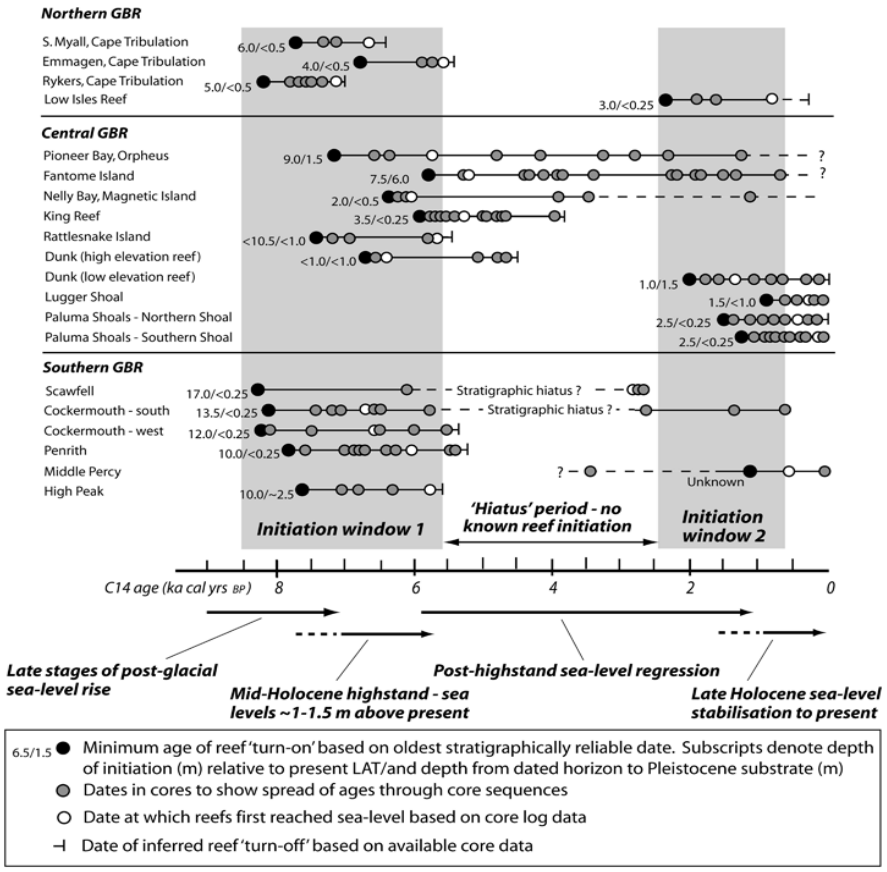

Figure 2: Plot showing reef initiation-accretion-demise for inner-shelf Great Barrier Reef sites from Perry and Smithers (2011) based on available chronostratigraphic (core) data. Perry and Smithers (2011) identified two distinct reef 'initiation windows' (grey boxed areas), separated by a 'hiatus'.

Varying scale mechanisms have been invoked as the likely cause of these hiatus including; eustatic sea level (ESL) oscillations (Hamanaka et al., 2012), regional relative sea level (RSL) changes (Smithers et al., 2006, Engels et al., 2008), shifting local wave regimes (Hongo and Kayanne, 2009), strengthening of the El Niño Southern Oscillation (ENSO; Rooney et al., 2004, Toth et al., 2012) and an increase in intense storm activity and subsequent sedimentation (Twiggs and Collins, 2010). Yet, the relative synchronicity of reef decline across the Indo-Pacific in the mid-Holocene is suggestive of a possible broad scale climatic and/or environmental shift. However high-resolution Holocene SL and climate data, especially for the southern hemisphere and GBR, are still poorly constrained. Therefore, to disentangle factors that have caused coral reef decline in the geological past, it is first necessary to establish centennial to sub-centennial scale environmental and climatic conditions that potentially led to the mid-Holocene coral hiatus.

Holocene sea level

Development of substantial three dimensional reef structures, such as those seen on the GBR, are governed by accommodation space which is regulated by both the stage of reef development and sea level (Veron, 1995, Dullo, 2005, Smithers et al., 2006, Perry and Smithers, 2011, Murray-Wallace and Woodroffe, 2014). Changes to total global mean sea level (i.e. eustatic sea level; ESL) is controlled by both changes in volume as a result of the transfer of water storage to or from land, and the mass of the ocean due to temperature/density changes (Lambeck et al., 2014). Following the last glacial maximum (LGM) large scale northern hemisphere ice melt and Antarctic contributions saw ESL rise by ~ 120m between 18,000 y BP and 6000 y BP (Clark and Lingle, 1979, Fairbanks, 1989). However water redistribution and glacio- hydroisostatic processes mean that relative sea level histories (RSL; the level of the ocean to land) are regionally specific (Clark et al., 1978, Milne and Mitrovica, 2008, Lambeck et al., 2014, Rovere et al., 2016). Generally, in the near field (i.e. near to former icesheets) ice removal from continents (glacio-hydro-isostasy) is the dominant control on the RSL signal, whereas in the far field (i.e. far from former glacial centres) the redistribution of water (e.g. ocean syphoning) and hydroisostatic response of continental shelves and ocean basins to increased water loads dominate (Clark et al., 1978, Nakada and Lambeck, 1989, Lambeck and Nakada, 1990, Mitrovica and Peltier, 1991, Pirazzoli and Pluet, 1991, Fleming et al., 1998, Lambeck, 2002, Mitrovica and Milne, 2002, Milne and Mitrovica, 2008, Lambeck et al., 2014).

Geophysical models of regional scale RSL response to ESL change place the Australian east coast (AEC) within a zone characterised by a mid-Holocene highstand (Fig. 3; Clark et al., 1978) followed by a RSL fall due to water redistribution and hydroisostasy on the continental shelf (Mitrovica and Milne, 2002). Reconstructions of RSL on the AEC using geomorphic features (e.g. Gagan et al., 1994, Switzer et al., 2010), fixed biological indicators (e.g. Hopley and Gill, 1972, Lewis et al., 2008), and fossil coral reefs and microatolls (Chappell, 1983b, Chappell, 1983a, McLean and Woodroffe, 1990, Woodroffe et al., 2000) generally support a mid-Holocene RSL highstand, although the exact magnitude and timing varies considerably with estimates ranging between +0.7m to +3.0m between ~7500 and 5500 yBP (Chappell, 1983b, Chappell, 1983a, Fleming et al., 1998, Sloss et al., 2007, Lewis et al., 2008, Yu and Zhao, 2010). Yet the most contentious issue is whether RSL regressed smoothly or oscillated to present levels since the mid-Holocene highstand (Chappell, 1983a, Baker and Haworth, 2000, Horton et al., 2005, Lewis et al., 2008, Lewis et al., 2013).

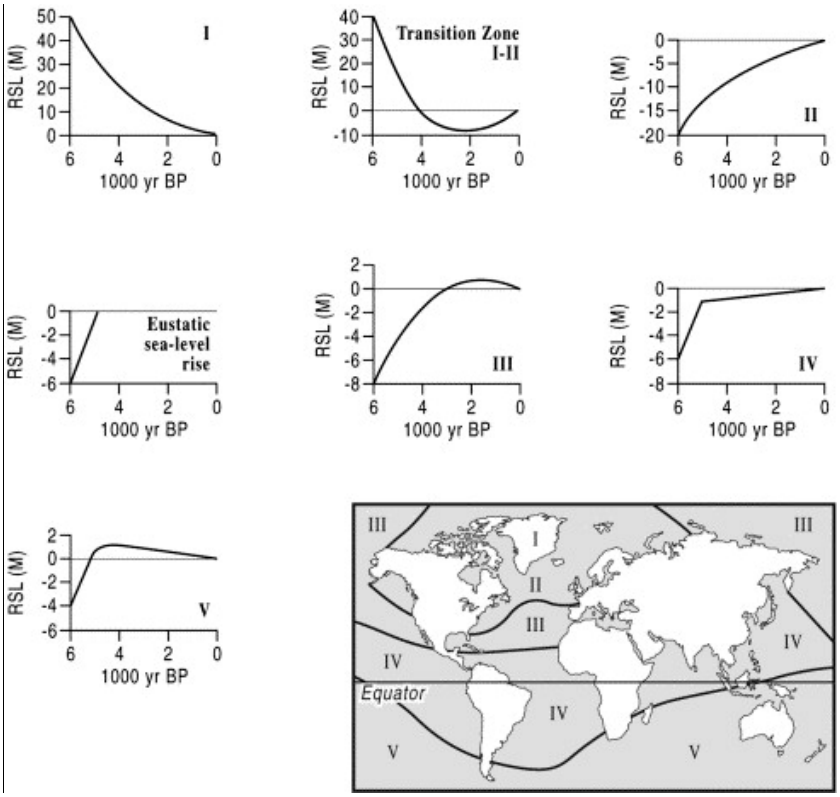

Figure 3: Geophysical model of relative sea level response (sea level zones) to post glacial melt where no eustatic change in ocean volume (i.e. eustatic change) has occurred since 5000 y BP from (from Clark et al., 1978, Woodroffe and Horton, 2005).

Using coral microatolls from a wide latitudinal range on the northern GBR, Chappell (1983a) concluded that a linear, or smooth, regression was most likely. However, evidence derived from fixed biological indicators (Baker and Haworth, 2000, Baker et al., 2005, Lewis et al., 2008, Lewis et al., 2015) and coral microatolls (Harris et al., 2015) suggests rapid and significant oscillations were a possibility. A comprehensive review by Lewis et al. (2008) recalibrated previously published ^{14}C dates of various sea level indicators from the AEC and proposed two negative RSL oscillations centred at ~4600 and 2800 yBP, however the persistence of the large age errors in this study limited sub-centennial interpretation (Fig. 4).

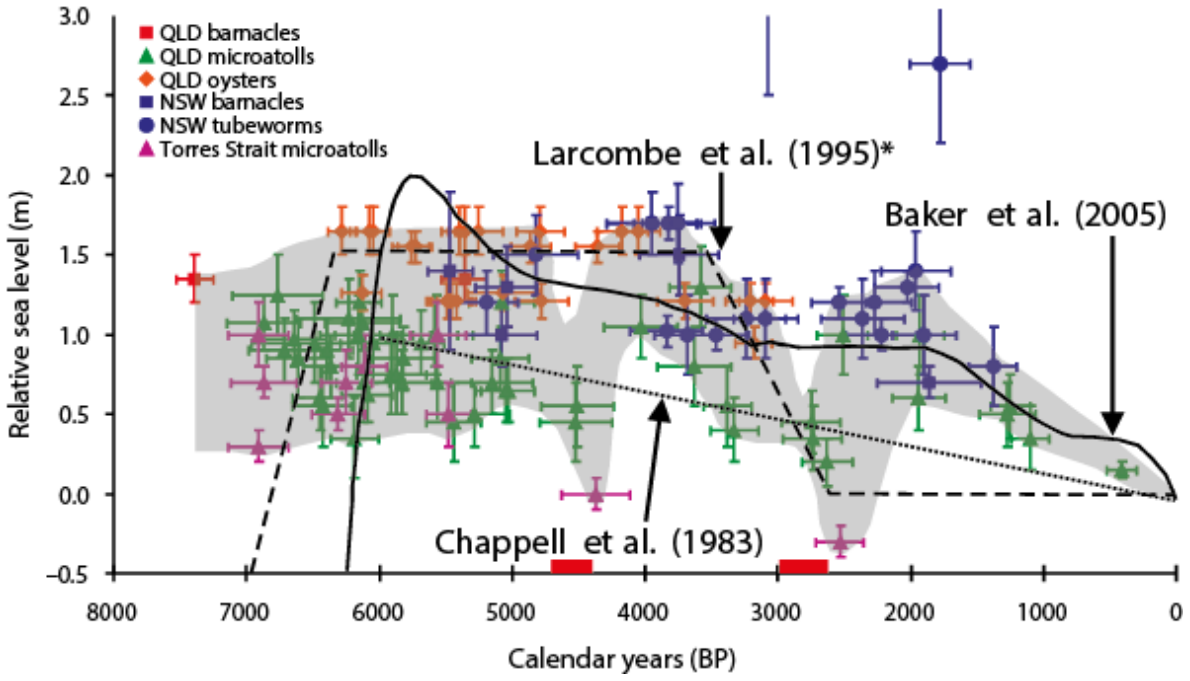

Figure 4: Recalibrated 14C sea level data from Lewis et al. (2008; and references therein) with superimposed past sea-level interpretations of Chappell et al. (1983), Larcombe et al. (1995) and Baker et al. (2005) for eastern Australia. The red bars represent growth hiatuses in oyster bed and tubeworm colonies identified by Lewis et al (2008).

Holocene climate

To enable a better understanding of coral reef response to predicted climate change and increasing anthropogenic pressure it is also important to investigate climate conditions during periods of reef "turn-off" throughout the Holocene. Until relatively recently the climate of the Holocene, particularly in the Southern Hemisphere, was considered to be relatively stable compared with prior geological epochs (Dansgaard et al., 1993, Petit et al., 1999). However, as the number and quality of palaeoclimate data improve it is becoming evident that

significant and sometimes rapid climatic changes have occurred the since the end of the last glacial maximum (Bond et al., 1997, Steig, 1999, Maslin et al., 2001, Mayewski et al., 2004, Sang-Ik et al., 2006, Donders et al., 2008, Harrison and Bartlein, 2012). In a comprehensive overview of global palaeoclimate records from both marine and terrestrial sources, Mayewski et al. (2004) detected at least six rapid climate change events (over centennial scales) during the Holocene at 9000–8000, 6000–5000, 4200–3800, 3500–2500, 1200–1000, and 600–150 y BP. It is notable that most high resolution palaeoclimate data is currently biased towards Northern Hemisphere records, and that complex ocean-atmospheric teleconnections that drive global climate means that the response to these events will vary at hemispherical to regional scales. For example, variations in the average position of the Inter-Tropical Convergence Zone (ITCZ; e.g. Haug et al., 2001, Fleitmann et al., 2007), historical expansion and contraction of the Indo-Pacific Warm Pool (IPWP; e.g. Abram et al., 2009, Xu et al., 2010) and changes in the frequency and/or strength of ENSO events (e.g. Woodroffe et al., 2003, McGregor and Gagan, 2004, Conroy et al., 2008, Cobb et al., 2013, McGregor et al., 2013, Lough et al., 2014, Zhang et al., 2014) will differentially effect coral reefs across the Indo-Pacific.

The El Niño Southern Oscillation (ENSO) is known to be a major driver of Australian climate, with the position and timing of positive SST anomalies in the equatorial Pacific controlling precipitation, storm events and general atmospheric circulation at inter-annual time scales (Lough, 1991, Cane, 2004, Cai and Cowan, 2009, Karumuri et al., 2009, Redondo-Rodriguez et al., 2012). The two phases of ENSO, El Niño and La Niña, produce significant changes in effective precipitation (EP) and storm/cyclone occurrence on the AEC, with La Niña years being wetter with higher than average SSTs and enhanced cyclone activity, and El Niño years associated with drier and calmer conditions during the Austral summer (Verdon et al., 2004, Meinke et al., 2005, Redondo-Rodriguez et al., 2012, Klingaman et al., 2013, King et al., 2014). Additionally, ENSO strength and periodicity is modulated by the Pacific Decadal Oscillation (PDO) and the Inter-decadal Pacific Oscillation (IPO) at longer timescales (Power et al., 1999, Power et al., 2006, Verdon and Franks, 2006, Klingaman et al., 2013, King et al., 2014, Rodriguez-Ramirez et al., 2014).

A number of reconstructions of ENSO periodicity throughout the Holocene have been developed for the wider Pacific region from both marine [e.g. coral luminescence, Sr/Ca, $\delta^{18}O$, foraminiferal Mg/Ca analyses] (Hendy et al., 2003, Woodroffe et al., 2003, McGregor and Gagan, 2004, Cobb et al., 2013, McGregor et al., 2013, Lough et al., 2014) and terrestrial

proxy records (e.g. lacustrine sedimentary properties, charcoal and palynology) (Shulmeister and Lees, 1995, Moy et al., 2002, Donders et al., 2007, Conroy et al., 2008) . It has been suggested by several authors that ENSO amplitude was subdued during the early to mid-Holocene [~ 9500-5000 cal. yr. BP; (Tudhope et al., 2001, McGregor and Gagan, 2004, Brown et al., 2006, Brown et al., 2008, Wanner et al., 2008, Chiang et al., 2009, Lough et al., 2014)] likely due to insolation characteristics (Clement et al., 2000), however spatial inconsistencies regarding warm/cool-wet/dry phases in the Southern Hemisphere, including the GBR region, are still unresolved (Wanner et al., 2008, Wanner et al., 2011) and may reflect internal rather than external mechanisms [e.g. overarching phases of Pacific Decadal Oscillations] (Debret et al., 2009, Cobb et al., 2013, Rodriguez-Ramirez et al., 2014, Emile-geay et al., 2016).

Where palynological and sedimentary records allow for interpretation of long continuous records of climate trends, they are limited in constraining chronologies to datable features found within the sediment cores (Kershaw, 1983). Subsequently, although an invaluable source of palaeoclimate data, these methods are restricted when trying to detect rapid and/or subtle sub-decadal to centennial changes in climate (Cobb et al., 2013). High resolution chronologically controlled coral cores address this issue, however proxy reconstructions from Holocene coral cores on the GBR are limited to a few studies (Gagan et al., 1998, Lough et al., 2014, Roche et al., 2014) which has resulted in a fragmented and sparse time series with spatial inconsistencies. Consequently, more records derived from fossil corals are needed to allow for better interpretation of high resolution environmental and climate conditions during the Holocene, with a focus on periods for which reef hiatus have been documented.

Objectives and Thesis Outline

The primary objective of this study is to investigate climatic and environmental conditions from the mid-Holocene to present on the Great Barrier Reef that controlled reef development and demise. Using high precision Uranium-Thorium (U-Th) dating techniques of sub-fossil coral microatolls (sea level) and novel treatment of coral luminescence index data from sub-fossil *Porites* sp. coral cores (climate/ENSO) this study aims to describe the possible mechanisms responsible for the previously documented reef “turn-off” event on the GBR in the mid-Holocene.

Refining sub-centennial relative sea level on the Great Barrier Reef

Refining the RSL history of the GBR is paramount to understanding Holocene reef growth histories and patterns of aggradation and progradation through time. Coral microatolls are discoid shaped corals that have living polyps around the perimeter but for which the upper dead flat surface has been constrained by the air-sea interface (Fig. 5a, Fig. 6 a, b) , generally within ± 10cm of MLWS on the GBR for *Porites sp.* (Chappell, 1983b).

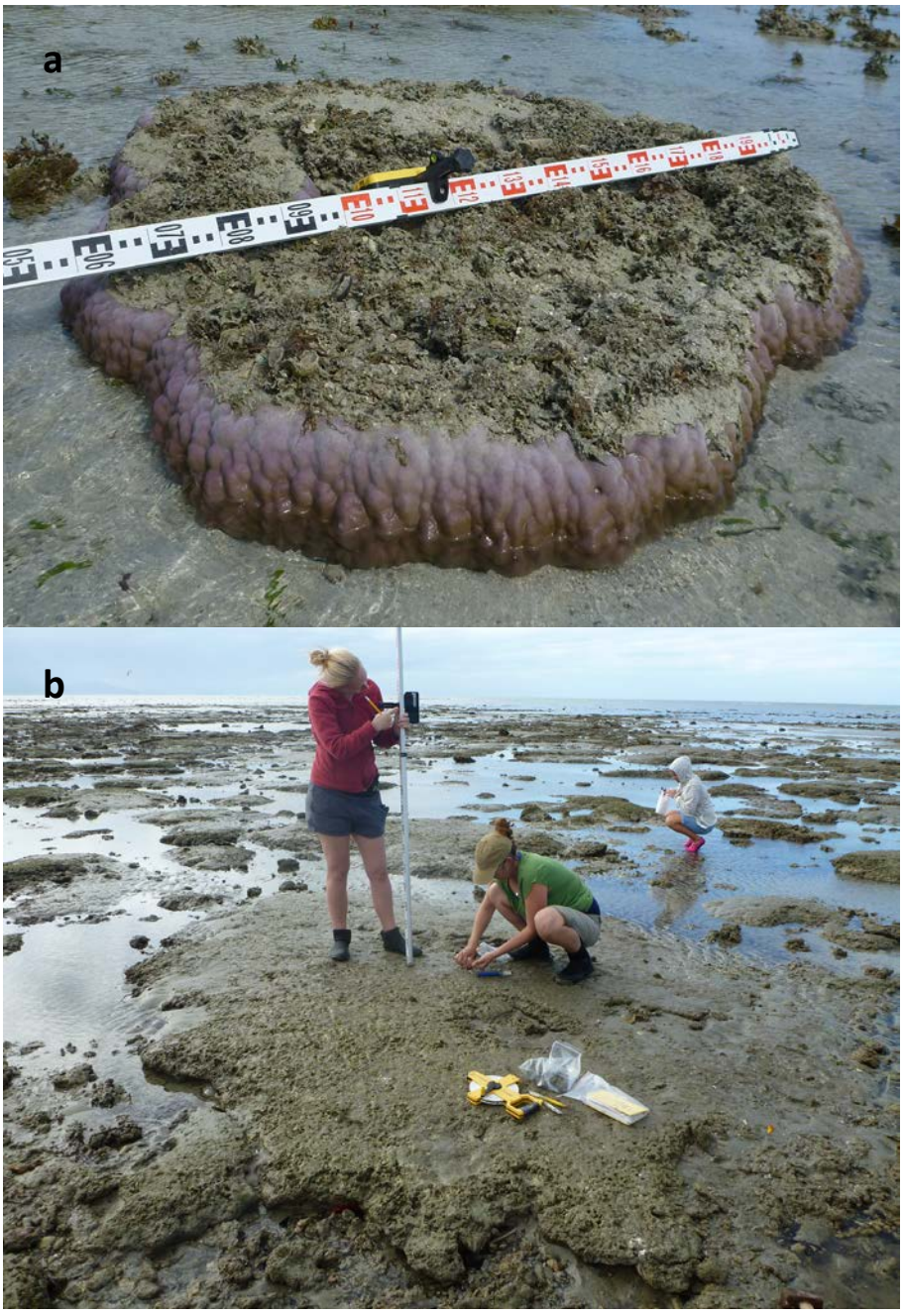

Figure 5: a) Modern microatoll emerged at lowest astronomical tide. The outer perimeter of the microatoll is living whilst the upper surface has died off as a result of exposure to the air-sea interface at ~mean low water spring tide level (MLWS). b) A field of fossil microatolls surveyed above present MLWS tide level at Alexandra Reef, Australia.

Individual coral microatoll morphologies can also provide information of the RSL history throughout the living history of the colony (Meltzner and Woodroffe, 2015) with a planar upper surface indicating RSL stability (Fig. 6b), a "hat" morphology indicating a fall in RSL (Fig. 6c) and a "cup" morphology (Fig. 6d) representing a rise in RSL (Scoffin et al., 1978, Hopley, 1982, Zachariasen et al., 1999)

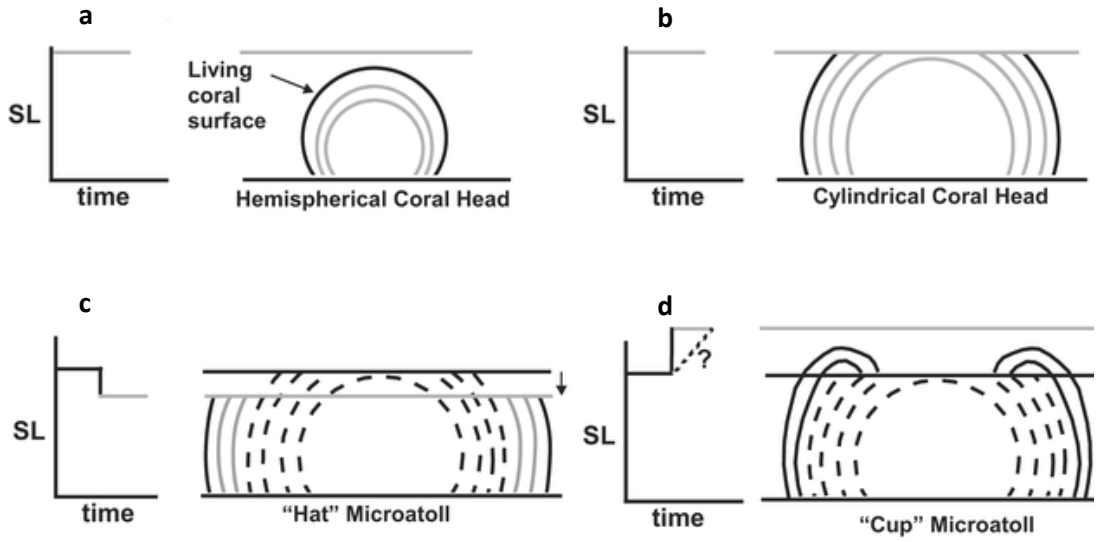

Figure 6: Schematic representation of coral microatoll formation and morphologies in response to relative sea level (RSL) changes. a) a massive coral growing below the air-sea interface forms a hemispherical growth form; b) when the coral reaches the constraining sea level (SL) the upper surface ceases to grow, but the coral edge retains living polyps; c) a RSL fall will result in a "hat" morphology where the outer living surface elevation is lowered; and d) a rise in RSL will result in a "cup" morphology where by the living outer polyps will grow up to the new SL height. Adapted from (Scoffin et al., 1978, Zachariasen et al., 1999)

Numerous emergent fossil coral reefs are evident on both inshore continental islands and mainland fringing reefs on the GBR, many of which retain *in situ* coral microatolls on former reef flats (e.g. Fig 5b). These fossil microatolls can be surveyed and referenced against modern MLWS tide levels to ascertain the height of the fossil communities relative to their modern counterparts (Chappell, 1983a).

Initial investigations of fossil microatolls relied on radiocarbon dating (^{14}C) to determine the age of these samples however, these were sometimes either uncalibrated, or inappropriately corrected for ^{14}C marine reservoir effects, or calibrated with the IntCal04 dataset using the Marine04 "global" marine calibration database (Hughen et al., 2004) that does not take into consideration the temporal variability of local/regional ΔR values which may fluctuate by >700 years on centennial to millennial scales in the Western Pacific region (McGregor et al.,

2008, Yu et al., 2010). More recently uranium-thorium (or U-series) dating has been adopted as a method for determining coral ages, with age errors significantly reduced compared to earlier ^{14}C techniques (Clark et al., 2014). U-Th dating relies on the radioactive decay chain of ^{238}U to ^{206}Pb via intermediate daughter products ^{234}U and ^{230}Th (Cheng et al., 2000, McCulloch and Mortimer, 2008). Where uranium is soluble in seawater and taken up by corals during skeletogenesis (between 2 - 4ppm), thorium is non-soluble and therefore generally negligible in coral aragonite at the time of formation. By measuring the ratio of ^{238}U to ^{230}Th in corals the absolute age can be calculated using the isotopic half- life values, with corrections made for detrital contamination calculated from ^{232}Th values measured simultaneously (Cheng et al., 2000, Cobb et al., 2003, Shen et al., 2008).

Using microatolls dated with high-precision U-Th dating techniques this thesis aims to refine the RSL history of the GBR throughout the Holocene. Results pertaining to this part of the thesis are presented in Chapters 2 and 3;

Theme 1: Holocene sea level

Hypothesis 1: Temporal variations of relative sea level have controlled reef development and demise in the Keppel Islands, GBR, throughout the Holocene.

- **Local scale relative sea level, Keppel Islands** – Evidence is still equivocal as to whether RSL regressed smoothly or oscillated following the mid-Holocene highstand. Previous sea level studies have been restricted from detecting small and possibly rapid changes in RSL due to uncertainties and errors associated with earlier dating techniques, and interpretation of a limited number of samples per site (generally < 10). To evaluate relative sea level (RSL), and the pattern of sea level regression, high precision U-Th age determinations and elevation surveys of numerous coral microatolls were conducted on three inshore continental island fringing fossil reefs in the Keppel Islands, southern GBR. Microatolls are precise indicators of reef phase shifts from a vertically accreting reef matrix ("catch up") to one that has reached RSL and is then constrained vertically to that point (Scoffin et al., 1978, Stoddart et al., 1978, Stoddart and Scoffin, 1979). This data provided the first evidence of a local scale oscillatory mode of SL regression using microatolls from multiple sites within the same region. The results of this study are presented in **Chapter 2:**

"Holocene sea level instability in the southern Great Barrier Reef, Australia: high-precision U-Th dating of fossil microatolls"

Leonard, N.D., Zhao, J-x., Welsh, K.J., Feng, Y-x., Smithers, S.G., Pandolfi, J.M., Clark, T.R

Coral Reefs (2016)

- **Regional scale sea level, Great Barrier Reef** - Previous studies and syntheses of SL on the GBR have included not only a variety of SL indicators with disparate elevation ranges (fixed biological indicators [FBI's], foraminiferal transfer functions, reef cores/microatolls and geomorphological evidence), but also data combined from wide latitudinal ranges (Hopley, 1975, Chappell, 1983a, Baker and Haworth, 2000, Baker, 2001, Sloss et al., 2007, Lewis et al., 2008, Lewis et al., 2013). This study presents 98 new microatoll U-Th age elevation points from 14 reefs presented separately across a wide latitudinal range on the GBR (11˚S - 23˚S) based on; a) proximity to each other; b) width of the continental shelf and; c) post-matching of SL trends. Data from this study and from **Chapter 2** are combined to further constrain Holocene RSL history on the GBR. The results are presented in **Chapter 3:**

"Holocene sea level oscillations on the Great Barrier Reef and links to climate"

Leonard, N.D., Zhao, J-x, Welsh, K.J., Feng, Y-x, Clark, T.R, Pandolfi, J.M.

(In prep) – Target Journal – Nature, Nature Geoscience

Theme 2: Holocene climate and novel techniques for palaeoclimate reconstructions

High resolution mid-Holocene climate records in the southern hemisphere are currently lacking. The second theme of this thesis is therefore concentrated on developing novel techniques for reconstructing past climatic and environmental conditions on the GBR using massive Porites sp. corals.

Annual resolution climate using coral luminescence

Fluorescent bands (or coral luminescence) revealed under ultraviolet (UV) light in annually banded massive corals were first described by Isdale (1984), with initial investigations suggesting that the distinct bands resulted from fluvially derived humic/fulvic acids (Boto and Isdale, 1985, Susic et al., 1991). However, a subsequent study by Barnes and Taylor (2005) suggests that luminescent lines are likely the result of skeletal architecture, where low density portions of skeleton are associated with reduced salinity. This was suggested as corals far removed from terrestrial influence were also sometimes found to exhibit luminescent lines that could not be explained by direct humic acid contribution. Regardless, at inshore locations luminescence bands represent river discharge events by either mechanism, and have been used extensively to reconstruct river discharge/rainfall on the GBR (Lough, 1991, Isdale et al., 1998, Lough et al., 2002, Fallon et al., 2003, Hendy et al., 2003, Lough, 2007, Lough, 2011b, Lough, 2011a, Lough et al., 2014, Rodriguez-Ramirez et al., 2014, Lough et al., 2015). As precipitation on the Queensland coast is strongly modulated by wider climatic mechanisms, luminescent lines in corals have also been used to reconstruct rainfall frequency with links to ENSO and the Pacific Decadal Oscillation, to extend the record beyond modern instrumentation to the past ~300 to 400 years (PDO; Isdale et al., 1998, Lough et al., 2002, Lough, 2007, Lough, 2011b, Lough et al., 2014, Rodriguez-Ramirez et al., 2014).

Fossil coral reconstructions of ENSO variability on the GBR are currently limited (Roche et al., 2014). Lough et al. (2014) used both modern and fossil (~6000 yBP) luminescence lines in massive *Porites* to reconstruct Burdekin River discharge events, and concluded that ENSO frequency and strength was reduced in the mid-Holocene compared to present. Roche et al. (2014) used geochemical analysis and spectral luminescence data from a modern and fossil microatoll from King Reef and suggested higher salinity variations, increased green/blue spectral ratios (i.e. increased terrestrial input) and reduced Sr/Ca seasonal SST range all represent a wetter and warmer phase on the GBR at~4600 yBP, reminiscent of modern La Niña like conditions. Clearly more Holocene ‘windows’ derived from both coral luminescence and geochemical proxy reconstructions are needed before a complete picture of ENSO variability can be assessed on the GBR throughout the Holocene, however data from elsewhere in Australia and in the wider Pacific generally supports reduced ENSO variability and strength during the mid-Holocene (Shulmeister and Lees, 1995, Moy et al., 2002, Rodo

and Rodriguez-Arias, 2004, Wanner et al., 2008, Chiang et al., 2009, Carré et al., 2012, Cobb et al., 2013, McGregor et al., 2013, Zhang et al., 2014, Emile-geay et al., 2016).

Continuous wavelet transform

Continuous wavelet transforms (CWTs) are increasingly being used for identifying frequencies or periodicities of non-stationary climate data through time. The Morlet wavelet is a cosine wavelet modulated with a Gaussian envelope which allows for detection of peaks and troughs within time series data (Morlet et al., 1982a, Nakken, 1999). Compared to Fourier transforms where the "window" of transformation is of a fixed size, thus limiting either the time or frequency resolution of climatic data, CWT allows for extension of the wavelet in the time band to reflect low frequency (dilation) of the climate signal (i.e. low resolution periodicities) and high frequency (contraction) of the wavelet for shorter time fields (Morlet et al., 1982b, Torrence and Compo, 1998, Cazelles et al., 2007). This allows for visualisation of one dimensional time series data in two dimensional time-frequency space (Morlet et al., 1982b, Lau and Weng, 1995) displayed as power spectrum for which significance of the signal can be ascertained (Torrence and Compo, 1998).

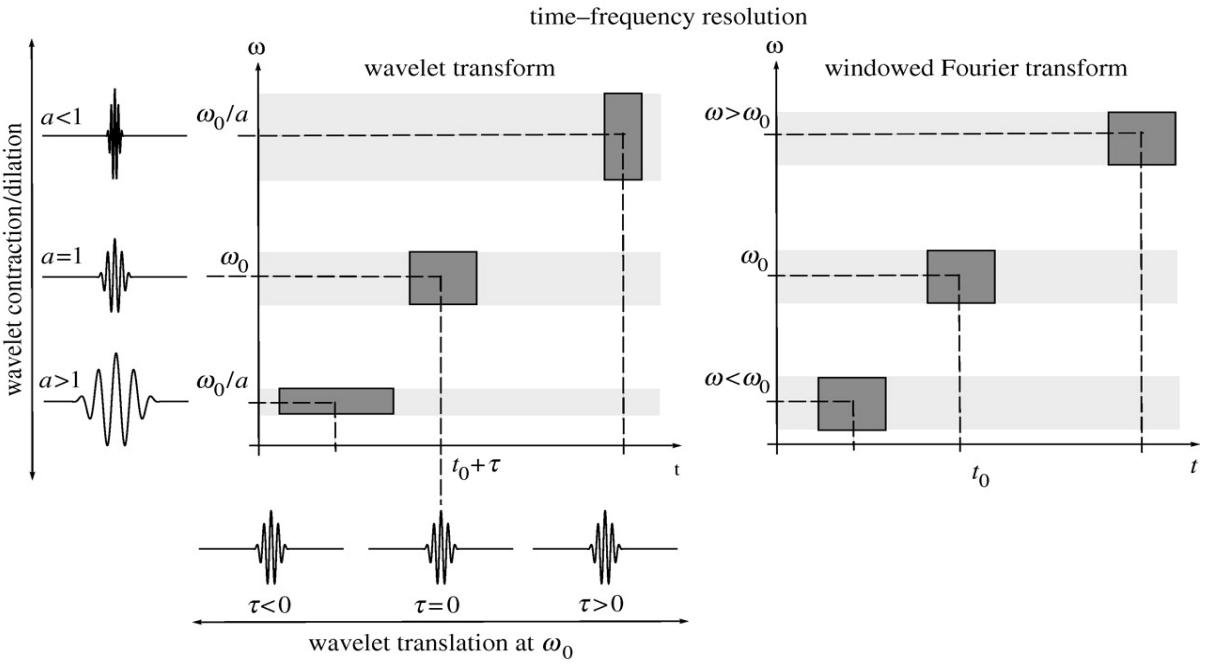

Figure 7: Schematic showing the difference between Morlet continuous wavelet transform and Fourier transform. (a) Wavelets and their time–frequency boxes representing the corresponding variance (energy) distribution (Where τ = time; a = scale of the wavelet and ω = frequency). When the scale a changes the time resolution and frequency resolution both change. (b) In Fourier decomposition of a signal the boxes of the transform are obtained by a time- or frequency shift, which yields the same variance spreads over the entire time–frequency reconstruction. (from Cazelles et al., 2007)

Hypothesis 2: Wavelet analysis of visually assessed ultraviolet (UV) luminescent lines in corals enables reconstruction of past ENSO variability on the GBR.

Numerous studies are now taking advantage of continuous wavelet transforms (CWT) of time-series environmental data (Gu and Philander, 1995, Torrence and Compo, 1998, Grinsted et al., 2004, Debret et al., 2009, Grove et al., 2013, Walther et al., 2013, Soon et al., 2014, Lough et al., 2015) which allows for interpretation in two dimensional time-frequency space (Torrence and Compo, 1998). This study used a previously published record of visually assessed luminescence data from a modern *Porites* sp. coral from Great Palm Island (GPI), central GBR, and Niño 3 region SST data to assess the utility of CWTs (Morlet) in reconstructing ENSO frequency and variability. The same method was then applied to three fossil *Porites* sp. cores from GPI U-Th dated to ~5200, 4900 and 4300 yBP. The results of this research are presented in **Chapter 4**:

"Evidence of reduced mid-Holocene ENSO variance on the Great Barrier Reef, Australia"
Leonard, N.D., Welsh, K.J., Lough J.M., Pandolfi, J.M., Clark, T.R., Zhao, J-x.

Paleoceanography (2016)

Coral geochemistry

It is undeniable that fluvial terrigenous outputs have been altered since European settlement on the east coast of Australia. The region has seen a fourfold increase in agriculture and farming practise within the 38 fluvial catchments entering the GBR over the last 150 years (Neil et al., 2002, Lawrence, 2010). Further, rapid population increases and a burgeoning mining industry along the length of the Queensland coast has led to increased land clearing for infrastructure (e.g. urban growth, port expansions, road development), yet limited continuous data are available for total sediment load onto inshore reefs. Modelling studies have reported that sediment loads to the GBR have increased 4 to 10 times since the 1850's (e.g. Neil et al., 2002, Kroon et al., 2012) however these models incorporate a number of assumptions about fluvial and climatic patterns pre-disturbance for which data is limited due

to lack of instrumental monitoring beyond a few decades. Consequently, a number of methods have been developed to obtain riverine sedimentary histories beyond instrumental records either directly (e.g. sediment cores; Cavanagh et al., 1999), or by proxy (e.g. coral geochemistry such as Barium/Calcium [Ba/Ca] and luminescence banding; Lough and Barnes, 1997, McCulloch et al., 2003, Lewis et al., 2007).

Massive long-lived corals offer a unique opportunity to both extend the modern instrumental record, and to reconstruct environmental conditions throughout the Holocene. When sliced and X-radiographed, drilled cores of corals can be chronologically constrained by uranium-thorium (U-Th) dating techniques and band counting, where one couplet of high density (dark) and low density (light) banding in the aragonite skeleton is equal to one year of growth (Knutson et al., 1972). Early evaluation of the geochemical composition of the aragonite of corals recognised that trace elements and stable isotopes within the skeletal architecture recorded numerous environmental parameters. For example, incorporation of Barium (Ba), rare earth elements (REEs) and Yttrium (Y)have been shown to reflect the ambient chemistry of the sea water in which the coral grew (Sholkovitz and Shen, 1995, Sinclair et al., 1998, McCulloch et al., 2003, Dubinin, 2004). This is significant in that oceanic surface waters are normally depleted in Ba, REEs and Y (REY), with the major source (>90%) of REYs in coastal water is derived from suspended and dissolved riverine input (Dubinin, 2004). Therefore, measuring the geochemically incorporated Ba and REYs in the skeletons of long-lived massive corals can be used as a proxy to evaluate terrigenous riverine input (Shen and Sanford, 1990).

Although numerous attempts have been made to reconcile Ba/Ca records with instrumental data of rainfall/flood events (Alibert et al., 2003, McCulloch et al., 2003, Jupiter et al., 2008) or known land use changes (Lewis et al., 2007), anomalous peaks and background variability of Ba/Ca that is decoupled from flood flow data or known land use changes restricts the interpretation of this proxy beyond the instrumental record. A number of hypothesis have been suggested to explain possible causes of observed Ba/Ca anomalies including, tidal mangrove sediment release of stored Ba under hyper-saline conditions during dry seasons (Alibert et al., 2003), the significance of Ba in biological systems such as phytoplankton blooms/scavenging processes (Lewis et al., 2007) and upwelling (McCulloch et al., 2003), however more critical research is needed to fully understand the sources and sinks of Ba at regional scales.

Low resolution (biannual) analysis of Yttrium, using solution ICP-MS, has shown promise as a gauge of fine sediment budget to the GBR, due to its role in secondary (biological) processes being considered insignificant (Lewis et al., 2007). Earlier studies applying LA-ICP-MS analysis of Y also demonstrated a decreasing concentration away from sources of sedimentary input, further suggesting that peaks may coincide with flood events (Alibert et al., 2003), but the lower precision in this study renders interpretation equivocal. Seasonally resolute studies of REEs, that may reflect high flow rainfall events, are to date relatively under-examined in geochemical investigations of coral aragonite, mainly due to previously low detection limits available and sample preparation time (Wyndham et al., 2004). As sample protocols and detection limits of solution ICP-MS improve, investigations into utility of REEs as a proxy of riverine terrigenous input to nearshore reefs are now more accessible.

Therefore, high-resolution analysis of REEs in chronologically-controlled annual banding of massive corals, with particular attention to Ce and La (LREEs), are suggested to provide a more cohesive separation of high flow riverine input onto reefs versus signals resulting from secondary biological processes as seen in exclusive Ba/Ca analysis.

Hypothesis 3: Time series of rare earth elements and Yttrium from chronologically controlled coral cores provides a proxy of riverine sedimentary input to coral reefs.

- **Coral geochemical proxies for terrigenous input** – The rare earth elements (REEs) offer potential as a proxy for reconstructing rainfall/flood events (Wyndham et al., 2004) and turbidity as, in coastal waters, ~90% are derived from suspended and dissolved riverine input (Dubinin, 2004). However, few records coral REE chemistry in massive corals from the GBR at sub-annual resolution are currently available. This study used cores from four massive *Porites* sp. corals live collected from the Frankland Islands and Sudbury Cay, a region that experiences a known water quality gradient driven by discharge from the Russell-Mulgrave River. The geochemical proxy data from these cores is compared with *in situ* data loggers (Australian Institute of Marine Science) and river discharge, rainfall (Australian Bureau of Meteorology) and wind data (DERM). These records have been used to determine regional relationships between geochemical proxies in corals that can record reliable riverine input events to inshore turbid reefs that allow for a more cohesive view of reef sediment input histories and environmental conditions. Results of this study are presented in **Chapter 5:**

“High resolution geochemical analysis of massive Porites sp. corals, Wet Tropics, GBR; Rare Earth Elements and Yttrium as indicators of terrigenous input”

Leonard, N.D., Welsh, K.J., Nguyen, A.D., Sadler, J., Pandolfi, J.M., Clark, T.R., Zhao, J-x., Webb, G.E.

(In prep) - Target Journal – Geochimica et Cosmochimica Acta

A synthesis and general discussion of the main results of this thesis and directions for future research is presented in **Chapter 6**.

References

Abram, N. J., Mcgregor, H. V., Gagan, M. K., Hantoro, W. S. & Suwargadi, B. W. 2009. Oscillations in the southern extent of the Indo-Pacific Warm Pool during the mid-Holocene. *Quaternary Science Reviews* **28,** 2794-2803.

Alibert, C., Kinsley, L., Fallon, S. J., Mcculloch, M. T., Berkelmans, R. & Mcallister, F. 2003. Source of trace element variability in Great Barrier Reef corals affected by the Burdekin flood plumes. *Geochimica et Cosmochimica Acta* **67,** 231-246.

Baker, R. 2001. Inter-tidal fixed indicators of former Holocene sea levels in Australia: a summary of sites and a review of methods and models. *Quaternary International* **83-85,** 257-273.

Baker, R. & Haworth, R. J. 2000. Smooth or oscillating late Holocene sea-level curve? Evidence from the palaeo-zoology of fixed biological indicators in east Australia and beyond. *Marine Geology* **163,** 367-386.

Baker, R. G. V., Haworth, R. J. & Flood, P. G. 2005. An Oscillating Holocene Sea-level? Revisiting Rottnest Island, Western Australia, and the Fairbridge Eustatic Hypothesis. *Journal of Coastal Research* **Special Issue,** 3-14.

Barnes, D. J. & Taylor, R. B. 2005. On the nature and causes of luminescent lines and bands in coral skeletons: II. Contribution of skeletal crystals. *Journal of experimental marine biology and ecology* **322,** 135-142.

Bellwood, D. R., Hughes, T. P., Folke, C. & Nyström, M. 2004. Confronting the coral reef crisis. *Nature* **429,** 827-833.

Bond, G., Bonani, G., Showers, W., Cheseby, M., Lotti, R., Almasi, P., Demenocal, P., Priore, P., Cullen, H. & Hajdas, I. 1997. A Pervasive Millennial-Scale Cycle in North Atlantic Holocene and Glacial Climates. *Science* **278,** 1257-1266.

Boto, K. & Isdale, P. 1985. Fluorescent bands in massive corals result from terrestrial fulvic acid inputs to nearshore zone. *Nature* **315,** 396-397.

Brodie, J. & Waterhouse, J. 2012. A critical review of environmental management of the 'not so Great' Barrier Reef. *Estuarine, Coastal and Shelf Science* **104-105,** 1.

Brown, J., Collins, M. & Tudhope, A. 2006. Coupled model simulations of mid-Holocene ENSO and comparisons with coral oxygen isotope records. *Advances in Geosciences* **6,** 29-33.

Brown, J., Collins, M., Tudhope, A. W. & Toniazzo, T. 2008. Modelling mid-Holocene tropical climate and ENSO variability: towards constraining predictions of future change with palaeo-data. *Climate Dynamics* **30,** 19-36.

Bruno, J. F. & Selig, E. R. 2007. Regional Decline of Coral Cover in the Indo-Pacific: Timing, Extent, and Subregional Comparisons. *PloS one* **2,** e711.

Buddemeier, R. W. & Hopley, D. Turn-ons and Turn-offs; Causes and mechanisms of the initiation and termination of coral reef growth. *In:* Proceedings of the 6th International Coral Reef Symposium, 1988 Australia. 253 - 261.

Cai, W. & Cowan, T. 2009. La Niña Modoki impacts Australia autumn rainfall variability. *Geophysical Research Letters* **36,** L12805.

Cane, M. A. 2004. The evolution of El Niño, past and future. *Earth and Planetary Science Letters* **230,** 227-240.

Carpenter, K. E., Abrar, M., Aeby, G., Aronson, R. B., Banks, S., Bruckner, A., Chiriboga, A., Cortés, J., Delbeek, J. C., Devantier, L., Edgar, G. J., Edwards, A. J., Fenner, D., Guzmán, H. M., Hoeksema, B. W., Hodgson, G., Johan, O., Licuanan, W. Y., Livingstone, S. R., Lovell, E. R., Moore, J. A., Obura, D. O., Ochavillo, D., Polidoro, B. A., Precht, W. F., Quibilan, M. C., Reboton, C., Richards, Z. T., Rogers, A. D., Sanciangco, J., Sheppard, A., Sheppard, C., Smith, J., Stuart, S., Turak, E., Veron, J. E. N., Wallace, C., Weil, E. & Wood, E. 2008. One-Third of Reef-Building Corals Face Elevated Extinction Risk from Climate Change and Local Impacts. *Science* **321,** 560-563.

Carré, M., Azzoug, M., Bentaleb, I., Chase, B. M., Fontugne, M., Jackson, D., Ledru, M.-P., Maldonado, A., Sachs, J. P. & Schauer, A. J. 2012. Mid-Holocene mean climate in the south eastern Pacific and its influence on South America. *Quaternary International* **253,** 55-66.

Cavanagh, J. E., Burns, K. A., Brunskill, G. J. & Coventry, R. J. 1999. Organochlorine Pesticide Residues in Soils and Sediments of the Herbert and Burdekin River Regions, North Queensland – Implications for Contamination of the Great Barrier Reef. *Marine Pollution Bulletin* **39,** 367-375.

Cazelles, B., Chavez, M., Magny, G. C. D., Guégan, J.-F. & Hales, S. 2007. Time-dependent spectral analysis of epidemiological time-series with wavelets. *Journal of The Royal Society Interface* **4,** 625-636.

Chappell, J. 1983a. Evidence for smoothly falling sea-level relative to North Queensland, Australia, during the past 6,000 yr. *Nature* **302,** 406-408.

Chappell, J. 1983b. Holocene palaeo-environmental changes, Central to North Great Barrier Reef inner zone. *BMR Journal of Australian Geology and Geophysics* **8,** 223-235.

Cheng, H., Edwards, R. L., Hoff, J., Gallup, C. D., Richards, D. A. & Asmerom, Y. 2000. The half-lives of uranium-234 and thorium-230. *Chemical Geology* **169,** 17-33.

Chiang, J. C. H., Fang, Y. & Chang, P. 2009. Pacific Climate Change and ENSO Activity in the Mid-Holocene. *Journal of Climate* **22,** 923-939.

Clark, J. A., Farrell, W. E. & Peltier, W. R. 1978. Global changes in postglacial sea level: A numerical calculation. *Quaternary Research* **9,** 265-287.

Clark, J. A. & Lingle, C. S. 1979. Predicted relative sea-level changes (18,000 years B.P. to present) caused by late-glacial retreat of the Antarctic Ice Sheet. *Quaternary Research* **11,** 279-298.

Clark, T. R., Roff, G., Zhao, J.-X., Feng, Y.-X., Done, T. J. & Pandolfi, J. M. 2014. Testing the precision and accuracy of the U–Th chronometer for dating coral mortality events in the last 100 years. *Quaternary Geochronology* **23,** 35-45.

Clement, A. C., Seager, R. & Cane, M. A. 2000. Suppression of El Niño during the Mid-Holocene by changes in the Earth's orbit. *Paleoceanography* **15,** 731-737.

Cobb, K. M., Charles, C. D., Cheng, H., Kastner, M. & Edwards, R. L. 2003. U/Th-dating living and young fossil corals from the central tropical Pacific. *Earth and Planetary Science Letters* **210,** 91-103.

Cobb, K. M., Westphal, N., Sayani, H. R., Watson, J. T., Di Lorenzo, E., Cheng, H., Edwards, R. L. & Charles, C. D. 2013. Highly variable El Niño-Southern Oscillation throughout the Holocene. *Science (New York, N.Y.)* **339,** 67.

Conroy, J. L., Overpeck, J. T., Cole, J. E., Shanahan, T. M. & Steinitz-Kannan, M. 2008. Holocene changes in eastern tropical Pacific climate inferred from a Galápagos lake sediment record. *Quaternary Science Reviews* **27,** 1166-1180.

Dansgaard, W., Johnsen, S., Clausen, H., Dahl-Jensen, D., Gundestrup, N., Hammer, C., Hvidberg, C., Steffensen, J., Sveinbjörnsdottir, A. & Jouzel, J. 1993. Evidence for general instability of past climate from a 250-kyr ice-core record. *Nature* **364,** 218-220.

De'ath, G. & Fabricius, K. 2010. Water quality as a regional driver of coral biodiversity and macroalgae on the Great Barrier Reef. *Ecological Applications* **20,** 840-850.

De'ath, G., Fabricius, K. E., Sweatman, H. & Puotinen, M. 2012. The 27-year decline of coral cover on the Great Barrier Reef and its causes. *Proceedings of the National Academy of Sciences of the United States of America* **109,** 17995-17999.

Debret, M., Sebag, D., Crosta, X., Massei, N., Petit, J. R., Chapron, E. & Bout-Roumazeilles, V. 2009. Evidence from wavelet analysis for a mid-Holocene transition in global climate forcing. *Quaternary Science Reviews* **28,** 2675-2688.

Donders, T. H., Haberle, S. G., Hope, G., Wagner, F. & Visscher, H. 2007. Pollen evidence for the transition of the Eastern Australian climate system from the post-glacial to the present-day ENSO mode. *Quaternary Science Reviews* **26,** 1621-1637.

Donders, T. H., Wagner-Cremer, F. & Visscher, H. 2008. Integration of proxy data and model scenarios for the mid-Holocene onset of modern ENSO variability. *Quaternary Science Reviews* **27,** 571-579.

Dubinin, A. V. 2004. Geochemistry of Rare Earth Elements in the Ocean. *Lithology and Mineral Resources* **39,** 289-289.

Dullo, W.-C. 2005. Coral growth and reef growth: a brief review. *Facies* **51,** 33-48.

Emile-Geay, J., Cobb, K. M., Carré, M., Braconnot, P., Leloup, J., Zhou, Y., Harrison, S. P., Corrège, T., Mcgregor, H. V., Collins, M., Driscoll, R., Elliot, M., Schneider, B. & Tudhope, A. 2016.

Links between tropical Pacific seasonal, interannual and orbital variability during the Holocene. *Nature Geoscience* **9,** 168.

Engels, M. S., Fletcher, C. H., Field, M., Conger, C. L. & Bochicchio, C. 2008. Demise of reef-flat carbonate accumulation with late Holocene sea-level fall: evidence from Molokai, Hawaii. *Coral Reefs* **27,** 991-996.

Fabricius, K. E. 2005. Effects of terrestrial runoff on the ecology of corals and coral reefs: review and synthesis. *Marine Pollution Bulletin* **50,** 125-146.

Fairbanks, R. G. 1989. A 17,000-year glacio-eustatic sea level record: influence of glacial melting rates on the Younger Dryas event and deep-ocean circulation. *Nature* **342,** 637.

Fallon, S., Wyndham, T., Hendy, E., Lough, J. & Barnes, D. 2003. Coral record of increased sediment flux to the inner Great Barrier Reef since European settlement. *Nature* **421,** 727-730.

Fleitmann, D., Burns, S. J., Mangini, A., Mudelsee, M., Kramers, J., Villa, I., Neff, U., Al-Subbary, A. A., Buettner, A., Hippler, D. & Matter, A. 2007. Holocene ITCZ and Indian monsoon dynamics recorded in stalagmites from Oman and Yemen (Socotra). *Quaternary Science Reviews* **26,** 170-188.

Fleming, K., Johnston, P., Zwartz, D., Yokoyama, Y., Lambeck, K. & Chappell, J. 1998. Refining the eustatic sea-level curve since the Last Glacial Maximum using far- and intermediate-field sites. *Earth and Planetary Science Letters* **163,** 327-342.

Gagan, M. K., Ayliffe, L. K., Hopley, D., Cali, J. A., Mortimer, G. E., Chappell, J., Mcculloch, M. T. & Head, M. J. 1998. Temperature and Surface-Ocean Water Balance of the Mid-Holocene Tropical Western Pacific. *Science* **279,** 1014-1018.

Gagan, M. K., Johnson, D. P. & Crowley, G. M. 1994. Sea level control of stacked late Quaternary coastal sequences, central Great Barrier Reef. *Sedimentology* **41,** 329-351.

Greenstein, B., Curran, H. & Pandolfi, J. 1998. Shifting ecological baselines and the demise of Acropora cervicornis in the western North Atlantic and Caribbean Province: a Pleistocene perspective. *Coral Reefs* **17,** 249-261.

Grinsted, A., Moore, J. C. & Jevrejeva, S. 2004. Application of the cross wavelet transform and wavelet coherence to geophysical time series. *Nonlinear Processes in Geophysics* **11,** 561-566.

Grove, C. A., Zinke, J., Peeters, F., Park, W., Scheufen, T., Kasper, S., Randriamanantsoa, B., Mcculloch, M. T. & Brummer, G. J. A. 2013. Madagascar corals reveal a multidecadal signature of rainfall and river runoff since 1708. *Climate of the Past* **9,** 641-656.

Gu, D. & Philander, S. G. H. 1995. Secular Changes of Annual and Interannual Variability in the Tropics during the Past Century. *Journal of Climate* **8,** 864-876.

Hamanaka, N., Kan, H., Yokoyama, Y., Okamoto, T., Nakashima, Y. & Kawana, T. 2012. Disturbances with hiatuses in high-latitude coral reef growth during the Holocene: Correlation with millennial-scale global climate change. *Global and Planetary Change* **80-81,** 21-35.

Harris, D. L., Webster, J. M., Vila-Concejo, A., Hua, Q., Yokoyama, Y. & Reimer, P. J. 2015. Late Holocene sea-level fall and turn-off of reef flat carbonate production: Rethinking bucket fill and coral reef growth models. *Geology* **43,** 175-178.

Harrison, S. P. & Bartlein, P. 2012. Chapter 14 - Records from the Past, Lessons for the Future: What the Palaeorecord Implies about Mechanisms of Global Change. *In:* Ann, H.-S. & Kendal, M. (eds.) *The Future of the World's Climate (Second Edition)*. Boston: Elsevier.

Haug, G. H., Hughen, K. A., Sigman, D. M., Peterson, L. C. & Röhl, U. 2001. Southward migration of the intertropical convergence zone through the Holocene. *Science (New York, N.Y.)* **293,** 1304-1308.

Hendy, E. J., Gagan, M. K. & Lough, J. 2003. Chronological control of coral records using luminescent lines and evidence for non-stationary ENSO teleconnections in northeast Australia. *The Holocene* **13,** 187-199.

Hongo, C. & Kayanne, H. 2009. Holocene coral reef development under windward and leeward locations at Ishigaki Island, Ryukyu Islands, Japan. *Sedimentary Geology* **214,** 62-73.

Hopley, D. 1975. Contrasting evidence for Holocene sea levels with special reference to the Bowen-Whitsunday area of Queensland. *Douglas, I., I-Iobbs, JE and Pigram, JJ (eds.) Geographical Essays in Honour ofGilbert J Butland, Dept. Geogr., Univ. New England, Armidale* **5,** 1-84.

Hopley, D. 1982. *The geomorphology of the Great Barrier Reef: quaternary development of coral reefs*, New York, Wiley.
Hopley, D. 2006. Fringing and Nearshore Coral Reefs of the Great Barrier Reef: Episodic Holocene Development and Future Prospects. *Journal of Coastal Research* **22,** 175-187.
Hopley, D. & Gill, E. 1972. Holocene sea levels in eastern Australia — A discussion. *Marine Geology* **12,** 223-233.
Hopley, D., Mclean, R. F., Marshall, J. F. & Smith, A. S. 1978. Holocene-Pleistocene boundary in a fringing reef:Hayman Island, North Queensland. *Search* **9,** 323-325.
Horton, B. P., Gibbard, P. L., Mine, G. M., Morley, R. J., Purintavaragul, C. & Stargardt, J. M. 2005. Holocene sea levels and palaeoenvironments, Malay-Thai Peninsula, southeast Asia. *The Holocene* **15,** 1199-1213.
Hughen, K., Lehman, S., Southon, J., Overpeck, J., Marchal, O., Herring, C. & Turnbull, J. 2004. 14C Activity and Global Carbon Cycle Changes over the past 50,000 Years. *Science* **303,** 202-207.
Hughes, T. P., Bellwood, D. R., Baird, A. H., Brodie, J., Bruno, J. F. & Pandolfi, J. M. 2011. Shifting base-lines, declining coral cover, and the erosion of reef resilience: comment on Sweatman et al. (2011). *Coral Reefs* **30,** 653-660.
Hughes, T. P., Day, J. C. & Brodie, J. 2015. Securing the future of the Great Barrier Reef. *Nature Climate Change* **5,** 508-511.
Isdale, P. 1984. Fluorescent bands in massive corals record centuries of coastal rainfall. *Nature* **310,** 578-579.
Isdale, P. J., Stewart, B. J., Tickle, K. S. & Lough, J. M. 1998. Palaeohydrological variation in a tropical river catchment: a reconstruction using fluorescent bands in corals of the Great Barrier Reef, Australia. *The Holocene* **8,** 1-8.
Jupiter, S., Roff, G., Marion, G., Henderson, M., Schrameyer, V., Mcculloch, M. & Hoegh-Guldberg, O. 2008. Linkages between coral assemblages and coral proxies of terrestrial exposure along a cross-shelf gradient on the southern Great Barrier Reef. *Coral Reefs* **27,** 887-903.
Karumuri, A., Tam, C. Y. & Lee, W. J. 2009. ENSO Modoki impact on the Southern Hemisphere storm track activity during extended austral winter. *Geophysical Research Letters* **36,** L12705.
Kershaw, A. P. 1983. A Holocene Pollen Diagram from Lynch's Crater, North-Eastern Queensland, Australia. *New Phytologist* **94,** 669-682.
King, A. D., Klingaman, N. P., Alexander, L. V., Donat, M. G., Jourdain, N. C. & Maher, P. 2014. Extreme Rainfall Variability in Australia: Patterns, Drivers, and Predictability. *Journal of Climate* **27,** 6035.
Kleypas, J. A. & Hopley, D. Reef Development Across a Broad Continental Shelf, Southern Great Barrier Reef, Australia. *In:* Richmond, R. H., ed. Seventh International Coral Reef Symposium, 1992 Guam. University of Guam Press, 1129-1141.
Klingaman, N. P., Woolnough, S. J. & Syktus, J. 2013. On the drivers of inter-annual and decadal rainfall variability in Queensland, Australia. *International Journal of Climatology* **33,** 2413-2430.
Knowlton, N. & Jackson, J. B. C. 2008. Shifting Baselines, Local Impacts, and Global Change on Coral Reefs. *PLoS Biol* **6,** e54.
Knutson, D. W., Buddemeier, R. W. & Smith, S. V. 1972. Coral chronometers: Seasonal growth bands in reef corals. *Science* **177,** 270-272.
Kroon, F. J., Kuhnert, P. M., Henderson, B. L., Wilkinson, S. N., Kinsey-Henderson, A., Abbott, B., Brodie, J. E. & Turner, R. D. R. 2012. River loads of suspended solids, nitrogen, phosphorus and herbicides delivered to the Great Barrier Reef lagoon. *Marine Pollution Bulletin* **65,** 167-181.
Lambeck, K. 2002. Sea level change from mid Holocene to recent time: an Australian example with global implications. *Geodynamics Series* **29,** 33-50.
Lambeck, K. & Nakada, M. 1990. Late Pleistocene and Holocene sea-level change along the Australian coast. *Palaeogeography, Palaeoclimatology, Palaeoecology (Global and Planetary Change Section)* **89,** 143-176.

Lambeck, K., Rouby, H., Purcell, A., Sun, Y. & Sambridge, M. 2014. Sea level and global ice volumes from the Last Glacial Maximum to the Holocene. *Proceedings of the National Academy of Sciences* **111,** 15296-15303.

Larcombe, P., Costen, A. & Woolfe, K. J. 2001. The hydrodynamic and sedimentary setting of nearshore coral reefs, central Great Barrier Reef shelf, Australia: Paluma Shoals, a case study. *Sedimentology* **48,** 811-835.

Larcombe, P. & Woolfe, K. J. 1999. Terrigenous sediments as influences upon Holocene nearshore coral reefs, central Great Barrier Reef, Australia. *Australian Journal of Earth Sciences* **46,** 141-154.

Lau, K.-M. & Weng, H. 1995. Climate Signal Detection Using Wavelet Transform: How to Make a Time Series Sing. *Bulletin of the American Meteorological Society* **76,** 2391-2402.

Lawrence, K. 2010. Social and economic profile of the Great Barrier Reef catchment 2009. Townsville, Qld.: Great Barrier Reef Marine Park Authority.

Lewis, S. E., Shields, G. A., Kamber, B. S. & Lough, J. M. 2007. A multi-trace element coral record of land-use changes in the Burdekin River catchment, NE Australia. *Palaeogeography, Palaeoclimatology, Palaeoecology* **246,** 471-487.

Lewis, S. E., Sloss, C. R., Murray-Wallace, C. V., Woodroffe, C. D. & Smithers, S. G. 2013. Post-glacial sea-level changes around the Australian margin: a review. *Quaternary Science Reviews* **74,** 115-138.

Lewis, S. E., Wu, R. a. J., Webster, J. M. & Shields, G. A. 2008. Mid-late Holocene sea-level variability in eastern Australia. *Terra Nova* **20,** 74-81.

Lewis, S. E., Wüst, R. a. J., Webster, J. M., Collins, J., Wright, S. A. & Jacobsen, G. 2015. Rapid relative sea-level fall along north-eastern Australia between 1200 and 800 cal. yr BP: An appraisal of the oyster evidence. *Marine Geology* **370,** 20-30.

Lough, J., Barnes, D. & Mcallister, F. 2002. Luminescent lines in corals from the Great Barrier Reef provide spatial and temporal records of reefs affected by land runoff. *Coral Reefs* **21,** 333-343.

Lough, J. M. 1991. Rainfall variations in Queensland, Australia: 1891–1986. *International Journal of Climatology* **11,** 745-768.

Lough, J. M. 2007. Tropical river flow and rainfall reconstructions from coral luminescence: Great Barrier Reef, Australia. *Paleoceanography* **22**.

Lough, J. M. 2011a. Great Barrier Reef coral luminescence reveals rainfall variability over northeastern Australia since the 17th century. *Paleoceanography* **26**.

Lough, J. M. 2011b. Measured coral luminescence as a freshwater proxy: comparison with visual indices and a potential age artefact. *Coral Reefs* **30,** 169-182.

Lough, J. M. & Barnes, D. J. 1997. Several centuries of variation in skeletal extension, density and calcification in massive Porites colonies from the Great Barrier Reef: A proxy for seawater temperature and a background of variability against which to identify unnatural change. *Journal of experimental marine biology and ecology* **211,** 29-67.

Lough, J. M., Lewis, S. E. & Cantin, N. E. 2015. Freshwater impacts in the central Great Barrier Reef: 1648–2011. *Coral Reefs* **34,** 739-751.

Lough, J. M., Llewellyn, L. E., Lewis, S. E., Turney, C. S. M., Palmer, J. G., Cook, C. G. & Hogg, A. G. 2014. Evidence for suppressed mid-Holocene northeastern Australian monsoon variability from coral luminescence. *Paleoceanography* **29,** 581-594.

Maslin, M., Stickley, C. & Ettwein, V. 2001. Holocene Climate Variability. *In:* Editors-in-Chief: john, H. S., Karl, K. T. & Steve, A. T. (eds.) *Encyclopedia of Ocean Sciences (Second Edition).* Oxford: Academic Press.

Mayewski, P. A., Holmgren, K., Lee-Thorp, J., Rosqvist, G., Rack, F., Staubwasser, M., Schneider, R. R., Steig, E. J., Rohling, E. E., Curt Stager, J., Karlén, W., Maasch, K. A., David Meeker, L., Meyerson, E. A., Gasse, F. & Van Kreveld, S. 2004. Holocene climate variability. *Quaternary Research* **62,** 243-255.

Mcculloch, M., Fallon, S., Wyndham, T., Hendy, E., Lough, J. & Barnes, D. 2003. Coral record of increased sediment flux to the inner Great Barrier Reef since European settlement. *Nature* **421,** 727-730.

Mcculloch, M. T. & Mortimer, G. E. 2008. Applications of the 238U–230Th decay series to dating of fossil and modern corals using MC-ICPMS. *Australian Journal of Earth Sciences* **55,** 955-965.

Mcgregor, H. V., Fischer, M. J., Gagan, M. K., Fink, D., Phipps, S. J., Wong, H. & Woodroffe, C. D. 2013. A weak El Niño/Southern Oscillation with delayed seasonal growth around 4,300 years ago. *Nature Geoscience* **6,** 949-953.

Mcgregor, H. V. & Gagan, M. K. 2004. Western Pacific coral $\delta^{18}O$ records of anomalous Holocene variability in the El-Nino-Southern Oscillation. *Geophysical Research Letters* **31,** 1-4.

Mcgregor, H. V., Gagan, M. K., Mcculloch, M. T., Hodge, E. & Mortimer, G. 2008. Mid-Holocene variability in the marine 14C reservoir age for northern coastal Papua New Guinea. *Quaternary Geochronology* **3,** 213-225.

Mclean, R. & Woodroffe, C. 1990. Microatolls and recent sea level change on coral atolls. *Nature* **344,** 531-534.

Mclean, R. F., Stoddart, D. R., Hopley, D. & Polach, H. 1978. Sea Level Change in the Holocene on the Northern Great Barrier Reef. *Philosophical Transactions of the Royal Society of London. Series A, Mathematical and Physical Sciences* **291,** 167-186.

Meinke, H., Devoil, P., Hammer, G. L., Power, S., Allan, R., Stone, R. C., Folland, C. & Potgieter, A. 2005. Rainfall Variability at Decadal and Longer Time Scales: Signal or Noise? *Journal of Climate* **18,** 89-96.

Meltzner, A. J. & Woodroffe, C. D. 2015. Coral microatolls. *Handbook of Sea-Level Research.* John Wiley & Sons, Ltd.

Miller, J., Muller, E., Rogers, C., Waara, R., Atkinson, A., Whelan, K., Patterson, M. & Witcher, B. 2009. Coral disease following massive bleaching in 2005 causes 60% decline in coral cover on reefs in the US Virgin Islands. *Coral Reefs* **28,** 925-937.

Milne, G. A. & Mitrovica, J. X. 2008. Searching for eustasy in deglacial sea-level histories. *Quaternary Science Reviews* **27,** 2292-2302.

Mitrovica, J. X. & Milne, G. A. 2002. On the origin of late Holocene sea-level highstands within equatorial ocean basins. *Quaternary Science Reviews* **21,** 2179-2190.

Mitrovica, J. X. & Peltier, W. R. 1991. On Postglacial Geoid Subsidence Over the Equatorial Oceans. *Journal of Geophysical Research* **96,** 20053-20071.

Montaggioni, L. F. 2005. History of Indo-Pacific coral reef systems since the last glaciation: Development patterns and controlling factors. *Earth Science Reviews* **71,** 1-75.

Montaggioni, L. F. & Braithwaite, C. J. R. 2009. Chapter One Introduction: Quaternary Reefs in Time and Space. *In:* Montaggioni, L. F. & Braithwaite, C. J. R. (eds.) *Developments in Marine Geology*. Elsevier.

Morlet, J., Arens, G., Fourgeau, E. & Giard, D. 1982a. Wave Propagation and Sampling Theory-Part 1: Complex Signal and Scattering in Multilayered Media. *Geophysics* **47,** 203-221.

Morlet, J., Arens, G., Fourgeau, E. & Giard, D. 1982b. Wave propagation and sampling Theory - Part II: Sampling theory and complex waves. *Geophysics* **47,** 222-236.

Moy, C. M., Anderson, D. M., Seltzer, G. O. & Rodbell, D. T. 2002. Variability of El Niño/Southern Oscillation activity at millennial timescales during the Holocene epoch. *Nature* **420,** 162-165.

Murray-Wallace, C. V. & Woodroffe, C. D. 2014. Quaternary sea-level changes: a global perspective. Cambridge;New York;: Cambridge University Press.

Nakada, M. & Lambeck, K. 1989. Late Pleistocene and Holocene sea-level change in the Australian region and mantle rheology. *Geophysical Journal International* **96,** 497-517.

Nakken, M. 1999. Wavelet analysis of rainfall–runoff variability isolating climatic from anthropogenic patterns. *Environmental Modelling and Software* **14,** 283-295.

Neil, D. T., Orpin, A. R., Ridd, P. V. & Yu, B. 2002. Sediment yield and impacts from river catchments to the Great Barrier Reef lagoon.

Neumann, A. C. & Macintyre, I. G. Reef response to sea level rise: keep-up, catch up or give-up. *In:* Proc. 5th Int Coral Reef Congr, 1985 Tahiti. 105-110.

Pandolfi, J. M. 2011. The Paleoecology of Coral Reefs. Dordrecht: Springer Netherlands.

Pandolfi, J. M. 2015. Incorporating Uncertainty in Predicting the Future Response of Coral Reefs to Climate Change. *Annual Review of Ecology, Evolution, and Systematics* **46,** 281-303.

Pandolfi, J. M., Bradbury, R. H., Sala, E., Hughes, T. P., Bjorndal, K. A., Cooke, R. G., Mcardle, D., Mcclenachan, L., Newman, M. J. H., Paredes, G., Warner, R. R. & Jackson, J. B. C. 2003. Global Trajectories of the Long-Term Decline of Coral Reef Ecosystems. *Science* **301,** 955-958.

Pauly, D. 1995. Anecdotes and the shifting baseline syndrome of fisheries. *Trends in Ecology and Evolution* **10,** 430.

Perry, C. & Smithers, S. 2011. Cycles of coral reef 'turn-on', rapid growth and 'turn-off' over the past 8500 years: a context for understanding modern ecological states and trajectories. *Global Change Biology* **17,** 76-86.

Petit, J.-R., Jouzel, J., Raynaud, D., Barkov, N. I., Barnola, J.-M., Basile, I., Bender, M., Chappellaz, J., Davis, M. & Delaygue, G. 1999. Climate and atmospheric history of the past 420,000 years from the Vostok ice core, Antarctica. *Nature* **399,** 429-436.

Pirazzoli, P. A. & Pluet, J. 1991. *World atlas of Holocene sea-level changes*, Amsterdam ; New York, Elsevier.

Power, S., Casey, T., Folland, C., Colman, A. & Mehta, V. 1999. Inter-decadal modulation of the impact of ENSO on Australia. *Climate Dynamics* **15,** 319-324.

Power, S., Haylock, M., Colman, R. & Wang, X. 2006. The predictability of interdecadal changes in ENSO activity and ENSO teleconnections. *Journal of Climate* **19,** 4755-4771.

Redondo-Rodriguez, A., Weeks, S. J., Berkelmans, R., Hoegh-Guldberg, O. & Lough, J. M. 2012. Climate variability of the Great Barrier Reef in relation to the tropical Pacific and El Niño-Southern Oscillation. *Marine and Freshwater Research* **63,** 34.

Risk, M. J. & Edinger, E. 2011. Encyclopedia of modern coral reefs: structure, form and process. *In:* Hopley, D. (ed.). Dordrecht: Springer.

Roche, R. C., Perry, C. T., Smithers, S. G., Leng, M. J., Grove, C. A., Sloane, H. J. & Unsworth, C. E. 2014. Mid-Holocene sea surface conditions and riverine influence on the inshore Great Barrier Reef. *The Holocene* **24,** 885-897.

Rodo, X. & Rodriguez-Arias, M.-A. 2004. El Nino-Southern Oscillation: Absent in the Early Holocene? *Journal of Climate* **17,** 423-426.

Rodriguez-Ramirez, A., Grove, C. A., Zinke, J., Pandolfi, J. M. & Zhao, J.-X. 2014. Coral Luminescence Identifies the Pacific Decadal Oscillation as a Primary Driver of River Runoff Variability Impacting the Southern Great Barrier Reef. *PloS one* **9,** e84305.

Roff, G., Clark, T. R., Reymond, C. E., Zhao, J.-X., Feng, Y., Mccook, L. J., Done, T. J. & Pandolfi, J. M. 2013. Palaeoecological evidence of a historical collapse of corals at Pelorus Island, inshore Great Barrier Reef, following European settlement. *Proceedings. Biological sciences / The Royal Society* **280**.

Rooney, J., Fletcher, C., Grossman, E., Engels, M. & Field, M. 2004. El Nino Influence on Holocene Reef Accretion in Hawai'i1. *Pacific Science* **58,** 305.

Rovere, A., Stocchi, P. & Vacchi, M. 2016. Eustatic and Relative Sea Level Changes. *Current Climate Change Reports,* 1-11.

Sang-Ik, S., Prashant, D. S., Robert, S. W., Robert, J. O. & Joseph, J. B. 2006. Understanding the Mid-Holocene Climate. *Journal of Climate* **19,** 2801.

Scoffin, T. P., Stoddart, D. R. & Rosen, B. R. 1978. The Nature and Significance of Microatolls. *Philosophical Transactions of the Royal Society of London. Series B, Biological Sciences* **284,** 99-122.

Shen, C.-C., Fan, T.-Y., Meltzner, A. J., Taylor, F. W., Quinn, T. M., Chiang, H.-W., Kilbourne, K. H., Li, K.-S., Sieh, K., Natawidjaja, D., Cheng, H., Wang, X., Edwards, R. L., Lam, D. D. & Hsieh, Y.-T. 2008. Variation of initial 230Th/ 232Th and limits of high precision U–Th dating of shallow-water corals. *Geochimica et Cosmochimica Acta* **72,** 4201-4223.

Shen, G. T. & Sanford, C. L. 1990. Trace element indicators of climate variability in reef-building corals. *Global ecological consequences of the 1982-83 El Nino-Southern Oscillation,* 255-283.

Sholkovitz, E. & Shen, G. T. 1995. The incorporation of rare earth elements in modern coral. *Geochimica et Cosmochimica Acta* **59,** 2749-2756.

Shulmeister, J. & Lees, B. G. 1995. Pollen evidence from tropical Australia for the onset of an ENSO-dominated climate at c. 4000 BP. *The Holocene* **5,** 10-18.

Sinclair, D. J., Kinsley, L. P. J. & Mcculloch, M. T. 1998. High resolution analysis of trace elements in corals by laser ablation ICP-MS. *Geochimica et Cosmochimica Acta* **62,** 1889-1901.

Sloss, C. R., Murray-Wallace, C. V. & Jones, B. G. 2007. Holocene sea-level change on the southeast coast of Australia: a review. *The Holocene* **17,** 999.

Smithers, S. G., Hopley, D. & Parnell, K. E. 2006. Fringing and Nearshore Coral Reefs of the Great Barrier Reef: Episodic Holocene Development and Future Prospects. *Journal of Coastal Research,* 175-187.

Soon, W., Velasco Herrera, V. M., Selvaraj, K., Traversi, R., Usoskin, I., Chen, C.-T. A., Lou, J.-Y., Kao, S.-J., Carter, R. M., Pipin, V., Severi, M. & Becagli, S. 2014. A review of Holocene solar-linked climatic variation on centennial to millennial timescales: Physical processes, interpretative frameworks and a new multiple cross-wavelet transform algorithm. *Earth-Science Reviews* **134,** 1-15.

Steig, E. J. 1999. Mid-Holocene Climate Change. *Science* **286,** 1485-1487.

Stoddart, D. R., Mclean, R. F., Scoffin, T. P., Thom, B. G. & Hopley, D. 1978. Evolution of Reefs and Islands, Northern Great Barrier Reef: Synthesis and Interpretation. *Philosophical Transactions of the Royal Society of London. Series B, Biological Sciences* **284,** 149-159.

Stoddart, D. R. & Scoffin, T. P. 1979. Microatolls: Review of Form, Origin and Terminology. *Atoll Research Bulletin* **No. 224,** 1-17.

Susic, M., Boto, K. & Isdale, P. 1991. Fluorescent humic acid bands in coral skeletons originate from terrestrial runoff. *Marine Chemistry* **33,** 91-104.

Switzer, A., Sloss, C. R., Jones, B. G. & Bristow, C. 2010. Geomorphic evidence for mid-late Holocene higher sea level from southeastern Australia. *Quaternary International* **221,** 13-22.

Torrence, C. & Compo, G. P. 1998. A practical guide to wavelet analysis. *Bulletin of the American Meteorological Society* **79,** 61-78.

Toth, L. T., Macintyre, I. G., Aronson, R. B., Vollmer, S. V., Hobbs, J. W., Urrego, D. H., Cheng, H., Enochs, I. C., Combosch, D. J. & Van Woesik, R. 2012. ENSO drove 2500-year collapse of eastern Pacific coral reefs. *Science (New York, N.Y.)* **337,** 81.

Tudhope, A. W., Chilcott, C. P., Mcculloch, M. T., Cook, E. R., Chappell, J., Ellam, R. M., Lea, D. W., Lough, J. M. & Shimmield, G. B. 2001. Variability in the El Niño-Southern Oscillation through a glacial-interglacial cycle. *Science (New York, N.Y.)* **291,** 1511-1517.

Twiggs, E. J. & Collins, L. B. 2010. Development and demise of a fringing coral reef during Holocene environmental change, eastern Ningaloo Reef, Western Australia. *Marine Geology* **275,** 20-36.

Uthicke, S., Patel, F. & Ditchburn, R. 2012. Elevated land runoff after European settlement perturbs persistent foraminiferal assemblages on the Great Barrier Reef. *Ecology* **93,** 111-121.

Verdon, D. C. & Franks, S. W. 2006. Long-term behaviour of ENSO: Interactions with the PDO over the past 400 years inferred from paleoclimate records. *Geophysical Research Letters* **33,** L06712.

Verdon, D. C., Wyatt, A. M., Kiem, A. S. & Franks, S. W. 2004. Multidecadal variability of rainfall and streamflow: Eastern Australia. *Water Resources Research* **40,** W10201.

Veron, J. E. N. 1995. *Corals in space and time: the biogeography and evolution of the Scleractinia,* Ithaca, Comstock/Cornell.

Walther, B. D., Kingsford, M. J. & Mcculloch, M. T. 2013. Environmental Records from Great Barrier Reef Corals: Inshore versus Offshore Drivers. *PloS one* **8,** e77091.

Wanner, H., Beer, J., Bütikofer, J., Crowley, T. J., Cubasch, U., Flückiger, J., Goosse, H., Grosjean, M., Joos, F., Kaplan, J. O., Küttel, M., Müller, S. A., Prentice, I. C., Solomina, O., Stocker, T. F., Tarasov, P., Wagner, M. & Widmann, M. 2008. Mid- to Late Holocene climate change: an overview. *Quaternary Science Reviews* **27,** 1791-1828.

Wanner, H., Solomina, O., Grosjean, M., Ritz, S. P. & Jetel, M. 2011. Structure and origin of Holocene cold events. *Quaternary Science Reviews* **30,** 3109-3123.

Woodroffe, C. D., Beech, M. R. & Gagan, M. K. 2003. Mid-late Holocene El Niño variability in the equatorial Pacific from coral microatolls. *Geophysical Research Letters* **30,** 1358.

Woodroffe, C. D. & Horton, B. P. 2005. Holocene sea-level changes in the Indo-Pacific. *Journal of Asian Earth Sciences* **25,** 29-43.

Woodroffe, C. D., Kennedy, D. M., Hopley, D., Rasmussen, C. E. & Smithers, S. G. 2000. Holocene reef growth in Torres Strait. *Marine Geology* **170,** 331-346.

Wooldridge, S. A. 2009. Water quality and coral bleaching thresholds: Formalising the linkage for the inshore reefs of the Great Barrier Reef, Australia. *Marine Pollution Bulletin* **58,** 745-751.

Wyndham, T., Mcculloch, M., Fallon, S. & Alibert, C. 2004. High-resolution coral records of rare earth elements in coastal seawater: biogeochemical cycling and a new environmental proxy. *Geochimica et Cosmochimica Acta* **68,** 2067-2080.

Xu, J., Kuhnt, W., Holbourn, A., Regenberg, M. & Andersen, N. 2010. Indo-Pacific Warm Pool variability during the Holocene and Last Glacial Maximum. *Paleoceanography* **25,** PA4230.

Yu, K.-F. & Zhao, J.-X. 2010. U-series dates of Great Barrier Reef corals suggest at least +0.7m sea level ~7000 years ago. *The Holocene* **20,** 161-168.

Yu, K., Hua, Q., Zhao, J.-X., Hodge, E., Fink, D. & Barbetti, M. 2010. Holocene marine 14C reservoir age variability: Evidence from 230Th-dated corals in the South China Sea. *Paleoceanography* **25**.

Zachariasen, J., Sieh, K., Taylor, F. W., Edwards, L. & Hantoro, W. S. 1999. Submergence and uplift associated with the giant 1833 Sumatran subduction earthquake: Evidence from coral microatolls. *Journal of Geophysical Research: Solid Earth* **104,** 895-919.

Zhang, Z., Leduc, G. & Sachs, J. P. 2014. El Nino evolution during the Holocene revealed by a biomarker rain gauge in the Galapagos Islands. *Earth and Planetary Science Letters* **404,** 420.

Chapter 2

Holocene sea level instability in the southern Great Barrier Reef, Australia: high-precision U-Th dating of fossil microatolls

Nicole D Leonard[1,2], Zhao, J-x.[1,2], Welsh, K.J.[1], Feng, Y-x[1,2], Smithers, S.G.[3], Pandolfi, J.M.[4], Clark, T.R[1,2].

1. School of Earth Sciences, The University of Queensland; St Lucia, Queensland, 4072.

2. Radiogenic Isotope Facility, The University of Queensland; St Lucia, Queensland, 4072.

3. School of Earth and Environmental Sciences, James Cook University; Townsville, Queensland, 4811.

4. Australian Research Council Centre of Excellence for Coral Reef Studies, Centre for Marine Science, School of Biological Sciences, The University of Queensland, Brisbane, Queensland 4072.

Published: Coral Reefs (2016) 35: 625

Keywords: Sea level; Holocene; Great Barrier Reef; microatoll; uranium-thorium; reef hiatus

Abstract

Three emergent sub-fossil reef flats from the inshore Keppel Islands, Great Barrier Reef (GBR), Australia, were used to reconstruct relative sea level (RSL). Forty-two high-precision uranium-thorium (U-Th) dates obtained from coral microatolls and non-microatoll colonies (2σ age errors from ± 8 to 37 years) in conjunction with elevation surveys provide evidence in support of a non-linear RSL regression throughout the Holocene. Results show that RSL was as least 0.75 m above present from ~6,500 – 5,500 years before present (yr. BP; before 1950). Following this highstand, two sites indicate a coeval lowering of RSL of at least 0.4 m from 5,500 – 5,300 yr. BP which was maintained for ~200 years. After the lowstand, RSL returns to higher levels before a 2,000 year hiatus in reef flat corals after 4,600 yr. BP at all three sites. A second possible RSL lowering event of ~0.3 m from ~2,800 –1,600 yr. BP is then detected before RSL stabilises ~0.2 m above present levels by 900 yr. BP. Whilst the mechanism of the RSL instability is still uncertain, the alignment with previously reported RSL oscillations, rapid global climate changes and mid-Holocene reef "turn-off" on the GBR are discussed.

Introduction

It is indisputable that coral reefs are under increasing pressure from anthropogenic influence globally (Pandolfi et al., 2003, Veron et al., 2009, Muthukrishnan and Fong, 2014). Nevertheless, natural processes have equally affected reef development throughout geological history, and worldwide coral reefs have suffered significant disturbances and hiatuses prior to anthropogenic influence (Buddemeier and Hopley, 1988, Hughes and Connell, 1999, Smithers et al., 2006, Perry and Smithers, 2011, Hamanaka et al., 2012, Toth et al., 2012). Determining the driving mechanisms of previous reef disturbance events is not only vital to interpreting Holocene reef histories, but allows for improved understanding of the future trajectory of reefs under changing climatic and environmental conditions.

Eustatic sea level (ESL) transgressive/regressive cycles are one of the primary controls of coral reef expansion/contraction throughout the Quaternary (Kennedy and Woodroffe, 2002, Hopley et al., 2007). Where ESL is dominated by changes in ice sheet volume and global steric variations, relative sea level (RSL) at any given coastline is governed by ESL contributions, as well as regional glacio-hydro-isostatic and tectonic effects (Lambeck and Nakada, 1990, Lambeck, 1993, Lambeck et al., 2014), water redistribution (Mitrovica and Milne, 2002) and climate (Hamanaka et al., 2012). At near-field sites (i.e. close to former icesheets and melt water) glacio-isostatic influence on RSL is dominant, however at far-field locations (distant from major ice accumulations) RSL at centennial to millennial timescales is mainly controlled by hydro-isostasy, equatorial ocean syphoning and steric effects which can produce significant spatial and temporal variability over just a few hundred kilometres (Lambeck and Nakada, 1990, Mitrovica and Milne, 2002).

Geophysical modelling of the regional response to glacio-hydro-isostatic processes has resulted in the identification of distinct zones of globally predicted RSL throughout the Holocene (Clark et al., 1978, Pirazzoli and Pluet, 1991). The islands and reefs of the inshore Great Barrier Reef (GBR), proximal to the mainland Queensland coast are characterised by a rapidly rising RSL from the early to mid-Holocene, culminating in a RSL highstand of +1 to +3 m by ~5,000 years before present after which significant meltwater contribution from the large northern hemisphere icesheets ceased (Clark et al., 1978, Nakada and Lambeck, 1989). Evidence of this highstand along the Australian east coast (AEC) between 7,000 – 5,000 years before present (yr. B.P; where present is 1950) is widespread and widely accepted (McLean et al., 1978, Hopley, 1980, Chappell et al., 1982, Chappell, 1983, Woodroffe et al.,

2000, Lewis et al., 2008, Yu and Zhao, 2010b, Leonard et al., 2013), although the magnitude and precise timing of the highstand is yet to be unequivocally refined (see Lewis et al., 2008 and , Lewis et al., 2013 for comprehensive reviews of Australian sea level throughout the Holocene).

Inshore reef development on the GBR reflects the rapid early to mid-Holocene RSL rise with coral initiation following inundation of the shallow Pleistocene shelf from ~8,500 yr. BP, followed by rapid reef accretion in either "catch up" or "keep up" modes of growth until ~5,500 yr. BP (Neumann and Macintyre, 1985, Kleypas and Hopley, 1992, Smithers et al., 2006, Perry and Smithers, 2011, Camoin and Webster, 2015). After ~5,500cal yr. BP however, both RSL and reef growth histories become increasingly ambiguous. Whether RSL regressed smoothly (Chappell, 1983) or oscillated/stepped down (Baker and Haworth, 2000, Baker, 2001, Lewis et al., 2008) on the AEC following the mid-Holocene highstand has been a contentious issue for over four decades. Indeed, different statistical treatments of the same sea level (SL) data suggests either regression mode to be equally likely (Woodroffe, 2009). At the same time, stratigraphic hiatuses in coral reef cores and a lack of reef initiation in the northern and southern inshore GBR have been documented from 5,500 – 2,800 yr. BP, suggestive of significant environmental change at this time, yet this hiatus is not detected in the central GBR (Perry and Smithers, 2011). Perry and Smithers (2011) proposed that a reduction in vertical accommodation space due to a slowly falling RSL in synergy with changes to environmental conditions at inshore locations (e.g. temperature, rainfall and shore progradation) limited significant reef aggradation/progradation in the mid-Holocene. However, such a synchronous and broad-scale response is suggestive of either a more abrupt change in RSL than currently proposed for the GBR (Chappell, 1983), or that rapid and wide scale climatic and environmental change was the primary driver of reef "turn-off" (Buddemeier and Hopley, 1988).

Whilst rapid changes or oscillations of RSL during the Holocene have been proposed for the AEC, they are most often dismissed as artefacts of the proxies used and uncertainties of age-error calculations (Perry and Smithers, 2011). In order to obtain a temporally continuous record it is often necessary to incorporate dissimilar SL indicators, or SL indicators from large latitudinal ranges, into a single interpretation potentially obscuring subtle variations (Chappell, 1983, Sloss et al., 2007, Lewis et al., 2008, Lewis et al., 2013). Additionally, directly comparing or combining data from separate studies is problematic as: a) the reference datum and the absolute elevation of the indicators being used may differ; b)

inconsistent methods between studies are used to establish elevation and age; c) large age errors may be associated with dating techniques [e.g. for ^{14}C dating, substantial age errors up to ± 500 years may be introduced if temporal changes in atmospheric production rates as well as global and regional marine ^{14}C reservoir effects are taken into consideration (McGregor et al., 2008, Yu et al., 2010, Hua et al., 2015)]; and d) the environmental context of the indicators is critically important but is often difficult to interpret and commonly not reported.

The primary objective of this study was to determine whether low magnitude RSL instability could be detected using highly precise U-Th dating techniques of coral microatolls from multiple sites in a tectonically stable far-field region. In addition, we also obtained samples of non-microatolls to relate dated microatolls to reef flat development at their time of growth. This sampling regime allowed for both intra- and inter-site comparisons of equivalent data, thereby increasing the confidence in the absolute RSL signal versus single reef geomorphological effects. This study is the first comprehensive evaluation of Holocene RSL and reef flat history in the Keppel Islands, a region for which data has been notably absent (Hopley et al., 2007, Lewis et al., 2013).

Materials and Methods

Regional Setting

The Keppel Islands are a group of continental islands located on the inner shelf of the southern GBR, Queensland, Australia (23˚10'S, 150˚59'E; Fig. 1). The islands are located in a macro tidal setting with a maximum tidal range of ~5 m. The region experiences a seasonally dry tropical climate in which most (on average 60%) of the rainfall typically occurs in the short wet season between December and March (B.O.M., 2011). Inter-annual variability is also high, with long dry periods often followed by episodic high flow rainfall events associated with tropical cyclones or monsoonal lows (Douglas et al., 2006, Brooke et al., 2008) which are modulated by complex interactions of the El Niño Southern Oscillation (ENSO) and Pacific Decadal Oscillation (Rodriguez-Ramirez et al., 2014). Due to frequent disturbance events (e.g. cyclones flood plumes) the modern Keppel Islands reefs are dominated by fast growing arborescent *Acropora* sp. (see Supp. 1). Although it has been suggested that in the Holocene suspended sediment loads from flood events were likely to be relatively high due to naturally sparse vegetative cover, no data are currently available for Holocene reef development or environmental conditions in this region (Douglas et al., 2006).

Three islands with evident emergent reef flats containing fossil corals and microatolls in growth position were visited from the 19th to 23rd June 2013 at low tide: North Keppel Island (NKI), Great Keppel Island (GKI) and Humpy Island (HI; Fig. 1). All sites displayed seaward sloping reef flats with no evidence of significant reef rims present. Microatolls of various sizes (diameter range 40 cm to 250 cm; Fig. 2; Table 1) were targeted to allow for the detection of possible shorter phases of RSL instability that may not be recognised if only the largest microatolls were sampled. Microatolls were elevated up to 0.4 m above the fossil reef flat substrate that was either overlain by thick unconsolidated mixed siliciclastic/carbonate sediments (Fig. 2a) or infilled with authogenic carbonate sands (Fig. 2d). At HI (microatolls n=12; non-microatolls n=10) and GKI (microatolls n=8), elevations were taken using a Magnum-Proshot 4.7 Laser Level and Apache Lightning 2 receiver and referenced against replicate timed-still tide levels. Due to limited time to access the reef flat at low tide at NKI, microatolls (n=13) were measured directly against still water level within groups that had elevation differences <5 cm. All elevations were determined using tide gauge data from Rosslyn Bay (Station-024011A; Fig. 1) provided by Maritime Safety Queensland (MSQ) and reduced to metres relative to present which we defined as the height above local mean low water spring tide (MLWS; 0.76 metres above lowest astronomical tide for the Keppel Islands); the level to which microatolls are constrained by the air-sea interface (Scoffin et al., 1978, Smithers and Woodroffe, 2000, Murray-Wallace and Woodroffe, 2014).

Even though conditions were calm on all days (<5 kt winds; mean sea-level pressure (MSLP) ~1,000 hPa), we acknowledge that measuring the absolute elevation of microatolls by referencing to timed-still tide levels is imprecise, mainly related to possible time lags between tide gauge location (Rosslyn Bay) and our sites. Although the difference in tide time in the Keppel Islands is only ± 5 minutes from the mainland (which was taken into consideration when calculating heights), so as not to underestimate errors associated with our methodology we calculated the propagated error terms of both the tide heights within a half hour period of our sea level tie points (<0.1 m) and the replicate tie points (<0.05 m) giving an error term of 0.11 m. We therefore assigned a conservative error of ±15 cm to our measurements to incorporate both sources of potential error associated with tide measurements. It must be noted however, that the error of the relative position of each coral sample to each other within each site is minimal and is a function of the laser level (accuracy of ± 1.0 mm/30 m; HI and GKI) or relative position to each other (< 0.05 m; NKI).

Samples of coral were collected with a hammer and chisel from the centre of each coral microatoll where the elevation and diameter were recorded (Table 1). The flat, upper surface of the centre of the coral microatoll where the corallites were observed to radiate (Fig. 2c) represents the surface of the colony that was originally constrained be the air-sea interface, and was used to justify our sampling strategy. Samples were also taken from the centre of non-microatoll fossil colonies (i.e. *in situ* remnant robust branching colonies and massive corals with no radial corallites) at HI (n=10) to determine the timing of reef flat development. Personal observations and previous dating trials have revealed that the centres of microatolls and corals are generally less prone to bio-erosion and detrital inclusions allowing for more precise U-Th age determinations.

Uranium-thorium dating

Samples were prepared for U-Th dating by Multi-Collector Inductively Coupled Mass Spectrometry (MC-ICP-MS) at the Radiogenic Isotope Facility, the University of Queensland, using methods described in Clark et al. (2012, 2014b) and Leonard et al. (2013). Full laboratory methods are described in detail in Supplementary 2 of the present paper. Samples of coeval material with different levels of cleaning protocol were measured for age validation of replicate samples and to determine local detrital $^{230}Th/^{232}Th$ ratios using $^{230}Th/^{232}Th$-$^{238}U/^{232}Th$ isochrons (Supp. Fig. 3.1). Sample ages were calculated using the decay constants of Cheng et al. (2000) using Isoplot/Ex software (Ludwig, 2003) and corrected for initial/detrital ^{230}Th using a two-component mixing correction scheme described by Clark et al. (2014a) using $^{230}Th/^{232}Th_{hyd}$ and $^{230}Th/^{232}Th_{det}$ ratios of 1.08 ± 0.23 and 0.62 ± 0.14, respectively.

Results

Uranium-thorium age data

Measured ^{232}Th for the corals collected from the Keppel Islands was variable, with 98% of samples ranging from 0.08–12.41 ppb (72% <3.5 ppb) suggesting relatively small to negligible initial ^{230}Th and/or non-radiogenic detrital ^{230}Th contamination in most of the samples we collected (Table 1). Elevated ^{232}Th (25.72 ppb) and a low $^{230}Th/^{232}Th$ ratio (6.84) was determined for sample GKI007, indicating significant contamination with detrital ^{230}Th and justifying the removal of this sample from further analysis (N.B. removal of this data point did not affect the interpretation of RSL). All samples appear to have remained a closed

system supported by $\delta^{234}U$ values falling within analytical error of the modern seawater value of 146.0 ± 3‰ and uranium concentrations similar to previously reported values for pristine coral, ranging from 2.6–3.5 ppm (Henderson, 2002, Cobb et al., 2003, Shen et al., 2008, Clark et al., 2012, Leonard et al., 2013). The average detrital $^{230}Th/^{232}Th$ ratio obtained from the Keppel Islands isochrons (0.62 ± 0.14; Supp. Fig. 3.1) is close to the 0.64 ± 0.04 ratio reported by Clark et al. (2014a) for massive *Porites* corals from the Palm Islands (18°43/146°35; Fig. 1) - a comparable inshore site ~650 km north of the present study area. The three replicate isochron samples used for age validation (GKI003, GKI004 and GKI005) are all within age error of the reported U-Th age of the final ultra-cleaned sample (Supp. Fig. 3.2).

Age-Elevation

Keppel Islands corrected ^{230}Th ages of non-microatoll corals and microatolls (n = 42; reported hereafter as calendar years before present – 1950) ranged from 6,864 - 968 yr. BP, although distributed discontinuously throughout this time (Table 1). Reef flats had developed at all three sites by the mid-Holocene, yet no reef flat samples were found to be dated at any site between ~4,600 – 2,800 yr. BP. All elevations are reported relative to MLWS tide height to which open water microatolls are constrained and therefore considered representative of height above/below present RSL.

Humpy Island is the smallest island and reef flat of the three sites investigated in this study. The modern leeward reef lies 150–350 m from the emerged reef flat, which is situated in a small embayment on the southwest of the island (Fig. 1 and Supp. 4a). The oldest microatoll at this site was *Cyphastrea* spp. (6,209 ± 27 yr. BP) at 0.4 m above present, however, large branching corals as early as 6,800 yr. BP are present (Fig. 3, Table 1). Both microatolls and non-microatolls are found from ~6,200 to 5,500 yr. BP at ~ 0.7 m above present, suggestive of a fully developed reef flat (Fig. 3). Four *Porites* sp. microatolls dated between ~5,300-5,100 yr. BP are ~0.4 – 0.7 m lower than their older counterparts (Fig. 3) with no corals found above this elevation for this period. After 5,100 yr. BP, only two late-Holocene microatolls ~0.2 m above present at ~970 yr. BP are found at this site.

On Great Keppel Island (Fig. 1, Supp. 4b), the modern reef is located almost perpendicular to a rocky headland at the seaward edge of an embayment on the south west of the island and is dominated by branching *Acropora* sp. (Fig. 2b). The relict emergent reef is located ~50 m towards the shore from the living coral zone and is partially covered by mixed

siliciclastic/carbonate sediment. Only one mid-Holocene sample (GKI 009) was dated at ~6,500 yr. BP at 0.52 m above present MLWS level. Whilst more mid-Holocene samples are most likely present at GKI, the occurrence of relatively thick unconsolidated sediments means that they are probably only intermittently exposed (Fig. 2a). The remaining samples from GKI are all late Holocene from 2,800 -1,400 yr. BP. Microatolls are at 0.3 m above present sea level at 2,856 yr. BP, -0.07 m by 1,640 yr. BP, 0.05 m at 1,550 yr. BP and 0.17 m at 1468 yr. BP (Fig.4a).

At North Keppel Island (NKI; Fig. 1, Supp. 4c) modern coral growth is mainly constrained to the reef slope, with small *Acropora* sp. recruits and a few modern microatolls (living tissue <5 cm thick on the edge of the colony; Supp. 4d) in areas of intermittent negative relief. Fossil microatolls at NKI are ~0.8 m above present sea level from 5,800 – 5,700 yr. BP and 0.4 m above present sea level between 5,350 – 5,125 yr. BP. From 5,000 – 4,600 yr. BP, microatolls are ~0.7 m above present sea level after which no further reef flat corals were sampled in this study at NKI (Fig 4a).

Discussion and interpretation

High-precision U-Th age-elevation data from corals and microatolls in the Keppel Islands provides evidence in support of a non-linear RSL regression throughout the Holocene on the southern GBR. Our study is based on 42 U-Th dates obtained from *in situ* fossil microatolls (n=32) and relict reef flat corals (non-microatolls; n=10) from three continental islands. This is the first account of centennial scale RSL instability documented from multiple reefs within the same region.

Mid-Holocene (6,500-4,600 yr. BP)

Models of glacio-hydro-isostatic response of RSL predict a highstand of +1 to + 3 m for the inshore GBR in the mid-Holocene (Clark et al., 1978, Chappell et al., 1982, Lambeck and Nakada, 1990, Lambeck, 2013). The earliest microatoll samples in the Keppel Islands are 0.4 – 0.5 m above present from ~6,500 – 6,200 yr. BP and ~ 0.7 m by 6,000 yr. BP (Fig. 3 and 4). Elevations of non-microatoll corals from HI suggests that the highstand was likely reached just after ~6,200 yr. BP, however, determining absolute RSL from non-microatolls is not possible (Fig. 3a). The highstand in the Keppel Islands, is both later and lower than previously proposed highstand for the AEC [e.g. 1.0 -1.5 m at 7,400 yr. BP (Sloss et al., 2007) and 7,000 yr. BP (Lewis et al., 2008)]. However, these previous highstand age and

elevation data must be treated with caution as they are based either on a limited number of radiocarbon ages obtained from supratidal deposits, for which upper elevation ranges are difficult to determine (Sloss et al., 2007), or recalibrated radiocarbon data from a number of different studies utilising different methods and indicators (Lewis et al., 2008). Early reef initiation in the Keppel Islands may have been inhibited by conditions unsuitable or marginal for coral growth due to the movement of the coastal terrigenous sediment wedge (TSW) and/or resuspension of pre-transgressive sediments (Larcombe and Woolfe, 1999). Nevertheless, RSL appears to have not peaked in the southern GBR until after 6,200 yr. BP. Furthermore, microatoll elevations designate the lower height estimate of RSL, commonly ~0.5 m lower than fixed biological indicators (FBI's; e.g. tubeworms and oyster beds; Lewis et al., 2008) or more when compared to mangrove deposits (Sloss et al., 2007), which makes our data comparable to previous elevation reconstructions. Furthermore, the magnitude and timing of the mid-Holocene highstand may vary between coastal and shelf sites due to mantle rheology, or by latitude as a function of Antarctic melt water contribution (Lambeck, 2002).

Following the highstand in the Keppel Islands, two sites (HI and NKI) show a rapid coeval fall in RSL of 0.4 m – 0.7 m at 5,500 yr. BP, with no microatolls or non-microatoll corals found above 0.4 m between 5,300 – 5,100 yr. BP. This lowering of RSL cannot be explained by a lack of accommodation space as microatolls reform at NKI at higher elevations (0.6 – 0.7 m) from 5,000 – 4,600 yr. BP at more landward locations on the reef flat (see Fig. 5). Although ponding must be considered when interpreting the return to higher RSL after 5,100 yr. BP, we consider this unlikely at NKI. A shore-to-sea survey showed that towards the reef slope the area of highest elevation (potentially causing ponding) is only 0.4 m above present (Supp. 4d). Thin ponded extant microatolls (<5 cm vertical living tissue above the substrate; Supp. 4e) are present on the reef flat at NKI at ~0.4 m above present MLWS, which is still 0.2 – 0.3 m lower than the microatolls dated between 5,000 – 4,600 yr. BP. The morphology of the modern microatolls also differs from their fossil counterparts with the former defined by planar surfaces formed by very still moated water levels and the latter being vertically more substantial with irregular surfaces (Fig. 2d) which is indicative of a free draining reef flat environment (Smithers and Woodroffe, 2000). Due to the temporal overlap of this lowstand at two reef sites we consider that the macro tidal setting, which can result in significant elevation differences between modern microatolls, is not sufficient to explain this lowstand. If elevation differences in this region were driven primarily by tidal range, the data

obtained in our study would consistently show temporally indiscreet elevation differences of > 0.3 m throughout the Holocene, which is not apparent.

The timing and magnitude of the sudden RSL lowering in the Keppel Islands is in strong agreement with FBI data from the southern AEC which exhibited a RSL fall of ~0.6 m between 5,400 – 5,000 yr. BP (Baker and Haworth, 2000, Sloss et al., 2007). On Magnetic Island, U-Th derived microatoll data also indicates that RSL was higher at 5,800 yr. BP compared to 5,400 – 5,000 yr. BP (Yu and Zhao, 2010b). When previously reported (recalibrated; Lewis et al., 2008) microatoll data from the GBR (Chappell, 1983) are compared with the Keppel Islands data, the lowered RSL between 5,300 – 5,100 yr. BP is still evident, with samples elevated higher found prior to and following the inferred lowstand (Fig. 4b).

The RSL lowering in the Keppel Islands at 5,500 yr. BP is contemporaneous with a period of significant change to reefs on the GBR (Smithers et al., 2006, Lybolt et al., 2011, Perry and Smithers, 2011, Leonard et al., 2013). Following the concept of reef "turn on" and "turn off" events initially proposed by Buddemeier and Hopley (1988), Perry and Smithers (2011) analysed data from 76 reef core records from the inshore GBR and noted that reef initiation ceased from ~5,500 yr. BP in both the northern (Cape Tribulation; 1,000 km north) and southern GBR (Cockermouth, Penrith, and Scawfell Islands; ~300 km north of the present study). Similarly, in Moreton Bay (~550 km south of the Keppel Islands) sudden reef flat termination (Leonard et al., 2013) and increasing coral depth followed by a reef hiatus (Lybolt et al., 2011) have been documented from ~ 5,600 yr. BP. Lack of vertical accommodation space, proximity to the coastal TSW and climate change were suggested as the likely cause of reef "turn-off" (i.e. reduction of accretion) on the inshore GBR (Perry and Smithers, 2011). However, it was noted by the authors that similar patterns and/or transitions from aggrading to prograding modes of growth were observed on mid- and outer -shelf reefs far from the effects of terrigenous input or resuspension. In Moreton Bay, a rapid fall in RSL and/or climatic change were suggested to have increased turbidity producing unfavourable conditions for coral growth (Leonard et al., 2013). However, a recent analysis of foraminiferal assemblages from Moreton Bay demonstrated water quality was continuously and consistently marginal to degraded from 7,400 yr. BP to present (Narayan et al., 2015), suggesting that a sudden increase in turbidity was likely not the primary driver of reef demise in this region.

The period of reduced accretion ("turn-off") was followed by a significant hiatus in reef growth from ~4,600 yr. BP that lasted for two millennia in the northern and southern GBR (Smithers et al., 2006, Perry and Smithers, 2011). Equally, no corals or microatolls were found in the Keppel Islands between 4,600 and 2,800 yr. BP. Previously presented RSL data from the AEC is contradictory, with some authors suggesting that SLs were 1 m (Flood and Frankel, 1989) to 1.7 m higher (Baker and Haworth, 2000) during this period, whilst others contest possible lowered RSLs at this time (Lewis et al., 2008). Lewis et al. (2008) proposed a significant negative oscillation of RSL at 4,600 yr. BP based on 115 recalibrated ^{14}C sea-level indicators from the AEC (Fig 4b). If RSLs were lowered during these periods, sediment loads to inshore reefs would increase due to mainland coastal sedimentary progradation, with flood plumes reaching further across the shelf and increased wave re-suspension of fine sediments which may have resulted in significantly reduced reef accumulation or hiatus at some locations as noted by Perry and Smithers (Perry and Smithers, 2011). Clearly, more SL proxies that temporally bracket, or are within, the GBR hiatus period are needed before any conclusions can be drawn. Nevertheless, the synchronicity of a RSL oscillation at 5,500 yr. BP and reef flat hiatus at 4,600 yr. BP in the Keppel Islands with significant reductions in reef initiation and reef hiatus elsewhere on the GBR is noteworthy.

Late Holocene re-initiation (2,800 yr. BP to present)

Microatoll records suggest that reef flats in the Keppel Islands reinitiated between 2,800 – 2,500 yr. BP, similar to the timing of reef re-initiation (~2,300 yr. BP) reported in the northern and southern GBR (Perry and Smithers, 2011). As only a limited number of samples at GKI and HI were found in the present study in the late Holocene, our interpretation of RSL is at this stage cautious. Microatoll evidence suggests that between 2,800 – 2,500 yr. BP RSL was 0.3 – 0.2 m above present, after which RSL appears to have been just below or close to present levels by 1,640 yr. BP. Microatolls are then found at increasing elevations up to 0.2 m above present from 1,470 – 970 yr. BP. Lewis et al. (2008) proposed a similar oscillation centred at 2,800 yr. BP at comparable elevations to our present record. More recently, Harris et al. (2015) reported a rapid fall in RSL after ~2,200 yr. BP at One Tree Island (southern GBR), however they suggested that RSL was ~1.0 m above present between 3,900 – 2,200 yr. BP. Baker and Haworth (2000) suggested that an absence of succession of various FBIs indicated a rapid RSL fall in Port Hacking (1,200 km south of the Keppel Islands) between 3,500 and 3,400 yr. BP, after which RSL was stable until ~2,800 yr. BP. However, following this period of RSL stability the Port Hacking data from two

sites within the same region displayed divergent trends, one falling and one rising (Baker and Haworth, 2000). Perry and Smithers (2011) inferred that reef re-initiation on the GBR during the late Holocene likely occurred due to RSL stabilisation and the associated retreat of the TSW and shoreline resulting in conditions becoming more favourable for accretion. However, data from the Keppel Islands and elsewhere on the GBR and AEC suggests that after 2,800 yr. BP RSL was unstable at centennial timescales. It is unclear at this stage as to why reefs re-initiated in the late Holocene even if RSL fell smoothly or oscillated.

Mechanisms of relative sea level oscillations

Neotectonics and hydro-isostasy

The AEC is considered to have been tectonically stable throughout the Holocene (Lambeck and Nakada, 1990, Lambeck, 2002, Woodroffe and Horton, 2005), however, neotectonic uplift of up to 1 m per 1,000 years to the east of the Broad Sound fault (~130 km north of the Keppel Islands) has been suggested (Kleypas and Hopley, 1992). At Broad Sound the continental shelf is at its widest (~200 km) compared with just south of the Keppel Islands where the shelf is approximately three times narrower (~70 km; Fig. 1). The resulting tidal range is the highest on the GBR (Cook and Mayo, 1977); being up to twice that of the Keppel Islands. It is possible that differential down warping (i.e. larger effect on the wider shelf) following the mid-Holocene highstand resulted in an increase in tidal range in the Keppel Islands region, which would result in a lowering of the MLWS level without a need for any RSL change or eustatic contribution (Kleypas and Hopley, 1992). Although feasible, we consider this unlikely as tidal adjustment would likely manifest as a more gradual change in the RSL curve which is not the case in the present study. This process would also fail to explain the extended period of RSL lowering then the return to higher RSL following the lowstand and cannot explain the oscillations reported from other sites both north and south of the Keppel Islands that occur synchronously.

Antarctic ice melt history in response to the Arctic melt water transgression is predicted to have continued throughout the mid- to late Holocene as a result of increasing ESL (Nakada and Lambeck, 1989), although the effect on RSL in the southern hemisphere is poorly constrained and rarely discussed. Antarctic contributions to the RSL history of the AEC have been predicted to result in lower amplitude highstands being reached in the southern GBR compared to the northern GBR (Nakada and Lambeck, 1989), which is broadly supported by

the data presented here; ~0.7 m above present compared to 0.7 - 2 m highstands reported in more northerly regions (Hopley, 1980, Chappell, 1983, Flood and Frankel, 1989, Baker, 2001, Lewis et al., 2008, Yu and Zhao, 2010a). Conversely, Bryant (1992) suggested that the peak highstands were trending opposite, with higher SL reached in the southeast of the continent and reducing northwards. Neither of these models is in agreement with the FBI data presented by Haworth et al. (2002), who suggested the AEC continental shelf had not responded differentially to hydro-isostatic down warping across north-south latitudinal gradient. Therefore, although the data presented here appears to support the earlier models of Nakada and Lambeck (1989), uncertainties regarding variation in continental shelf width and isostatic response to mass water loading during the mid-Holocene transgression are yet to be resolved. Although it is important to understanding regional responses of RSL to water loading, the rapidity of the oscillations detected in the present study also generally precludes continental tilting or shelf down warping as the driving mechanism of the RSL oscillations in the present study.

Climate and sea level

Evidence of rapid climate change events during the Holocene are numerous, and although attempts to reconcile a global Holocene climate signal have been made (Bond et al., 1997, Bond et al., 2001, Mayewski et al., 2004, Wanner et al., 2011, Wanner et al., 2015) the currently available records are significantly biased to the northern hemisphere, with continuous high resolution records from the southern hemisphere being relatively sparse (Wanner et al., 2015). Furthermore, whether rapid (sub-centennial to centennial) shifts in climate translated to either minor relative or eustatic SL variability is difficult to ascertain and rarely discussed. In the Northwest Pacific, Hamanaka et al. (2012) interpreted reef hiatus events at Kodakara Island in the Mid-Holocene to be associated with oscillations in RSL, and suggested links to possible eustatic oscillations driven by Atlantic and Pacific cold events and associated short lived ice build-up. Similarly, links between climate perturbations and SL oscillations in the Atlantic at ~6,500 and 2,200 yr. BP (Schellmann and Radtke, 2010) and in the Pacific in response to the “Little Climatic Optimum” and “Little Ice Age” of the late Holocene have also been proposed (Nunn, 1998, Nunn, 2000a, Nunn, 2000b). Conversely, glacio-isostatically adjusted mangrove and reef deposit data from the Seychelles (Indian Ocean) suggests that ESL has been largely insensitive to climate fluctuations over the past 2,000 years prior to anthropogenic influence (Woodroffe et al., 2015). Although a recent re-analysis of available “far-field” sea level data by Lambeck et al. (2014) concluded that no

oscillations of >0.2 m occurred during the last 6,000 years, this conclusion is limited to timescales of ≥200 years due to age uncertainties, which is above the temporal detection limit of the oscillations presented here for the Keppel Islands. Unfortunately, insufficient continuous high resolution climate data in the southern hemisphere (Wanner et al., 2011, Wanner et al., 2015) makes interpretation of Holocene regional and global climate signals on SL variability tenuous. Coral proxy derived (Sr/Ca and $\delta^{18}O$) sea surface temperature (SST) data from Orpheus Island (18.5˚S, 146.5˚E) and King Reef (17°46'S, 146°08'E) in the northern GBR suggest that SSTs were ~1.0 – 1.2˚C warmer than present at ~5,300 (Gagan et al., 1998) and 4,700 years before present (Roche et al., 2014). Warmer SSTs have also been inferred from foraminiferal $\delta^{18}O$ analysis from near Indonesia, with warm/wet and stable conditions prior to 5,500 – 5,300 yr. BP (Brijker et al., 2007). Conversely, coral data from Indonesia and Papua New Guinea suggests a cooling of ~1.2˚C at ~5,500 yr. BP (Abram et al., 2009). With consideration of the age errors in these records, a possible 1.0 – 2.0˚C change in SST affecting the Indo-Pacific during the mid-Holocene is possible, however this cannot be validated with the data currently available.

In this study we have demonstrated that by using high precision U-Th dating techniques, in conjunction with elevation surveys of a single SL indicator at multiple sites, it is possible to detect minor (<1 m) RSL fluctuations. The RSL oscillations presented here for the Keppel Islands are in good temporal agreement with episodes of significant change to reefs on the GBR throughout the Holocene ("turn-off" and hiatus events). With current models predicting a 0.2 - 0.6 m contribution to sea level rise for each 1˚C of global warming in the future (Church et al., 2013) is it not then possible that similar scale cooling events in the Holocene had comparable effects on at least RSL signals in the far-field? Given the rates and magnitudes of change in the present study, and lack of evidence for any other geological or geomorphological contributions, we consider significant sub-centennial to centennial climate perturbations the most likely driver of RSL oscillations in the Keppel Islands. Clearly, more high resolution RSL records are needed to determine whether this is a local, regional or global signal, and robust links to possible climate perturbations are required before any further conclusions can be drawn.

High resolution palaeo-sea level reconstructions are not only critical to interpreting reef growth history on the GBR, but will enable improved predictions of reef response to future SL variability (Camoin and Webster, 2015). Further, precisely dated RSL records in

conjunction with high resolution palaeo-climate data will enable refinement to model parameters for use in future sea level rise projections.

Acknowledgements

We thank C. Murray-Wallace and one anonymous reviewer for their constructive comments which greatly improved this manuscript. We would like to thank Hannah Markham, Mauro Lepore, Martina Prazeres, Ian Butler and all others involved in fieldwork and Dr Ai Duc Nguyen for invaluable laboratory assistance. Special thanks to the crew of the MV Adori, Len and John.

Funding

This study was funded by the National Environmental Research Programme (NERP) Tropical Ecosystems Hub Project 1.3 'Characterising the cumulative impacts of global, regional and local stressors on the present and past biodiversity of the GBR' to J-xZ, JMP, SGS, TRC, Y-xF and others, and Australian Research Council LIEF grant (LE0989067 for the purchase and installation of the MC-ICP-MS essential for this study) to J-xZ, JMP, Y-xF and others, as well as an Australian Postgraduate Award (APA) to NDL. Samples were collected under permit number G12/34979.1.

References

Abram, N. J., Mcgregor, H. V., Gagan, M. K., Hantoro, W. S. & Suwargadi, B. W. 2009. Oscillations in the southern extent of the Indo-Pacific Warm Pool during the mid-Holocene. *Quaternary Science Reviews* **28,** 2794-2803.

B.O.M. 2011. *Australian climate variability & change - Time series graphs* [Online]. Australian Bureau of Meteorology, Commonwealth of Australia. Available: http://www.bom.gov.au/cgi-bin/climate/change/timeseries. [Accessed 15th October 2011].

Baker, R. 2001. Inter-tidal fixed indicators of former Holocene sea levels in Australia: a summary of sites and a review of methods and models. *Quaternary International* **83-85,** 257-273.

Baker, R. & Haworth, R. J. 2000. Smooth or oscillating late Holocene sea-level curve? Evidence from the palaeo-zoology of fixed biological indicators in east Australia and beyond. *Marine Geology* **163,** 367-386.

Bond, G., Bonani, G., Kromer, B., Beer, J., Muscheler, R., Evans, M. N., Showers, W., Hoffmann, S., Lotti-Bond, R. & Hajdas, I. 2001. Persistent Solar Influence on North Atlantic Climate During the Holocene. *Science* **294,** 2130-2136.

Bond, G., Bonani, G., Showers, W., Cheseby, M., Lotti, R., Almasi, P., Demenocal, P., Priore, P., Cullen, H. & Hajdas, I. 1997. A Pervasive Millennial-Scale Cycle in North Atlantic Holocene and Glacial Climates. *Science* **278,** 1257-1266.

Brijker, J. M., Jung, S. J. A., Ganssen, G. M., Bickert, T. & Kroon, D. 2007. ENSO related decadal scale climate variability from the Indo-Pacific Warm Pool. *Earth and Planetary Science Letters* **253,** 67-82.

Brooke, B., Ryan, D., Pietsch, T., Olley, J., Douglas, G., Packett, R., Radke, L. & Flood, P. 2008. Influence of climate fluctuations and changes in catchment land use on Late Holocene and modern beach-ridge sedimentation on a tropical macrotidal coast: Keppel Bay, Queensland, Australia. *Marine Geology* **251,** 195-208.

Bryant, E. 1992. Last interglacial and Holocene trends in sea-level maxima around Australia: Implications for modern rates. *Marine Geology* **108,** 209-217.

Buddemeier, R. W. & Hopley, D. Turn-ons and Turn-offs; Causes and mechanisms of the initiation and termination of coral reef growth. *In:* Proceedings of the 6th International Coral Reef Symposium, 1988 Australia. 253 - 261.

Camoin, G. F. & Webster, J. M. 2015. Coral reef response to Quaternary sea-level and environmental changes: State of the science. *Sedimentology* **62,** 401-428.

Chappell, J. 1983. Evidence for smoothly falling sea-level relative to North Queensland, Australia, during the past 6,000 yr. *Nature* **302,** 406-408.

Chappell, J., Rhodes, E. G., Thom, B. G. & Wallensky, E. 1982. Hydro-isostasy and the sea-level isobase of 5500 B.P. in north Queensland, Australia. *Marine Geology* **49,** 81-90.

Cheng, H., Edwards, R. L., Hoff, J., Gallup, C. D., Richards, D. A. & Asmerom, Y. 2000. The half-lives of uranium-234 and thorium-230. *Chemical Geology* **169,** 17-33.

Church, J. A., Clark, P. U., Cazenave, A., Gregory, J. M., Jevrejeva, S., Levermann, A., Merrifield, M. A., Milne, G. A., Nerem, R. S., Nunn, P. D., Payne, A. J., Pfeffer, W. T., Stammer, D. & Unnikrishnan, A. S. 2013. Sea Level Change. *In:* Stocker, T. F., Qin, D., Plattner, G.-K., Tignor, M., Allen, S. K., Boschung, J., Nauels, A., Xia, Y., Bex, V. & Midgley, P. M. (eds.) *Climate Change 2013: The Physical Science Basis Contribution of Working Group I to the Fifth Assessment Report of the Intergovernmental Panel on Climate Change.* Cambridge, United Kingdom and New York, NY, USA.

Clark, J. A., Farrell, W. E. & Peltier, W. R. 1978. Global changes in postglacial sea level: A numerical calculation. *Quaternary Research* **9,** 265-287.

Clark, T. R., Roff, G., Zhao, J.-X., Feng, Y.-X., Done, T. J. & Pandolfi, J. M. 2014a. Testing the precision and accuracy of the U–Th chronometer for dating coral mortality events in the last 100 years. *Quaternary Geochronology* **23,** 35-45.

Clark, T. R., Zhao, J.-X., Feng, Y.-X., Done, T. J., Jupiter, S., Lough, J. & Pandolfi, J. M. 2012. Spatial variability of initial $^{230}Th/^{232}Th$ in modern Porites from the inshore region of the Great Barrier Reef. *Geochemica et Cosmochimca Acta* **78,** 99-118.

Clark, T. R., Zhao, J.-X., Roff, G., Feng, Y.-X., Done, T. J., Nothdurft, L. D. & Pandolfi, J. M. 2014b. Discerning the timing and cause of historical mortality events in modern Porites from the Great Barrier Reef. *Geochimica et Cosmochimica Acta* **138,** 57-80.

Cobb, K. M., Charles, C. D., Cheng, H., Kastner, M. & Edwards, R. L. 2003. U/Th-dating living and young fossil corals from the central tropical Pacific. *Earth and Planetary Science Letters* **210,** 91-103.

Cook, P. J. & Mayo, W. 1977. Sedimentology and Holocene history of a tropical estuary (Broad Sound, Queensland). *Bulletin 170.* Canberra: Bureau of Mineral Resources.

Cowie, B. A., Thornton, C. M. & Radford, B. J. 2007. The Brigalow Catchment Study: I*. Overview of a 40-year study of the effects of land clearing in the brigalow bioregion of Australia. *Soil Research* **45,** 479-495.

Douglas, G. B., Ford, P. W., Palmer, M., Noble, R. M. & Packett, R. 2006. Fitzroy River Basin, Queensland, Australia. I. Identification of Sediment Sources in Impoundments and Flood Events. *Environmental Chemistry* **3,** 364.

Elvidge, C., D, B. Dietz, J., B, Berkelmans, R., Andréfouët, S., Skirving, W., Strong, A., E & Tuttle, B., T 2004. Satellite observation of Keppel Islands (Great Barrier Reef) 2002 coral bleaching using IKONOS data. *Coral Reefs* **23,** 123-132.

Flood, P. G. & Frankel, E. 1989. Late Holocene higher sea level indicators from eastern Australia. *Marine Geology* **90,** 193-195.

Gagan, M. K., Ayliffe, L. K., Hopley, D., Cali, J., Mortimer, G., Chappell, J., Mcculloch, M. T. & Head, M. 1998. Temperature and surface-ocean water balance of the mid-Holocene tropical western Pacific. *Science* **279,** 1014-1018.

Great Barrier Reef Marine Park Authority 2006. Great Barrier Reef coral bleaching surveys 2006. *Research Publication 87.* Townsville, Queensland.

Hamanaka, N., Kan, H., Yokoyama, Y., Okamoto, T., Nakashima, Y. & Kawana, T. 2012. Disturbances with hiatuses in high-latitude coral reef growth during the Holocene: Correlation with millennial-scale global climate change. *Global and Planetary Change* **80-81,** 21-35.

Harris, D. L., Webster, J. M., Vila-Concejo, A., Hua, Q., Yokoyama, Y. & Reimer, P. J. 2015. Late Holocene sea-level fall and turn-off of reef flat carbonate production: Rethinking bucket fill and coral reef growth models. *Geology* **43,** 175-178.

Haworth, R. J., Flood, P. G. & Baker, R. G. V. 2002. Predicted and observed Holocene sea ‐ levels on the Australian coast: what do they indicate about hydro ‐ isostatic models in far ‐ field sites? *Journal of Quaternary Science* **17,** 581-591.

Henderson, G. M. 2002. Seawater ($^{234}U/^{238}U$) during the last 800 thousand years. *Earth and Planetary Science Letters* **199,** 97-110.

Hopley, D. 1980. Mid-Holocene high sea levels along the coastal plain of the Great Barrier Reef Province: A discussion. *Marine Geology* **35,** M1-M9.

Hopley, D., Smithers, S. G. & Parnell, K. 2007. *The Geomorphology of the Great Barrier Reef: Development, Diversity and Change,* Cambridge, Cambridge University Press.

Hua, Q., Webb, G. E., Zhao, J.-X., Nothdurft, L. D., Lybolt, M., Price, G. J. & Opdyke, B. N. 2015. Large variations in the Holocene marine radiocarbon reservoir effect reflect ocean circulation and climatic changes. *Earth and Planetary Science Letters* **422,** 33-44.

Hughes, T. P. & Connell, J. H. 1999. Multiple Stressors on Coral Reefs: A Long-Term Perspective. *Limnology and Oceanography* **44,** 932-940.

Jones, A. M. & Berkelmans, R. 2014. Flood impacts in Keppel Bay, southern Great Barrier Reef in the aftermath of cyclonic rainfall. *PloS one* **9,** 84739.

Kennedy, D. M. & Woodroffe, C. D. 2002. Fringing reef growth and morphology: a review. *Earth Science Reviews* **57,** 255-277.

Kleypas, J. A. & Hopley, D. Reef Development Across a Broad Continental Shelf, Southern Great Barrier Reef, Australia. *In:* Richmond, R. H., ed. Seventh International Coral Reef Symposium, 1992 Guam. University of Guam Press, 1129-1141.

Lambeck, K. 1993. Glacial rebound and sea-level change: An example of a relationship between mantle and surface processes. *Tectonophysics* **223,** 15-37.

Lambeck, K. 2002. Sea level change from mid Holocene to recent time: an Australian example with global implications. *Geodynamics Series* **29,** 33-50.

Lambeck, K. 2013. Sea Level Change from Mid Holocene to Recent Time: an Australian Example With Global Implications. *Ice Sheets, Sea Level and the Dynamic Earth.* American Geophysical Union.

Lambeck, K. & Nakada, M. 1990. Late Pleistocene and Holocene sea-level change along the Australian coast. *Palaeogeography, Palaeoclimatology, Palaeoecology (Global and Planetary Change Section)* **89,** 143-176.

Lambeck, K., Rouby, H., Purcell, A., Sun, Y. & Sambridge, M. 2014. Sea level and global ice volumes from the Last Glacial Maximum to the Holocene. *Proceedings of the National Academy of Sciences* **111,** 15296-15303.

Larcombe, P. & Woolfe, K. J. 1999. Terrigenous sediments as influences upon Holocene nearshore coral reefs, central Great Barrier Reef, Australia. *Australian Journal of Earth Sciences* **46,** 141-154.

Leonard, N. D., Welsh, K. J., Zhao, J.-X., Nothdurft, L. D., Webb, G. E., Major, J., Feng, Y.-X. & Price, G. J. 2013. Mid-Holocene sea-level and coral reef demise: U-Th dating of subfossil corals in Moreton Bay, Australia. *The Holocene* **23,** 1841-1852.

Lewis, S. E., Sloss, C. R., Murray-Wallace, C. V., Woodroffe, C. D. & Smithers, S. G. 2013. Post-glacial sea-level changes around the Australian margin: a review. *Quaternary Science Reviews* **74,** 115-138.

Lewis, S. E., Wu, R. a. J., Webster, J. M. & Shields, G. A. 2008. Mid-late Holocene sea-level variability in eastern Australia. *Terra Nova* **20,** 74-81.

Ludwig, K. R. 2003. Isoplot/Ex, version 3: a Geochronological Toolkit for Microsoft Excel. *Berkeley Geochronology Center Special Publications*.

Lybolt, M., Neil, D. T., Zhao, J., Feng, Y., Yu, K. & Pandolfi, J. 2011. Instability in a marginal coral reef: the shift from natural variability to a human-dominated seascape. *Frontiers in Ecology and the Environment* [Online].

Mayewski, P. A., Holmgren, K., Lee-Thorp, J., Rosqvist, G., Rack, F., Staubwasser, M., Schneider, R. R., Steig, E. J., Rohling, E. E., Curt Stager, J., Karlén, W., Maasch, K. A., David Meeker, L., Meyerson, E. A., Gasse, F. & Van Kreveld, S. 2004. Holocene climate variability. *Quaternary Research* **62,** 243-255.

Mcgregor, H. V., Gagan, M. K., Mcculloch, M. T., Hodge, E. & Mortimer, G. 2008. Mid-Holocene variability in the marine 14C reservoir age for northern coastal Papua New Guinea. *Quaternary Geochronology* **3,** 213-225.

Mclean, R. F., Stoddart, D. R., Hopley, D. & Polach, H. 1978. Sea Level Change in the Holocene on the Northern Great Barrier Reef. *Philosophical Transactions of the Royal Society of London. Series A, Mathematical and Physical Sciences* **291,** 167-186.

Mitrovica, J. X. & Milne, G. A. 2002. On the origin of late Holocene sea-level highstands within equatorial ocean basins. *Quaternary Science Reviews* **21,** 2179-2190.

Murray-Wallace, C. V. & Woodroffe, C. D. 2014. Quaternary sea-level changes: a global perspective. Cambridge;New York;: Cambridge University Press.

Muthukrishnan, R. & Fong, P. 2014. Multiple anthropogenic stressors exert complex, interactive effects on a coral reef community. *Coral Reefs* **33,** 911-921.

Nakada, M. & Lambeck, K. 1989. Late Pleistocene and Holocene sea-level change in the Australian region and mantle rheology. *Geophysical Journal International* **96,** 497-517.

Narayan, Y. R., Lybolt, M., Zhao, J.-X., Feng, Y. & Pandolfi, J. M. 2015. Holocene benthic foraminiferal assemblages indicate long-term marginality of reef habitats from Moreton Bay, Australia. *Palaeogeography, Palaeoclimatology, Palaeoecology* **420,** 49-64.

Neumann, A. C. & Macintyre, I. G. Reef response to sea level rise: keep-up, catch up or give-up. *In:* Proc. 5th Int Coral Reef Congr, 1985 Tahiti. 105-110.

Nunn, P. D. 1998. Sea-Level Changes over the past 1,000 Years in the Pacific. *Journal of Coastal Research* **14,** 23-30.

Nunn, P. D. 2000a. Environmental catastrophe in the Pacific Islands around A.D. 1300. *Geoarchaeology* **15,** 715-740.

Nunn, P. D. 2000b. Illuminating Sea ‐ Level Fall around AD 1220 ‐ 1510 (730 ‐ 440 cal yr BP) in the Pacific Islands: Implications for Environmental Change and Cultural Transformation. *New Zealand Geographer* **56,** 46-54.

Pandolfi, J. M., Bradbury, R. H., Sala, E., Hughes, T. P., Bjorndal, K. A., Cooke, R. G., Mcardle, D., Mcclenachan, L., Newman, M. J. H., Paredes, G., Warner, R. R. & Jackson, J. B. C. 2003. Global Trajectories of the Long-Term Decline of Coral Reef Ecosystems. *Science* **301,** 955-958.

Perry, C. & Smithers, S. 2011. Cycles of coral reef 'turn-on', rapid growth and 'turn-off' over the past 8500 years: a context for understanding modern ecological states and trajectories. *Global Change Biology* **17,** 76-86.

Pirazzoli, P. A. & Pluet, J. 1991. *World atlas of Holocene sea-level changes,* Amsterdam ; New York, Elsevier.

Roche, R. C., Perry, C. T., Smithers, S. G., Leng, M. J., Grove, C. A., Sloane, H. J. & Unsworth, C. E. 2014. Mid-Holocene sea surface conditions and riverine influence on the inshore Great Barrier Reef. *The Holocene* **24,** 885-897.

Rodriguez-Ramirez, A., Grove, C. A., Zinke, J., Pandolfi, J. M. & Zhao, J.-X. 2014. Coral Luminescence Identifies the Pacific Decadal Oscillation as a Primary Driver of River Runoff Variability Impacting the Southern Great Barrier Reef. *PloS one* **9,** e84305.

Schellmann, G. & Radtke, U. 2010. Timing and magnitude of Holocene sea-level changes along the middle and south Patagonian Atlantic coast derived from beach ridge systems, littoral terraces and valley-mouth terraces. *Earth-Science Reviews* **103,** 1-30.

Scoffin, T. P., Stoddart, D. R. & Rosen, B. R. 1978. The Nature and Significance of Microatolls. *Philosophical Transactions of the Royal Society of London. Series B, Biological Sciences* **284,** 99-122.

Shen, C.-C., Fan, T.-Y., Meltzner, A. J., Taylor, F. W., Quinn, T. M., Chiang, H.-W., Kilbourne, K. H., Li, K.-S., Sieh, K., Natawidjaja, D., Cheng, H., Wang, X., Edwards, R. L., Lam, D. D. & Hsieh, Y.-T. 2008. Variation of initial 230Th/ 232Th and limits of high precision U–Th dating of shallow-water corals. *Geochimica et Cosmochimica Acta* **72,** 4201-4223.

Sloss, C. R., Murray-Wallace, C. V. & Jones, B. G. 2007. Holocene sea-level change on the southeast coast of Australia: a review. *The Holocene* **17,** 999.

Smithers, S. G., Hopley, D. & Parnell, K. E. 2006. Fringing and Nearshore Coral Reefs of the Great Barrier Reef: Episodic Holocene Development and Future Prospects. *Journal of Coastal Research,* 175-187.

Smithers, S. G. & Woodroffe, C. D. 2000. Microatolls as sea-level indicators on a mid-ocean atoll. *Marine Geology* **168,** 61-78.

Toth, L. T., Macintyre, I. G., Aronson, R. B., Vollmer, S. V., Hobbs, J. W., Urrego, D. H., Cheng, H., Enochs, I. C., Combosch, D. J. & Van Woesik, R. 2012. ENSO drove 2500-year collapse of eastern Pacific coral reefs. *Science (New York, N.Y.)* **337,** 81.

Van Woesik, R. 1991. Immediate impact of the January 1991 floods on the coral assemblages of the Keppel Islands. *Research Publication No. 23*. Townsville: Great Barrier Reef Marine Park Authority.

Van Woesik, R. & Done, T. J. 1997. Coral communities and reef growth in the southern Great Barrier Reef. *Coral Reefs* **16,** 103-115.

Veron, J. E. N., Hoegh-Guldberg, O., Lenton, T. M., Lough, J. M., Obura, D. O., Pearce-Kelly, P., Sheppard, C. R. C., Spalding, M., Stafford-Smith, M. G. & Rogers, A. D. 2009. The coral reef crisis: The critical importance of <350 ppm CO2. *Marine Pollution Bulletin* **58,** 1428-1436.

Wanner, H., Mercolli, L., Grosjean, M. & Ritz, S. P. 2015. Holocene climate variability and change; a data-based review. *Journal of the Geological Society* **172,** 254-263.

Wanner, H., Solomina, O., Grosjean, M., Ritz, S. P. & Jetel, M. 2011. Structure and origin of Holocene cold events. *Quaternary Science Reviews* **30,** 3109-3123.

Woodroffe, C. D. & Horton, B. P. 2005. Holocene sea-level changes in the Indo-Pacific. *Journal of Asian Earth Sciences* **25,** 29-43.

Woodroffe, C. D., Kennedy, D. M., Hopley, D., Rasmussen, C. E. & Smithers, S. G. 2000. Holocene reef growth in Torres Strait. *Marine Geology* **170,** 331-346.

Woodroffe, S. A. 2009. Testing models of mid to late Holocene sea-level change, North Queensland, Australia. *Quaternary Science Reviews* **28,** 2474-2488.

Woodroffe, S. A., Long, A. J., Milne, G. A., Bryant, C. L. & Thomas, A. L. 2015. New constraints on late Holocene eustatic sea-level changes from Mahé, Seychelles. *Quaternary Science Reviews* **115,** 1-16.

Yu, K., Hua, Q., Zhao, J.-X., Hodge, E., Fink, D. & Barbetti, M. 2010. Holocene marine 14C reservoir age variability: Evidence from 230Th-dated corals in the South China Sea. *Paleoceanography* **25**.

Yu, K. & Zhao, J. 2010a. U-series dates of Great Barrier Reef corals suggest at least +0.7 m sea level ~7000 years ago. *The Holocene* **20,** 161-168.

Yu, K. F. & Zhao, J. X. 2010b. U-series dates of Great Barrier Reef corals suggest at least+0.7 m sea level similar to 7000 years ago. *Holocene* **20,** 161-168.

Tables

Table 1: Results of MC-ICP-MS uranium–thorium dating and elevation surveys of fossil microatolls from the Keppel Islands, Southern Great Barrier Reef, Australia. Elevation is relative to modern mean low water spring tide level (MLWS). Elevation errors for microatolls are based on the standard deviation of tidal datum measurements (1σ) and positive elevation errors for non-microatolls (≥0.35m) reflect the uncertainty of depth range of non-microatoll samples.

Sample Name	U (ppm)	^{232}Th (ppb)	(^{230}Th/ ^{232}Th)	(^{230}Th/^{238}U)	(^{234}U/^{238}U)	Uncorr. Age (a)	Corr. Age (b)	Age (yr BP - 1950)	initial δ^{234}U (c)	Genus/Growth form (*)	Coral Diam. (cm)	Elev. (m)	Elevation error	Latitude	Longitude
HUMP 001	2.8147 ± 0.0017	1.3017 ± 0.0028	385.5 ± 1.7	0.05875 ± 0.00024	1.1435 ± 0.0013	5753 ± 25	5739 ± 25	5676 ± 25	145.9 ± 1.3	Leptastrea	85	0.66	±0.15	23˚12'46.4	150˚58'10.8
HUMP 002	2.6366 ± 0.0018	0.1065 ± 0.0012	4294 ± 49	0.05705 ± 0.00019	1.1449 ± 0.007	5576 ± 19	5570 ± 19	5507 ± 19	147.2 ± 0.7	Cyphastrea	150	0.64	±0.15	23˚12'46.4	150˚58'11.0
HUMP 003	3.3272 ± 0.0024	1.6978 ± 0.0025	364.9 ± 1.6	0.61366 ± 0.00026	1.1436 ± 0.0010	6015 ± 27	6002 ± 27	5939 ± 27	143.6 ± 1.0	Pavona*	120	0.23	-0.15/≥0.35	23°12'45.9	150°58'09.5
HUMP 004	3.3226 ± 0.0024	7.366 ± 0.013	82.5 ± 0.3	0.06026 ± 0.00021	1.1449 ± 0.0009	5898 ± 22	5849 ± 25	5785 ± 25	147.4 ± 0.9	Branching*	180	0.46	-0.15/≥0.35	23˚12'46.8	150˚58'10.5
HUMP 006	3.4795 ± 0.0013	2.4757 ± 0.0038	227.4 ± 1.0	0.05332 ± 0.00021	1.1422 ± 0.0010	5215 ± 21	5197 ± 22	5134 ± 22	144.4 ± 1.0	Porites	250	0.16	±0.15	23˚12'46.0	150˚58'08.6
HUMP 007	3.5303 ± 0.0017	1.4009 ± 0.0021	404.0 ± 1.4	0.05284 ± 0.00017	1.1436 ± 0.0011	5161 ± 18	5149 ± 18	5086 ± 18	145.7 ± 1.1	Porites	70	0.09	±0.15	23˚12'45.9	150˚58'08.6
HUMP 008	3.0912 ± 0.0027	2.3010 ± 0.0044	225.2 ± 1.2	0.05525 ± 0.00028	1.1437 ± 0.0011	5402 ± 28	5382 ± 29	5319 ± 29	145.9 ± 1.1	Porites	75	0.2	±0.15	23˚12'45.8	150˚58'08.9
HUMP 009	3.3431 ± 0.0019	5.5019 ± 0.0075	112.5 ± 0.5	0.06104 ± 0.00024	1.1455 ± 0.0010	5973 ± 24	5930 ± 32	5867 ± 32	145.6 ± 1.0	Pavona*	110	0.19	-0.15/≥0.35	23°12'45.6	150°58'09.7
HUMP 010	3.4909 ± 0.0021	3.6409 ± 0.0049	205.6 ± 0.7	0.07067 ± 0.00023	1.1442 ± 0.0009	6953 ± 24	6928 ± 25	6864 ± 25	147.1 ± 1.0	Branching*	250	0.1	-0.15/≥0.35	23˚12'44.1	150˚58'10.1
HUMP 011	2.8329 ± 0.0018	0.4291 ± 0.0015	1283.4 ± 6.8	0.06407 ± 0.00026	1.1449 ± 0.0012	6281 ± 27	6273 ± 27	6209 ± 27	147.5 ± 1.2	Cyphastrea	75	0.4	±0.15	23˚12'44.4	150˚58'10.7
HUMP 012	3.0712 ± 0.0014	1.2108 ± 0.0022	514.7 ± 2.0	0.06688 ± 0.00022	1.1440 ± 0.0010	6570 ± 23	6558 ± 24	6495 ± 24	146.7 ± 1.0	Porites Cylindrica*	90	0.46	-0.15/≥0.35	23˚12'44.4	150˚58'11.0
HUMP 013	3.0504 ± 0.0022	12.409 ± 0.021	48.6 ± 0.2	0.06519 ± 0.00029	1.1443 ± 0.0009	6398 ± 30	6310 ± 37	6247 ± 37	147.1 ± 0.9	Porites Cylindrica*	110	0.58	-0.15/≥0.35	23˚12'44.9	150˚58'11.5
HUMP 014	3.1765 ± 0.0019	6.4363 ± 0.0087	95.8 ± 0.4	0.06395 ± 0.00026	1.1443 ± 0.0011	6272 ± 27	6227 ± 29	6163 ± 29	147.0 ± 1.1	Porites Cylindrica*	210	0.58	-0.15/≥0.35	23˚12'44.8	150˚58'11.4
HUMP 015	3.5019 ± 0.0016	2.3805 ± 0.0042	298.8 ± 1.3	0.06694 ± 0.00028	1.1437 ± 0.0007	6579 ± 28	6561 ± 28	6497 ± 28	146.4 ± 0.7	Porites Cylindrica*	70	0.59	-0.15/≥0.35	23˚12'45.1	150˚58'11.3
HUMP 016	3.5124 ± 0.0021	2.8456 ± 0.0033	248.9 ± 0.8	0.06645 ± 0.00022	1.1448 ± 0.0009	6522 ± 23	6502 ± 23	6438 ± 23	147.5 ± 0.9	Porites Cylindrica*	100	0.64	-0.15/≥0.35	23˚12'45.3	150˚58'11.3
HUMP 017	3.3614 ± 0.0021	2.2358 ± 0.0039	265.5 ± 0.9	0.05820 ± 0.00017	1.1426 ± 0.0009	5702 ± 18	5685 ± 18	5621 ± 18	145.0 ± 0.9	Porites Cylindrica*	200	0.1	-0.15/≥0.35	23˚12'46.8	150˚58'07.7
HUMP 018	2.8587 ± 0.0014	0.4336 ± 0.0012	219.2 ± 1.9	0.010959 ± 0.000090	1.1468 ± 0.0007	1048 ± 9	1041 ± 9	977 ± 9	147.3 ± 0.7	Cyphastrea	230	0.1	±0.15	23˚12'47.9	150˚58'08.2
HUMP 019	3.0813 ± 0.0014	0.4114 ± 0.0014	246.7 ± 2.0	0.010854 ± 0.000080	1.1460 ± 0.0013	1039 ± 8	1032 ± 8	968 ± 8	146.4 ± 1.3	Cyphastrea	170	0.2	±0.15	23˚12'46.7	150˚58'08.5
HUMP 020	3.4097 ± 0.0015	0.4805 ± 0.0014	1176.3 ± 6.3	0.05464 ± 0.00025	1.1463 0.0011	5328 ± 25	5321 ± 25	5257 ± 25	148.6 ± 1.1	Porites	150	0.3	±0.15	23˚12'47.1	150˚58'08.7
HUMP 021	2.7724 ± 0.0017	0.054188 ± 0.00066	9150± 120	0.05867 ± 0.00023	1.1449 ± 0.0012	5739 ± 24	5734 ± 24	5670 ± 24	147.2 ± 1.3	Cyphastrea	180	0.7	±0.15	23˚12'46.4	150˚58'11.1
HUMP 022	3.2932 ± 0.0014	1.8478 ± 0.0023	327.9 ± 1.3	0.06065 ± 0.00024	1.1452 ± 0.0007	5935 ± 24	5920 ± 24	5856 ± 24	147.6 ± 0.7	Porites	210	0.66	±0.15	23˚12'46.4	150˚58'11.0

Sample Name	U (ppm)	^{232}Th (ppb)	(^{230}Th/ ^{232}Th)	(^{230}Th/^{238}U)	(^{234}U/^{238}U)	Uncorr. Age (a)	Corr. Age (b)	Age (yr BP - 1950)	initial δ^{234}U (c)	Genus/Growth form (*)	Coral Diam. (cm)	Elev. (m)	Elevation error	Latitude	Longitude
HUMP 023	3.5361 ± 0.0016	1.2274 ± 0.0019	546.7 ± 2.0	0.06254 ± 0.00021	1.1456 ± 0.0008	6123 ± 21	6112 ± 21	6048 ± 21	148.2 ± 0.8	Leptastrea	130	0.68	±0.15	23˚12'46.2	150˚58'11.0
NKI 001	3.1841 ± 0.0022	0.5042 ± 0.0016	1018.0 ± 6.0	0.05313 ± 0.00027	1.1422 ± 0.0008	5196 ± 27	5189 ± 27	5125 ± 27	144.3 ± 0.8	Porites	250	0.39	±0.15	23°04'57.6	150°53'52.8
NKI 002	2.8433 ± 0.0014	7.5792 ± 0.0084	63.9 ± 0.2	0.05615 ± 0.00017	1.1457 ± 0.0010	5482 ± 18	5423 ± 23	5359 ± 23	148.0 ± 1.0	Porites	120	0.39	±0.15	23°04'57.6	150°53'52.2
NKI 003	2.9487 ± 0.0011	0.0203 ± 0.0010	2238 ± 14	0.05082 ± 0.00018	1.1434 ± 0.0008	4960 ± 18	4954 ± 18	4891 ± 18	145.5 ± 0.8	Cyphastrea	70	0.63	±0.15	23°04'52.7	150°53'51.7
NKI 004	3.2567 ± 0.0015	2.5073 ± 0.0039	205.9 ± 0.9	0.05224 ± 0.00021	1.1438 ± 0.0010	5101 ± 21	5081 ± 21	5017 ± 21	145.9 ± 1.0	Porites	110	0.63	±0.15	23°04'52.4	150°53'51.6
NKI 005	3.2033 ± 0.0014	3.7824 ± 0.0044	134.1 ± 0.5	0.05218 ± 0.00018	1.1448 ± 0.0009	5089 ± 19	5061 ± 20	4997 ± 20	147.0 ± 1.0	Porites	100	0.63	±0.15	23°04'52.4	150°53'51.1
NKI 006	2.6269 ± 0.0012	0.2884 ± 0.0014	1382.9 ± 9.6	0.05004 ± 0.00024	1.1454 ± 0.0008	4874 ± 25	4867 ± 25	4803 ± 25	147.4 ± 0.8	Favites	90	0.73	±0.15	23°04'50.5	150°53'50.8
NKI 007	3.2162 ± 0.0011	0.2171 ± 0.0011	2202 ± 15	0.04899 ± 0.00020	1.1450 ± 0.0010	4770 ± 21	4764 ± 21	4701 ± 21	147.0 ± 1.0	Cyphastrea	100	0.73	±0.15	23°04'49.8	150°53'50.9
NKI 008	3.2828 ± 0.0016	10.544 ± 0.013	50.1 ± 0.2	0.05303 ± 0.00025	1.1442 ± 0.0010	5177 ± 25	5108 ± 30	5044 ± 30	146.4 ± 1.0	Porites	90	0.73	±0.15	23°04'49.6	150°53'50.9
NKI 009	2.9348 ± 0.0012	3.4989 ± 0.0050	130.6 ± 0.5	0.05132 ± 0.00018	1.1443 ± 0.0010	5006 ± 19	4977 ± 20	4913 ± 20	146.4 ± 1.0	Porites	80	0.73	±0.15	23°04'49.2	150°53'50.6
NKI 010	2.7258 ± 0.0012	0.5414 ± 0.0016	792.8 ± 4.7	0.05189 ± 0.00027	1.1448 ± 0.0008	5061 ± 27	5052 ± 27	4988 ± 27	146.9 ± 0.8	Favites	160	0.77	±0.15	23°04'48.5	150°53'49.3
NKI 011	3.2569 ± 0.0014	0.0837 ± 0.0010	5687 ± 72	0.04819 ± 0.00020	1.1475 ± 0.0008	4680 ± 20	4676 ± 20	4612 ± 20	149.5 ± 0.8	Cyphastrea	120	0.77	±0.15	23°04'48.4	150°53'48.9
NKI 012	2.7301 ± 0.0015	3.1752 ± 0.0039	158.5 ± 0.7	0.06075 ± 0.00024	1.1448 ± 0.0010	5948 ± 25	5919 ± 26	5856 ± 26	147.2 ± 1.0	Porites	200	0.77	±0.15	23°04'48.0	150°53'49.0
NKI 013	2.8941 ± 0.0011	0.3032 ± 0.0011	1716 ± 10	0.05925 ± 0.00027	1.1452 ± 0.0008	5795 ± 27	5789 ± 27	5725 ± 27	147.6 ± 0.8	Cyphastrea	140	0.79	±0.15	23°04'47.1	150°53'49.3
GKI 001	3.2827 ± 0.0012	2.3108 ± 0.0033	131.0 ± 0.6	0.03039 ± 0.00015	1.1445 ± 0.0007	2938 ± 15	2919 ± 15	2856 ± 15	145.7 ± 0.7	Porites	130	0.29	±0.15	23°11'48.2	150°56'19.4
GKI 002	3.1006 ± 0.0012	11.496 ± 0.017	14.5 ± 0.1	0.01772 ± 0.00012	1.1456 ± 0.0009	1702 ± 12	1623 ± 23	1559 ± 23	146.3 ± 0.9	Porites	90	0.1	±0.15	23°11'47.8	150°56'18.8
GKI 003	2.9822 ± 0.0011	4.4127 ± 0.0058	33.5 ± 0.3	0.01632 ± 0.00012	1.1456 ± 0.0008	1566 ± 12	1532 ± 15	1468 ± 15	146.3 ± 0.8	Porites	130	0.17	±0.15	23°11'47.3	150°56'19.5
GKI 004	2.7803 ± 0.0010	1.4822 ± 0.0023	96.6 ± 0.7	0.01698 ± 0.00012	1.1482 ± 0.0011	1626 ± 12	1611 ± 13	1547 ± 13	148.9 ± 1.1	Cyphastrea	150	0.05	±0.15	23°11'45.9	150°56'19.8
GKI 005	3.1125 ± 0.0010	7.356 ± 0.011	23.5 ± 0.2	0.01827 ± 0.00011	1.1448 ± 0.0009	1756 ± 11	1704 ± 17	1640 ± 17	145.6 ± 0.9	Porites	50	-0.07	±0.15	23°11'44.9	150°56'19.6
GKI 007#	3.1193 ± 0.0010	25.717 ± 0.034	6.8 ± 0.1	0.01859 ± 0.00014	1.1478 ± 0.0007	1783 ± 14	1611 ± 45	1548 ± 45	147.9 ± 0.9	Porites	70	0.12	±0.15	23°11'46.0	150°56'20.1
GKI 008	3.0879 ± 0.0013	2.3435 ± 0.0033	110.8 ± 0.4	0.02770 ± 0.00010	1.1456 ± 0.0009	2672 ± 10	2652 ± 11	2588 ± 11	146.7 ± 0.9	Cyphastrea	100	0.2	±0.15	23°11'45.4	150°56'21.4
GKI 009	3.0791 ± 0.0014	0.7192 ± 0.0014	867.2 ± 4.1	0.06676 ± 0.00029	1.1442 ± 0.0010	6557 ± 30	6548 ± 30	6484 ± 30	146.9 ± 1.1	Goniastrea	40	0.52	±0.15	23°11'45.3	150°56'24.0

Ratios in parentheses are activity ratios calculated from atomic ratios using decay constants of Cheng et al. (2000) (2000) (2000) (2000)(a) Uncorrected ^{230}Th age was calculated using Isoplot/EX 3.0 program (Ludwig, 2003).(b) ^{230}Th ages were corrected using the two-component correction method of Clark et al. (2014a) Th/^{232}Th$_{hyd}$ and ^{230}Th/^{232}Th$_{det}$ activity ratios of 1.08 ± 0.23 and 0.62 ± 0.14, respectively.
(c) ^{234}U = [(^{234}U/^{238}U) − 1] × 1000. * Indicates non- microatoll # Sample removed from analysis.# Sample removed from analysis.

Figures

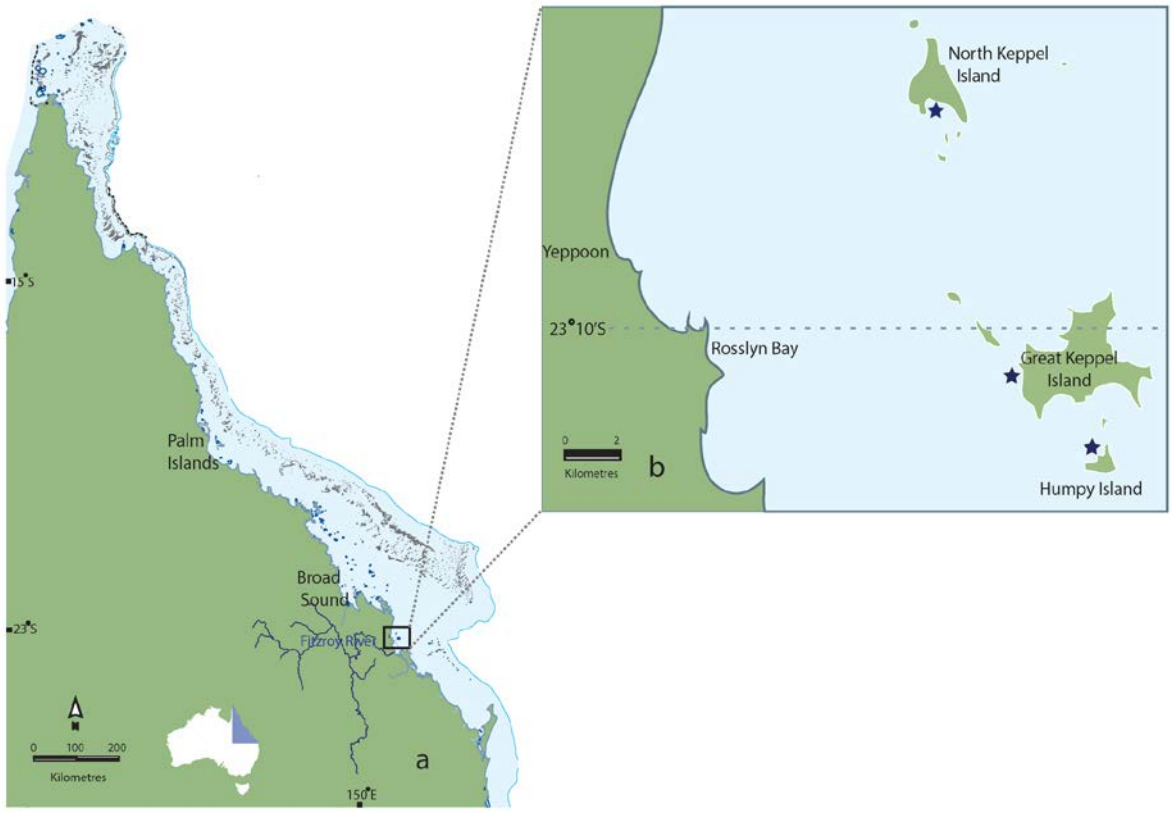

Figure 1: Queensland, Australia, showing the Great Barrier Reef (in grey) and the location of the Keppel Islands. Blue line is 200 m isobath; the continental shelf is shaded in blue; b) Locations of the Keppel Islands (North Keppel, Great Keppel and Humpy Islands) and fossil reef flat sites (black stars).

Figure 2: a) Microatoll at Great Keppel Island. Note thick unconsolidated sediment surrounding sample. b) Modern reef seaward of relict reef at Great Keppel Island dominated by branching and plate *Acropora* sp. c) Surface morphology of *Cyphastrea* sp. microatoll demonstrating radiation of corallites from the centre of the colony d) Large microatoll at the seaward edge of North Keppel Island reef (survey rod in centre of microatoll is ~1.3m)

.

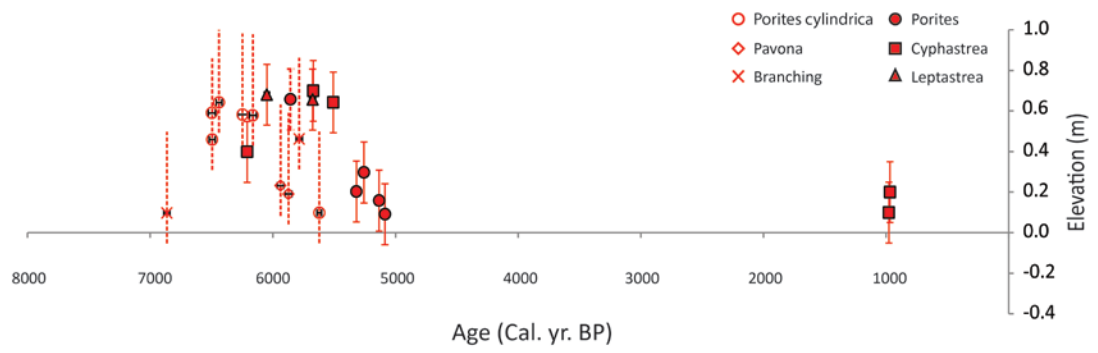

Figure 3: Uranium-thorium (U-Th) age-elevation data for microatolls and non-microatoll samples from Humpy Island, Great Barrier Reef, Australia. Solid symbols are microatoll samples (elevation errors of ±0.15 m; see methods). Open symbols are non-microatoll samples. As non-microatoll corals are not constrained equally by the air-sea interface, positive elevation errors are given as ≥0.35 m. Elevation is metres (m) above present mean low water spring tide. U-Th ages are years before present (yr. BP; before 1950) with errors at 2σ level (N.B. some age error bars are smaller than symbol width).

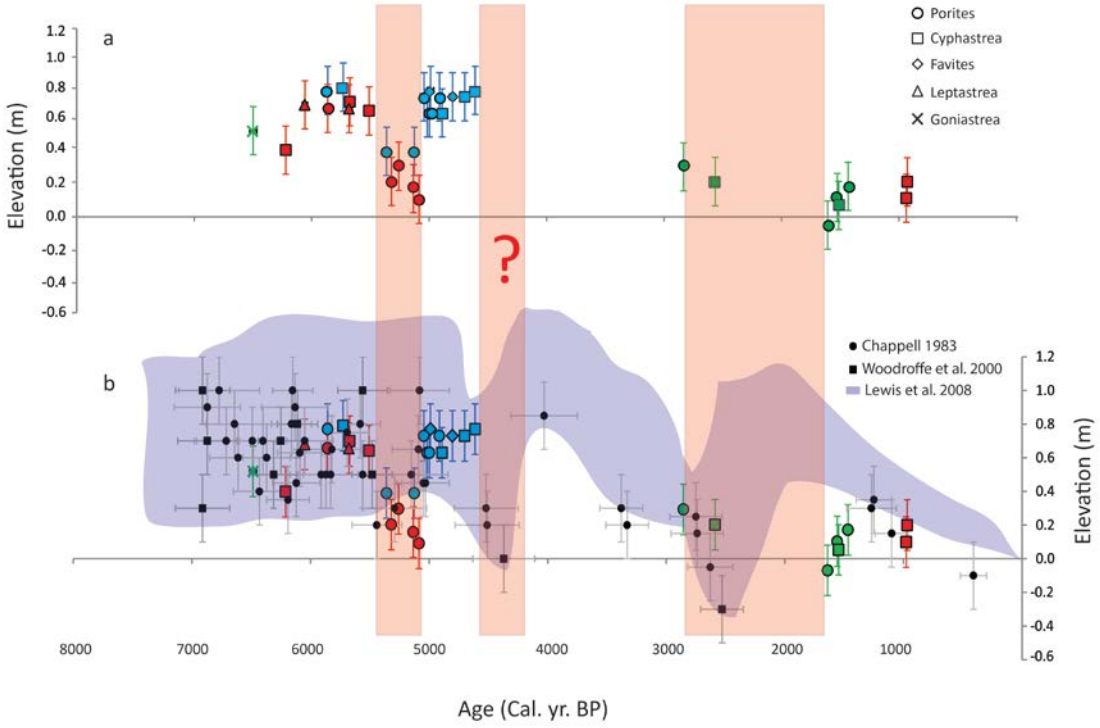

Figure 4: a) Uranium-Thorium (U-Th) age-elevation data for microatolls from the Keppel Islands, Great Barrier Reef (GBR), Australia; Great Keppel Island (GKI; green), North Keppel Island (NKI; blue) and Humpy Island (HUMP; red). Elevation is metres (m) above present mean low water Spring tide. U-Th ages are years before present (yr. BP; before 1950) with errors at 2σ level (N.B. some age error bars are smaller than symbol width). b) Microatoll data from the Keppel Islands (same as [a]) compared to previously published recalibrated (Lewis et. al 2008) microatoll data from the Great Barrier Reef; black circles - Chappell (1983) minimum elevation and grey shaded area – Lewis et al. (2008) sea level envelope for the Australian east coast. Shaded red bars are periods of suggested relative sea level (RSL) oscillations.

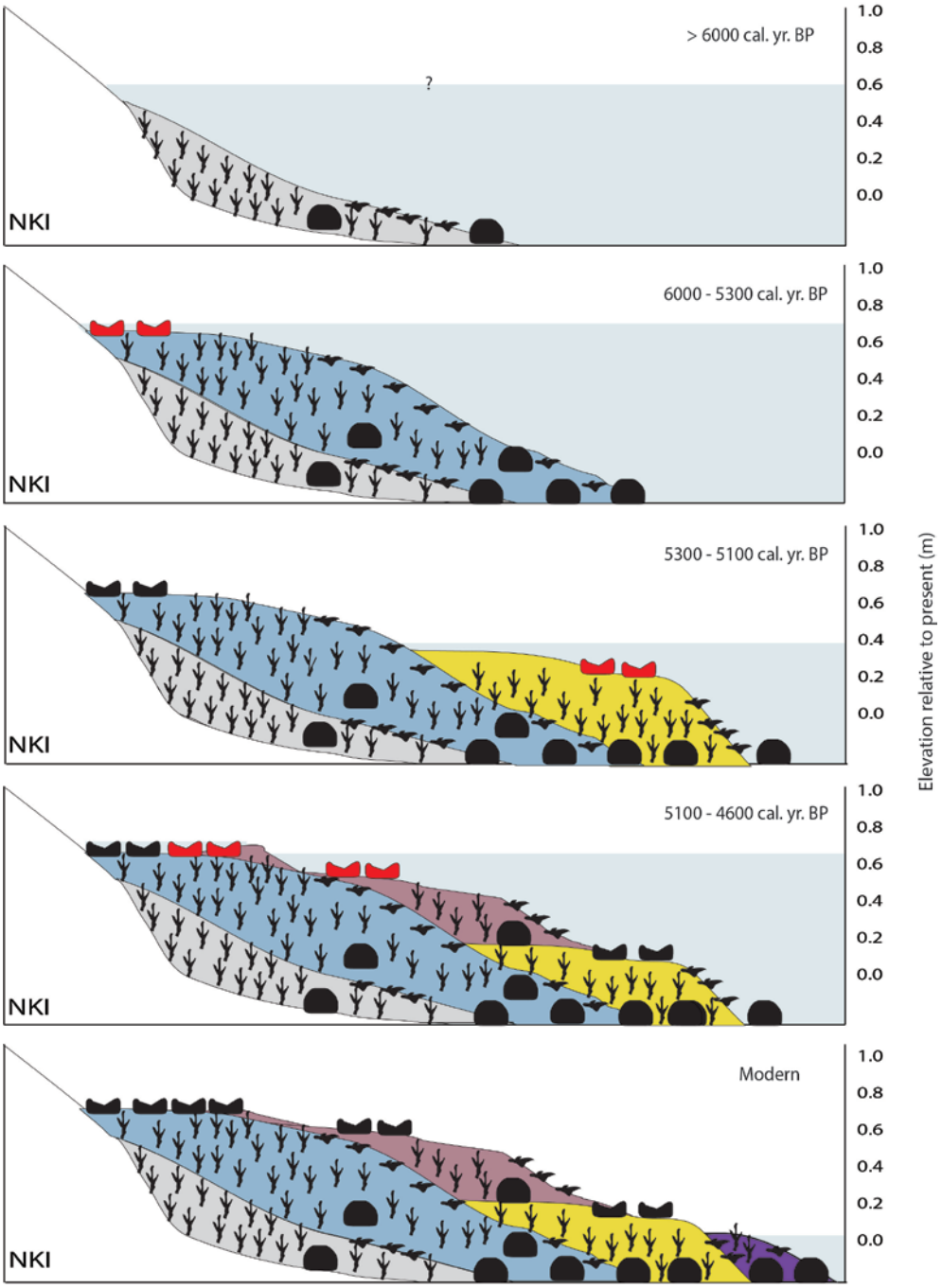

Figure 5: Schematic of inferred Holocene reef flat development at North Keppel Island, Great Barrier Reef, Australia. Microatoll positions are based on actual position on the reef flat and reef age is from U-Th derived ages. Elevation is metres relative to present mean low water spring tide. Red microatoll symbols represent those being formed at that time period (i.e. living); black microatoll symbols represent fossil corals at that time period. Blue shaded area represents RSL for each phase. N.B. Subsurface corals are an assumption based on general models of reef development.

Supplementary

Supplementary 1: Keppel Islands

Situated ~18 km from the Queensland coastal town of Yeppoon and ~40 km north of the mouth of the Fitzroy River (Fig. 1 main text), the Keppel Islands group is impacted by intermittent flood plumes and high turbidity events. It has been suggested that throughout the Holocene, suspended sediment loads from flood events were likely to be relatively high in the Fitzroy River basin due to naturally sparse vegetative cover in the region (Douglas et al., 2006). However, commencing in 1962 as part of the Brigalow Land Development Fitzroy Basin Scheme, 4.5 million hectares of native vegetation were cleared for agricultural and grazing development (Cowie et al., 2007). Long-term monitoring of these sites indicate an increase in run-off within cleared catchments from 5% to 9-11% (Cowie et al., 2007). Recent major flood events have resulted in mass mortality of corals in the Keppel Islands; most notably in 1991 (up to 85% mortality; Van Woesik, 1991) and 2011 (up to 100% in some locations; Jones and Berkelmans, 2014). Mass coral bleaching due to positive thermal anomalies combined with increased turbidity were also documented in this region during the 2002 and 2006 El Niño events, with up to 100% of coral affected to some degree in both events, and ~40% mortality reported in 2006 (GBRMPA Elvidge et al., 2004, 2006). These acute and relatively frequent disturbance events, in conjunction with the latitudinal marginality of the Keppel Island reefs, have been suggested as the primary driver for the dominant mono-specific stands of fast growing arborescent *Acropora* sp.[Fig. 2b – main text] (van Woesik and Done, 1997).

Supplementary 2: Uranium-thorium methods

All coral aragonite samples in the present study were prepared at the Radiogenic Isotope Facility, University of Queensland, Australia. Sub-samples of the coral were cut using a diamond blade saw, avoiding areas of obvious bio-erosion and surficial organics. For further removal of detrital and organic contaminants, sub-samples were crushed to a small grain size (~1 mm diameter) and soaked in 15% H_2O_2 overnight. The crushed sub-samples were then ultra-sonicated for 15 minutes, rinsed with Milli-Q water (18.2 $M\Omega cm^{-1}$), ultra-sonicated and rinsed until the water ran clear and then dried on a hotplate in the ultra-clean lab at <40˚C overnight. Once dried, approximately 15-50 mg of sample material was inspected under a compound microscope to select the purest aragonite material (i.e. no inclusion of

detritus/organics, sediment, calcite, or pyrite) for dating. Samples were spiked with a ^{233}U-^{229}Th mixed tracer and fully dissolved in a pre-cleaned Teflon beaker with 15.8N quartz-double-distilled HNO_3. To ensure complete homogenisation of the spike-sample solution, 3-4 drops of 30% H_2O_2 was added to remove any organic contaminants, each beaker was tightly capped, and the solution heated on a hotplate with a temperature setting of 120°C overnight. Once the sample was completely dissolved, each beaker was uncapped and the spiked solution dried down at 90°C on a hot-plate. Dried samples were then re-dissolved using 1-2 drops of 7N HNO_3 and passed through ion-exchange columns containing Bio-Rad AG1X8 anion resin to separate U from Th using column separation procedures described in detail in Clark et al. (2014). After collection, separate U and Th solutions were centrifuged at 3,500 rpm for 10 min, remixed in appropriate proportions based on quadrupole ICP-MS pre-screening of U-Th concentrations in the stock solutions, and then measured on a Nu Plasma multi-collector inductively coupled plasma mass spectrometer (MC ICP-MS) fully automatically using a Cetac ASX110 auto-sampler (see Clark et al., 2014b for detailed procedure).

Supplementary 3: U-Th validation

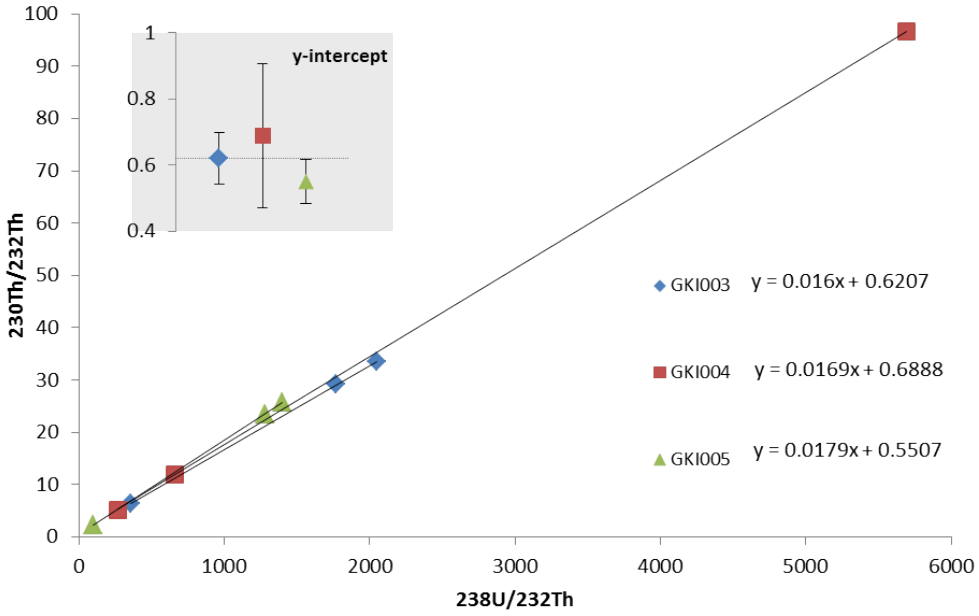

Supplementary Figure 3.1: $^{230}Th/^{232}Th$ versus $^{238}U/^{232}Th$ isochrons for three sub-samples of fossil microatolls from Great Keppel Island, Australia. Inset shows the isochron-inferred averaged $^{230}Th/^{232}Th$ ratio of 0.62 ± 0.14, which is comparable to the ratio reported by Clark et al. (2014a) for massive *Porites* corals from the Palm Islands of 0.64 ± 0.04.

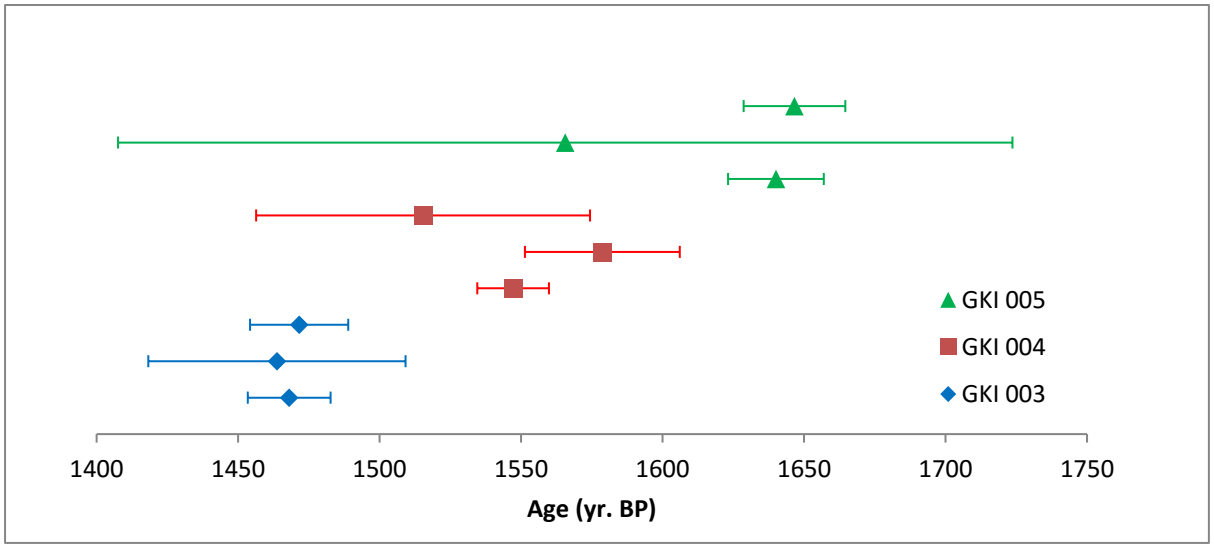

Supplementary Figure 3.2: Uranium-Thorium (U-Th) age determination of replicate samples with no cleaning, H_2O_2 cleaning and ultra-cleaned samples for the Keppel Islands, Great Barrier Reef. Note all replicate ages are within error (2σ). Largest age errors are "uncleaned" samples.

Supplementary 4: Microatoll locations and ages

Figure 4: Satellite imagery of islands and reefs of the Keppel Islands, Great Barrier Reef showing microatoll and non-microatoll coral locations and elevations relative to present (where present is equivalent to Mean Low water Spring tide). a) Humpy Island; b) Great Keppel Island and c) North Keppel Island.

a) Humpy Island microatolls (black) and non microatolls (red)

Humpy Island

N.B. - Black samples are microatolls, Red samples are non-microatolls.

Sample Name	Age (cal. yr. BP)	Elevation above present (m)	Sample Name	Age (cal. yr. BP)	Elevation above present (m)
HUMP 001	5676 ± 25	0.66	HUMP 013	6247 ± 37	0.58
HUMP 002	5507 ± 19	0.64	HUMP 014	6163 ± 29	0.58
HUMP 003	5939 ± 27	0.23	HUMP 015	6497 ± 28	0.59
HUMP 004	5785 ± 25	0.46	HUMP 016	6438 ± 23	0.64
HUMP 006	5134 ± 22	0.16	HUMP 017	5621 ± 18	0.10
HUMP 007	5086 ± 18	0.09	HUMP 018	977 ± 9	0.10
HUMP 008	5319 ± 29	0.20	HUMP 019	968 ± 8	0.20
HUMP 009	5867 ± 32	0.19	HUMP 020	5257 ± 25	0.30
HUMP 010	6864 ± 25	0.10	HUMP 021	5670 ± 24	0.70
HUMP 011	6209 ± 27	0.40	HUMP 022	5856 ± 24	0.66
HUMP 012	6495 ± 24	0.46	HUMP 023	6048 ± 21	0.68

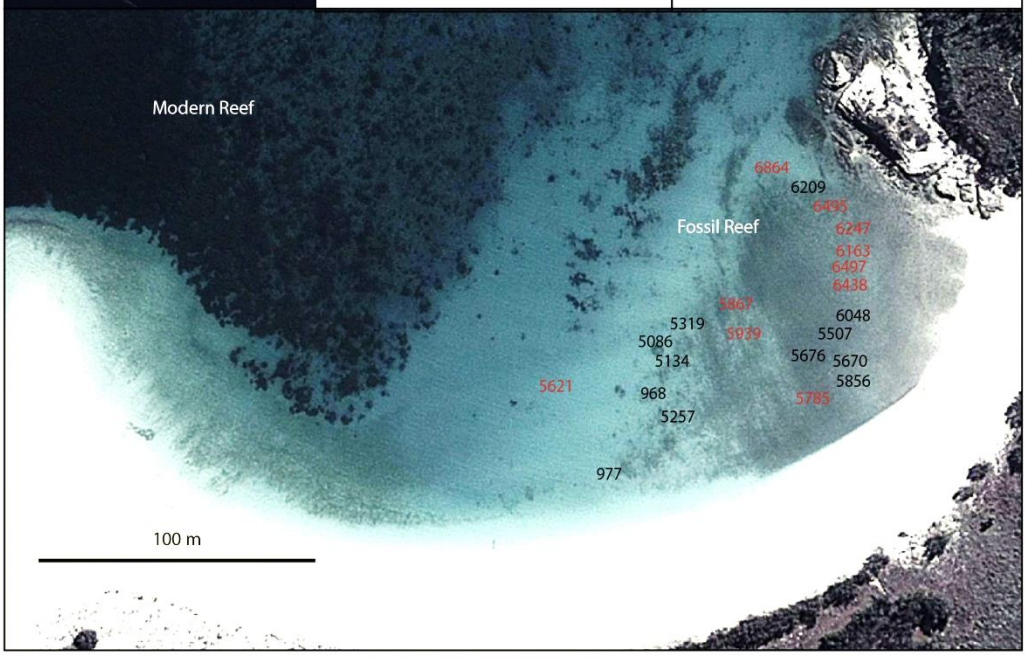

b) Great Keppel Island microatolls

Great Keppel Island		
Sample Name	Age (cal. yr. BP)	Elevation above present (m)
GKI 001	2856 ± 15	0.29
GKI 002	1559 ± 23	0.10
GKI 003	1468 ± 15	0.17
GKI 004	1547 ± 13	0.05
GKI 005	1640 ± 17	-0.07
GKI 007	1548 ± 45	0.12
GKI 008	2588 ± 11	0.20
GKI 009	6484 ± 30	0.52

c) North Keppel Island microatolls

North Keppel Island

Sample Name	Age (cal. yr. BP)	Elevation above present (m)
NKI MA 001	5125	0.39
NKI MA 002	5359	0.39
NKI MA 003	4891	0.63
NKI MA 004	5017	0.63
NKI MA 005	4997	0.63
NKI MA 006	4803	0.73
NKI MA 007	4701	0.73
NKI MA 008	5044	0.73
NKI MA 009	4913	0.73
NKI MA 010	4988	0.77
NKI MA 011	4612	0.77
NKI MA 012	5856	0.77
NKI MA 013	5725	0.79

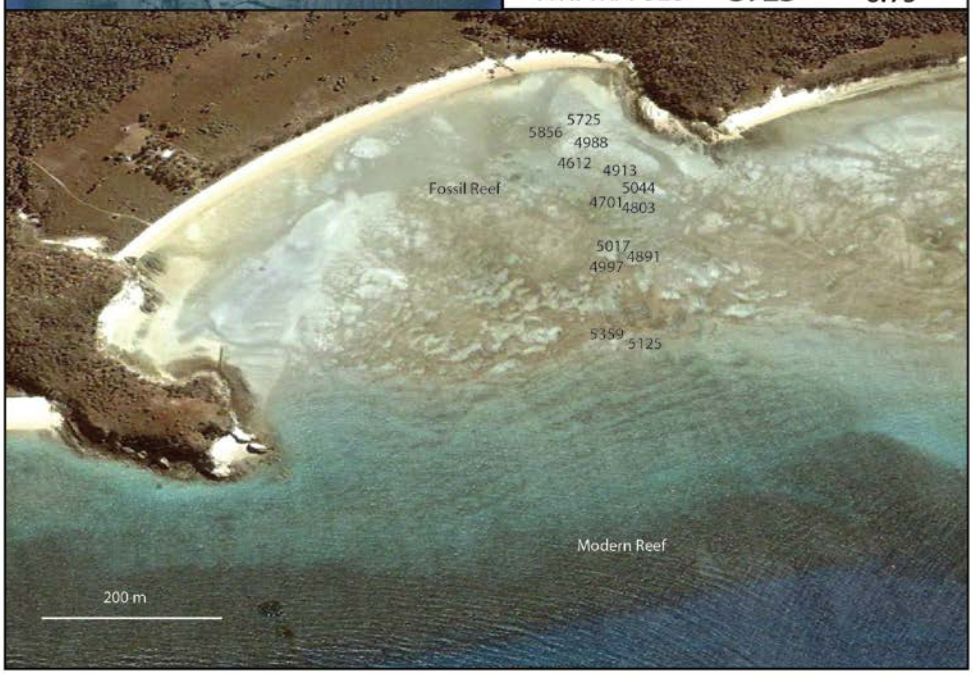

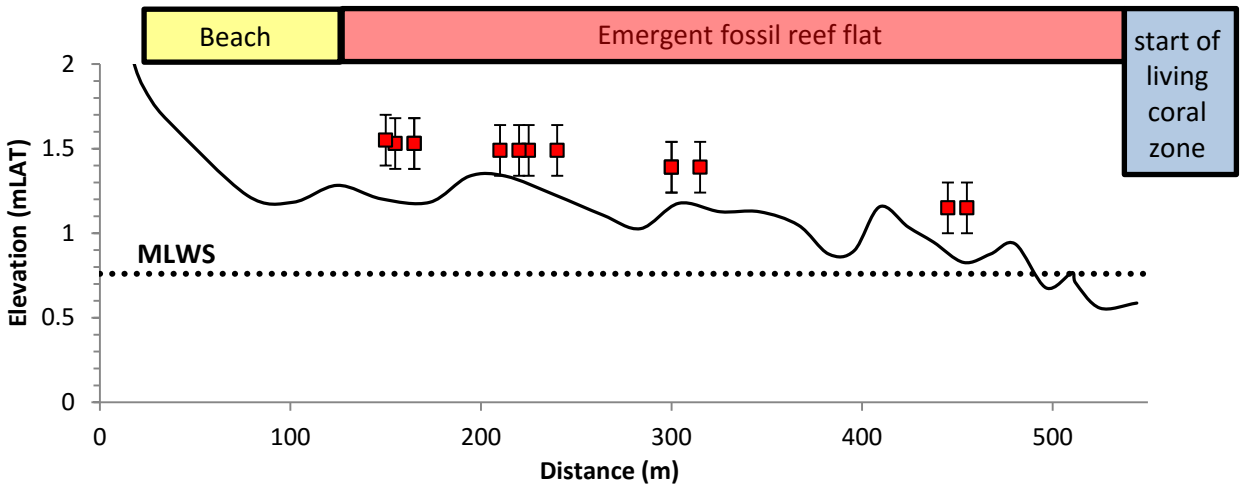

Supplementary Figure 4d: Substrate survey from shore to reef slope of the emerged fossil reef at North Keppel Island, Great Barrier Reef, Australia. Elevation is in metres lowest astronomical tide (MLAT), vertical distance is in metres. Dashed line is modern mean low water spring tide (MLWS) and red squares are approximate fossil microatoll locations across the reef flat with elevation error of ± 0.15m.

Supplementary Figure 4e: Photograph of a thin ponded modern microatoll (<0.05 m depth of living tissue) and small *Acropora* spp. recruits on the reef flat at North Keppel Island, southern Great Barrier Reef, Australia.

Supplementary References

Clark TR, Roff G, Zhao J-x, Feng Y-x, Done TJ, Pandolfi JM (2014a) Testing the precision and accuracy of the U–Th chronometer for dating coral mortality events in the last 100 years. Quaternary Geochronology 23:35-45

Clark TR, Zhao J-x, Roff G, Feng Y-x, Done TJ, Nothdurft LD, Pandolfi JM (2014b) Discerning the timing and cause of historical mortality events in modern Porites from the Great Barrier Reef. Geochimica et Cosmochimica Acta 138:57-80

Cowie BA, Thornton CM, Radford BJ (2007) The Brigalow Catchment Study: I; Overview of a 40-year study of the effects of land clearing in the Brigalow bioregion of Australia. Soil Research 45:479-495

Douglas GB, Ford PW, Palmer M, Noble RM, Packett R (2006) Fitzroy River Basin, Queensland, Australia. I. Identification of Sediment Sources in Impoundments and Flood Events. Environmental Chemistry 3:364

Elvidge C, D, B. Dietz J, B, Berkelmans R, Andréfouët S, Skirving W, Strong A, E, Tuttle B, T (2004) Satellite observation of Keppel Islands (Great Barrier Reef) 2002 coral bleaching using IKONOS data. Coral Reefs 23:123-132

Great Barrier Reef Marine Park Authority (2006) Great Barrier Reef coral bleaching surveys 2006 Research Publication 87, Townsville, Queensland

Jones AM, Berkelmans R (2014) Flood impacts in Keppel Bay, southern Great Barrier Reef in the aftermath of cyclonic rainfall. PloS one 9:84739

Lewis SE, Wu RAJ, Webster JM, Shields GA (2008) Mid-late Holocene sea-level variability in eastern Australia. Terra Nova 20:74-81

Van Woesik R (1991) Immediate impact of the January 1991 floods on the coral assemblages of the Keppel Islands Research Publication No 23. Great Barrier Reef Marine Park Authority, Townsville 1-33

Van Woesik R, Done TJ (1997) Coral communities and reef growth in the southern Great Barrier Reef. Coral Reefs 16:103-115

This page is intentionally left blank

Chapter 3

Holocene sea level oscillations on the Great Barrier Reef and links to climate

Leonard, N.D.[1], Welsh, K.J.[1], Clark, T.R.[1], Feng, Y-x.[1], Pandolfi, J.M.[2], Zhao, J-x.[1]

[1]School of Earth Sciences, The University of Queensland, Brisbane, Qld 4072, Australia

[2]Centre for Marine Science, Australian Research Council Centre of Excellence for Coral Reef Studies, School of Biological Sciences, The University of Queensland, Brisbane, Qld 4072, Australia

***Corresponding author: Nicole Leonard; email: nicole.leonard@uqconnect.edu.au**

Target Journal: Nature

Keywords: Holocene, sea level, microatolls, Great Barrier Reef, U-Th dating, oscillations, climate

Abstract

Rising sea level is of significant concern in the coming century, yet predicting the rate and magnitude of eustatic and relative sea level rise in response to global climate change is complex. Potential analogues are provided within the recent geological past, yet previous links between palaeo-climate and -sea level have been tenuous due to large age uncertainties and paucity in relative sea level records. Here we present a sea level history for the Great Barrier Reef, Australia derived from 94 high precision uranium-thorium dates of sub-fossil coral microatolls across a wide latitudinal range (11˚S – 20˚S). Our results provide evidence for two periods of relative sea level instability (>-0.3m) at ~5500 and 4600 years before present which coincide with significant reef “turn-off” events. We suggest that these sea level events may be synchronous with periods Indo-Pacific sea surface temperature anomalies, of dampened El Niño Southern Oscillation activity, rapid global cooling events and glacial advances. We conclude that the magnitude of these events suggests a eustatic/thermosteric contribution operating in conjunction with regional climatic controls.

Introduction

Within the coming century rising sea level is one of the greatest consequences of climate change (Haigh et al., 2014). Not only are millions of people living in coastal communities at threat of being displaced, but the vulnerabilities of coastal ecosystems are still relatively uncertain (Hamylton et al., 2014). At local to regional scales the immediate and future impacts of sea level rise (SLR) will be governed largely by the rate of change and adaptation thresholds (Hamylton et al., 2014), yet understanding the spatial heterogeneity of relative sea level (RSL) change in response to eustatic SLR is complex (Wong et al., 2014, Milne et al., 2009, Milne and Mitrovica, 2008). The Holocene offers a potential analogy for understanding future sea level variability with temperatures and sea levels higher than present comparable in magnitude to those projected for the coming century (Hodell et al., 2001). Yet whether sea level has oscillated significantly at centennial timescales in response to climate perturbations during the Holocene is controversial (Fairbridge, 1961, Baker and Haworth, 2000, Baker et al., 2005, Baker et al., 2001, Woodroffe and Horton, 2005, Lambeck et al., 2014).

Efforts to reconstruct eustatic sea level (ESL) since the termination of the Last Glacial Maximum (LGM) are often hampered by differentiating true eustatic signals from hydro-glacio- isostatic adjustment and local tectonics (Lambeck et al., 2014, Milne and Mitrovica, 2008). Therefore, precisely dated geological indicators in tectonically stable "far-field" regions (far from former glaciations) such as Australia offer the best potential to develop RSL histories that may shed light on global ESL history (Milne and Mitrovica, 2008, Lambeck, 2002, Lambeck and Nakada, 1990).

Geophysical models place the Australian East Coast (AEC) within Zone IV of post-glacial melt response (Clark et al., 1978) which is characterised by a mid-Holocene RSL highstand, representing the cessation of northern hemisphere ice melt (glacio-eustasy), followed by a RSL regression to present levels where ocean mass redistribution and hydro-isostasy dominate the signal (Nakada and Lambeck, 1989, Mitrovica and Milne, 2002). These models were supported by the seminal work of Chappell (1983) using coral microatoll data from the GBR which demonstrated a mid-Holocene highstand of 1.0 - 1.5m above modern levels by ~6000 years before present (yBP), followed by a linear (smooth fall) RSL regression to modern levels. However, reports of an oscillating or stepped RSL signal both relative to Australia (Woodroffe and Horton, 2005, Baker and Haworth, 2000, Baker et al., 2005, Fairbridge, 1961, McGowan and Baker, 2014) and elsewhere in the Indo-Pacific are

numerous (Hamanaka et al., 2012, Compton, 2001, Compton, 2006, Rashid et al., 2013). Whilst geophysical models are informative of centennial to millennial scale processes pertaining to rheological and water redistribution response of RSL to ESL changes, they do not take into consideration climatic perturbations that may have played a role in sub-centennial ESL or RSL variability.

Here we present the results of 94 high-precision uranium-thorium (U-Th) dates of coral microatolls (*Porites sp.*), in conjunction with elevation surveys, across ~ 10 degrees of latitude on the GBR (Fig 1b). Coral microatolls, especially *Porites* sp., are considered one of the most reliable palaeo-sea-level indicators, as the upper flat surface of the colony is constrained by the air-sea interface (Murray-Wallace and Woodroffe, 2014), with modern microatoll elevations lying generally within a vertical range of ~10cm of mean low water spting (MLWS) tide level (Chappell et al., 1983). We therefore report all elevations relative to modern site specific MLWS level (see Methods) with all U-Th ages reported as years before present (yBP), where present is defined as 1950.

Holocene sea level

Our results show that continental island reefs flats had developed by 7000 yBP along ~10˚ of latitude on the inshore GBR (Fig 1, Fig. 2; Extended Data Table 1). In the northern GBR (Fig 2a, c - High, Haggerstone and Gore Islands) microatolls are found at least 0.5 ± 0.15m above modern MLWS from ~7000 – 5500 yBP (Ext. data Fig. 1a). The timing of this highstand is in good agreement with previous data from the GBR (Lewis et al., 2008) and AEC (Sloss et al., 2007) although we found no evidence of RSLs >1m in the mid-Holocene. Higher mid-Holocene RSLs cannot be discounted however, as microatolls delineate the MLWS tide level. Lewis et al (2008) reported a systematic -0.5m offset between microatoll RSL data when compared data obtained from fixed biological indicator data likely due to site specific environmental conditions (e.g. wave energy). Furthermore, we acknowledge the limitation of deriving absolute RSLs using our methodology, and therefore concentrate on the relative elevations of the microatolls both within and between sites (instrumental precision ± 0.001m/30m; see Methods).

Compared to the Northern GBR, data from the central GBR indicates a rising RSL from 6900 to 6600 yBP at an average rate of ~1.4mmyr^{-1} (Fig. 2d – Stone Island). This rate of RSL rise is similar to a contemporaneous record from the Keppel Islands (southern GBR) of ~0.5 –

1.1mmyr^{-1} between ~6900 and 6200 yBP (Fig 2e; Leonard et al., 2016). This pattern of RSL rise in the southern and central GBR suggests that either a) the timing of the RSL highstand is latitudinally displaced due to a lag in water mass redistribution; or more likely b) hydro-isostatic adjustment occurred on this wider section of the continental shelf in the early mid-Holocene, with regional variation possibly related to the NE-SW structural lineament boundaries across the shelf in this region (Kleypas and Hopley, 1992).

After 5500 yBP reef flat growth ceased abruptly at High Island (Fig. 2c) and north Gore Island (Fig. 2a). Evidence that Holocene MLWS level was close to present MLWS levels between 5200 – 5000 yBP is found both at Fitzroy Island (-0.2m) and Hayman Island (~0.0m; Fig. 2c-d). At Alexandra Reef, a mainland fringing reef, substantial microatoll development at ~0.5 ± 0.15m above present did not commence until after 5000 yBP (Fig 2b). This later initiation was likely due to turbid conditions being unfavourable for substantial coral growth due to reworking of coastal pre-transgressive sediments (Larcombe and Woolfe, 1999). A rapid RSL lowering of -0.3 - 0.5m then occurs at Alexandra Reef ~4600 yBP lasting for at least 400 years (Fig. 2b). Whilst there is overlap of microatoll U-Th dates at the time of the transition from higher to lower RSL this can be explained by both our sampling strategy and the individual coral morphologies at this site. Whilst we sampled and measured the microatolls from the centre of the colony, the outer rims of the microatolls of the higher population displayed lowered rims indicating a RSL fall during their lifetime, whilst the lower population were planar suggesting they grew up to lower RSL (Supp. Fig. 1). This lowstand is also further supported by evidence from the leeward reef flat of Gore Island where microatolls occur close to the elevation (~+0.08m) of their modern counterparts between 4300 and 4000 yBP (Fig. 2a; Ext. data Fig.1b) and at Fitzroy Island where microatolls were found to be below their modern counterparts at 4400 yBP (Fig. 2c). After 4000 yBP RSL appears to have risen 0.2 - 0.3m to 2800 yBP, after which no further samples were dated in our present work.

Linear and Gaussian models (with 95% confidence bounds) of the microatoll data from the present study combined with previously published data from the Keppel Islands (obtained using the same methodology; Leonard et al., 2016) indicates that a four term Gaussian model is the best fit for the data (adjusted r-squared– 0.36) compared with the linear model (0.15; Suppl. Table 2). Significance in the normality of residuals ($p = 0.05$, $n=130$; Filliben, 1975) is also only achieved with an increase in terms (Gauss 4; Supp. Fig 4). Both the linear and lower term Gaussian functions (Gauss 1) over estimate the microatoll RSL height from 5500

– 5000 yBP and 4500 – 4000 yBP (negative residuals) and under estimate RSL from 5000 – 4500 yBP (positive residuals; Supp. Fig 4), supporting RSL oscillations in the mid-Holocene.

Rapid sea level lowering events

In agreement with previous AEC sea-level records and geophysical models (Fig.3a; Nakada and Lambeck, 1989) our data indicates a RSL regression from a mid-Holocene highstand at ~7000 yBP to present levels largely attributable to ocean syphoning (Chappell, 1983, Mitrovica and Milne, 2002). However we find the regression to be punctuated by rapid lowering events at 5500 and 4600 yBP (Fig. 2, Fig. 3a).

The RSL lowering event at 5500 yBP in the central GBR and the Keppel Islands of at least -0.4m after 5500 yBP (Leonard et al., 2016) also coincides with significant reductions in reef flat progradation (Smithers et al., 2006, Perry and Smithers, 2011) as well as a sudden reef "turn-off" in Moreton Bay by 5600 yBP (Fig. 2e; Leonard et al., 2013). The second RSL level lowering event of ~0.2 - 0.4m at 4600 yBP in the present study agrees well with the oscillation proposed by Lewis et al. (2008) which was based on a comprehensive review and re-calibration of sea level data from the AEC (Fig 2e). This negative oscillation is also synchronous with reef flat "turn-off" in the Keppel Islands (Leonard et al., 2016) and a significant reef "hiatus" event in the southern and northern GBR (Perry and Smithers, 2011). The lack of samples after 2800 yBP in our far north GBR record, albeit tentative, adds support to another possible RSL fall previously identified on the AEC (Lewis et al., 2008, Leonard et al., 2016). Despite the response of individual reefs being variable, the configuration of the combined RSL signal and synchronicity of re/initiation at some sites between these lowstand periods suggests a return to higher levels.

The question then remains as to the cause of these oscillations in the Australian coastal zone. Firstly, the coherence of the oscillations across an extensive latitudinal range rules out regional neotectonic activity or local reef/coastal dynamics, although local variations in the absolute level of the RSL reconstruction may be affected. Secondly, the centennial timescales of the oscillations precludes hydroisostasy/ocean syphoning as the primary driver however, these factors explain well the overall regressive trend following the highstand. Therefore, we infer that the oscillations detected in our record are of a eustatic, thermosteric or regional climatic origin, or a combination of these factors. In an attempt to resolve the mechanism/s

for these oscillations, we compare our data to both regional and global records of sea level, temperature and climatic conditions throughout the Holocene.

Eustasy

Mid- to late- Holocene eustatic sea level oscillations of over 1m, as first proposed by Fairbridge (1961), have been debated for over half a century. If the oscillations we present are of eustatic origin, then oscillations with comparable chronologies should be detectable in other tectonically stable far-field locations, although the magnitude may differ due to local response and the indicators used. As stated previously the oscillations we present here are in good agreement with data from elsewhere on the GBR and AEC at 5500, 4600 and after 2800 yBP (Lewis et al., 2008, Leonard et al., 2016). In the north west Pacific at Kodakara Island (Fig. 1A) disconformities (and hiatus) in an uplifted coral reef at ~5800, ~4200 and ~3200 yBP were reported, with the latter two events associated with sea level oscillations linked to northern hemisphere cooling (Hamanaka et al., 2012). Geomorphic evidence from the Atlantic coast of South Africa (Fig 1A) indicates a rapid SL drop to below present after ~5500 yBP and between 4800 - 4200 yBP (Compton, 2006) consistent with the GBR record presented here, although of much larger amplitudes. Facies and faunal interpretations on the coast of Bangladesh (Fig 1A) also record a stepped RSL regression with rapid lowering from 5900 – 5700 yBP, and at 5500 yBP and a minor regression after 4800 yBP (Rashid et al., 2013). Yet, a recent comprehensive analysis of far-field RSL and global ice volume data since the LGM by Lambeck et al. (Lambeck et al., 2014) reported that no oscillations of >0.2m were detectable during the last 6000 years of the Holocene. However, limitations apply to using differing sea-level indicators with various elevation errors from a number of studies, and may only provide information on the upper or lower limits of the SL signal within any one region (Lambeck et al., 2014).

The most chronologically continuous far-field RSL record for the Holocene is that from Kiritimati (Fig. 1AWoodroffe et al., 2012). Derived from microatoll age-elevation data, this record has two limitations as acknowledged by the authors (Woodroffe et al., 2012). Firstly, an unexpectedly large (~1m) geoidal gradient was discovered in the living microatoll populations across the atoll (Woodroffe et al., 2012). This was rectified by comparing fossil microatoll elevations to their nearest living counterparts, which is common practice, yet requires that the geoid has remained stable over millennia. More significantly, no living comparisons were available on the emergent atoll interior (Woodroffe and McLean, 1998), so

the interior populations were aligned with reef flat populations (Woodroffe et al., 2012). This method of elevation reduction, although unavoidable in this instance, is somewhat limiting as it negates the effects of ponding or tide attenuation associated with lagoon populations, which makes determination of absolute sea level difficult (Woodroffe and McLean, 1998). Separating the interior microatoll population data from reef flat data greatly affects the continuity of the record, resulting in a RSL history that cannot state explicitly against possible oscillations of >0.25m. The elevation of the fossil reef flat microatolls close to present sea level between 4700 – 4100 yBP and after 2800 yBP does not disagree with the timing of the negative SL oscillations proposed here for the GBR (Ext. data Fig 2b). Interestingly, the highest (uncorrected) microatoll population from the centre of the atoll occur between our lowstand periods, suggesting that populations inside the former reticulate lagoon may have been either isolated from oceanic influence or have reduced tidal flushing leading to coral demise between 4600 - 4000 yBP and 2800-2100 yBP (within dating uncertainties). Unfortunately the age errors (> ±500 years) of the two earliest reef flat samples between 6000 – 5000 yBP make comparisons with our data difficult. We therefore suggest that current studies in support of a stable ESL during the mid to late Holocene are still open to alternate interpretation.

Links to climate

At a regional scale, the largest annual to decadal modulating climate system on the GBR is the El Niño Southern Oscillation (ENSO), with La Niña (El Niño) associated with increased (decreased) precipitation in the Austral summer. Although the effect of El Niño/La Niña events on sea surface height (SSH) on the AEC is not well understood, in the central Pacific SSH can vary by as much as 0.3 – 0.4m due to the varying phases of ENSO (Woodroffe and McLean, 1998). Recent evidence also suggests that during La Niña phases low latitude glaciers advance (Francou et al., 2004) and Antarctic glacier melting is greatly reduced (Dutrieux et al., 2014) increasing the potential of terrestrial water storage in the Southern Hemisphere (SH).

Marine based reconstructions of ENSO variability on the GBR in the Holocene are restricted to short time windows. Sea surface temperature (SST-Sr/Ca) and sea surface salinity (SSS - $\delta^{18}O$) at ~6200 (re-calibrated ^{14}C) and 4700 yBP SSTs were shown to be ~1˚ warmer than present on the GBR with a suggested increase in evaporation and salinity ranges associated with strong flood events (Gagan et al., 1998, Roche et al., 2014). A multi-proxy terrestrial

record of pluvial conditions in southern Australia (Fig. 1A) also shows a La Niña like mean state of climate inferred from rainfall maximums at ~5800 – 5200, ~4500 and from ~3500 – 2700 yBP (Gliganic et al., 2014). These periods are also synchronous with phases of dampened El Niño events identified at Laguna Pallcacocha, Ecuador (Moy et al., 2002) and to cooling (or contraction) of the Indo-Pacific warm pool (IPWP) in the western Pacific (Fig. 1A; Supp. Fig. 3e-f; Abram et al., 2009). Coral based SST anomaly data from the Indo-Pacific also demonstrates warmer than present conditions ~6500 followed by a transition to cooler temperatures by ~5500 y BP (Fig. 3b; Sadler et al., 2016 and references therein).

At a broader scale, foraminiferal abundance and $\delta^{18}O$ analysis of a deep sea core off the South Australian coast (Fig. 1A –CORE 1) demonstrates distinct marine cooling events at 5800, 4300 and 2700 yBP of possibly ~2˚C (Ext. data Fig 3b), which are observed to be aligned with cooling events in the EPICA DOME C ice core (Moros et al., 2009). Significant SST cooling and ice expansion was also detected in the South Atlantic sector of the Southern Ocean between ~5500 – 4700 yBP (Fig. 1A – CORE 2; Hodell et al., 2001). In the northern hemisphere, evidence from Greenland (GISP2; Fig.1A) suggests rapid cooling events of 1.5 – 2.0˚C from 5600 – 5400 yBP, 5000 – 4700 yBP and a stepped cooling trend from 2100 – 1200 yBP (Ext. data Fig 2d; Alley, 2004). Rapid cooling also occurs in the North Atlantic (Bond Cycles 4, 3 and 2) at 5900, 4200 and 2800 yBP (Supp. Fig. 5c; Bond et al., 1997) which is aligned with periods of global glacier advances (Supp. Fig .5a; Mayewski et al., 2004, Denton and Karlén, 1973). With modelled projections of future SLR suggesting a 0.2 – 0.6m per +1°C (Church et al., 2013), a first order approximation of observed cooling events of ~1˚C in the northern and southern hemisphere during the Holocene may reconcile the RSL oscillations on the GBR. Although marine and terrestrial palaeo-temperature reconstructions within a given study are not indicative of global mean response, the synchronicity of cooling events and the RSL oscillations described here for the GBR are noteworthy and require further investigation.

Conclusions

Based upon measurements of coral microatoll elevations dated with high-precision U-Th techniques, our study is the first to show coherent rapid RSL oscillations represented across a large geographic range, supporting a model of SL instability throughout the Holocene. We suggest that although the response of individual coral reefs to RSL lowering events on the GBR has been variable throughout the Holocene, the broad scale synchronicity of responses

at 5500 and 4600 yBP and after 2800 yBP, co-occurring oscillations reported at other far-field locations, and links to documented climate shifts is noteworthy. The RSL oscillations detected in our study are of a much smaller magnitude (<0.5m) than previously suggested ESL oscillations (>1m). Although still open for debate, we propose that the RSL oscillations presented here are likely the result of ocean-atmosphere climatic perturbations affecting SSTs and sensitive mountain ice-cap and non-polar icesheet water storage balances in both the northern and southern hemispheres. These climate signals may have further been emphasized locally due to the response of the ENSO system.

With recent advancements in the accuracy and precision of geochronological techniques we suggest that future research effort be concentrated on high resolution SL data from other regions (where tectonic history is negligible) and on reconstructing high resolution palaeoclimate records, especially in the southern hemisphere. Establishing links between sea level and climate in the recent geological past, and refining RSL histories with regards to eustatic changes will ultimately improve models of future climate change scenarios, which are imperative for coastal planning and management.

Methods

As part of a multi-faceted project conducted under the National Environmental Research Program (NERP) numerous islands and coral reefs of the inshore GBR (11˚S to 23˚S) were visited between 2012 and 2014 (see Supp. 1 for site descriptions). Reef flats were visited at the lowset tides possible to be able to target fossil *Porites* sp. microatolls for RSL reconstructions. Corals were deemed to be *in situ* based on the orientation of corallite growth direction and relationship to the surrounding substrate (i.e. relative position of other fossil microatolls and other fossil reef features). It must be considered however that some samples may have been transported as a result of high energy storm/cyclone events so careful evaluation of the final data is necessary.

Using only a single type of sea-level indicator that is well constrained to a predictable level mean low water spring (MLWS) tide reduces the uncertainty of interpretation between sites and negates the need for elevation interpolation required when a variety of sea level indicators are used. As current hydro-and-glacio-isostatic models for the region are based on a limited number of previously published sea level records that are geographically and chronologically discontinuous, we present our age-elevation data separated into four

latitudinal zones ranging between 11˚S - 20˚S (<25km from the mainland) based on relative location of sites to each other, and width of the continental shelf. No correction has been applied for glacial isostatic adjustment (GIA), as although this would affect the absolute RSL elevation, it has little effect on the relative position of microatolls to each other within one region.

Sample collection and elevation surveys

Elevations of microatolls were taken using a Magnum-Proshot 4.7 Laser Level and Apache Lightning 2 receiver and referenced against a timed-still tide level and, where possible, modern living counterparts. The elevation was taken from the centre of each microatoll along with the coral surface diameter and GPS location (Ext. Data TBL 1). Elevations were calculated using the nearest tide gauge data from Maritime Safety Queensland (MSQ), time adjusted, and reduced to elevation relative to present mean low water spring tide (MLWS; semi-diurnal tides) or mean lowest low water (MLLW; diurnal tides) as given by the Australian Bureau of Meteorology. Although elevation errors between each sample within sites is minimal and a function of the laser level accuracy (± 0.001m/30m), we acknowledge the uncertainties of deriving absolute elevations from timed-still tide levels and assign a vertical error term to measurements of ± 18cm for Haggerstone Island and a conservative error term of ±15 cm to the remaining sites (based on the propagation of tidal error correction and tide tie points of the living population of microatolls at this site compared to modern MLWS/MLLW levels; Supp. Fig. 6).

Our previous dating experience indicated that the centre of the microatolls generally had lower detrital inclusions and micro-borings than the edges, which greatly improves the uranium-thorium (U-Th) age accuracy. Therefore, samples of each microatoll were collected for dating from the centre of each colony using a hammer and chisel. Sometimes the centre of the colony was more bio-eroded than the edge, or the exact centre unclear, so samples were taken from the edge of these colonies as indicated in as (E) in Extended Data Table 1.

U-Th dating

Samples were prepared for U-Th dating at the Radiogenic Isotope Facility, at The University of Queensland, using a pre-cleaning treatment as described in Leonard et al. (2015). Crushed and ultra-cleaned samples were picked manually under a binocular microscope to allow the best aragonite to be selected for dating (i.e. lacking any detritus, alteration or cements).

Picked samples were then weighed (15-50mg), spiked with a ^{233}U-^{229}Th mixed tracer and dissolved in pre-cleaned Teflon beakers with 15.8N quartz-double-distilled HNO_3. Additionally, 6-10 drops of 30% H_2O_2 was added to the dissolved sample solutions to remove any remaining organics and ensure complete homogenisation of the spike-sample solution. The Teflon beakers were capped, and the solution heated to 90˚C on a hotplate overnight to ensure complete digestion. The solution was then dried down completely on a hotplate set at 90°C. Following complete drying, samples were re-dissolved using 700µl of 7N HNO_3 and passed through pre-conditioned Bio-Rad AG1X8 anion resin ion-exchange columns to separate U from Th. Quadrupole ICP-MS pre-screening of the collected U and Th solutions was conducted, and where necessary, U and Th solutions were remixed in appropriate proportions. After thorough mixing of the U-Th solution samples were centrifuged at 3500 rpm for 10 minutes and then measured fully automatically using a Cetac ASX110 auto-sampler on a Nu Plasma multi-collector inductively coupled plasma mass spectrometer (MC ICP-MS) as described in Clark et al. (2014). Sample ages were calculated using the decay constants of Cheng et al. (2000) using Isoplot/Ex software (Ludwig, 2003), and corrected for initial detrital ^{230}Th using a two-component mixing correction scheme described by Clark et al. (2014).

Statistical Analysis

Relative sea level microatoll data from this study as well as U-Th dated microatoll data obtained from the Keppel Islands by Leonard et al. (2016) was combined to a derive a single sea level envelope for the GBR. The mode of RSL fall to present levels was tested by applying linear and Gaussian models (two – four terms employed) to the data points with 95% confidence in Matlab®. The significance of the normality of the residuals from the models were assessed using the correlation coefficient of the probability in PAST statistical programme.

Acknowledgements

This study was funded by the National Environmental Research Programme (NERP) Tropical Ecosystems Hub Project 1.3 ‘Characterising the cumulative impacts of global, regional and local stressors on the present and past biodiversity of the GBR’ to J-xZ, JMP, SGS, TRC, Y-xF and others, and Australian Research Council LIEF grant (LE0989067 for the purchase and installation of the MC-ICP-MS essential for this study) to J-xZ, JMP, Y-xF and others, as well as an Australian Postgraduate Award (APA) to NDL. We are grateful to the skippers and crews of the MV Coral Emperor, MV Phoenix and MV Adori.

References

Abram, N. J., Mcgregor, H. V., Gagan, M. K., Hantoro, W. S. & Suwargadi, B. W. 2009. Oscillations in the southern extent of the Indo-Pacific Warm Pool during the mid-Holocene. *Quaternary Science Reviews,* 28**,** 2794-2803.

Alley, R. B. 2004. GISP2 Ice Core Temperature and Accumulation Data. *In:* PALEOCLIMATOLOGY, I. P. W. D. C. F. (ed.). Boulder CO, USA: NOAA/NGDC Paleoclimatology Program.

Baker, R. & Haworth, R. J. 2000. Smooth or oscillating late Holocene sea-level curve? Evidence from the palaeo-zoology of fixed biological indicators in east Australia and beyond. *Marine Geology,* 163**,** 367-386.

Baker, R. G. V., Haworth, R. J. & Flood, P. G. 2001. Warmer or cooler late Holocene marine palaeoenvironments?: interpreting southeast Australian and Brazilian sea-level changes using fixed biological indicators and their δ18O composition. *Palaeogeography, Palaeoclimatology, Palaeoecology,* 168**,** 249-272.

Baker, R. G. V., Haworth, R. J. & Flood, P. G. 2005. An Oscillating Holocene Sea-level? Revisiting Rottnest Island, Western Australia, and the Fairbridge Eustatic Hypothesis. *Journal of Coastal Research,* Special Issue**,** 3-14.

Bond, G., Bonani, G., Showers, W., Cheseby, M., Lotti, R., Almasi, P., Demenocal, P., Priore, P., Cullen, H. & Hajdas, I. 1997. A Pervasive Millennial-Scale Cycle in North Atlantic Holocene and Glacial Climates. *Science,* 278**,** 1257-1266.

Chappell, J. 1983. Evidence for smoothly falling sea-level relative to North Queensland, Australia, during the past 6,000 yr. *Nature,* 302**,** 406-408.

Chappell, J., Chivas, A., Wallensky, E., Polach, H. & Aharon, P. 1983. Holocene palaeo-environmental changes, central to north Great Barrier Reef inner zone. *BMR Journal of Australian Geology and Geophysics,* 8**,** 223-235.

Cheng, H., Edwards, R. L., Hoff, J., Gallup, C. D., Richards, D. A. & Asmerom, Y. 2000. The half-lives of uranium-234 and thorium-230. *Chemical Geology,* 169**,** 17-33.

Church, J. A., Clark, P. U., Cazenave, A., Gregory, J. M., Jevrejeva, S., Levermann, A., Merrifield, M. A., Milne, G. A., Nerem, R. S., Nunn, P. D., Payne, A. J., Pfeffer, W. T., Stammer, D. & Unnikrishnan, A. S. 2013. Sea Level Change. *In:* STOCKER, T. F., QIN, D., PLATTNER, G.-K., TIGNOR, M., ALLEN, S. K., BOSCHUNG, J., NAUELS, A., XIA, Y., BEX, V. & MIDGLEY, P. M. (eds.) *Climate Change 2013: The Physical Science Basis Contribution of Working Group I to the Fifth Assessment Report of the Intergovernmental Panel on Climate Change.* Cambridge, United Kingdom and New York, NY, USA.

Clark, J. A., Farrell, W. E. & Peltier, W. R. 1978. Global changes in postglacial sea level: A numerical calculation. *Quaternary Research,* 9**,** 265-287.

Clark, T. R., Roff, G., Zhao, J.-X., Feng, Y.-X., Done, T. J. & Pandolfi, J. M. 2014. Testing the precision and accuracy of the U–Th chronometer for dating coral mortality events in the last 100 years. *Quaternary Geochronology,* 23**,** 35-45.

Compton, J. 2001. Holocene sea-level fluctuations inferred from the evolution of depositional environments of the southern Langebaan Lagoon salt marsh, South Africa. *The Holocene,* 11**,** 395-405.

Compton, J. S. 2006. The mid-Holocene sea-level highstand at Bogenfels Pan on the southwest coast of Namibia. *Quaternary Research,* 66**,** 303-310.

Denton, G. H. & Karlén, W. 1973. Holocene climatic variations—their pattern and possible cause. *Quaternary Research,* 3**,** 155IN1175-174IN2205.

Dutrieux, P., De Rydt, J., Jenkins, A., Holland, P. R., Ha, H. K., Lee, S. H., Steig, E. J., Ding, Q., Abrahamsen, E. P. & Schröder, M. 2014. Strong sensitivity of Pine Island ice-shelf melting to climatic variability. *Science,* 343**,** 174-178.

Fairbridge, R. W. 1961. Eustatic changes in sea level. *Physics and Chemistry of the Earth,* 4**,** 99-185.

Filliben, J. J. 1975. The Probability Plot Correlation Coefficient Test for Normality. *Technometrics,* 17**,** 111-117.

Francou, B., Vuille, M., Favier, V. & Cáceres, B. 2004. New evidence for an ENSO impact on low-latitude glaciers: Antizana 15, Andes of Ecuador, 0 28′ S. *Journal of Geophysical Research: Atmospheres*, 109.

Gagan, M. K., Ayliffe, L. K., Hopley, D., Cali, J., Mortimer, G., Chappell, J., Mcculloch, M. T. & Head, M. 1998. Temperature and surface-ocean water balance of the mid-Holocene tropical western Pacific. *Science*, 279**,** 1014-1018.

Gliganic, L. A., Cohen, T. J., May, J.-H., Jansen, J. D., Nanson, G. C., Dosseto, A., Larsen, J. R., Aubert, M., Stockholms, U., Naturvetenskapliga, F. & Institutionen För Naturgeografi Och, K. 2014. Late-Holocene climatic variability indicated by three natural archives in arid southern Australia. *The Holocene*, 24**,** 104-117.

Haigh, I. D., Wahl, T., Rohling, E. J., Price, R. M., Pattiaratchi, C. B., Calafat, F. M. & Dangendorf, S. 2014. Timescales for detecting a significant acceleration in sea level rise. *Nat Commun*, 5.

Hamanaka, N., Kan, H., Yokoyama, Y., Okamoto, T., Nakashima, Y. & Kawana, T. 2012. Disturbances with hiatuses in high-latitude coral reef growth during the Holocene: Correlation with millennial-scale global climate change. *Global and Planetary Change*, 80-81**,** 21-35.

Hamylton, S. M., Leon, J. X., Saunders, M. I. & Woodroffe, C. D. 2014. Simulating reef response to sea-level rise at Lizard Island: A geospatial approach. *Geomorphology*, 222**,** 151-161.

Hodell, D. A., Kanfoush, S. L., Shemesh, A., Crosta, X., Charles, C. D. & Guilderson, T. P. 2001. Abrupt Cooling of Antarctic Surface Waters and Sea Ice Expansion in the South Atlantic Sector of the Southern Ocean at 5000 cal yr B.P. *Quaternary Research*, 56**,** 191-198.

Kleypas, J. A. & Hopley, D. Reef Development Across a Broad Continental Shelf, Southern Great Barrier Reef, Australia. *In:* RICHMOND, R. H., ed. Seventh International Coral Reef Symposium, 1992 Guam. University of Guam Press, 1129-1141.

Lambeck, K. 2002. Sea level change from mid Holocene to recent time: an Australian example with global implications. *Geodynamics Series*, 29**,** 33-50.

Lambeck, K. & Nakada, M. 1990. Late Pleistocene and Holocene sea-level change along the Australian coast. *Palaeogeography, Palaeoclimatology, Palaeoecology (Global and Planetary Change Section)*, 89**,** 143-176.

Lambeck, K., Rouby, H., Purcell, A., Sun, Y. & Sambridge, M. 2014. Sea level and global ice volumes from the Last Glacial Maximum to the Holocene. *Proceedings of the National Academy of Sciences*, 111**,** 15296-15303.

Larcombe, P. & Woolfe, K. J. 1999. Terrigenous sediments as influences upon Holocene nearshore coral reefs, central Great Barrier Reef, Australia. *Australian Journal of Earth Sciences*, 46**,** 141-154.

Leonard, N. D., Welsh, K. J., Zhao, J.-X., Nothdurft, L. D., Webb, G. E., Major, J., Feng, Y.-X. & Price, G. J. 2013. Mid-Holocene sea-level and coral reef demise: U-Th dating of subfossil corals in Moreton Bay, Australia. *The Holocene*, 23**,** 1841-1852.

Leonard, N. D., Zhao, J.-X., Welsh, K. J., Feng, Y.-X., Smithers, S. G., Pandolfi, J. M. & Clark, T. R. 2016. Holocene sea level instability in the southern Great Barrier Reef, Australia: high-precision U–Th dating of fossil microatolls. *Coral Reefs*, 35**,** 625-639.

Lewis, S. E., Wu, R. a. J., Webster, J. M. & Shields, G. A. 2008. Mid-late Holocene sea-level variability in eastern Australia. *Terra Nova*, 20**,** 74-81.

Ludwig, K. R. 2003. Isoplot/Ex, version 3: a Geochronological Toolkit for Microsoft Excel. *Berkeley Geochronology Center Special Publications*.

Mayewski, P. A., Holmgren, K., Lee-Thorp, J., Rosqvist, G., Rack, F., Staubwasser, M., Schneider, R. R., Steig, E. J., Rohling, E. E., Curt Stager, J., Karlén, W., Maasch, K. A., David Meeker, L., Meyerson, E. A., Gasse, F. & Van Kreveld, S. 2004. Holocene climate variability. *Quaternary Research*, 62**,** 243-255.

Mcgowan, S. A. & Baker, R. G. 2014. How past sea-level changes can inform future planning: A case study from the Macleay River estuary, New South Wales, Australia. *The Holocene*, 24**,** 1591-1601.

Milne, G. A., Gehrels, W. R., Hughes, C. W. & Tamisiea, M. E. 2009. Identifying the causes of sea-level change. *Nature Geoscience*, 2**,** 471-478.

Milne, G. A. & Mitrovica, J. X. 2008. Searching for eustasy in deglacial sea-level histories. *Quaternary Science Reviews*, 27**,** 2292-2302.

Mitrovica, J. X. & Milne, G. A. 2002. On the origin of late Holocene sea-level highstands within equatorial ocean basins. *Quaternary Science Reviews,* 21**,** 2179-2190.

Moros, M., De Deckker, P., Jansen, E., Perner, K. & Telford, R. J. 2009. Holocene climate variability in the Southern Ocean recorded in a deep-sea sediment core off South Australia. *Quaternary Science Reviews,* 28**,** 1932-1940.

Moy, C. M., Anderson, D. M., Seltzer, G. O. & Rodbell, D. T. 2002. Variability of El Niño/Southern Oscillation activity at millennial timescales during the Holocene epoch. *Nature,* 420**,** 162-165.

Murray-Wallace, C. V. & Woodroffe, C. D. 2014. Quaternary sea-level changes: a global perspective. Cambridge;New York;: Cambridge University Press.

Nakada, M. & Lambeck, K. 1989. Late Pleistocene and Holocene sea-level change in the Australian region and mantle rheology. *Geophysical Journal International,* 96**,** 497-517.

Perry, C. & Smithers, S. 2011. Cycles of coral reef 'turn-on', rapid growth and 'turn-off' over the past 8500 years: a context for understanding modern ecological states and trajectories. *Global Change Biology,* 17**,** 76-86.

Rashid, T., Suzuki, S., Sato, H., Monsur, M. H. & Saha, S. K. 2013. Relative sea-level changes during the Holocene in Bangladesh. *Journal of Asian Earth Sciences,* 64**,** 136-150.

Roche, R. C., Perry, C. T., Smithers, S. G., Leng, M. J., Grove, C. A., Sloane, H. J. & Unsworth, C. E. 2014. Mid-Holocene sea surface conditions and riverine influence on the inshore Great Barrier Reef. *The Holocene,* 24**,** 885-897.

Sadler, J., Webb, G. E., Leonard, N. D., Nothdurft, L. D. & Clark, T. R. 2016. Reef core insights into mid-Holocene water temperatures of the southern Great Barrier Reef. *Paleoceanography***,** n/a-n/a.

Sloss, C. R., Murray-Wallace, C. V. & Jones, B. G. 2007. Holocene sea-level change on the southeast coast of Australia: a review. *The Holocene,* 17**,** 999.

Smithers, S. G., Hopley, D. & Parnell, K. E. 2006. Fringing and Nearshore Coral Reefs of the Great Barrier Reef: Episodic Holocene Development and Future Prospects. *Journal of Coastal Research***,** 175-187.

Wong, P. P., Losada, J.-P., Hinkel, J., Khattabi, A., Mcinnes, K. L., Saito, Y. & Sallenger, A. 2014. Coastal systems and low-lying areas. *In:* FIELD, C. B., BARROS, V. R., DOKKEN, D. J., MACH, K. J., MASTRANDREA, M. D., BILIR, T. E., CHATTERJEE, M., EBI, K. L., ESTRADA, R. C., GENOVA, R. C., GIRMA, B., KISSEL, E. S., LEVY, A. N., MACCRACKEN, S., MANSTRANDREA, P. R. & WHITE, L. L. (eds.) *Climate Change 2014: Impacts, Adaptation, and Vulnerability. Part A:Global and Sectoral Aspects. Contribution of Working Group II to the Fifth Assessment Report of the Intergovernmental Panel on Climate Change.* Cambridge, United Kingdom and New York, NY, USA.

Woodroffe, C. D. & Horton, B. P. 2005. Holocene sea-level changes in the Indo-Pacific. *Journal of Asian Earth Sciences,* 25**,** 29-43.

Woodroffe, C. D., Mcgregor, H. V., Lambeck, K., Smithers, S. G. & Fink, D. 2012. Mid-Pacific microatolls record sea-level stability over the past 5000 yr. *Geology,* 40**,** 951.

Woodroffe, C. D. & Mclean, R. F. 1998. Pleistocene morphology and Holocene emergence of Christmas (Kiritimati) Island, Pacific Ocean. *Coral Reefs,* 17**,** 235-248.

Figures

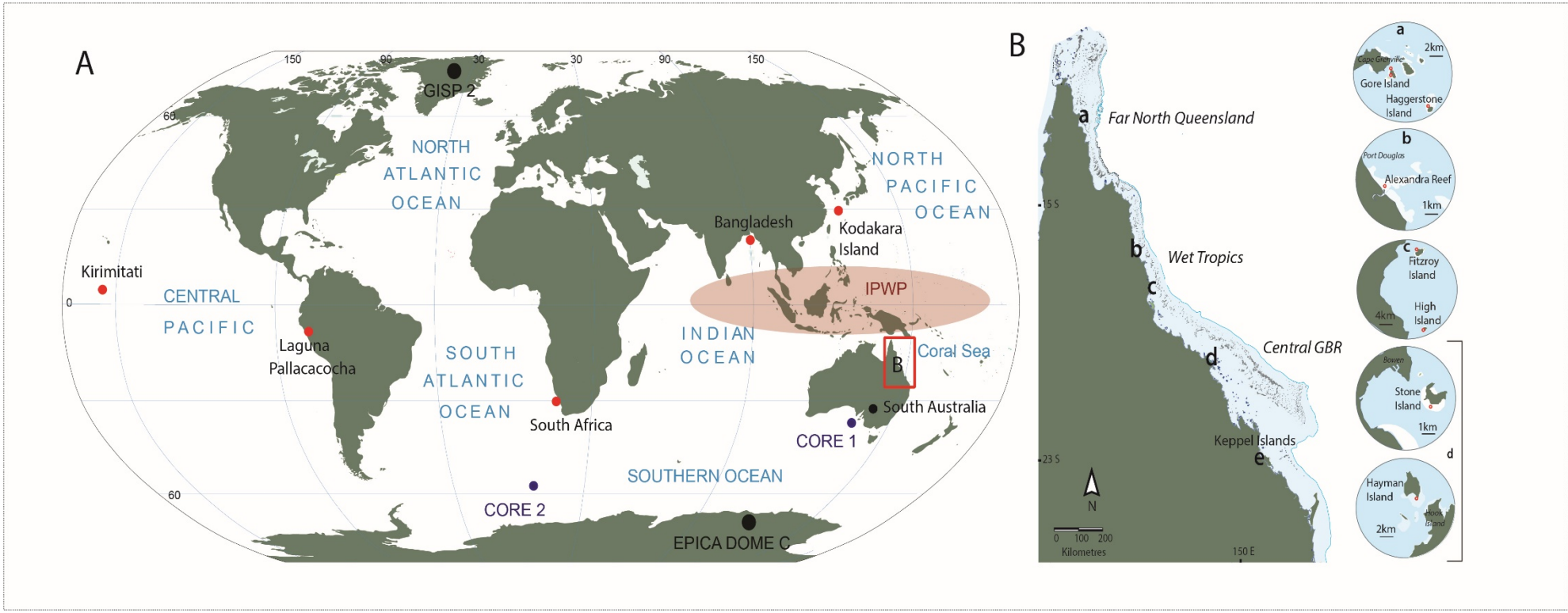

Figure 1: A) World map showing locations of climate and sea level data referred to in the main text of the present study. Red square with (B) indicates Queensland, Australia, the region of this study. B) Map of Queensland, Australia and the Great Barrier Reef showing the locations of sites in the present study, red circles indicating site locations within each region.

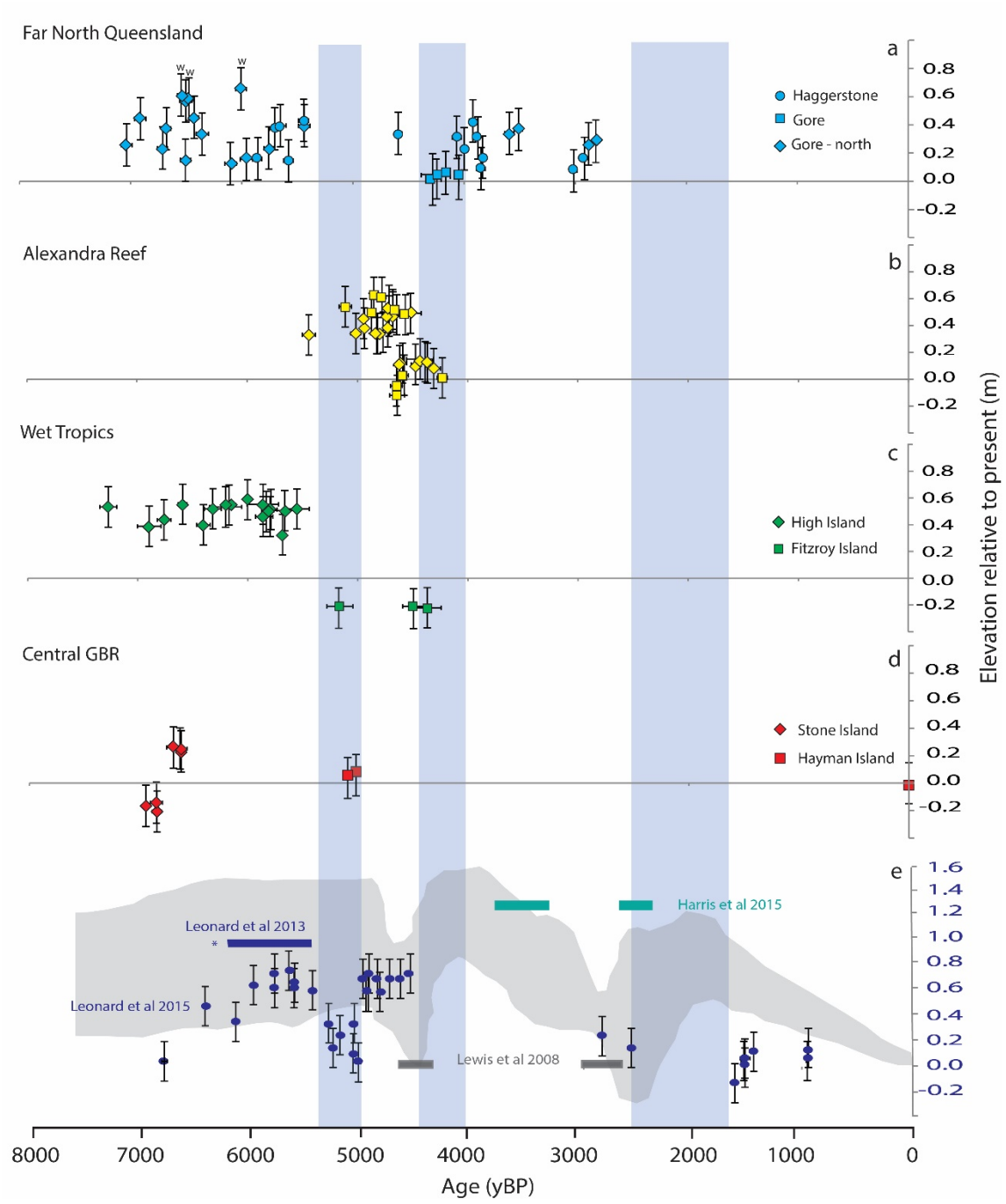

Figure 2: (a-d) U-Th age - elevation plots of fossil *Porites* microatolls for four regions on the Great Barrier Reef (GBR), Australia (e) compared with previously published sea-level records from the Australian east coast (AEC). Elevation is given as height in metres above present mean low water spring tides with errors of ±0.15m. All age errors are 2σ (note some age errors are smaller than the icon width). a) Far North (small w above samples from Gore North indicate windward location); b) Alexandra Reef – samples and surveys conducted in 2012 (squares) and 2013 (diamonds); c) High Island (diamonds) and Fitzroy Island (squares) and d) Stone Island (diamonds) and Hayman Island (squares). e) U-Th age – elevation plot of Leonard et al. 2016 from the Keppel Islands, southern GBR (blue circles), sea level envelope of Lewis et al. 2008 (grey shaded) with suggested lowstands (grey bars) and microatoll data from the southern Great Barrier Reef of Harris et al. 2015 (aqua bars).

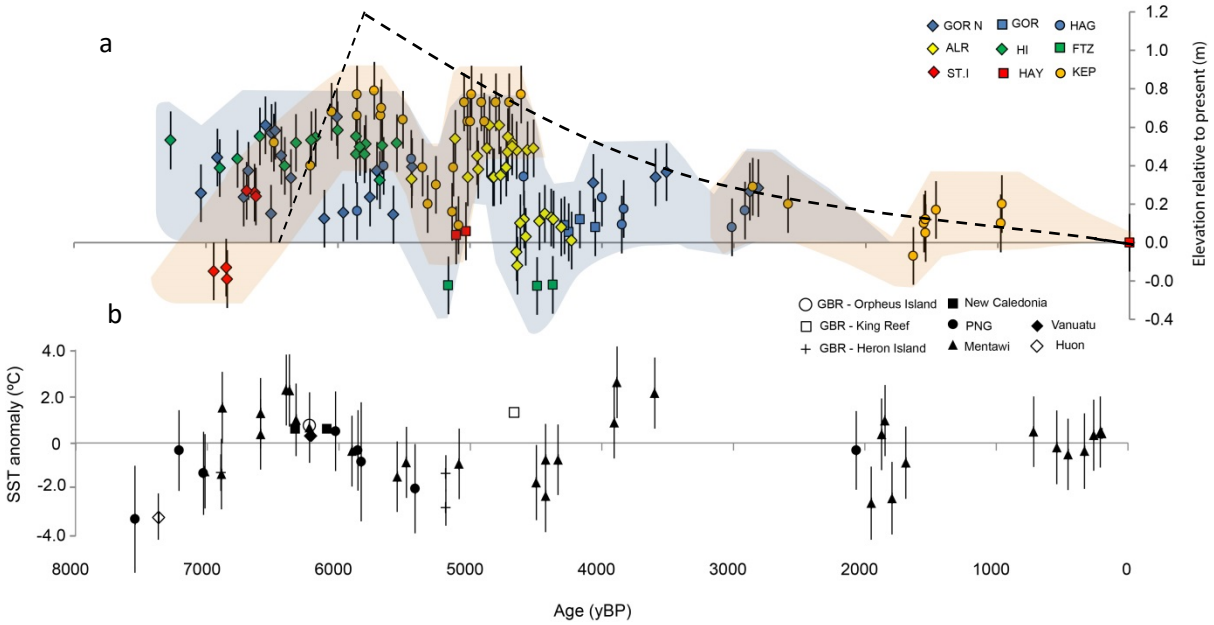

Figure 3: a) U-Th dated microatoll elevation data (metres [m] relative to modern mean low water spring tide) for the Great Barrier Reef (GBR), Australia (GOR N – Gore North, GOR – Gore Island, HAG –Haggerstone Island, ALR – Alexandra Reef, HI – High Island, FTZ – Fitzroy Island, St. I – Stone Island, HAY – Hayman Island - this study) and including U-Th dated microatoll data of Leonard et al. (2016) from the Keppel Islands (KEP; southern GBR). Blue shaded area represents the relative sea level (RSL) envelope of the northern GBR and orange shading represents the central – southern GBR. Dashed line is the geophysical model of Nakada and Lambeck (1989) from Halifax Bay (GBR). b) Coral derived (Sr/Ca) sea surface temperature (SST) anomaly data from the Indo-Pacific (˚C; Sadler et al., 2016 and references therein).

Supplementary

Regional site descriptions

The Great Barrier Reef is the largest coral reef system in the world, with over 2900 reefs and 900 coral cays and islands. The region is recognised as an international World Heritage area, however the overall health of the GBR was recently brought into question by the United Nations Educational, Scientific and Cultural Organization (Hughes et al., 2015). Increasing anthropogenic pressures combined with global climate change has resulted in a significant decline in coral cover in recent decades (Hughes et al., 2015). However this is not the first time the GBR has suffered significant disturbance, with a ~2000 year hiatus or reef "turn-off" event reported in the northern and southern sectors during the mid-Holocene (Perry and Smithers, 2011, Smithers et al., 2006). Whilst it has been recognised that understanding these natural reef "turn-on" and "turn-off" cycles is imperative to better predicting future reef trajectories (Perry and Smithers, 2011), the cause of the mid-Holocene hiatus is still equivocal.

Three possible drivers of the mid-Holocene "turn-off" have been suggested being; a) conditions marginal to reef growth caused by changes in climatic conditions; b) reef flat senescence limiting accretion potential; c) a regressing sea level following the mid-Holocene highstand resulting in emergence of reef flats (Perry and Smithers, 2011) and d) an oscillating Holocene RSL (Leonard et al., 2015, Harris et al., 2015).

Far North Great Barrier Reef

Far North (12˚S, 143˚E)

Gore (11˚59S, 143˚14E) and Haggerstone Islands (12˚02S, 143˚17E) lie ~1km and 10km off the south east of Cape Grenville respectively. Two reef flats were visited in August 2014 at Gore Island (north-north-east and west) and one site to the southwest of Haggerstone Island (Fig. 1B (a) main text)). The emergent reef flats at Gore Island are well developed, and contained numerous fossil microatolls. The modern reef community is mainly restricted to the reef crest and slope, with some tabulate and branching Acropora, massive forms of Goniastrea and Porites, soft corals and foliose algae present. Although living corals on the modern reef crest were patchy, *in situ* samples appear to have been recently covered in a relatively thick layer of mud, and extensive fields of large Acropora rubble clasts indicate this is likely the result of tropical cyclone Ita earlier in 2014 (Supp. Fig 2a). These reef flats are

largely infilled and lack any structural complexity. Comparatively, the south east portion of the reef flat visited at Haggerstone Island was less well developed. Whilst some areas of the reef flat were infilled, a considerable back reef lagoon is still present where modern coral growth is prolific (Supp. Fig 2b).

Northern Great Barrier Reef

Alexandra Reef (16°31S, 145°28E)

Alexandra Reef is an extensive interconnecting complex of reefs that extend from Yule Point in the south to Port Douglas in the north. Although largely considered an amalgamation of mainland fringing reefs, geomorphological studies in this region by Bird (1971) suggests that these reefs actually established as shore detached reefs, and subsequent sea level regression and coastal progradation has led to infilling of a former back reef lagoon with clastic fluvial deposits from the Mowbray River and its tributaries. The emerged reef flat contains extensive fields of large (>2m) *Porites* microatolls. The modern reef flat is largely infilled, and is at the limit of vertical growth. Live coral cover is patchy, with only a few small *Acropora* sp., *Goniastrea* sp. and *Porites* sp. microatolls. Sediments are mainly biogenic carbonate rubble mixed with quartzose sands and muds.

Wet Tropics

Fitzroy Island (16˚55S, 145˚59E)

Fitzroy Island is located ~6km from the mainland coast. The fringing reefs are narrow, and coral cover is low and declined significantly after the 1998 bleaching event (10-30% in 1986 to <5% in 2002) (Sweatman et al., 2008). The fossil microatolls here are located under a thin veneer of living corals and microatolls.

High Island (17˚09S, 146˚00E)

High Island is a small continental island located ~5km from the mainland coast (Liu et al., 2014). The leeward reef flat is ~300m wide and the reef slope drops off rapidly (~45˚) to a muddy sediment wedge where coral growth is limited (Wolanski et al., 2005). The emergent reef flat contains numerous large fossil Porites microatolls (>2m diameter), with live coral limited to mainly juvenile recruits. The island is impacted regularly by flood plumes derived from the Russell-Mulgrave River, and by tropical storms and cyclones (Liu et al., 2014, Chin et al., 2006).

Central Great Barrier Reef

Stone Island (20˚02S, 148˚17E)

Stone Island is located <2km from the mainland coast in the central GBR. The emerged reef flat is extensive however we avoided the most elevated regions due to possible ponding. This was interpreted from the reef having a "step" running shore parallel on the south western portion of the reef flat (Supp. Fig 3). The lower level reef flat substrate is largely infilled and lacks any structural complexity, although intermittent branching and plate Acropora are present. The reef flat at Stone Island was reportedly completely destroyed by a cyclone in 1918, however anecdotal evidence suggests that the reef was recovering 20-30 years ago, however the living coral communities we observed in 2012 were extremely limited.

Hayman Island (20˚03S, 148˚53E)

Hayman Island is a large continental island located ~25km from the coast within the Whitsundays Group in the central GBR. The Whitsundays experience tidal ranges of up to 4m (meso-tidal) and the climate is dominated by seasonal rainfall occurring from December to March. Whilst initial investigations suggested that the reef on Hayman Island developed as a shore detached reef crest, followed by subsequent infilling of the lagoon (Hopley, 1982), more recent dating has indicated a shore to sea progradational mode of growth (Kan et al., 1996). Modern reef growth is mainly limited to the reef crest and slopes. Discontinuous banks of rubble and large coral boulders have been deposited due to previous storms behind the modern reef crest. The reef flat has reached sea level and is mostly infilled, lacking any significant topographic variation.

Supplementary References

Bird, E. C. F. 1971. The fringing reefs near Yule Pont, North Queensland. *Australian Geographical Studies* **9,** 107-115.

Chin, A., Davidson, J. & Diaz, G. 2006. Initial survey of the impact of Tropical Cyclone Larry on reefs and islands in the Central Great Barrier Reef. Great Barrier Reef Marine Park Authority.

Harris, D. L., Webster, J. M., Vila-Concejo, A., Hua, Q., Yokoyama, Y. & Reimer, P. J. 2015. Late Holocene sea-level fall and turn-off of reef flat carbonate production: Rethinking bucket fill and coral reef growth models. *Geology* **43,** 175-178.

Hopley, D. 1982. *The geomorphology of the Great Barrier Reef: quaternary development of coral reefs*, New York, Wiley.

Hughes, T. P., Day, J. C. & Brodie, J. 2015. Securing the future of the Great Barrier Reef. *Nature Climate Change* **5,** 508-511.

Kan, H., Nakashima, Y. & Hopley, D. Year. Coral communities during structural development of a fringing reef flat, Hayman Island, the Great Barrier Reef. *In:* Proceedings of the 8th International Coral Reef Symposium, 1996 Panama. 465-470.

Leonard, N., Zhao, J. X., Welsh, K. J., Feng, Y. X., Smithers, S. G., Pandolfi, J. M. & Clark, T. R. 2015. Holocene sea level instability in the southern Great Barrier Reef, Australia: high-precision U–Th dating of fossil microatolls. *Coral Reefs***,** 1-15.

Liu, E.-T., Zhao, J.-X., Clark, T. R., Feng, Y.-X., Leonard, N. D., Markham, H. L. & Pandolfi, J. M. 2014. High-precision U–Th dating of storm-transported coral blocks on Frankland Islands, northern Great Barrier Reef, Australia. *Palaeogeography, Palaeoclimatology, Palaeoecology* **414,** 68-78.

Perry, C. & Smithers, S. 2011. Cycles of coral reef 'turn-on', rapid growth and 'turn-off' over the past 8500 years: a context for understanding modern ecological states and trajectories. *Global Change Biology* **17,** 76-86.

Smithers, S. G., Hopley, D. & Parnell, K. E. 2006. Fringing and Nearshore Coral Reefs of the Great Barrier Reef: Episodic Holocene Development and Future Prospects. *Journal of Coastal Research***,** 175-187.

Sweatman, H., Cheal, A., Coleman, G., Emslie, M., Johns, K., Jomnker, M., Miller, I. & Osborne, K. 2008. Long-term monitoring of the Great Barrier Reef Status Report Number 8. Australian Institute of Marine Science.

Wolanski, E., Fabricius, K., Spagnol, S. & Brinkman, R. 2005. Fine sediment budget on an inner-shelf coral-fringed island, Great Barrier Reef of Australia. *Estuarine, Coastal and Shelf Science* **65,** 153-158.

Supplementary Table

Supplementary Table 1: Results from MC-ICP -MS Uranium Thorium dating and elevation surveys of fossil *Porites* microatolls from the Great Barrier Reef, Australia. Microatoll elevations are given as metres relative to lowest astronomical tide (mLAT) and relative to regionally specific mean low water spring tide (MLWS). Elevation errors are ± 15cm except for Haggerstone Island (HAG) which is ±18cm based on the standard deviation of the living (modern) population.

Sample Name	U (ppm)	232Th (ppb)	(230Th/ 232Th)	(230Th/238U)	Corr. (234U/ 238U)	Uncorr. Age	Corr. Age	**Age (yBP)**	δU^{234}	Diam (cm)	Elev. mLAT	Elev. rel. to present (MLWS)	Latitude	Longitude
GOR N 002	2.8823 ± 0.0016	13.787 ± 0.018	19.6 ± 0.2	0.03086 ± 0.00027	1.1470 ± 0.0007	2976 ± 26	2880 ± 33	**2815 ± 33**	147.0 ± 0.7	160	**0.80**	0.28	11˚59'02.1	143˚14'48.6
GOR N 003	3.1165 ± 0.0016	8.946 ± 0.013	32.9 ± 0.3	0.03109 ± 0.00028	1.1456 ± 0.0009	3002 ± 27	2943 ± 30	**2878 ± 30**	145.6 ± 0.9	190	**0.79**	0.27	11˚59'02.3	143˚14'48.4
GOR N 004	2.5509 ± 0.0012	7.858 ± 0.011	37.0 ± 0.4	0.03760 ± 0.00035	1.1465 ± 0.0010	3639 ± 34	3575 ± 37	**3510 ± 37**	146.5 ± 1.0	150	**0.89**	0.37	11˚59'02.6	143˚14'48.1
GOR N 005	2.6300 ± 0.0013	17.168 ± 0.023	18.2 ± 0.2	0.03913 ± 0.00035	1.1469 ± 0.0010	3788 ± 35	3658 ± 43	**3593 ± 43**	146.9 ± 1.0	150	**0.86**	0.34	11˚59'02.5	143˚14'48.3
GOR N 006	2.5218 ± 0.0011	19.994 ± 0.026	16.9 ± 0.1	0.04411 ± 0.00029	1.1452 ± 0.0008	4287 ± 28	4129 ± 42	**4065 ± 42**	145.2 ± 0.8	70	**0.83**	0.31	11˚59'02.9	143˚14'48.1
GOR N 007	2.5822 ± 0.0016	24.429 ± 0.029	18.7 ± 0.1	0.05823 ± 0.00038	1.1469 ± 0.0010	5689 ± 38	5503 ± 53	**5438 ± 53**	146.9 ± 1.0	130	**0.91**	0.39	11˚59'03.0	143˚14'48.0
GOR N 008	2.5805 ± 0.0011	5.4510 ± 0.0086	85.3 ± 0.6	0.05940 ± 0.00042	1.1449 ± 0.0008	5816 ± 42	5770 ± 43	**5705 ± 43**	144.9 ± 0.8	120	**0.89**	0.37	11˚59'03.1	143˚14'47.8
GOR N 009	2.7130 ± 0.0016	2.7941 ± 0.0055	193.4 ± 1.6	0.06563 ± 0.00054	1.1447 ± 0.0009	6446 ± 55	6421 ± 55	**6356 ± 55**	144.7 ± 0.9	170	**0.86**	0.34	11˚59'03.2	143˚14'47.4
GOR N 010	2.6430 ± 0.0011	17.678 ± 0.017	26.8 ± 0.2	0.05906 ± 0.00035	1.1457 ± 0.0011	5778 ± 35	5645 ± 44	**5580 ± 44**	145.7 ± 1.1	170	**0.67**	0.15	11˚59'03.0	143˚14'46.9
GOR N 011	2.6807 ± 0.0015	4.6588 ± 0.0079	110.7 ± 0.9	0.06342 ± 0.00051	1.1476 ± 0.0010	6207 ± 51	6168 ± 52	**6103 ± 52**	147.6 ± 1.0	180	**0.65**	0.13	11˚59'03.2	143˚14'46.6
GOR N 012	2.3603 ± 0.0009	14.398 ± 0.017	33.9 ± 0.2	0.06819 ± 0.00038	1.1467 ± 0.0010	6694 ± 39	6571 ± 46	**6507 ± 46**	146.7 ± 1.0	110	**0.67**	0.15	11˚59'03.5	143˚14'46.2
GOR N 013	2.7231 ± 0.0012	10.392 ± 0.014	55.2 ± 0.3	0.06947 ± 0.00036	1.1471 ± 0.0007	6822 ± 37	6743 ± 40	**6679 ± 40**	147.1 ± 0.7	160	**0.89**	0.37	11˚59'05.3	143˚14'50.3
GOR N 014	3.0441 ± 0.0016	18.349 ± 0.025	33.9 ± 0.2	0.06742 ± 0.00029	1.1472 ± 0.0006	6614 ± 29	6494 ± 38	**6429 ± 38**	147.2 ± 0.6	80	**0.97**	0.45	11˚59'05.5	143˚14'50.3
GOR N 015	2.5883 ± 0.0012	6.621 ±0.012	84.8 ± 0.6	0.07152 ± 0.00047	1.1465 ± 0.0010	7033 ± 49	6979 ± 50	**6914 ± 50**	146.5 ± 1.0	200	**0.96**	0.44	11˚59'05.3	143˚14'50.6
GOR N 016	2.7168 ± 0.0016	22.455 ± 0.026	25.2 ± 0.2	0.06866 ± 0.00043	1.1483 ± 0.0008	6732 ± 44	6569 ± 54	**6504 ± 54**	148.3 ± 0.8	230	**1.09**	0.57	11˚59'05.3	143˚14'51.1

GOR N 019	2.8329 ± 0.0013	6.8821 ± 0.0092	75.0 ± 0.5	0.06005 ± 0.00041	1.1465 ± 0.0009	5873 ± 42	5822 ± 43	**5757 ± 43**	146.5 ± 0.9	210	**0.76**	0.24	11˚59'05.3	143˚15'52.6
GOR N 020	2.5204 ± 0.0013	11.340 ± 0.016	42.1 ± 0.4	0.06249 ± 0.00053	1.1472 ± 0.0011	6115 ± 54	6024 ± 57	**5959 ± 57**	147.2 ± 1.1	90	**0.68**	0.16	11˚59'05.9	143˚14'52.3
GOR N 021	3.1270 ± 0.0015	3.5266 ± 0.0076	195.1 ± 1.3	0.07253 ± 0.00047	1.1476 ± 0.0011	7129 ± 48	7103 ± 48	**7038 ± 48**	147.6 ± 1.1	240	**0.78**	0.26	11˚59'06.8	143˚14'51.3
GOR N 022	2.8696 ± 0.0015	9.007 ± 0.012	67.4 ± 0.4	0.06971 ± 0.00045	1.1474 ± 0.0007	6844 ± 46	6779 ± 47	**6714 ± 47**	147.4 ± 0.7	70	**0.76**	0.24	11˚59'06.1	143˚14'51.0
GOR N 023	2.8876 ± 0.0010	4.8027 ± 0.0072	122.2 ± 0.6	0.06698 ± 0.00029	1.1459 ± 0.0010	6576 ± 29	6540 ± 30	**6475 ± 30**	145.9 ± 1.0	110	**1.10**	0.58	11˚59'09.3	143˚14'52.6
GOR N 024	3.0197 ± 0.0012	2.2988 ± 0.0065	269.3 ± 1.3	0.06756 ± 0.00027	1.1461 ± 0.0011	6633 ± 28	6614 ± 29	**6549 ± 29**	146.1 ± 1.1	70	**1.13**	0.61	11˚59'09.5	143˚14'52.7
GOR N 025	3.0528 ± 0.0017	3.9747 ± 0.0065	145.3 ± 1.1	0.06234 ± 0.00046	1.1468 ± 0.0011	6102 ± 47	6072 ± 47	**6008 ± 47**	146.8 ± 1.1	60	**1.17**	0.65	11˚59'09.5	143˚14'52.7
GOR 001	2.3476 ± 0.0011	6.642 ± 0.010	47.5 ± 0.4	0.04427 ± 0.00038	1.1481 ± 0.0011	4291 ± 37	4231 ± 39	**4166 ± 39**	148.1 ± 1.3	120	**0.64**	0.12	11˚59'27.2	143˚14'42.1
GOR 002	2.5954 ± 0.0013	31.290 ± 0.044	11.3 ± 0.1	0.04481 ± 0.00057	1.1469 ± 0.0013	4350 ± 57	4114 ± 74	**4049 ± 74**	146.9 ± 0.7	170	**0.60**	0.08	11˚59'27.2	143˚14'42.1
GOR 004	2.5986 ± 0.0017	64.354 ± 0.096	6.03 ± 0.05	0.04923 ± 0.00042	1.1455 ± 0.0007	4797 ± 42	4316 ± 105	**4251 ± 105**	145.5 ± 1.0	100	**0.57**	0.05	11˚59'27.0	143˚14'42.2
GOR 005	2.4778 ± 0.0016	6.176 ± 0.013	55.2 ± 0.6	0.04532 ± 0.00046	1.1463 ± 0.0010	4403 ± 46	4349 ± 47	**4284 ± 47**	146.3 ± 0.9	90	**0.61**	0.09	11˚59'27.1	143˚14'42.1
HAG 002	2.6509 ± 0.0012	6.3338 ± 0.0099	61.4 ± 0.4	0.04836 ± 0.00031	1.1454 ± 0.0008	4708 ± 31	4657 ± 33	**4592 ± 33**	145.4 ± 0.8	170	**0.86**	0.34	12˚02'24.3	143˚17'45.6
HAG 003	2.5732 ± 0.0012	0.4684 ± 0.0039	699.5 ± 7.4	0.04196 ± 0.00028	1.1453 ± 0.0010	4073 ± 28	4064 ± 28	**3999 ± 28**	145.3 ± 1.0	120	**0.75**	0.23	12˚02'24.0	143˚17'45.4
HAG 010	3.3752 ± 0.0019	25.850 ± 0.036	13.3 ± 0.1	0.03344 ± 0.00033	1.1467 ± 0.0008	3229 ± 32	3079 ± 44	**3014 ±44**	146.7 ± 0.8	80	**0.60**	0.08	12˚02'14.4	143˚17'43.9
HAG 011	3.3160 ± 0.0014	38.081 ± 0.044	8.8 ± 0.1	0.03315 ± 0.00023	1.1460 ± 0.0009	3204 ± 22	2979 ± 50	**2915 ±50**	146.0 ± 0.9	200	**0.68**	0.17	12˚02'14.1	143˚17'44.6
HAG 012	2.4244 ± 0.0011	2.5762 ± 0.0058	115.6 ± 0.8	0.04049 ± 0.00027	1.1461 ± 0.0009	3925 ± 27	3899 ± 27	**3834 ± 27**	146.1 ± 0.9	160	**0.69**	0.18	12˚02'13.1	143˚17'44.4
HAG 013	4.8141 ± 0.0022	22.859 ± 0.027	39.2 ± 0.2	0.06138 ± 0.00034	1.1451 ± 0.0011	6014 ± 35	5920 ± 40	**5855 ± 40**	145.1 ± 1.1	230	**0.68**	0.16	12˚02'12.1	143˚17'43.0
HAG 014	2.5354 ± 0.0058	8.2182 ±0.0099	38.4 ± 0.3	0.04098 ± 0.00034	1.1442 ± 0.0008	3980 ± 34	3913 ± 37	**3848 ± 37**	144.2 ± 0.8	170	**0.61**	0.09	12˚02'18.0	143˚17'43.2
HAG 017	2.6635 ± 0.0012	0.9449 ± 0.0042	483.7 ± 4.1	0.05656 ± 0.00041	1.1467 ± 0.0009	5521 ± 42	5509 ± 42	**5444 ± 42**	146.7 ± 0.9	130	**0.95**	0.44	12˚02'26.0	143˚17'45.1
HAG 018	2.5872 ± 0.0013	3.9198 ± 0.0068	117.9 ± 0.8	0.05887 ± 0.00041	1.1469 ± 0.0011	5752 ± 41	5718 ± 42	**5653 ±42**	146.9 ± 1.1	110	**0.91**	0.40	12˚02'26.3	143˚17'45.2
ALR 001	2.5021 ± 0.0009	10.296 ± 0.013	40.0 ± 0.1	0.05420 ± 0.00015	1.1472 ± 0.0012	5280 ± 16	5174 ± 55	**5111 ± 55**	149.5 ± 1.2	150	**1.26**	0.54	16˚31'17.9	145˚28'36.2

ALR 002	2.7799 ± 0.0013	7.5724 ± 0.0084	57.3 ± 0.1	0.05140 ± 0.00010	1.1464 ± 0.0010	5005 ± 11	4934 ± 37	**4871 ± 37**	148.6 ± 1.0	160	**1.21**	0.49	16˚31'18.1	145˚28'36.4
ALR 003	2.7066 ± 0.0020	12.286 ± 0.041	32.7 ± 0.1	0.04893 ± 0.00013	1.1499 ± 0.0010	4774 ± 14	4627 ± 60	**4564 ± 60**	152.0 ± 1.1	380	**1.19**	0.48	16˚31'17.7	145˚28'36.2
ALR 004	2.5278 ± 0.0016	2.3775 ± 0.0041	158.3 ± 0.4	0.04908 ± 0.00010	1.1480 ± 0.0010	4767 ± 11	4743 ± 16	**4680 ± 16**	150.0 ± 1.0	210	**1.24**	0.52	16˚31'17.7	145˚28'36.2
ALR 009	2.8455 ±0.0027	9.744 ± 0.014	40.1 ± 0.1	0.04520 ± 0.00011	1.1482 ± 0.0009	4382 ± 11	4293 ± 45	**4230 ± 45**	150.1 ± 0.9	150	**0.72**	0.01	16˚31'13.6	145˚28'42.8
ALR 010	2.8546 ± 0.0011	11.599 ± 0.022	37.0 ± 0.1	0.04949 ± 0.00010	1.1467 ± 0.0008	4814 ± 10	4709 ± 53	**4646 ± 53**	148.8 ± 0.8	180	**0.67**	-0.05	16˚31'12.4	145˚28'43.3
ALR 011	2.8471 ± 0.0020	8.4773 ± 0.0090	49.5 ± 0.1	0.04852 ± 0.00012	1.1468 ± 0.0008	4717 ± 12	4640 ± 40	**4577 ± 40**	148.9 ± 0.8	110	**0.75**	0.03	16˚31'12.6	145˚28'44.0
ALR 012	2.9301 ± 0.0016	15.163 ± 0.028	29.1 ± 0.1	0.04969 ± 0.00013	1.1458 ± 0.0011	4837 ± 14	4703 ± 68	**4640 ± 68**	148.0 ± 1.1	120	**0.60**	-0.12	16˚31'19.2	145˚28'33.0
ALR 014	2.7393 ± 0.0015	6.6920 ± 0.0081	62.5 ± 0.2	0.05034 ± 0.00015	1.1453 ± 0.0008	4904 ± 16	4841 ± 35	**4778 ± 35**	147.4 ± 0.8	160	**1.33**	0.61	16˚31'20.1	145˚28'33.5
ALR 015	2.7196 ±0.0019	25.966 ± 0.034	16.8 ± 0.1	0.05299 ± 0.00017	1.1467 ± 0.0009	5161 ± 17	4914 ± 124	**4851 ± 124**	149.2 ± 1.0	130	**1.33**	0.61	16˚31'20.2	145˚28'33.3
ALR 022	2.7068 ±0.0013	4.735 ± 0.013	85.9 ± 0.5	0.04951 ± 0.00029	1.1474 ± 0.0013	4821 ± 29	4776 ± 37	**4713 ± 37**	147.4 ± 1.3	250	**1.17**	0.47	16˚31'18.7	145˚28'35.7
ALR 024	2.7294 ± 0.0021	13.662 ± 0.035	30.0 ± 0.1	0.04949 ± 0.00018	1.1431 ± 0.0009	4838 ± 18	4708 ± 67	**4645 ± 67**	143.1 ± 0.9	247	**1.18**	0.48	16˚31'19.1	145˚28'36.1
ALR 028	2.9374 ± 0.0023	7.161 ± 0.018	70.7 ± 0.3	0.05681 ± 0.00022	1.1442 ± 0.0011	5568 ± 23	5504 ± 39	**5441 ± 39**	144.2 ± 1.1	99	**1.02**	0.33	16˚31'20.8	145˚28'36.7
ALR-030	2.9289 ± 0.0026	2.035 ± 0.005	214.9 ± 1.2	0.04920 ± 0.00026	1.1436 ± 0.0013	4806 ± 26	4788 ± 28	**4725 ± 28**	143.6 ± 1.3	220	**1.08**	0.39	16˚31.18.7	145˚28.37.5
ALR 033	2.8562 ± 0.0019	12.821 ± 0.021	35.9 ± 0.2	0.05307 ± 0.00020	1.1435 ± 0.0011	5195 ± 21	5078 ± 62	**5015 ± 62**	143.5 ±1.1	130	**1.04**	0.34	16˚31'19.3	145˚28'37.4
ALR 034	2.8753 ± 0.0015	5.982 ± 0.013	73.7 ± 0.4	0.05055 ± 0.00023	1.1436 ± 0.0010	4942 ± 24	4888 ± 36	**4825 ± 36**	143.6 ± 1.0	205	**1.04**	0.34	16˚31'17.5	145˚28'37.6
ALR 035	3.2863 ± 0.0021	7.266 ± 0.015	69.5 ± 0.4	0.05061 ± 0.00027	1.1460 ± 0.0009	4937 ± 27	4880 ± 39	**4817 ± 39**	146.0 ±0.9	110	**1.04**	0.34	16˚31'18.6	145˚28'37.2
ALR 036	2.5220 ± 0.0016	5.574 ± 0.012	68.8 ± 0.3	0.05008 ± 0.00020	1.1452 ± 0.0015	4887 ± 21	4830 ± 36	**4767 ± 36**	145.2 ± 1.5	215	**1.05**	0.35	16˚31'17.5	145˚28'37.2
ALR 037	2.9145 ± 0.0018	3.3063 ± 0.0091	137.8 ± 0.8	0.05150 ± 0.00028	1.1452 ± 0.0017	5030 ± 29	5000 ± 32	**4937 ± 32**	145.2 ± 1.7	330	**1.08**	0.38	16˚31'17.4	145˚28'37.1
ALR-038	2.7090 ± 0.0018	17.704 ± 0.042	22.2 ± 0.2	0.04782 ± 0.00042	1.1447 ± 0.0012	4665 ± 43	4495 ± 95	**4432 ± 95**	144.7 ± 1.2	295	**0.94**	0.15	16˚31'15.7	145˚28'41.0
ALR 040	2.8280 ± 0.0011	5.175 ± 0.013	80.1 ± 0.5	0.04829 ± 0.00030	1.1473 ± 0.0008	4701 ± 30	4653 ±38	**4590 ± 38**	147.3 ± 0.8	250	**0.91**	0.12	16˚31'15.3	145˚28'41.3
ALR 041	2.7872 ± 0.0016	21.026 ± 0.042	19.2 ± 0.2	0.04771 ± 0.00040	1.1475 ± 0.0013	4642 ± 40	4447 ± 105	**4384 ± 105**	147.5 ± 1.3	180	**0.92**	0.13	16˚31'14.4	145˚28'41.2

ALR 043	2.8267 ± 0.0014	9.463 ± 0.013	43.0 ± 0.2	0.04749 ± 0.00020	1.1468 ± 0.0015	4622 ± 21	4536 ± 48	**4473 ± 48**	146.8 ± 1.5	205	**0.90**	0.11	16˚31'14.2	145˚28'40.7
ALR 045	2.9426 ± 0.0020	12.334 ± 0.023	33.7 ± 0.2	0.04660 ± 0.00027	1.1460 ± 0.0010	4537 ± 27	4429 ± 61	**4366 ± 61**	146.0 ± 1.0	185	**0.91**	0.12	16˚31'14.5	145˚28'40.9
ALR 046	2.6213 ± 0.0014	14.081 ± 0.034	26.1 ± 0.2	0.04627 ± 0.00025	1.1449 ± 0.0012	4509 ± 26	4370 ± 74	**4307 ± 74**	144.9 ± 1.2	190	**0.87**	0.08	16˚31'13.8	145˚28'41.5
ALR 047	2.9077 ± 0.0020	19.800 ± 0.043	22.2 ± 0.1	0.04991 ± 0.00022	1.1484 ± 0.0014	4857 ± 22	4681 ± 90	**4618 ± 90**	148.4 ± 1.4	360	**0.88**	0.10	16˚31'13.2	145˚28'41.7
ALR 050	2.4478 ± 0.0016	7.731 ± 0.014	47.6 ± 0.3	0.04952 ± 0.00027	1.1472 ± 0.0012	4823 ± 27	4742 ± 49	**4679 ± 49**	147.2 ± 1.2	240	**1.32**	0.5	16˚31'19.7	145˚28'33.8
ALR 052	2.5661 ± 0.0015	14.758 ± 0.029	27.9 ± 0.2	0.05278 ± 0.00026	1.1453 ± 0.0013	5158 ± 27	5008 ± 79	**4945 ± 79**	145.3 ± 1.3	215	**1.27**	0.45	16˚31'20.2	145˚28'33.7
ALR 057	2.8427 ± 0.0017	25.345 ± 0.042	17.5 ± 0.1	0.05138 ± 0.00027	1.1481 ± 0.0013	5006 ± 28	4775 ± 118	**4712 ± 118**	148.1 ± 1.3	170	**1.37**	0.55	16˚31'22.2	145˚28'33.0
ALR 060	2.7202 ± 0.0016	17.993 ± 0.041	22.4 ± 0.1	0.04885 ± 0.00023	1.1484 ± 0.0012	4751 ± 23	4580 ± 88	**4517 ± 88**	148.4 ± 1.2	120	**1.31**	0.49	16˚31'22.8	145˚28'33.2
FI 001	2.6878 ± 0.0014	30.024 ± 0.040	13.0 ± 0.1	0.0479 ± 0.0002	1.1472 ± 0.0014	4662 ± 18	4434 ± 115	**4371 ± 115**	147.2 ± 1.4	~300	**0.16**	-0.22	16˚55'35.9	145˚59'24.2
FI 002	2.4995 ± 0.0025	25.332 ± 0.037	14.6 ± 0.1	0.0488 ± 0.0002	1.1460 ± 0.0011	4760 ± 18	4553 ± 105	**4490 ± 105**	146.0 ± 1.1	~300	**0.15**	-0.23	16˚55'35.7	145˚59'24.3
FI 003	2.8224 ± 0.0010	32.575 ± 0.047	14.68 ± 0.04	0.0558 ± 0.0001	1.1457 ± 0.0013	5462 ± 14	5226 ± 118	**5163 ± 118**	145.7 ± 1.3	~300	**0.15**	-0.22	16˚55'35.4	145˚59'24.3
HIG 002	3.0050 ± 0.0016	13.693 ± 0.016	44.8 ± 0.1	0.06729 ± 0.00014	1.1515 ± 0.0012	6583 ± 15	6466 ± 60	**6403 ± 60**	151.7 ± 1.2	270	**1.00**	0.40	17˚09'29.0	146˚00'20.2
HIG 003	3.2503 ± 0.0021	16.349 ± 0.019	37.4 ± 0.1	0.06203 ± 0.00014	1.1511 ± 0.0012	6056 ± 15	5926 ± 66	**5863 ± 66**	151.2 ± 1.2	310	**1.06**	0.46	17˚09'28.9	146˚00'20.4
HIG 005	3.0075 ± 0.0023	13.857 ± 0.030	46.6 ± 0.2	0.07069 ± 0.00017	1.1490 ± 0.0010	6943 ± 18	6824 ± 62	**6761 ± 62**	149.1 ± 1.0	300	**1.04**	0.44	17˚09'28.8	146˚00'21.2
HIG 006	2.8269 ± 0.0017	22.838 ± 0.031	27.4 ± 0.1	0.07281 ± 0.00021	1.1476 ± 0.0009	7168 ± 22	6958 ± 106	**6895 ± 106**	147.9 ± 0.9	465	**0.99**	0.39	17˚09'28.6	146˚00'21.2
HIG 008	2.8994 ± 0.0021	12.187 ± 0.011	44.0 ± 0.1	0.06091 ± 0.00012	1.1479 ± 0.0009	5961 ± 13	5852 ± 56	**5789 ± 56**	148.1 ± 0.9	215	**1.11**	0.51	17˚09'29.5	146˚00'21.3
HIG 009	2.8710 ± 0.0021	8.3394 ± 0.079	63.8 ± 0.2	0.06107 ± 0.00019	1.1489 ± 0.0009	5971 ± 19	5896 ± 42	**5833 ± 42**	149.0 ± 0.9	510	**1.10**	0.50	17˚09'29.7	146˚00'21.2
HIG 011	3.2979 ± 0.0018	19.261 ± 0.032	39.5 ± 0.1	0.07595 ± 0.00016	1.1484 ± 0.0011	7482 ± 18	7331 ± 77	**7268 ± 77**	148.6 ± 1.1	260	**1.13**	0.53	17˚09'29.1	146˚00'21.9
HIG 013	2.9202 ± 0.0018	13.626 ± 0.036	42.1 ± 0.2	0.06477 ± 0.00016	1.1472 ± 0.0013	6354 ± 17	6233 ± 62	**6170 ± 62**	147.3 ± 1.3	335	**1.15**	0.55	17˚09'27.7	146˚00'21.3
HIG 001-E	2.9298 ± 0.0017	5.916 ± 0.0093	89.2 ± 0.2	0.05935 ± 0.00014	1.1489 ± 0.0009	5798 ± 30	5746 ± 30	**5683 ± 30**	149.0 ± 0.9	110	**0.93**	0.33	17˚09'29.1	146˚00'19.8
HIG 003-E	2.8322 ± 0.0021	4.2349 ± 0.0083	122.5 ± 0.4	0.06039 ± 0.00017	1.1495 ± 0.0011	6055 ± 18	5861 ± 26	**5798 ± 26**	149.5 ± 1.1	310	**1.06**	0.46	17˚09'28.9	146˚00'20.4

HIG 004-E	2.6600 ± 0.0027	20.860 ± 0.024	24.6 ± 0.1	0.06347 ± 0.00016	1.1493 ± 0.0015	6210 ± 18	6008 ± 102	**5664 ± 102**	149.6 ± 1.5	175	**1.10**	0.50	17˚09'29.0	146˚00'20.7
HIG 006-E	2.9066 ± 0.0021	16.342 ± 0.022	35.9 ± 0.1	0.06656 ± 0.00021	1.1489 ± 0.0013	6525 ± 23	6379 ± 76	**6317 ± 76**	149.1 ± 1.3	465	**1.12**	0.52	17˚09'28.6	146˚00'21.2
HIG 007-E	2.4044 ± 0.0014	21.311 ± 0.021	20.4 ± 0.1	0.05967 ± 0.00015	1.1458 ± 0.0010	5846 ± 16	5617 ± 115	**5554 ± 115**	146.1 ± 1.0	440	**1.12**	0.52	17˚09'29.0	146˚00'21.3
HIG 011-E	2.8991 ± 0.0017	32.591 ± 0.051	18.0 ± 0.1	0.06676 ± 0.00017	1.1470 ± 0.0010	6556 ± 18	6265 ± 146	**6202 ± 146**	147.3 ± 1.1	260	**1.13**	0.53	17˚09'29.1	146˚00'21.9
HIG 012-E	2.8797 ± 0.0019	5.0386 ± 0.0063	108.4 ± 0.3	0.06248 ± 0.00015	1.1494 ± 0.0011	6110 ± 16	6065 ± 28	**6002 ± 28**	149.5 ± 1.1	410	**1.19**	0.59	17˚09'28.1	146˚00'21.5
HIG 014-E	2.5618 ± 0.0008	35.505 ± 0.086	13.88 ± 0.04	0.06341 ± 0.00011	1.1459 ± 0.0013	6209 ± 13	5926 ± 141	**5863 ± 141**	148.8 ± 1.3	335	**1.15**	0.55	17˚09'27.5	146˚00'21.5
HIG 015-E	2.8629 ± 0.0011	9.775 ± 0.015	60.8 ± 0.1	0.06837 ± 0.00016	1.1433 ± 0.0008	6724 ± 17	6655 ± 39	**6592 ± 39**	146.1 ± 0.8	450	**1.15**	0.55	17˚09'27.2	146˚00'21.5
ST.I 002	3.0884 ± 0.0018	13.75 ± 0.028	47.2 ± 0.2	0.0692 ± 0.0003	1.1465 ± 0.0012	6810 ± 30	6694 ± 64	**6631 ± 64**	146.5 ± 1.2	70	**0.92**	0.26	20˚02'31.7	148˚17'09.3
ST.I 003	2.9531 ± 0.0023	11.06 ± 0.020	56.5 ± 0.3	0.0697 ± 0.0003	1.1482 ± 0.0013	6852 ± 34	6755 ± 59	**6692 ± 59**	148.2 ± 1.3	200	**0.93**	0.27	20˚02'31.6	148˚17'09.4
ST.I 004	3.0112 ± 0.0025	6.061 ± 0.013	103.4 ± 0.6	0.0686 ± 0.0004	1.1480 ± 0.0013	6736 ± 37	6684 ± 45	**6621 ± 45**	148.0 ± 1.3	130	**0.90**	0.24	20˚02'31.9	148˚17'09.4
ST.I 005	2.69525 ± 0.00094	2.0210 ± 0.0035	288.9 ± 0.7	0.0714 ± 0.0001	1.1480 ±0.0012	7020 ± 14	7004 ± 16	**6941 ± 16**	148.0 ± 1.2	290	**0.51**	-0.15	20˚02'32.0	148˚17'09.5
ST.I 007	2.9438 ± 0.0021	10.45 ± 0.022	60.9 ± 0.3	0.0712 ± 0.0003	1.1485 ± 0.0013	7002 ± 33	6910 ± 56	**6847 ± 56**	148.5 ± 1.3	240	**0.53**	-0.13	20˚02'32.2	148˚17'09.7
ST.I 012	2.9567 ± 0.0016	6.17 ± 0.018	102.7 ± 0.5	0.0706 ± 0.0003	1.1458 ± 0.0011	6958 ± 32	6903 ± 42	**6840 ± 42**	145.8 ± 1.1	120	**0.46**	-0.19	20˚02'34.9	148˚17'11.8
HAY 001*	2.3655 ± 0.0010	17.941 ± 0.047	0.74 ± 0.01	0.0018 ± 0.0000	1.1471 ± 0.0010	176 ± 3	21 ± 78	**1992 ± 78**	147.1 ± 1.0	50	**0.61**	0.00	20˚03'16.9	148˚53'52.4
HAY 002	3.0096 ± 0.0010	28.453 ± 0.059	17.6 ± 0.1	0.0549 ± 0.0001	1.1467 ± 0.0009	5360 ± 15	5167 ± 97	**5104 ± 97**	146.7 ± 0.9	90	**0.65**	0.04	20˚03'17.1	148˚53'52.1
HAY 003E	3.1494 ± 0.0016	26.76 ± 0.35	19.3 ± 0.1	0.0539 ± 0.0001	1.1467 ± 0.0015	5266 ± 14	5093 ± 87	**5030 ± 87**	146.7 ± 1.5	130	**0.67**	0.06	20˚03'17.4	148˚53'51.3

Ratios in parentheses are activity ratios calculated from atomic ratios using decay constants of Cheng et al. (2000). All values have been corrected for laboratory procedural blanks. All errors reported in this table are quoted as 2σ.

a. Uncorrected ^{230}Th age was calculated using Isoplot/EX 3.0 program (Ludwig, 2003).

b. ^{230}Th ages were corrected using the two-component correction method of Clark et al. (2014) using ^{230}Th/^{232}Th$_{hyd}$ and ^{230}Th/^{232}Th$_{det}$ activity ratios of 1.08 ± 0.23 and 0.62 ± 0.14, respectively.

c. $\delta^{234}U = [(^{234}U/^{238}U) - 1] \times 1000$.

Supplementary Table 2: Summary statistics for linear and Gaussian models (see Supp. Fig. 4) of relative sea level (RSL) on the Great Barrier Reef, Australia. Where SSE is the Sum of Squares due to error, R-square is the square of the correlation between the predicted response values and response values, Adjusted R-square is adjusted using the residuals degrees of freedom, RMSE is the root mean squared error.

Goodness of Fit	SSE	R-square	Adjusted R-square	RMSE
Linear	6.52	0.15	0.15	0.22
Gaussian 1	5.85	0.24	0.23	0.21
Gaussian 2	5.02	0.35	0.32	0.20
Gaussian 3	4.93	0.36	0.32	0.20
Gaussian 4	4.52	0.41	0.36	0.20

Supplementary Figures

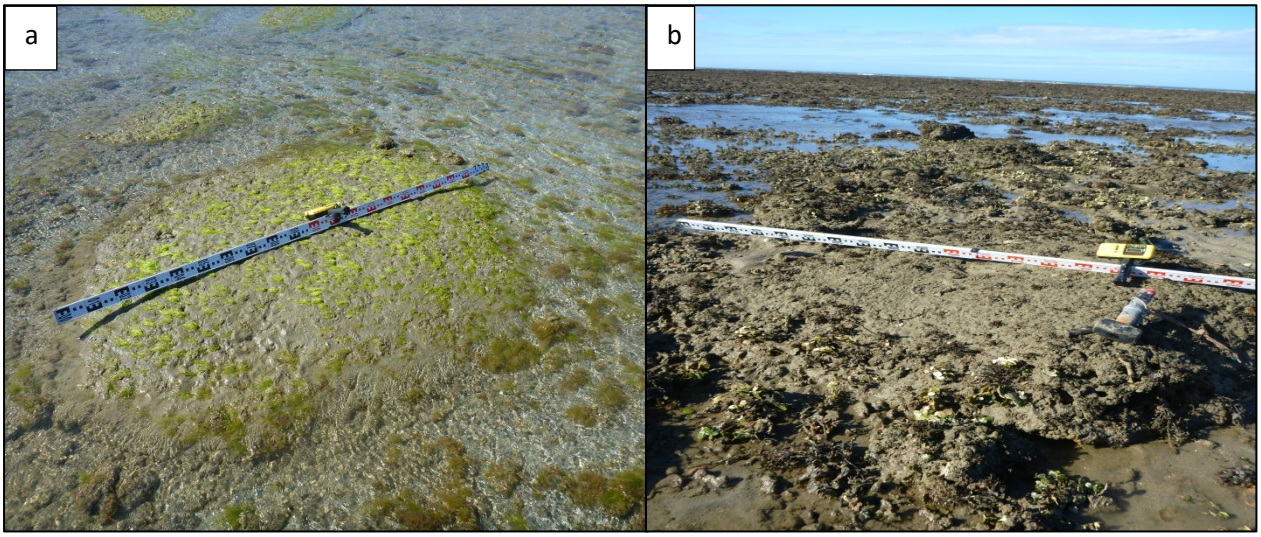

Supplementary Figure 1: Photographs of fossil microatolls from Alexandra Reef, Queensland, Australia. a) microatoll showing a reduction in height around the outer rim indicative of a fall in RSL and; b) microatoll with a planar upper surface indicating growth up to a constant RSL.

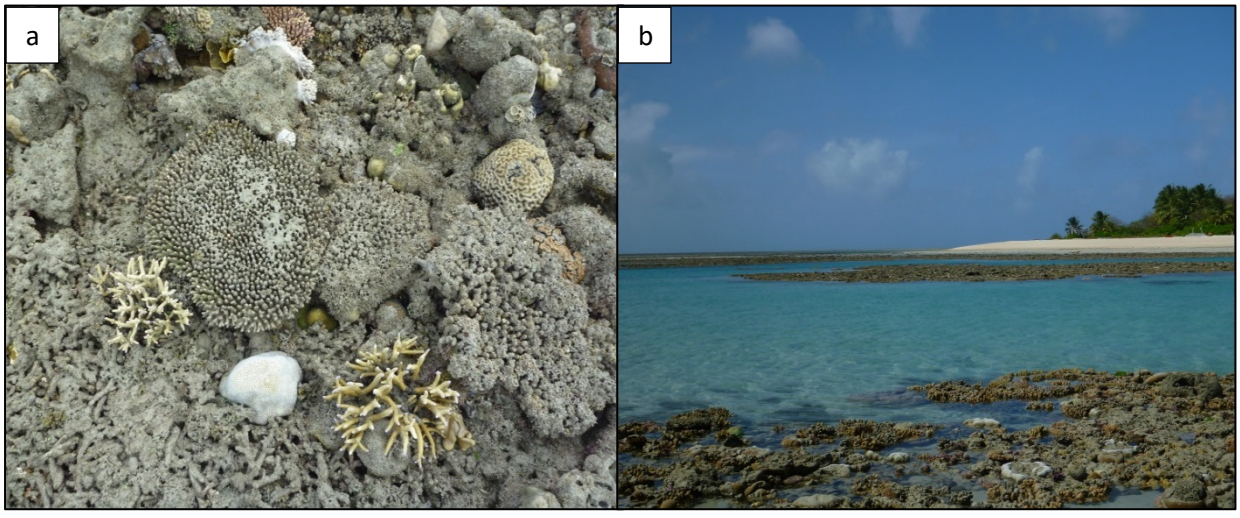

Supplementary Figure 2: Photographs from far north Queensland Great Barrier Reef a) *In situ* branching, plating and small massive corals covered in thick sediment on the seaward edge of the reef flat at leeward Gore Island and b) Haggerstone Island back reef lagoon.

Supplementary Figure 3: Photograph of Stone Island (20˚02S, 148˚17E), Great Barrier Reef, Australia, looking towards the island (with Bowen in the background). Note the shore parallel "step" which is an emerged coral reef suggestive of possible ponding. Microatolls for this study were only taken from the lower reef terrace.

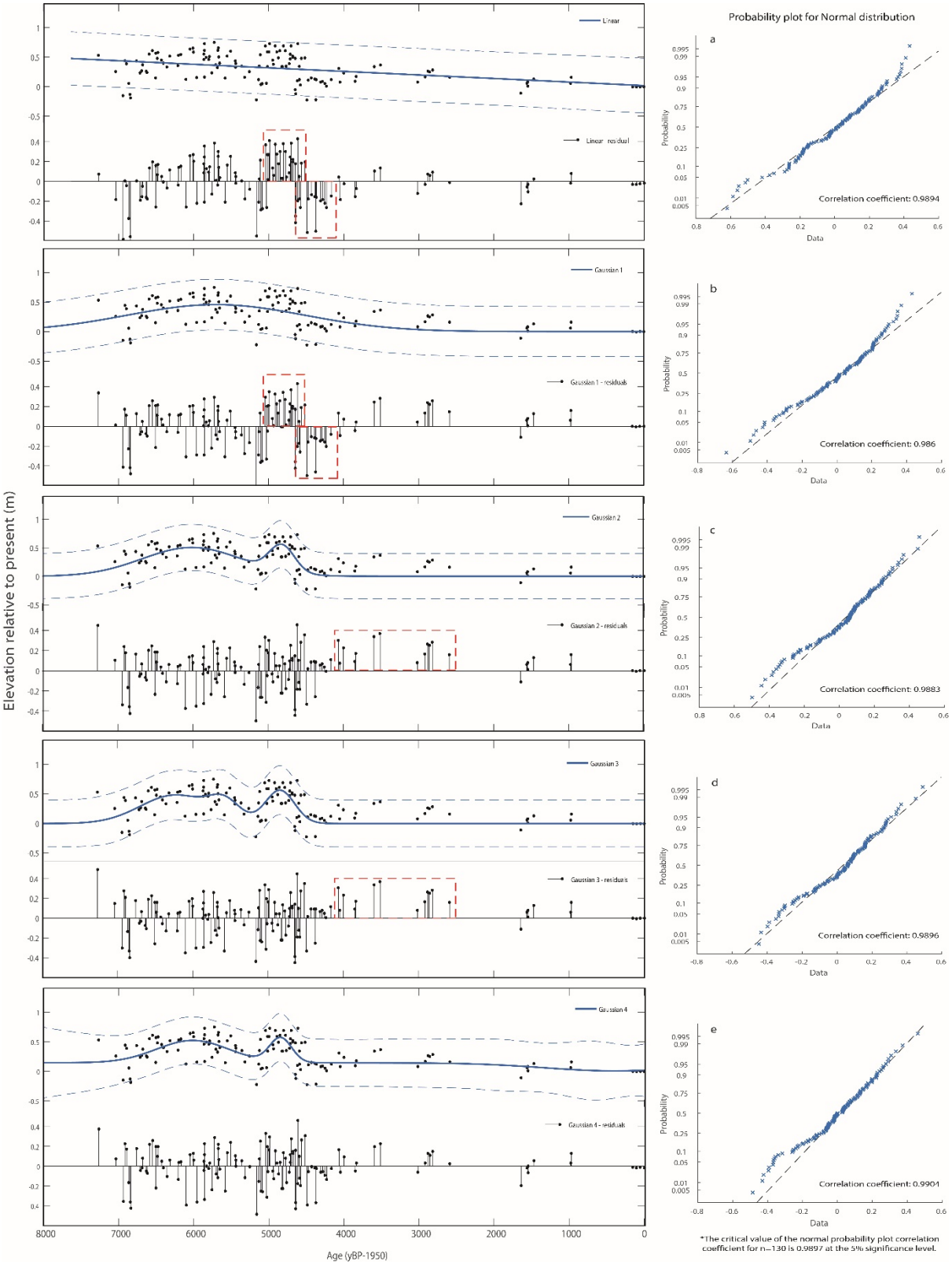

Supplementary Figure 4: Linear and Gaussian models of RSL based on U-Th dated coral microatolls and probability plots (normal distribution of the model residuals) from the Great Barrier Reef, Australia. Elevation is in metres (m) relative to present mean low water spring tide (MLWS), Age is in years before present (yBP) where present is defined as 1950. Gaussian 1-4 represents number of terms included in the analysis. Dotted blue lines are 95% confidence bounds, red dashed squares indicate predictive tendency of the residuals of the models indicating poor fit to the data. The correlation coefficient of normal distribution of the residuals is only significant (p = 0.05) for the highest term Gaussian model (Gaussian 4).

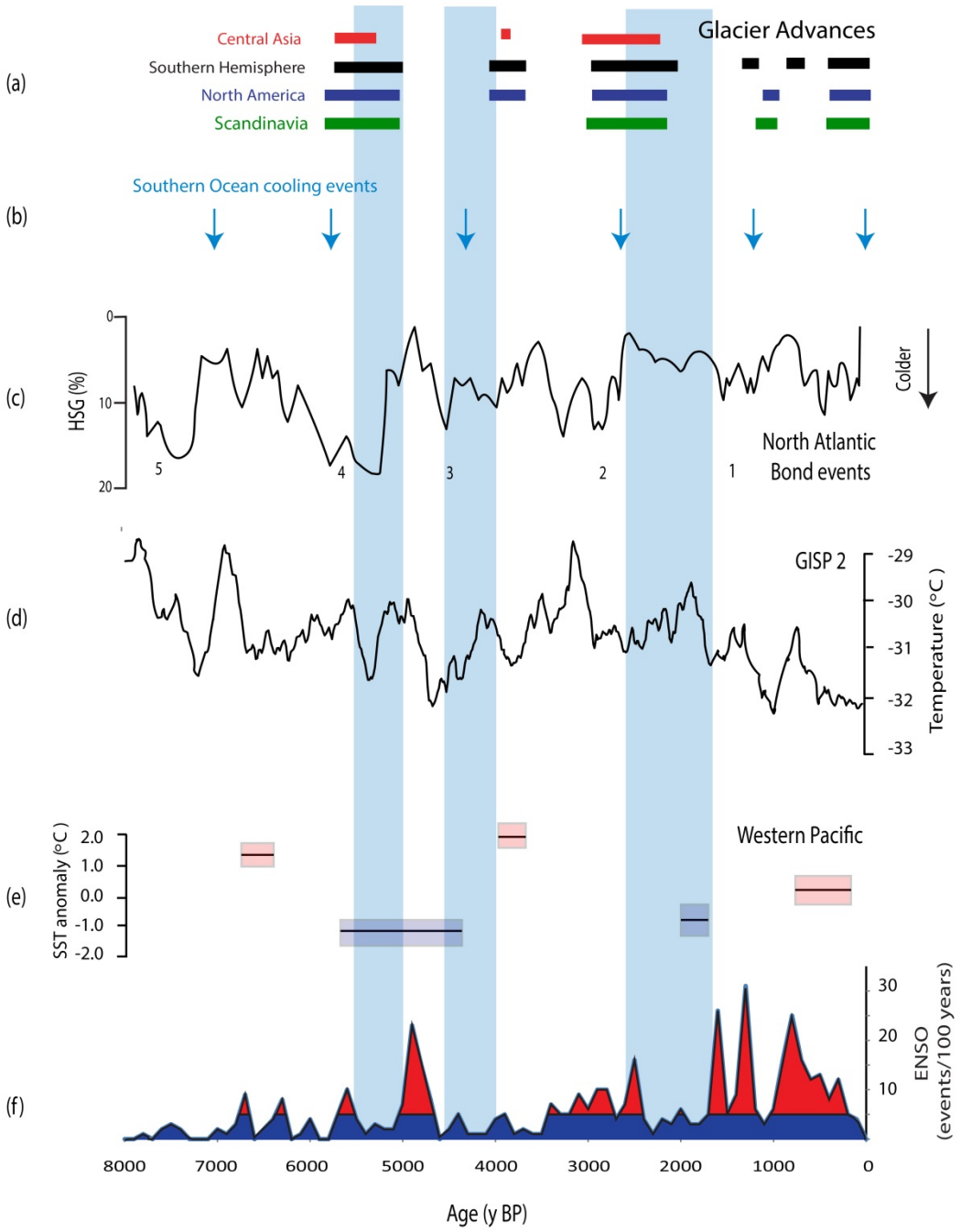

Supplementary Figure 5: Holocene climate records of; a) Northern and Southern hemisphere glacier advances (Denton and Karlén, 1973, Mayewski et al., 2004); b) δ18O derived Southern Ocean cooling events (Moros et al., 2009); c) percent haematite stained grains from North Atlantic cold events (Bond et al., 2001, Bond et al., 1997); d) Greenland ice core GISP 2 temperature record (Alley, 2004); e) Sr/Ca coral proxy derived SST from the western Pacific (Abram et al., 2009) and; f) Number of El Niño Southern Oscillation (ENSO) events in the eastern Pacific (Moy et al., 2002; Ecuador sediment record).

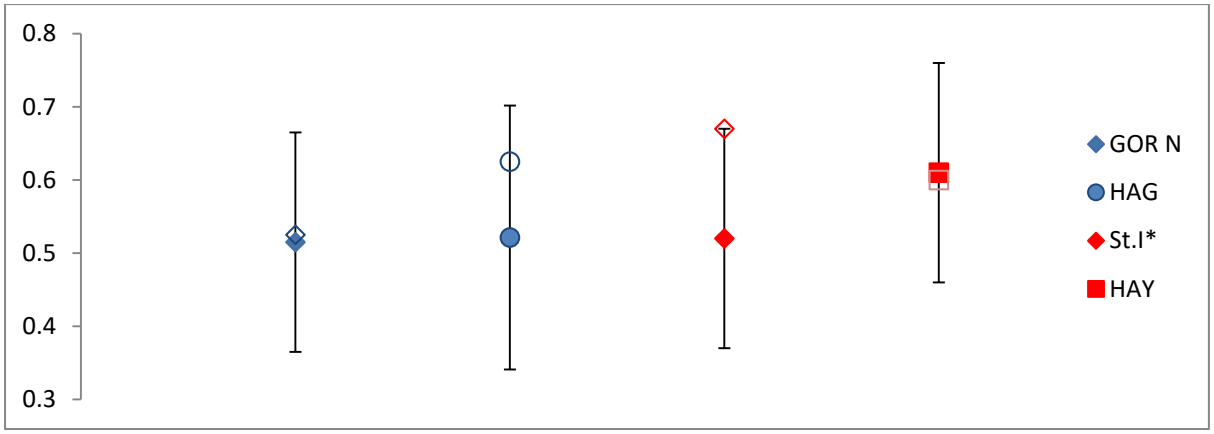

Supplementary Figure 6: Elevations of modern *Porites* sp. microatolls (closed symbols) compared to site specific modern mean low water spring tide level (MLWS; open symbols) obtained from the Australian Bureau of Meteorology. Errors are ± 15cm for Gore North (GOR N), Stone Island (St.I) and Hayman Island (HAY) calculated from laser level accuracy and still tide timed data. Haggerstone Island (HAG) elevation error is ± 18cm calculated from the standard deviation of modern microatoll elevations. * The modern microatoll used for Stone Island comparison was obtained from Bramston Reef located 3 km from the site.

Chapter 4

Evidence for reduced ENSO variance in the mid-Holocene: wavelet analysis of modern and fossil coral luminescence indices from the Great Barrier Reef

Leonard, N.D.[1,2], Welsh, K.J.[2], Lough J.M.[3], Feng, Y-x.[1,2], Pandolfi, J.M.[4], Clark, T.R.[1,2], Zhao, J-x.[1,2]

[1]Radiogenic Isotope Facility, School of Earth Sciences, The University of Queensland, Brisbane, Qld 4072, Australia

[2]School of Earth Sciences, The University of Queensland, Brisbane, Qld 4072, Australia

[3]Australian Institute of Marine Science, Townsville, Queensland, Australia

[4]Centre for Marine Science, Australian Research Council Centre of Excellence for Coral Reef Studies, School of Biological Sciences, The University of Queensland, Brisbane, Qld 4072, Australia

***Corresponding author: Nicole Leonard; email: nicole.leonard@uqconnect.edu.au**

Keywords: Wavelet transforms, coral luminescence, ENSO, palaeoclimate, mid-Holocene

Published: Paleoceanography 31(9), 1248-1260.

Abstract

Globally, coral reefs are under increasing pressure both through direct anthropogenic influence and increases in climate extremes. Understanding past climate dynamics that negatively affected coral reef growth is imperative for improving management strategies, and modelling of future coral reef responses to a changing climate. The El Niño Southern Oscillation (ENSO) is the primary source of climate variability at inter-annual timescales on the Great Barrier Reef (GBR), Australia. Applying continuous wavelet transforms to visually assessed coral luminescence intensity in massive *Porites* corals from the central GBR, we demonstrate that these records reliably reproduce ENSO variance patterns for the period 1880 – 1985. We then applied this method to three sub-fossil corals from the same reef to reconstruct ENSO variance from ~5200 – 4300 years before present (yBP). We show that ENSO events were less extreme and less frequent after ~5200 yBP on the GBR compared to modern records. Growth characteristics of the corals are consistent with cooler sea surface temperatures (SST) between 5200 and 4300 yBP compared to both the millennia prior (~6000 yBP) and modern records. Understanding ENSO dynamics in response to SST variability at geological timescales is instrumental to improving predictions of future ENSO response to a rapidly warming climate.

Introduction

With the future of coral reefs uncertain due to local and global environmental change, elucidating the controls on reef growth and decline in the recent geological past, prior to anthropogenic impacts, is imperative for developing realistic future management strategies (Pandolfi, 2015). Records of globally significant reef 'turn-off' (Buddemeier and Hopley, 1988) or hiatus events in the mid-Holocene (~6500 – 4500 years before present; yBP) are numerous, and have been attributed to various exogenic processes such as sea-level variability (Hamanaka et al., 2012, Leonard et al., 2013, Harris et al., 2015, Leonard et al., 2015), broad-scale climate shifts (Smithers et al., 2006, Perry and Smithers, 2011) or changed frequency and intensity of El Niño Southern Oscillation events (ENSO; Lybolt et al., 2011, Toth et al., 2012).

The effects of extreme ENSO events on the health of coral reef ecosystems has gained interest since the globally unprecedented mass coral bleaching event of 1998 which, due to anomalously high summer sea surface temperatures (SST; Hoegh-Guldberg, 1999, Lough, 2000), resulted in up to 87% of inshore corals on the Great Barrier Reef (GBR), Australia, being affected to some extent (Berkelmans and Oliver, 1999). This event was aligned with the strongest El Niño event recorded over the past century, and possibly over the past millennium (Lough, 2000). Alarmingly, first assessments (aerial and underwater surveys) of the effects of the 2015-2016 El Niño event have reported on moderate to severe bleaching for large tracts of coral reefs north of Townsville on the GBR, however the full extent of mortality and recovery will not be known for some time (GBRMPA, 2016).

Extreme La Niña events are also detrimental to coral reefs, with increased and persistent rainfall and increased tropical cyclogenesis (Kuleshov et al., 2008) resulting in amplified sediment and pollutant input and physical destruction to the GBR lagoon, causing coral mortality (Butler et al., 2013, Jones and Berkelmans, 2014). Therefore, understanding ENSO dynamics on the GBR in the Mid-Holocene is not only vital to disentangling the cause/s of reef hiatuses in the past, but offers an opportunity to understand potential response to changes to ENSO in the future.

A suite of proxies in both terrestrial and marine environments have been developed to interpret climatic and environmental dynamics at geological timescales (Wanner et al., 2008, Jones et al., 2009). Both geochemical and ecological information can be extracted from sediment cores, offering long histories of climatic data to be inferred, but at relatively low

(centennial – millennial) resolution (e.g. Gupta et al., 2003, Conroy et al., 2008, Marcott et al., 2013). Conversely, annually banded coral skeletons enable high-resolution analysis of palaeoclimate proxies, often at intra-annual scales, yet are normally restricted to short time windows for sub-fossil corals (Zinke et al., 2015).

One of the simplest and most efficient methods of extracting information from massive coral cores is by measuring growth characteristics, such as linear extension, calcification rate and skeletal density. These growth characteristics have been linked to both environmental and climatic controls on modern corals from the GBR (Lough et al., 1999, Lough and Barnes, 2000, Cooper et al., 2008, De'ath et al., 2009, Cantin and Lough, 2014), Thailand (Tanzil et al., 2009, Tanzil et al., 2013), the Maldives (Storz and Gischler, 2010) and the central Red Sea (Cantin et al., 2010). Annual density bands in corals (Knutson et al., 1972) enable measurement of the linear extension rates in massive, long-lived *Porites*, where high density and low density couplets represent one year of coral growth. A report of the growth characteristics of 264 colonies and 35 cores obtained from *Porites* on the GBR demonstrated broad scale geographic responses, and latitudinal patterns in extension and calcification rates, with lower rates linked to cooler sea surface temperatures (SSTs) in the southern GBR (Lough et al., 1999).

A second rapid assessment method is the visual assessment of coral luminescent lines under ultra-violet (UV) light (Isdale et al., 1998, Lough and Barnes, 2000, Hendy et al., 2003, Lough, 2007). The correlation between luminescent lines in nearshore corals of the GBR and river discharge/rainfall was first described by Isdale (1984), with initial investigations suggesting that the distinct luminescent lines resulted from terrestrial humic/fulvic acids transported in river flood plumes (Boto and Isdale, 1985, Susic et al., 1991), a link further supported by Llewellyn et al. (2012). Rainfall, and thus river flow, in northeast Queensland coastal river catchments is strongly modulated by ENSO with El Niño (La Niña) events supressing (increasing) rainfall (Lough, 1991). Consequently, luminescent lines in corals used to reconstruct rainfall and river flow for the region have also been used to infer the frequency and strength of driving climatic mechanisms such as ENSO and the Pacific Decadal Oscillation (PDO) beyond instrumental records (Isdale et al., 1998, Lough et al., 2002, Lough, 2007, Lough, 2011b, Lough et al., 2014, Rodriguez-Ramirez et al., 2014). Holocene records of ENSO derived from GBR coral luminescence suggests that the frequency and intensity of ENSO was reduced ~6000 yBP (Lough et al., 2014). Coral luminescence and $\delta^{18}O$ from a microatoll at King Reef suggests generally wetter conditions

by ~4700 yBP, in agreement with palynological evidence from north Queensland of more La Niña like mean state of climate at this time (Shulmeister and Lees, 1995). Similar evidence of reduced ENSO variance has also been found in central Pacific corals at 4300 yBP (McGregor et al., 2013); although an alternative explanation suggests that Mid-Holocene ENSO variance was not reduced, but that modern ENSO variance is comparatively greater than that of the last 7000 years (Cobb et al., 2013).

A number of environmental and climatic studies are now taking advantage of wavelet analysis of time-series data (Gu and Philander, 1995, Torrence and Compo, 1998, Grinsted et al., 2004, Debret et al., 2009, Grove et al., 2013, Walther et al., 2013, Soon et al., 2014, Lough et al., 2015). Wavelet power spectrums allow interpretation of one dimensional time series data in two dimensional time-frequency space, allowing for modes of climate variability, and climate variability through time, to be assessed simultaneously (Torrence and Compo, 1998). Grove et al. (2013) used cross-wavelet coherency to demonstrate links between coral luminescence and proxy records of the PDO in Madagascar. On the GBR, wavelet analysis of coral Ba/Ca signals showed high inter-annual variability, with periodicity possibly linked to ENSO (Walther et al., 2013). Lough et al. (2015) used regression analysis of luminescence data from a 364-year coral core from Havannah Island to reconstruct Burdekin River flow, with a subsequent wavelet analysis revealing weakened ENSO variance (in the 2-8 year band) prior to 1860, and increasing variability in the latter part of the 19th century (Lough et al., 2015).

The focus of the present study is the application of rapid visual assessment of luminescence intensity as a proxy for river flow (Lough, 2011b), combined with wavelet power spectrum analysis, to assess mid-Holocene climate variability and ENSO dynamics. This approach is applied to a previously published modern luminescence record from Great Palm Island (GPI), central GBR (Hendy et al., 2003), and three fossil corals retrieved as part of a dredging program from the same reef. ENSO dynamics are determined through analysis of the Niño 3 (5N-5S 150W-120W) and Niño 3.4 (5N-5S 170W-120W) sea surface temperature (SST) anomaly ENSO index (see www.ncdc.noaa.gov/teleconnections/enso/indicators/sst.php; and Trenberth and Stepaniak, 2001).

Methods

Regional Setting

Great Palm Island (GPI, 18˚44, 146˚34) is a nearshore (~30km from the mainland) granitic island located in the Queensland dry tropics (Fig. 1; Jompa and McCook, 2003). The region experiences most of its annual rainfall in the austral spring - summer (October-March); however, inter-annual variability is high (Lough, 1991) driven mainly by ENSO variability (Risbey et al., 2009, Klingaman et al., 2013). Located ~60km north-west of Townsville, GPI is regularly affected by freshwater flows from the Burdekin River (King et al., 2001), the largest contributor to terrestrially derived sediments onto the GBR (Brodie et al., 2010, Schroeder et al., 2012, Bainbridge et al., 2014).

Fossil core collection and processing

Between January and May 2009, ~11 000m^3 of material was dredged from the main channel to GPI to allow for better access to the jetty. The resultant dredge material was transported by barge to a landfill site in Townsville. Amongst the dredge material were several massive "bommies" (1.5 to 2.5 m diameter) of which, in July 2012, five *Porites* (Palm Island - PAM 1.0, 2.0, 3.0, 5.0 and 6.0) and one *Favia* (PAM 4.0) were cored using a pneumatic drill (water lubricated), with additional surface samples of two *Porites* (PAM 7.0 and 8.0) collected by hammer and chisel. As the original orientation of the corals was unknown, small pilot cores were drilled and the cores were extracted to check the alignment of the annual density bands. Once the orientation was established, cores were drilled using a ~6 cm diameter coring barrel. In an effort to improve alignment, some corals were sampled 2-3 times at different locations on the colony (e.g. PAM 3.0 - 3.3). Cores were rinsed in water prior to transportation. To further assess the orientation of the cores, computed tomography (CT) scans were conducted at St Vincent's Hospital, Brisbane. Images were viewed in the software programme Osirex® where the best alignment was determined using 3D visualisation of the annual density bands. Based on the density band alignment viewed in the CT scans, corals PAM 1.0, 2.0, 3.0, 3.1 and 5.0 were selected for further preparation. These coral cores were cut longitudinally along the inferred major growth axes into ~6 mm thick slices, ultra-sonicated in Milli-Q water for 15 minutes three times, and dried in a carbonate only oven at ~60˚C in facilities at the School of Earth and Environment, University of Western Australia.

To examine the annual density bands in the coral slabs, the selected corals were X-rayed at Queensland Diagnostic Imaging, Indooroopilly, Queensland (Supp. Figs. 1a-c). The clearest and most continuous density bands were observed in PAM 5.0, PAM 2.0 and PAM 3.1, so these were selected for further analysis. Annual linear extension rates were measured between adjacent high density bands using the X-ray positive prints (austral summer – summer) which was also used to establish the core chronological length (i.e. one couplet of high and low density banding is equal to one year of growth) (Lough and Barnes, 1990). Eight separate fossil coral colonies from GPI were dated by high precision U-Th dating at the Radiogenic Isotope Facility at the University of Queensland following the methods of Leonard et al. (2015) and Clark et al. (2014b). Approximately 50mg of ultra-cleaned aragonite was used for dating both near the base of the coral cores (n = 6; PAM 1.0 –PAM 6.0) and surface samples from colonies that were not cored (PAM 7.0 – PAM 8.0). Core replicates (from adjacent annual bands and different cores from the same colony) were dated in 2012 and 2014 to cross-check the age of the colonies. Sample ages were calculated using the decay constants of Cheng et al.(2000) using Isoplot/Ex software (Ludwig, 2003) and corrected for initial detrital ^{230}Th using a two-component mixing correction (Clark et al., 2014a).

Corals slabs were viewed under UV light in a darkened room and visual assessment of luminescent lines was conducted following the methods of Hendy et al. (2003) and Lough (2007) where luminescent lines are graded; 0 = no visible line; 1 = faint luminescent line; 2 = moderate luminescent line and; 3 = strong luminescent line (Supp. Figs. 1a-c). This simple visual assessment has been shown to be reproducible to 81% between different assessors (Lough et al., 2002), and has been successfully used to cross correlate chronologies between coral cores on the GBR (Hendy et al., 2003). Luminescent line intensity was first viewed for a modern coral core collected from nearby Havannah Island in 2009 (Fig. 1) for comparison with luminescence strength in the fossil corals. We then assigned visual assessment indices to the annual luminescent signals in the fossil corals with the clearest and most continuous luminescent lines (PAM 5.0 – 55 years, PAM 2.0 – 21 years and PAM 3.1 -53 years).

Data analysis

To determine whether the fossil coral luminescence index data could reliably reconstruct ENSO, continuous wavelet transforms were first applied to a previously published luminescence index record from a modern coral record spanning 1880 – 1985 from GPI

(Hendy et al., 2003) and to ENSO (Niño 3.0 and Niño 3.4) SST indices for the same period. As luminescent signals are annual, monthly (extended) HadISST1 data for Niño 3 (www.esrl.noaa.gov/psd/gcos_wgsp/Timeseries/Data/nino3.long.anom.data) and Niño 3.4 (www.esrl.noaa.gov/psd/gcos_wgsp/Timeseries/Data/nino34.long.anom.data) data were converted to average annual indices (Jan-Dec). Continuous wavelet transforms (Morlet) were performed in Matlab® statistical programme using the online toolkit of Grinsted et al. (2004) available from www.glaciology.net/wavelet-coherence, which is modified from and includes, the toolkit of Torrence and Compo (1998; http://paos.colorado.edu/research/wavelets/).
Cross wavelet transform (XWT) and wavelet coherency transform (WCT) were then applied to the luminescence data and averaged annual Niño 3 and Niño 3.4 SST anomaly data to determine periods of high common power and covariance, respectively. Morlet wavelet transforms were then applied to the three fossil coral records from GPI with the clearest annual density banding and luminescence lines for comparison (PAM 5.0, PAM 2.0 and PAM 3.1).

Results

Uranium-thorium dating

Eight separate massive colonies were U-Th dated from the GPI dredge material, comprising six coral cores and two surface samples (Table 1). The oldest colony was dated to 6079 ± 23 and the youngest to 3784 ± 13 years before present (yBP – where present is 1950); however, six of the eight colonies all lived and died in the period between ~5300 and 4300 yBP. Core PAM 5.1 showed an interruption in growth, ~16.5 cm from the top of the core, where the corallites at the surface were preserved, likely due to partial mortality. Dating of the coral core below and above this horizon revealed indistinguishable ages (5120 ± 46 and 5125 ± 42 respectively). This core contained conspicuous brown bands just prior to and after this surface, with an increase in micro- and macro-borings. Under binocular microscope these bands were found to be caused by organic filaments threading through the pores of the skeleton parallel to the growth surface. These bands are possibly a micro-algae or remnants of macro-algae; however, further work is needed to identify the exact cause.

Density banding was not always clear throughout all the cores collected, which can be due to coring not being perfectly oriented along the major growth axes of the colonies and convoluted growth patterns (Lough and Barnes, 1992). Clear annual density bands were observed in PAM 5.0, 3.1 and 2.0 (Supp. Figs. 1a-c). The average linear extension rates of

coherent density bands of these cores were all <10mmyr^{-1}, with the top ~10cm of PAM 3.1 <5mmyr^{-1} (Supp. Fig 1c). These three corals also showed the clearest luminescent lines when viewed under UV light and were therefore selected for visual luminescence assignment (Supp. Figs. 1a-c). Luminescence index assignment in the top ~8 – 10 cm of each core was not possible due to significant detritus interfering with the luminescent signal. The resultant luminescent index record lengths based on clear annual density patterns were thus; PAM 5.0 – 55 years, PAM 2.0 – 21 years and PAM 3.1 - 53 years.

Wavelet analysis of modern coral luminescence

As numerous fossil corals from multiple sites that chronologically overlap are rare (Lough et al., 2014), we used only the single modern luminescence record from GPI to test the efficacy of wavelet transforms in reproducing ENSO signals. Visual comparison of wavelet power spectra of modern coral luminescent index records from GPI (Hendy et al., 2003) and annually averaged Niño 3 and Niño 3.4 SST index records show coherent power of variance for periods of relatively strong ENSO in the 2-8 band frequency (1890-1920 and 1970-1980) and reduced ENSO variance (1930-1950; Fig. 2). The Niño 3.4 wavelet analysis shows no significant power for 1890 – 1920; however it is still notably high for this period (Fig. 2b). Cross wavelet transform (XWT) of Niño 3 and Niño 3.4 with GPI luminescence index data shows high common power (95% significance level) in the ~2-4 year band for 1890-1910, in the 4-7 year band for 1910-1920 and the 1-4 year band for 1970-1980 (Fig. 3). Arrows in the significant regions of the 4-7 year band indicate a lag in the response between Niño 3, Niño 3.4 and the GPI coral luminescence index data. A test of wavelet coherency (WTC) indicates more significant covariance between the GPI luminescence index data and Niño 3.4 than Niño 3, especially in the 8 year band for 1935 – 1960 (Fig. 4). Significant covariance occurs between GPI luminescence and both ENSO index regions in the 2-8 year band for ~ 1890-1920 and in the early 1970's. A strong power and significant coherency are observed in the ~15- 30 year band, although this is largely within the cone of influence (COI), so is interpreted cautiously.

Wavelet analysis of fossil coral luminescence

Continuous wavelet transforms (Morlet) of the fossil coral core luminescent indices shows significance in the power spectra (95% confidence interval) for PAM 5.0 (~5200 yBP) and PAM 3.1 (~4300 y BP) however, not for PAM 2.0 (~4900 yBP) (Fig. 5). The lack of significance in the PAM 2.0 coral is likely due to the limited number of years in this record

(21 years) which may only reflect three normal ENSO cycles (2-7 years). This coral does however indicate a relatively weak signal of variance in the 1-3 year band. At 5200 yBP (PAM 5.0; Fig 5a), significant power is observed in the 5-8 year band for the earliest part of the record, then only briefly significant in the 2-3 year band before no further significance in period is observed. At 4300 yBP, PAM 3.1 (Fig. 5c) is only intermittently significant in the 1-6 year band, with increased power also observed in the ~10 -16 year band (although largely within the COI).

Discussion

Currently there is a lack of continuous high-resolution palaeoclimate data from the Southern Hemisphere (Neukom and Gergis, 2012, Wanner et al., 2015) largely due to difficulties in obtaining suitable samples for sub-annual to decadal proxy reconstructions. Massive fossil corals offer the ability to conduct high-resolution sampling at sub-annular scales (Cobb et al., 2013, Zhang et al., 2014); however, finding a continuous temporal sequence of samples across millennia is difficult, and the preservation state of the corals greatly affects geochemical signal reliability (McGregor and Gagan, 2003, McGregor and Abram, 2008). At nearshore locations on the GBR, measured and visually assessed annual coral UV luminescence signals have been shown to reliably record river flow and rainfall variability associated with both ENSO (Hendy et al., 2003, Lough, 2011a) and the PDO (Rodriguez-Ramirez et al., 2014) thus offering potential as a valuable archive for reconstructing palaeo-ENSO activity. Here we demonstrate the potential for wavelet transforms of rapid visual assessment of luminescent lines in corals to reconstruct ENSO-related climate variability in the central GBR.

Wavelet transform of modern coral luminescence

The visually assessed modern coral luminescence data from GPI used in the present study was first reported by Hendy et al. (2003) as part of a luminescence cross chronology calibration effort, with a subsequent study using measured luminescence values on the same coral (Lough, 2007). A significant correlation was found between the luminescence master chronology based on up to 8 coral luminescence records for the central GBR and an instrumental and modelled Burdekin river discharge record (Isdale et al., 1998) for 1894-1985 ($r = 0.82$; Hendy et al., 2003), and the GPI only core ($r = 0.69$; Lough, 2007) indicating that coral luminescence is a reliable proxy for river discharge volume. Hendy et al. (2003) also reported a weak but significant ($r = -33$) correlation between their luminescence master

chronology and reconstructed Niño 3 SST index (Mann et al., 2000) from 1650-1980. However, the strength of the relationship between ENSO and Queensland rainfall and river flow does vary through time (Hendy et al., 2003), being modulated on multi-decadal time scales by the PDO (Kiem et al., 2003, Verdon et al., 2004, Meinke et al., 2005, Rodriguez-Ramirez et al., 2014)

In the present study, continuous wavelet transform of the GPI coral luminescent index record (Hendy et al., 2003) for the period 1880 – 1985 is comparable to both the Niño 3 and Niño 3.4 SST indices, with significant peaks in the ~3-7 year band ($p = 0.05$) in 1890–1900, the early 1950's, and 1970-1980 (Fig. 2). The only difference between the Niño 3 and Niño 3.4 region data is a significant power in the ~7 year band in the Niño 3 record between 1910 - 1920. Although this band has relatively high power in the Niño 3.4index, it is not significant. This phase is evident (and significant) in the GPI luminescence record, suggesting that central Queensland rainfall responds to SST anomalies in both ENSO index regions. The luminescent index record also shows reduced ENSO variance between ~1925-1950 which is coincident with a PDO warm phase (1916-1943), which has been shown to weaken ENSO teleconnections and reduce the inter-annual variability of Queensland rainfall (Lough, 1991, Lough, 2007).

Wavelet coherency (Fig. 4) indicates higher and stronger covariance between the GPI coral record and the Niño 3.4 region, indicating that SST anomalies in the central Pacific are more strongly linked to Queensland rainfall than Niño 3, as noted in previous coral records from the same region (Lough et al., 2015). Higher power is also observed in the annual cycle when ENSO variance is reduced, which is in agreement with observations that increased annual cycle amplitudes decreases ENSO variance (Wang, 1994, Gu and Philander, 1995), although the relationship between these two cycles is not fully resolved (Qian et al., 2011, Emile-geay et al., 2016). High power and sometimes significant covariance between Niño 3 and GPI, and Niño 3.4 and GPI also occurs in the ~16-35 year band, which is likely a manifestation of the PDO; however, as most of this record falls outside the cone of influence (COI) it is interpreted cautiously (Fig. 4). Overall the modern GPI luminescence record reflects both phases of increased and decreased ENSO activity in the 3-7 year band over the 100 year record compared to both Niño 3 and Niño 3.4 ENSO indices, and is therefore considered appropriate for interpreting palaeo-ENSO signatures from the fossil coral cores.

Fossil coral analysis and ENSO

Examination of the UV luminescence index of the fossil coral cores from GPI provide windows into mid-Holocene ENSO variability at ~5200 y BP (PAM 5.0), 4900 y BP (PAM 2.0) and ~4300 y BP (PAM 3.1) on the GBR. The intensity of the luminescent lines in the fossil cores was reduced when compared to a modern core from nearby Havannah Island and with the modern luminescent index data of Hendy et al. (2003) from GPI. Although the depth at which the fossil corals grew is unknown, previous results derived from massive *Porites* corals from nearby by Rib Reef (~35km to the NE) demonstrated no significant difference in either luminescent signal or linear extension rates in corals collected from between 0 - 20 metres depth (Carricart-Ganivet et al., 2007) suggesting that fossil coral depth is unlikely to affect our results.

A second caveat for consideration is that the reduced luminescent intensity observed in the fossil corals may be due to either less intense discharge events in the mid-Holocene or to modern rainfall to run-off ratio increases due to anthropogenic catchment modifications in the Burdekin region (Lough et al., 2015). Yet, regardless of differences observed in luminescent intensity, the relative variability of the inter-annual luminescent signal is informative for understanding the periodicity of Burdekin River discharge events and thus ENSO variability.

The modern GPI average luminescence index value (0.9 ± 1.1; standard deviation) is similar to the average values for PAM 5.0 (0.8 ± 0.8), PAM 2.0 (1.0 ± 0.75) and PAM 3.1 (1.0 ± 0.7). However, the standard deviations for the modern coral are higher than for the fossil corals, suggesting reduced ENSO variability in the mid-Holocene. Further visual inspection of the luminescent index time series shows far fewer intense (strong La Niña) and absent luminescent line (strong El Niño) events occurred in the Holocene record compared to the modern luminescence record, indicating that the strength of ENSO was also subdued in the mid-Holocene compared to the late 20th century (Supp. Figs. 2a-d).

Wavelet transform (Morlet) of the luminescent signal at 5200 y BP (PAM 5.0) indicates an active ENSO in the 5-8 year band in the earlier part of the coral record, similar to modern ENSO variance (Fig. 5a). This was followed by a shift to increased frequency (~3 year band) and then no significant periodicity towards the end of the record. At ~4900 y BP (PAM 2.0) there was no significant spectral power across the series although there is slight power at the annual to biannual level (Fig. 5b). This may be partly a function of the shorter record (21 years) available from this core which does not cover an entire ENSO cycle (Walther et al.,

2013); however, a reduction in ENSO frequency after ~5100 y BP was also evident in core PAM 5.0. At ~4300 y BP (PAM 3.1) there were temporally shorter significant periods of variance in the 1-4 year band and 11-20 year band, suggesting less frequent ENSO events at this time (Fig. 5c). Our combined coral luminescence record is in agreement with previous climate reconstructions indicating reduced frequency of ENSO between ~5500 and 3500 y BP in the eastern Pacific Galapagos Islands (Zhang et al., 2014), central Pacific Line Islands (Cobb et al., 2013), and Kiritimati Island (McGregor et al., 2013). Reduced intensity and variability of luminescent signals have also been reported for a series of fossil corals (~6000 y BP) from Magnetic Island (~40 km south of GPI), which is also influenced by Burdekin River discharge (Lough et al., 2014). A marked difference between the fossil corals from GPI fossil and Magnetic Island is a substantially lower linear extension rate at GPI. The mid-Holocene corals from Magnetic Island exhibited similar extension rates to their modern counterparts (12.14 ± 3.58 mm.yr^{-1} and 13.34 ± 4.43 mm.yr^{-1}, respectively). Comparatively, average modern linear extension rates for *Porites* on GPI are with nearby massive *Porites* at Pandora and Havannah Islands having modern extension rates of 15.3 ± 2.6 mm.yr^{-1} and 12.1 ± 3.3 mm.yr^{-1}, respectively(Lough and Barnes, 1997, Lough et al., 1999). This gives an average regional growth rate of *Porites* of 15.4 ± 3.3 mm.yr^{-1} compared to the 5200 yBP GPI coral which had an average linear extension of only 6.9 ± 1.4 mm.yr^{-1}, with similarly low extension rates for the 4900 and 4300 y BP colonies (generally <10mm.yr^{-1}). As annual extension rates have been shown to be greater in large (1.6 - 8.0 m height) versus small colonies (0.1 -0.7 m) on the GBR (Lough and Barnes, 2000), and the GPI fossil corals are all >1.5 m diameter, the lower extension rate is inferred to be indicative of an environmental or climatic influence. On the GBR (and throughout the Indo-Pacific) average linear extension rates have been linked to average SST, with more southerly locations (lower SST) showing reduced linear extension (Lough and Barnes, 2000, Lough and Cantin, 2014), thus suggesting cooler SST conditions at GPI at 5200 yBP compared to present. In a comprehensive review of growth characteristic of *Porites* corals on the GBR, Lough and Barnes (2000) demonstrated that for each 1˚C rise in SST, average linear extension increased by 3.1 mmyr^{-1}. Using this as a first order assumption for the fossil GPI corals this suggests SST were ~2.5˚C cooler at 5200 yBP than at 6000 yBP (Lough et al., 2014). Cooler than present SSTs of -2.0˚C at 5200 yBP have recently been inferred from Sr/Ca records from a *Porites* coral core from Heron Island, southern GBR, which corroborates with the evidence presented here for GPI. This recent paleo-SST record from Heron Island differs from an earlier Sr/Ca resolved

SST reconstruction that suggested 1˚C warmer conditions at 5300 yBP in the central GBR (Gagan et al., 1998); however, recalibration of the C^{14} date of this coral places it at ~6200 yBP (Sadler et al., *in review*), supporting evidence of similar extension rates to modern corals at 6000 y BP at Magnetic Island (Lough et al., 2014). As linear extension has also been shown to be lower at offshore than inshore sites in the modern record (Lough et al., 1999), an alternate interpretation of lower linear extension rates at GPI is that the waters surrounding these reefs were more oligotrophic in the mid-Holocene. Further work on high-resolution paleo-SST is clearly required on the GBR before any firm conclusions can be drawn. However, the documented cooling at Heron Island and in the wider Pacific after ~5500 y BP (Sadler et al., *in review*) suggests that reduced SSTs are the most likely source of limited linear extension at GPI in the mid-Holocene.

Conclusions

Deriving high-resolution paleoclimatic and paleoenvironmental data from massive corals is generally time intensive and expensive. In the present study we have shown that simple visual assessment of luminescent lines in annually banded *Porites,* used in conjunction with continuous wavelet transforms (Morlet), enables reconstruction of major characteristics of ENSO variability in time-frequency space. Besides the obvious advantages of reduced processing times compared to geochemical analysis, this method also allows for evaluation of fossil *Porites* cores that may not be perfectly aligned with the growth axis, or are diagenetically altered. Furthermore, as luminescence in corals is visible as a surface phenomenon, distortions due to convoluted colony growth are negligible compared to assessments of linear extension, calcification and density (Lough and Barnes, 1990). Consequently, this method can potentially be applied to massive colonies that had been previously rejected because alignment with the growth axis was imperfect such as those collected as part of reef matrix coring efforts.

Results from wavelet transforms of coral luminescence indices between ~5200 and 4300 yBP at GPI suggests less frequent and less intense ENSO events during the mid-Holocene, which agrees well with previous observations from elsewhere on the GBR (Lough et al., 2014) and in the wider Pacific (Cobb et al., 2013, McGregor et al., 2013, Zhang et al., 2014). The reduction in ENSO frequency in the 2-7 year band after 5200 y BP is also coincident with lower linear extension rates in the fossil corals compared to modern values, suggestive of cooler SSTs, which is in agreement with a recent Sr/Ca reconstruction from the southern

GBR (Sadler et al. 2016 – in review). This record encompasses the period when significant and widespread reef flat declines and reef "turn off" events occurred on the GBR at 5500 yBP and 4600 yBP, respectively (Smithers et al., 2006, Perry and Smithers, 2011). Although the majority of the corals dredged from GPI all lived and died within the period of reef decline on the GBR, we find no evidence of increased intensity or frequency in ENSO that would drive mid-Holocene reef mortality on the GBR. This is contrary to evidence for the eastern Pacific reef hiatus after 4200 yBP for which presumed El Niño related bleaching, and La Niña related increases in turbidity were attributed to reef "turn-off" and hiatus, respectively (Toth et al., 2012).

Future work should concentrate on applying this method to fossil *Porites* cores retrieved from reef matrix cores to enable more ENSO windows of the past to be reconstructed, and to previously published luminescent records from the GBR covering the past few centuries. Understanding ENSO dynamics in response to SST variability over longer time scales than the instrumental record period is important for predicting how this dominant mode of tropical inter-annual climate variability may respond to a rapidly warming climate, and what effect this may have on the future of the GBR.

Acknowledgments

This study was funded by the National Environmental Research Programme (NERP) Tropical Ecosystems Hub Project 1.3 'Characterising the cumulative impacts of global, regional and local stressors on the present and past biodiversity of the GBR' to J-xZ, JMP, SGS, TRC, Y-xF and others, and Australian Research Council LIEF grant (LE0989067 for the purchase and installation of the MC-ICP-MS essential for this study) to J-xZ, JMP, Y-xF and others, as well as an Australian Postgraduate Award (APA) to NDL. We are grateful to Eric Matson from the Australian Institute of Marine Science (AIMS) for technical assistance in obtaining the fossil coral cores and to Hard Rock Earth Works (Rod Morelli and associates) in Townsville for allowing access to the corals. We also thank St Vincent's Private Hospital, Brisbane for CT scans and Queensland Diagnostic Imaging, Indooroopilly for X-rays.

References

Bainbridge, Z. T., Lewis, S. E., Smithers, S. G., Kuhnert, P. M., Henderson, B. L. & Brodie, J. E. 2014. Fine-suspended sediment and water budgets for a large, seasonally dry tropical catchment: Burdekin River catchment, Queensland, Australia. *Water Resources Research* **50,** 9067-9087.

Berkelmans, R. & Oliver, K. J. 1999. Large-scale bleaching of corals on the Great Barrier Reef. *Coral Reefs* **18,** 55-60.

Boto, K. & Isdale, P. 1985. Fluorescent bands in massive corals result from terrestrial fulvic acid inputs to nearshore zone. *Nature* **315,** 396-397.

Brodie, J., Schroeder, T., Rohde, K., Faithful, J., Masters, B., Dekker, A., Brando, V. & Maughan, M. 2010. Dispersal of suspended sediments and nutrients in the Great Barrier Reef lagoon during river-discharge events: conclusions from satellite remote sensing and concurrent flood-plume sampling. *Marine & Freshwater Research* **61,** 651.

Buddemeier, R. W. & Hopley, D. Year. Turn-ons and Turn-offs; Causes and mechanisms of the initiation and termination of coral reef growth. *In:* Proceedings of the 6th International Coral Reef Symposium, 1988 Australia. 253 - 261.

Butler, I., Sommer, B., Zann, M., Zhao, J.-X. & Pandolfi, J. 2013. The impacts of flooding on the high-latitude, terrigenoclastic influenced coral reefs of Hervey Bay, Queensland, Australia. *Coral Reefs* **32,** 1149-1163.

Cantin, N. E., Cohen, A. L., Karnauskas, K. B., Tarrant, A. M. & Mccorkle, D. C. 2010. Ocean warming slows coral growth in the central Red Sea. *Science* **329,** 322-325.

Cantin, N. E. & Lough, J. M. 2014. Surviving Coral Bleaching Events: *Porites* Growth Anomalies on the Great Barrier Reef. *PloS one* **9,** e88720.

Carricart-Ganivet, J. P., Lough, J. M. & Barnes, D. J. 2007. Growth and luminescence characteristics in skeletons of massive Porites from a depth gradient in the central Great Barrier Reef. *Journal of experimental marine biology and ecology* **351,** 27-36.

Cheng, H., Edwards, R. L., Hoff, J., Gallup, C. D., Richards, D. A. & Asmerom, Y. 2000. The half-lives of uranium-234 and thorium-230. *Chemical Geology* **169,** 17-33.

Clark, T. R., Roff, G., Zhao, J.-X., Feng, Y.-X., Done, T. J. & Pandolfi, J. M. 2014a. Testing the precision and accuracy of the U–Th chronometer for dating coral mortality events in the last 100 years. *Quaternary Geochronology* **23,** 35-45.

Clark, T. R., Zhao, J.-X., Roff, G., Feng, Y.-X., Done, T. J., Nothdurft, L. D. & Pandolfi, J. M. 2014b. Discerning the timing and cause of historical mortality events in modern Porites from the Great Barrier Reef. *Geochimica et Cosmochimica Acta* **138,** 57-80.

Cobb, K. M., Westphal, N., Sayani, H. R., Watson, J. T., Di Lorenzo, E., Cheng, H., Edwards, R. L. & Charles, C. D. 2013. Highly variable El Niño-Southern Oscillation throughout the Holocene. *Science (New York, N.Y.)* **339,** 67.

Conroy, J. L., Overpeck, J. T., Cole, J. E., Shanahan, T. M. & Steinitz-Kannan, M. 2008. Holocene changes in eastern tropical Pacific climate inferred from a Galápagos lake sediment record. *Quaternary Science Reviews* **27,** 1166-1180.

Cooper, T. F., De'ath, G., Fabricius, K. E. & Lough, J. M. 2008. Declining coral calcification in massive Porites in two nearshore regions of the northern Great Barrier Reef. *Global Change Biology* **14,** 529-538.

De'ath, G., Lough, J. M. & Fabricius, K. E. 2009. Declining coral calcification on the Great Barrier Reef. *Science (New York, N.Y.)* **323,** 116-119.

Debret, M., Sebag, D., Crosta, X., Massei, N., Petit, J. R., Chapron, E. & Bout-Roumazeilles, V. 2009. Evidence from wavelet analysis for a mid-Holocene transition in global climate forcing. *Quaternary Science Reviews* **28,** 2675-2688.

Emile-Geay, J., Cobb, K. M., Carré, M., Braconnot, P., Leloup, J., Zhou, Y., Harrison, S. P., Corrège, T., Mcgregor, H. V., Collins, M., Driscoll, R., Elliot, M., Schneider, B. & Tudhope, A. 2016. Links between tropical Pacific seasonal, interannual and orbital variability during the Holocene. *Nature Geoscience* **9,** 168.

Gagan, M. K., Ayliffe, L. K., Hopley, D., Cali, J., Mortimer, G., Chappell, J., Mcculloch, M. T. & Head, M. 1998. Temperature and surface-ocean water balance of the mid-Holocene tropical western Pacific. *Science* **279,** 1014-1018.

Gbrmpa. 2016. *Statement on coral bleaching surveys* [Online]. Australian Government. Available: http://www.gbrmpa.gov.au/media-room/latest-news/coral-bleaching/2016/statement-on-coral-bleaching-surveys [Accessed 08/07/2016 2016].

Grinsted, A., Moore, J. C. & Jevrejeva, S. 2004. Application of the cross wavelet transform and wavelet coherence to geophysical time series. *Nonlinear Processes in Geophysics* **11,** 561-566.

Grove, C. A., Zinke, J., Peeters, F., Park, W., Scheufen, T., Kasper, S., Randriamanantsoa, B., Mcculloch, M. T. & Brummer, G. J. A. 2013. Madagascar corals reveal a multidecadal signature of rainfall and river runoff since 1708. *Climate of the Past* **9,** 641-656.

Gu, D. & Philander, S. G. H. 1995. Secular Changes of Annual and Interannual Variability in the Tropics during the Past Century. *Journal of Climate* **8,** 864-876.

Gupta, A. K., Anderson, D. M. & Overpeck, J. T. 2003. Abrupt changes in the Asian southwest monsoon during the Holocene and their links to the North Atlantic Ocean. *Nature* **421,** 354-357.

Hamanaka, N., Kan, H., Yokoyama, Y., Okamoto, T., Nakashima, Y. & Kawana, T. 2012. Disturbances with hiatuses in high-latitude coral reef growth during the Holocene: Correlation with millennial-scale global climate change. *Global and Planetary Change* **80-81,** 21-35.

Harris, D. L., Webster, J. M., Vila-Concejo, A., Hua, Q., Yokoyama, Y. & Reimer, P. J. 2015. Late Holocene sea-level fall and turn-off of reef flat carbonate production: Rethinking bucket fill and coral reef growth models. *Geology* **43,** 175-178.

Hendy, E. J., Gagan, M. K. & Lough, J. 2003. Chronological control of coral records using luminescent lines and evidence for non-stationary ENSO teleconnections in northeast Australia. *The Holocene* **13,** 187-199.

Hoegh-Guldberg, O. 1999. Climate change, coral bleaching and the future of the world's coral reefs. *Marine and Freshwater Research* **50,** 839-866.

Isdale, P. 1984. Fluorescent bands in massive corals record centuries of coastal rainfall. *Nature* **310,** 578-579.

Isdale, P. J., Stewart, B. J., Tickle, K. S. & Lough, J. M. 1998. Palaeohydrological variation in a tropical river catchment: a reconstruction using fluorescent bands in corals of the Great Barrier Reef, Australia. *The Holocene* **8,** 1-8.

Jompa, J. & Mccook, L. J. 2003. Contrasting effects of turf algae on corals: massive Porites spp. are unaffected by mixed-species turfs, but killed by the red alga Anotrichium tenue. *Marine Ecology Progress Series* **258,** 79-86.

Jones, A. M. & Berkelmans, R. 2014. Flood impacts in Keppel Bay, southern Great Barrier Reef in the aftermath of cyclonic rainfall. *PloS one* **9,** 84739.

Jones, P. D., Briffa, K. R., Osborn, T. J., Lough, J. M., Van Ommen, T. D., Vinther, B. M., Luterbacher, J., Wahl, E. R., Zwiers, F. W., Mann, M. E., Schmidt, G. A., Ammann, C. M., Buckley, B. M., Cobb, K. M., Esper, J., Goosse, H., Graham, N., Jansen, E., Kiefer, T., Kull, C., Kuttel, M., Mosley-Thompson, E., Overpeck, J. T., Riedwyl, N., Schulz, M., Tudhope, A. W., Villalba, R., Wanner, H., Wolff, E. & Xoplaki, E. 2009. High-resolution palaeoclimatology of the last millennium: a review of current status and future prospects. *The Holocene* **19,** 3-49.

Kiem, A. S., Franks, S. W. & Kuczera, G. 2003. Multi-decadal variability of flood risk. *Geophysical Research Letters* **30,** n/a-n/a.

King, B., Mcallister, F., Wolanski, E., Done, T. & Spagnol, S. 2001. River Plume Dynamics in the Central Great Barrier Reef. *Oceanographic Processes of Coral Reefs.* CRC Press.

Klingaman, N. P., Woolnough, S. J. & Syktus, J. 2013. On the drivers of inter-annual and decadal rainfall variability in Queensland, Australia. *International Journal of Climatology* **33,** 2413-2430.

Knutson, D. W., Buddemeier, R. W. & Smith, S. V. 1972. Coral chronometers: Seasonal growth bands in reef corals. *Science* **177,** 270-272.

Kuleshov, Y., Qi, L., Fawcett, R. & Jones, D. 2008. On tropical cyclone activity in the Southern Hemisphere: Trends and the ENSO connection. *Geophysical Research Letters* **35,** L14S08.

Leonard, N., Zhao, J. X., Welsh, K. J., Feng, Y. X., Smithers, S. G., Pandolfi, J. M. & Clark, T. R. 2015. Holocene sea level instability in the southern Great Barrier Reef, Australia: high-precision U–Th dating of fossil microatolls. *Coral Reefs***,** 1-15.

Leonard, N. D., Welsh, K. J., Zhao, J.-X., Nothdurft, L. D., Webb, G. E., Major, J., Feng, Y.-X. & Price, G. J. 2013. Mid-Holocene sea-level and coral reef demise: U-Th dating of subfossil corals in Moreton Bay, Australia. *The Holocene* **23,** 1841-1852.

Llewellyn, L. E., Everingham, Y. L. & Lough, J. M. 2012. Pharmacokinetic modelling of multi-decadal luminescence time series in coral skeletons. *Geochimica et Cosmochimica Acta* **83,** 263-271.

Lough, J. 2000. 1997-98: Unprecedented thermal stress to coral reefs? *Geophysical Research Letters* **27,** 3901-3904.

Lough, J. & Barnes, D. 2000. Environmental controls on growth of the massive coral Porites. *Journal of experimental marine biology and ecology* **245,** 225-243.

Lough, J., Barnes, D. & Mcallister, F. 2002. Luminescent lines in corals from the Great Barrier Reef provide spatial and temporal records of reefs affected by land runoff. *Coral Reefs* **21,** 333-343.

Lough, J. M. 1991. Rainfall variations in Queensland, Australia: 1891–1986. *International Journal of Climatology* **11,** 745-768.

Lough, J. M. 2007. Tropical river flow and rainfall reconstructions from coral luminescence: Great Barrier Reef, Australia. *Paleoceanography* **22**.

Lough, J. M. 2011a. Great Barrier Reef coral luminescence reveals rainfall variability over northeastern Australia since the 17th century. *Paleoceanography* **26**.

Lough, J. M. 2011b. Measured coral luminescence as a freshwater proxy: comparison with visual indices and a potential age artefact. *Coral Reefs* **30,** 169-182.

Lough, J. M. & Barnes, D. J. 1990. Intra-annual timing of density band formation of Porites coral from the central Great Barrier Reef. *Journal of experimental marine biology and ecology* **135,** 35-57.

Lough, J. M. & Barnes, D. J. 1992. Comparisons of skeletal density variations in Porites from the central Great Barrier Reef. *Journal of experimental marine biology and ecology* **155,** 1-25.

Lough, J. M. & Barnes, D. J. 1997. Several centuries of variation in skeletal extension, density and calcification in massive Porites colonies from the Great Barrier Reef: A proxy for seawater temperature and a background of variability against which to identify unnatural change. *Journal of experimental marine biology and ecology* **211,** 29-67.

Lough, J. M., Barnes, D. J., Devereux, M. J., Tobin, B. J. & Tobin, S. 1999. Variability in growth characteristics of massive Porites on the Great Barrier Reef. *Technical Report No. 28.* Townsville: CRC Reef Research Centre.

Lough, J. M. & Cantin, N. E. 2014. Perspectives on Massive Coral Growth Rates in a Changing Ocean. *Biological Bulletin* **226,** 187-202.

Lough, J. M., Lewis, S. E. & Cantin, N. E. 2015. Freshwater impacts in the central Great Barrier Reef: 1648–2011. *Coral Reefs* **34,** 739-751.

Lough, J. M., Llewellyn, L. E., Lewis, S. E., Turney, C. S. M., Palmer, J. G., Cook, C. G. & Hogg, A. G. 2014. Evidence for suppressed mid-Holocene northeastern Australian monsoon variability from coral luminescence. *Paleoceanography* **29,** 581-594.

Ludwig, K. R. 2003. Isoplot/Ex, version 3: a Geochronological Toolkit for Microsoft Excel. *Berkeley Geochronology Center Special Publications*.

Lybolt, M., Neil, D. T., Zhao, J., Feng, Y., Yu, K. & Pandolfi, J. 2011. Instability in a marginal coral reef: the shift from natural variability to a human-dominated seascape. *Frontiers in Ecology and the Environment* [Online].

Mann, M. E., Gille, E., Overpeck, J., Gross, W., Bradley, R. S., Keimig, F. T. & Hughes, M. K. 2000. Global Temperature Patterns in Past Centuries: An Interactive Presentation. *Earth Interactions* **4,** 1.

Marcott, S. A., Shakun, J. D., Clark, P. U. & Mix, A. C. 2013. A reconstruction of regional and global temperature for the past 11,300 years. *Science (New York, N.Y.)* **339,** 1198.

Mcgregor, H. & Gagan, M. K. 2003. Diagenesis and geochemistry of *Porites* corals from Papua New Guinea: Implications for paleoclimate reconstruction. *Geochemica et Cosmochimica Acta* **67,** 2147-2156.

Mcgregor, H. V. & Abram, N. 2008. Images of diagenetic textures in Porites corals from Papua New Guinea and Indonesia. *Geochemistry, Geophysics, Geosystems* **9**.

Mcgregor, H. V., Fischer, M. J., Gagan, M. K., Fink, D., Phipps, S. J., Wong, H. & Woodroffe, C. D. 2013. A weak El Niño/Southern Oscillation with delayed seasonal growth around 4,300 years ago. *Nature Geoscience* **6,** 949-953.

Meinke, H., Devoil, P., Hammer, G. L., Power, S., Allan, R., Stone, R. C., Folland, C. & Potgieter, A. 2005. Rainfall Variability at Decadal and Longer Time Scales: Signal or Noise? *Journal of Climate* **18,** 89-96.

Neukom, R. & Gergis, J. 2012. Southern Hemisphere high-resolution palaeoclimate records of the last 2000 years. *The Holocene* **22,** 501-524.

Pandolfi, J. M. 2015. Incorporating Uncertainty in Predicting the Future Response of Coral Reefs to Climate Change. *Annual Review of Ecology, Evolution, and Systematics* **46,** 281-303.

Perry, C. & Smithers, S. 2011. Cycles of coral reef 'turn-on', rapid growth and 'turn-off' over the past 8500 years: a context for understanding modern ecological states and trajectories. *Global Change Biology* **17,** 76-86.

Qian, C., Wu, Z., Fu, C. & Wang, D. 2011. On Changing El Niño: A View from Time-Varying Annual Cycle, Interannual Variability, and Mean State. *Journal of Climate* **24,** 6486-6500.

Risbey, J. S., Pook, M. J., Mcintosh, P. C., Wheeler, M. C. & Hendon, H. H. 2009. On the Remote Drivers of Rainfall Variability in Australia. *Monthly Weather Review* **137,** 3233-3253.

Rodriguez-Ramirez, A., Grove, C. A., Zinke, J., Pandolfi, J. M. & Zhao, J.-X. 2014. Coral Luminescence Identifies the Pacific Decadal Oscillation as a Primary Driver of River Runoff Variability Impacting the Southern Great Barrier Reef. *PloS one* **9,** e84305.

Sadler, J., Webb, G. E., Leonard, N. D., Nothdurft, L. D. & Clark, T. R. *in review*. Reef core insights into mid-Holocene water temperatures of the southern Great Barrier Reef. *Paleoceanography*.

Schroeder, T., Devlin, M. J., Brando, V. E., Dekker, A. G., Brodie, J. E., Clementson, L. A. & Mckinna, L. 2012. Inter-annual variability of wet season freshwater plume extent into the Great Barrier Reef lagoon based on satellite coastal ocean colour observations. *Marine Pollution Bulletin* **65,** 210-223.

Shulmeister, J. & Lees, B. G. 1995. Pollen evidence from tropical Australia for the onset of an ENSO-dominated climate at c. 4000 BP. *The Holocene* **5,** 10-18.

Smithers, S. G., Hopley, D. & Parnell, K. E. 2006. Fringing and Nearshore Coral Reefs of the Great Barrier Reef: Episodic Holocene Development and Future Prospects. *Journal of Coastal Research,* 175-187.

Soon, W., Velasco Herrera, V. M., Selvaraj, K., Traversi, R., Usoskin, I., Chen, C.-T. A., Lou, J.-Y., Kao, S.-J., Carter, R. M., Pipin, V., Severi, M. & Becagli, S. 2014. A review of Holocene solar-linked climatic variation on centennial to millennial timescales: Physical processes, interpretative frameworks and a new multiple cross-wavelet transform algorithm. *Earth-Science Reviews* **134,** 1-15.

Storz, D. & Gischler, E. 2010. Coral extension rates in the NW Indian Ocean I: reconstruction of 20th century SST variability and monsoon current strength. *Geo-Marine Letters* **31,** 141-154.

Susic, M., Boto, K. & Isdale, P. 1991. Fluorescent humic acid bands in coral skeletons originate from terrestrial runoff. *Marine Chemistry* **33,** 91-104.

Tanzil, J. T. I., Brown, B. E., Dunne, R. P., Lee, J. N., Kaandorp, J. A. & Todd, P. A. 2013. Regional decline in growth rates of massive Porites corals in Southeast Asia. *Global Change Biology* **19,** 3011-3023.

Tanzil, J. T. I., Brown, B. E., Tudhope, A. W. & Dunne, R. P. 2009. Decline in skeletal growth of the coral Porites lutea from the Andaman Sea, South Thailand between 1984 and 2005. *Coral Reefs* **28,** 519-528.

Torrence, C. & Compo, G. P. 1998. A practical guide to wavelet analysis. *Bulletin of the American Meteorological Society* **79,** 61-78.

Toth, L. T., Macintyre, I. G., Aronson, R. B., Vollmer, S. V., Hobbs, J. W., Urrego, D. H., Cheng, H., Enochs, I. C., Combosch, D. J. & Van Woesik, R. 2012. ENSO drove 2500-year collapse of eastern Pacific coral reefs. *Science (New York, N.Y.)* **337,** 81.

Trenberth, K. E. & Stepaniak, D. P. 2001. Indices of El Niño Evolution. *Journal of Climate* **14,** 1697-1701.

Verdon, D. C., Wyatt, A. M., Kiem, A. S. & Franks, S. W. 2004. Multidecadal variability of rainfall and streamflow: Eastern Australia. *Water Resources Research* **40,** W10201.

Walther, B. D., Kingsford, M. J. & Mcculloch, M. T. 2013. Environmental Records from Great Barrier Reef Corals: Inshore versus Offshore Drivers. *PloS one* **8,** e77091.

Wang, X. L. 1994. The Coupling of the Annual Cycle and ENSO Over the Tropical Pacific. *Journal of the Atmospheric Sciences* **51,** 1115-1136.

Wanner, H., Beer, J., Bütikofer, J., Crowley, T. J., Cubasch, U., Flückiger, J., Goosse, H., Grosjean, M., Joos, F., Kaplan, J. O., Küttel, M., Müller, S. A., Prentice, I. C., Solomina, O., Stocker, T. F., Tarasov, P., Wagner, M. & Widmann, M. 2008. Mid- to Late Holocene climate change: an overview. *Quaternary Science Reviews* **27,** 1791-1828.

Wanner, H., Mercolli, L., Grosjean, M. & Ritz, S. P. 2015. Holocene climate variability and change; a data-based review. *Journal of the Geological Society* **172,** 254-263.

Zhang, Z., Leduc, G. & Sachs, J. P. 2014. El Nino evolution during the Holocene revealed by a biomarker rain gauge in the Galapagos Islands. *Earth and Planetary Science Letters* **404,** 420.

Zinke, J., Mcgregor, H. V., Abram, N. J., Lough, J. M., Gagan, M., O'leary, M., Mcculloch, M., Webster, J. & Woodroffe, C. 2015. Dealing with climate change through understanding past tropical ocean-atmosphere climate interactions and their impacts on marine ecosystems. *Quaternary Australasia* **32,** 25-31.

Tables

Table 1: Results of multi-collector inductively coupled plasma mass spectrometry (MC-ICP-MS) uranium-thorium dating of fossil corals cores and surface samples from Great Palm Island, central Great Barrier Reef, Australia.

Sample Name	Date of Chemistry	U (ppm)	232Th (ppb)	(230Th/ 232Th)	(230Th/238U)	Corr. (234U/ 238U)	Uncorr. Age (a)	Corr. Age (b)	Age (y BP - 1950)	δU234 (c)	Genus	Core length (cm)
PAM 1.0	15/02/2014	2.6890 ± 0.0012	1.2338 ± 0.0048	307.0 ± 2.5	0.04642 ± 0.00033	1.1450 ± 0.0009	4517 ± 33	4503 ± 33	4438 ± 33	145.0 ± 0.9	*Porites*	34
PAM 1.1	13/02/2012	2.8058 ± 0.0024	1.2874 ± 0.0018	303.4 ± 1.1	0.04588 ± 0.00016	1.1470 ± 0.0007	4462 ± 16	4450 ± 17	4388 ± 17	147.0 ± 0.7	*Porites*	30
PAM 2.0	13/02/2012	2.7591 ± 0.0015	0.45560 ± 0.00063	936.1 ± 2.5	0.05094 ± 0.00012	1.1463 ± 0.0012	4969 ± 13	4965 ± 13	4902 ± 13	146.3 ± 1.2	*Porites*	82
PAM 2.0	15/02/2014	2.5638 ±0.0015	0.6552 ± 0.0041	605.5 ± 5.8	0.05100 ± 0.00037	1.1447 ± 0.0007	4974 ± 37	4964 ± 37	4899 ± 37	144.7 ± 0.7	*Porites*	35
PAM 3.0	13/02/2012	2.7118 ± 0.0028	0.45363 ± 0.00086	821.4 ± 2.9	0.04528 ± 0.00014	1.1471 ± 0.0009	4401 ± 14	4397 ± 15	4335 ± 15	147.1 ± 0.9	*Porites*	42
PAM 3.0	15/02/2014	2.7214 ± 0.0014	0.4343 ± 0.0040	857 ± 11	0.04510 ± 0.00040	1.1473 ± 0.0008	4377 ± 40	4368 ± 40	4303 ± 40	147.3 ± 0.8	*Porites*	42
PAM 3.1	15/02/2014	2.5429 ± 0.0013	0.4355 ± 0.0035	796.7 ± 8.4	0.04497 ± 0.00031	1.1456 ±0.0011	4370 ± 31	4362 ± 31	4297 ± 31	145.6 ± 1.1	*Porites*	44
PAM 3.2	13/02/2012	2.6785 ±0.0016	0.42553 ± 0.00087	860.8 ± 2.4	0.045069 ± 0.000092	1.1471 ± 0.0007	4381 ± 10	4376 ± 10	4314 ± 10	147.1 ± 0.7	*Porites*	47
PAM 3.3	15/02/2014	2.8155 ± 0.0017	2.6904 ± 0.0060	142.8 ± 1.1	0.04498 ± 0.00034	1.1483 ± 0.0008	4361 ± 34	4338 ± 34	4273 ± 34	148.3 ± 0.8	*Porites*	32
PAM 4.0	13/02/2012	2.6108 ± 0.0014	0.15531 ± 0.00053	2530 ± 11	0.04959 ± 0.00015	1.1481 ± 0.0007	4826 ± 15	4762 ± 15	4698 ± 15	148.1 ± 0.7	*Favia*	40
PAM 5.0	13/02/2012	2.6597 ± 0.0011	0.23197 ± 0.00038	1865.9 ± 5.2	0.05363 ± 0.00012	1.1464 ± 0.0010	5237 ± 13	5235 ± 13	5173 ± 13	146.4 ± 1.0	*Porites*	48
PAM 5.0	15/02/2014	2.6747 ± 0.0012	0.6904 ± 0.0042	644.4 ± 5.7	0.05481 ± 0.00034	1.1461 ± 0.0010	5350 ± 35	5339 ± 35	5274 ± 35	146.1 ±1.0	*Porites*	48
PAM 5.1 *(below death surface)*	15/02/2014	2.6203 ± 0.0013	0.1732 ± 0.0042	2442 ± 62	0.05320 ± 0.00046	1.1454 ± 0.0010	5191 ± 46	5185 ± 46	5120 ± 46	145.4 ± 1.0	*Porites*	82
PAM 5.1 *(above death surface)*	15/02/2014	2.8330 ± 0.0011	0.4821 ± 0.0037	951 ± 10	0.05332 ± 0.00042	1.1466 ± 0.0010	5198 ± 42	5190 ± 42	5125 ± 42	146.6 ± 1.0	*Porites*	82
PAM 6.0	13/02/2012	2.6642 ± 0.0017	1.4520 ± 0.0011	221.5 ± 0.6	0.03979 ± 0.00011	1.1463 ± 0.0009	3860 ± 11	3846 ± 13	3784 ± 13	146.3 ± 0.9	*Porites*	50
PAM 7.0	13/02/2012	2.5900 ± 0.0016	3.3012 ± 0.0036	149.6 ± 0.4	0.06286 ± 0.00016	1.1448 ± 0.0009	6174 ± 17	6141 ± 23	6079 ± 23	144.8 ± 0.9	*Porites*	-
PAM 8.0	13/02/2012	2.6450 ± 0.0020	4.2888 ± 0.0061	90.4 ± 0.3	0.04831 ± 0.00013	1.1469 ± 0.0010	4704 ± 14	4662 ± 25	4600 ± 25	146.9 ± 1.0	*Porites*	~50

Ratios in parentheses are activity ratios calculated from atomic ratios using decay constants of Cheng et al. (2000). All values have been corrected for laboratory procedural blanks. All errors reported in this table are quoted as 2σ. (a) Uncorrected ^{230}Th age was calculated using Isoplot/EX 3.0 program (Ludwig 2003). (b) ^{230}Th ages were corrected using the two-component correction method of Clark et al. (2014a) using $^{230}Th/^{232}Th_{hyd}$ and $^{230}Th/^{232}Th_{det}$ activity ratios of 1.08 ± 0.23 and 0.62 ± 0.14, respectively. (c) $\delta^{234}U = [(234U/238U) - 1] *1000$

Figures

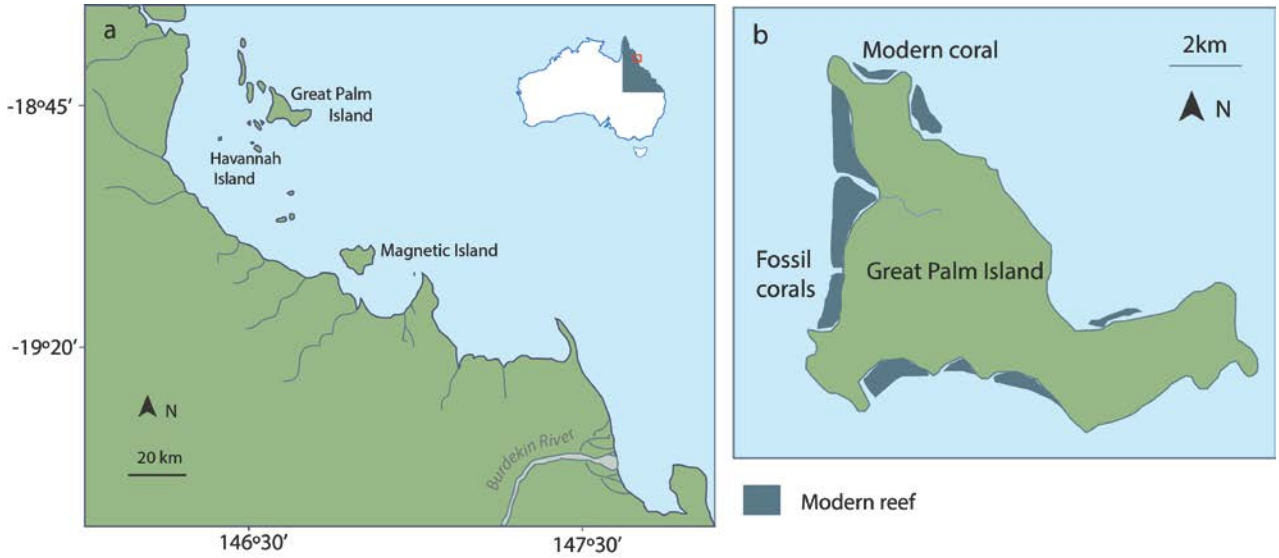

Figure 1: Map showing location of the Palm Islands Group, central Great Barrier Reef, Australia, in relation to the Burdekin River and; b) Great Palm Island indicating location of the modern and fossil *Porites* corals.

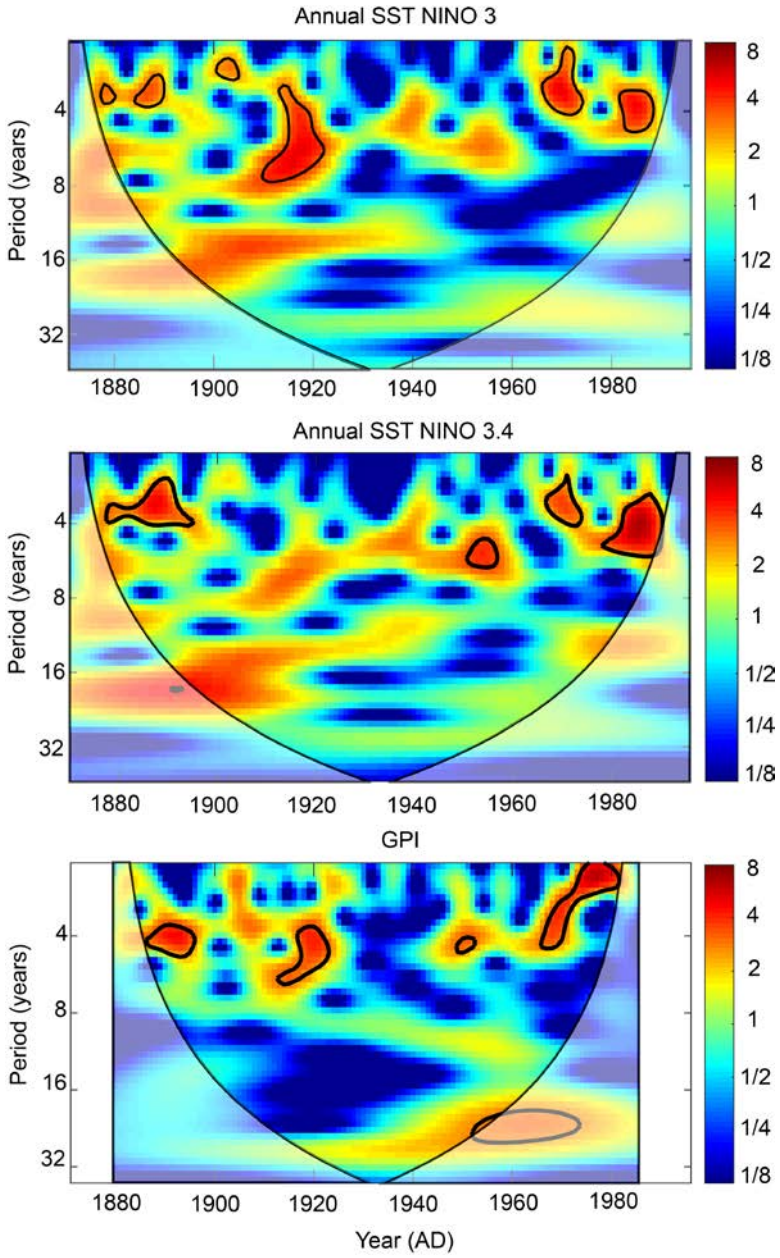

Figure 2: Continuous wavelet transform (Morlet) of annual averaged Niño 3.0 (a) and Niño 3.4 (b) sea surface temperature (SST) anomaly data and coral luminescence index data (c) from Great Palm Island (GPI; Hendy et al. 2003). Period is in years, black contour line indicates significance in power spectrum (p = 0.05), shaded area indicates values outside the cone of influence (COI). Colour graded bar (right) is the wavelet power spectrum. Note the coral luminescence record visually predicts well the overall phases of increased (significant) El Niño Southern Oscillation (ENSO) periods in the 2-7 year band.

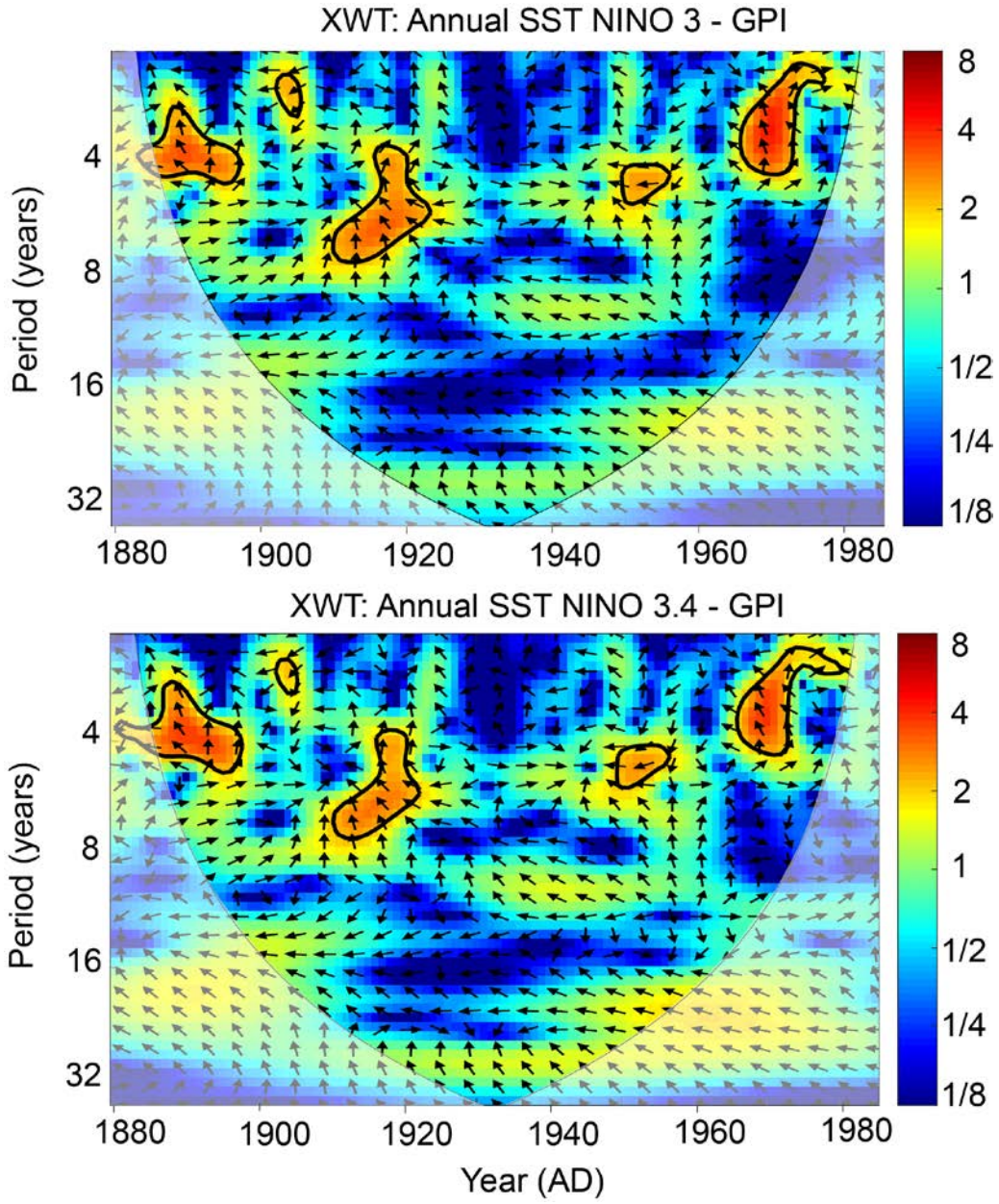

Figure 3: Cross wavelet transform (XWT) of annual averaged Niño 3.0 (a) and Niño 3.4 (b) sea surface temperature (SST) anomaly data and Great Palm Island (GPI) coral luminescence index data (Hendy et al. 2003). Period is in years, black contour line indicates significance in high common power (p = 0.05), shaded area indicates values outside the cone of influence (COI). Colour graded bar (right) is the wavelet power spectrum Arrows indicate in-phase (right), anti-phased (left) response of luminescence to SST.

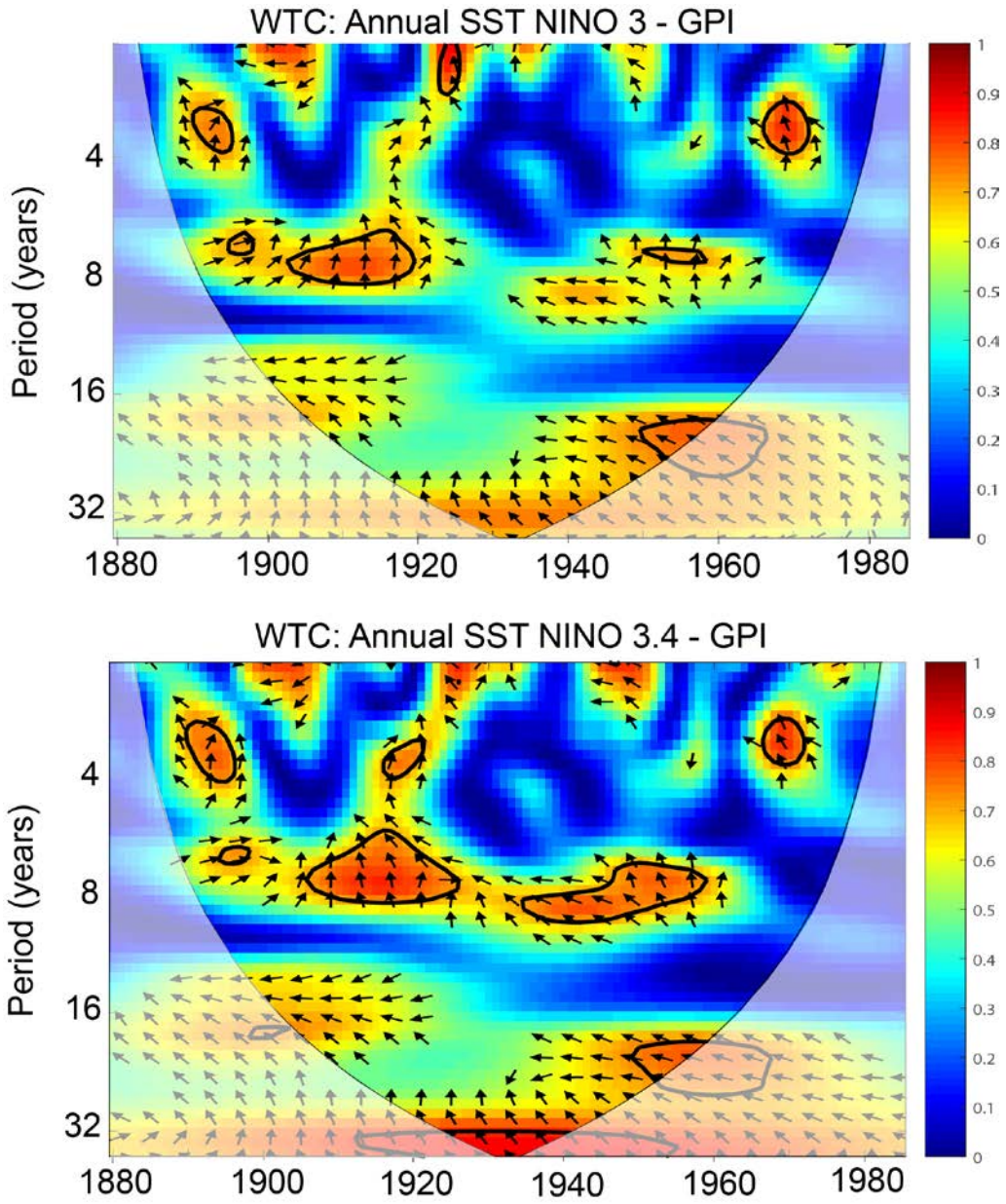

Figure 4: Wavelet coherence (WTC) of annual averaged Niño 3 (a) and Niño 3.4 (b) sea surface temperature (SST) data and Great Palm Island (GPI) coral luminescence index data (Hendy et al. 2003). The WTC finds regions in time frequency space where the two time series co-vary but don't necessarily have high power (Grinsted et al. 2004). Period is in years , black contours are the 5% significance level against red noise background and arrow directions indicate in phase (right) and anti-phased responses (left). Colour graded bar (right) is the wavelet power spectrum.

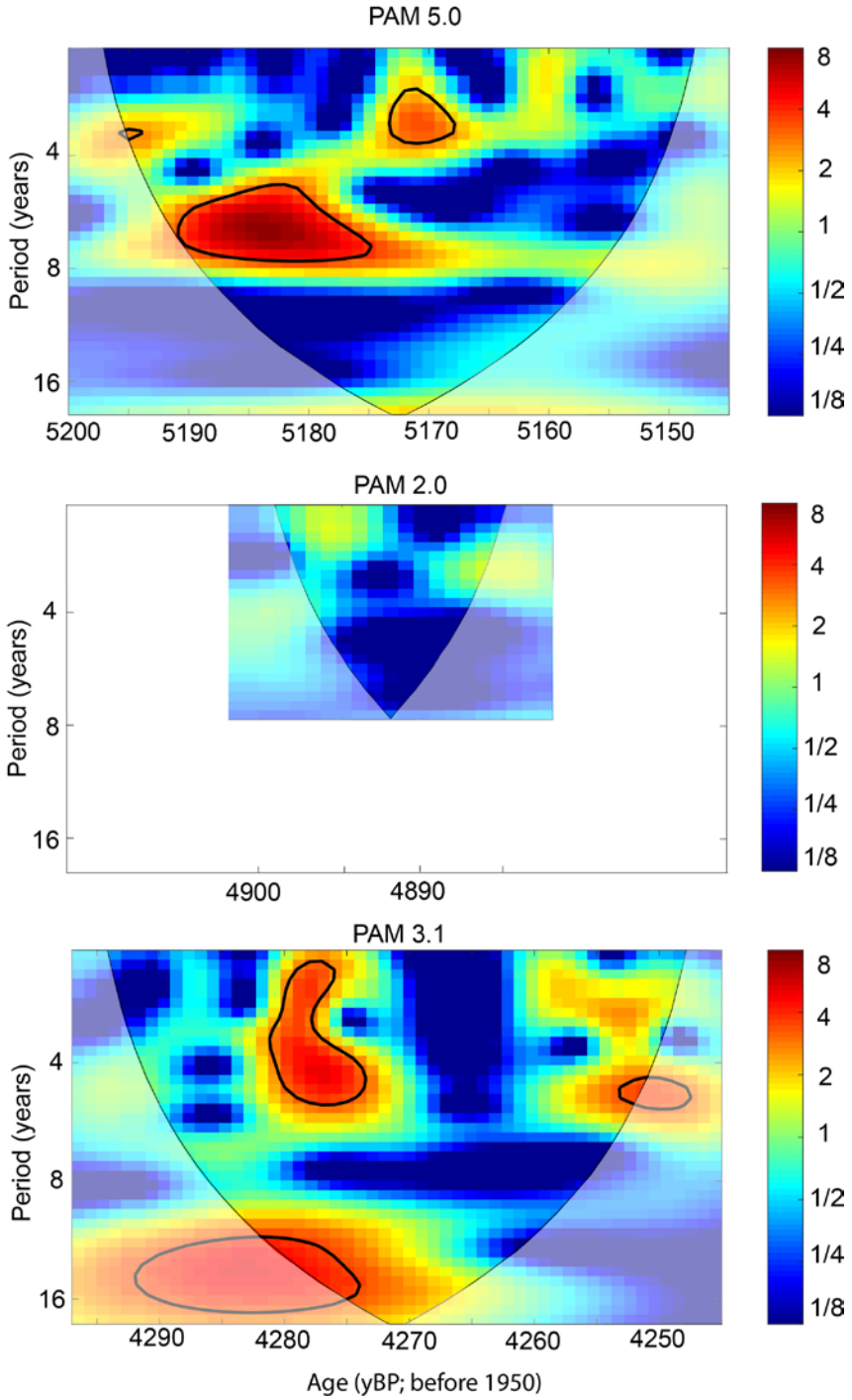

Figure 5: Continuous wavelet transform of mid-Holocene coral luminescence index data from Great Palm Island, central Great Barrier Reef, Australia. Period is in years, black contour line indicates significance in power spectrum (p = 0.05), shaded area indicates values outside the cone of influence (COI). Colour graded bar (right) is the wavelet power spectrum; a) PAM 5.0 – 53 year record; b) PAM 2.0 – 21 year record and; c) PAM 3.1 – 53 year record.

Supplementary

a)

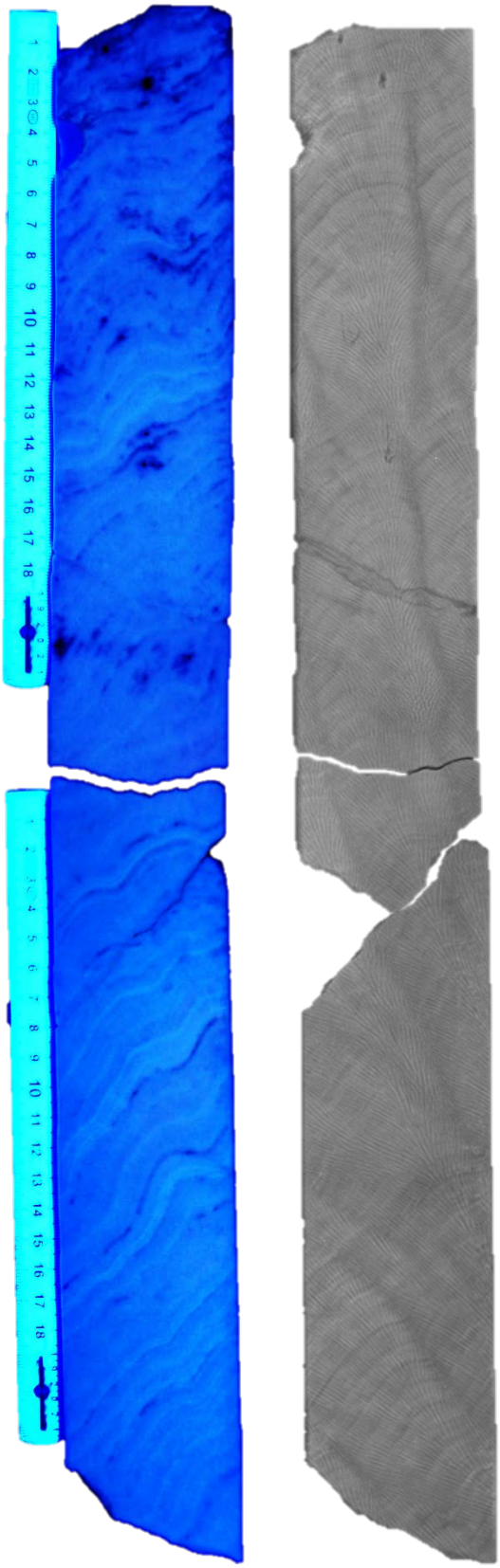

PAM 5.0

b)

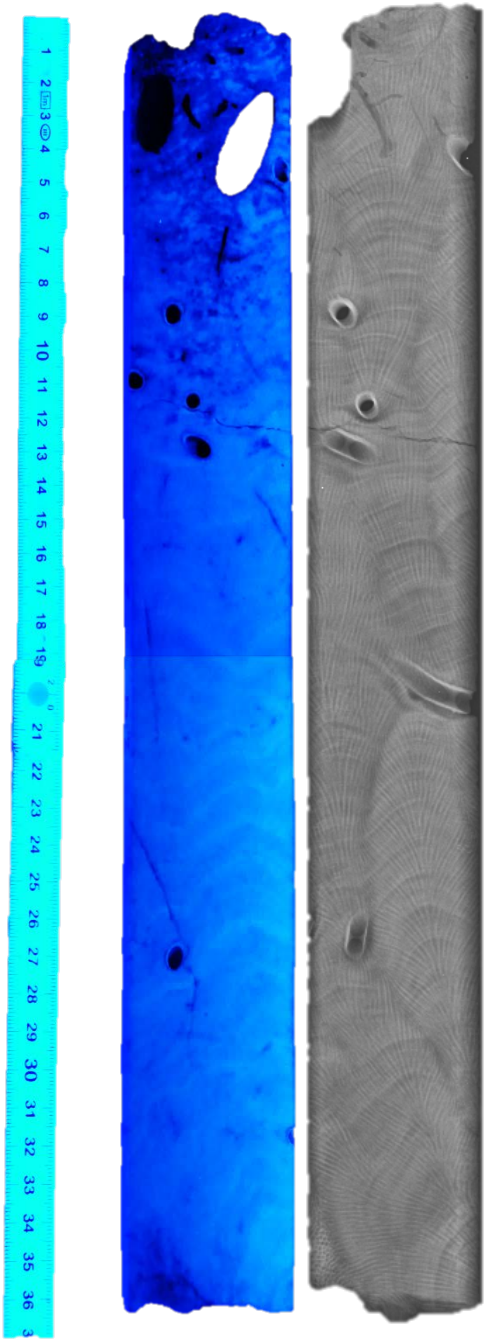

PAM 2.0

c)

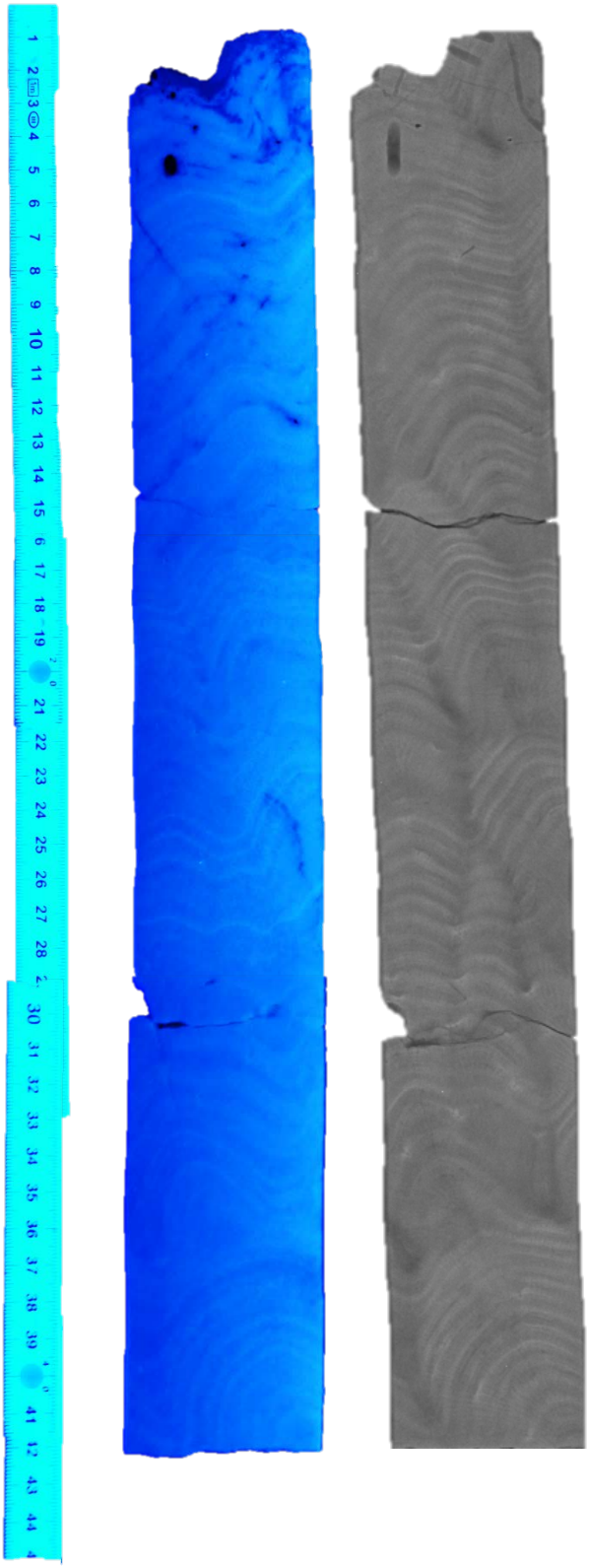

PAM 3.1

Supplementary Figure 1: Digitally enhanced photographs of ultraviolet (UV) luminescence lines (left) and X-ray images of fossil Porites from Great Palm Island, central Great Barrier Reef, Australia (ruler scale is cm). a) PAM 5.0 (~5200 years before present (yBP –where present is 1950); b) PAM 2.0 (~4900 y BP) and; c) PAM 3.1 (~4300 y BP).

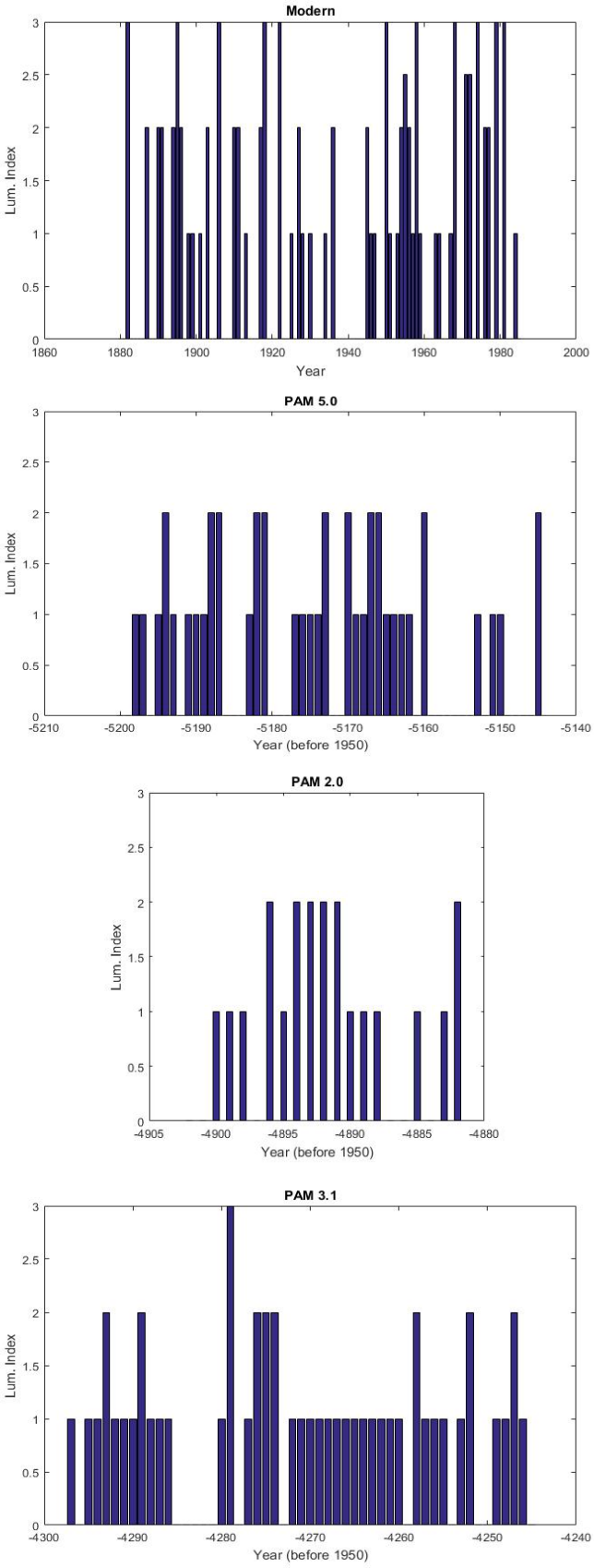

Supplementary Figure 2: Visually assessed ultra-violet (UV) luminescence index data from Great Palm Island, central Great Barrier Reef, Australia (see Methods in main text). a) Modern coral core (year is AD; Hendy et al. 2003); and fossil corals b) PAM 5.0; c) PAM 2.0 and; d) PAM 3.1. Years for the fossil corals are before present (y BP) where present is defined as 1950.

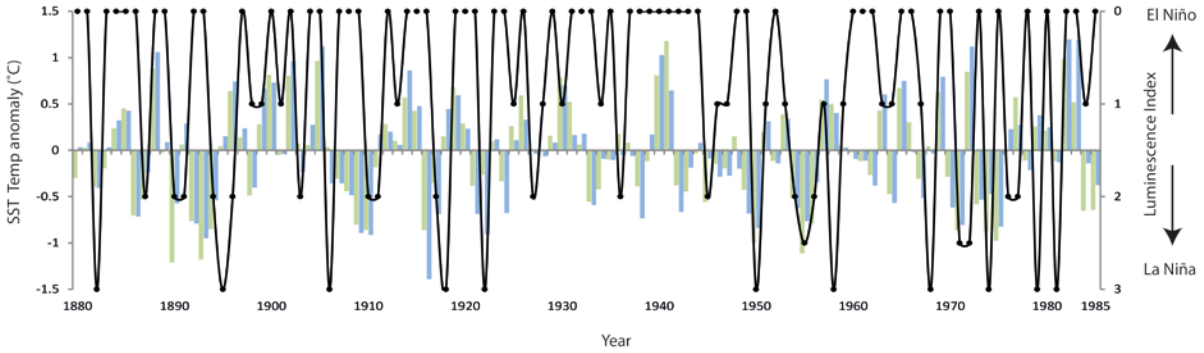

Supplementary Figure 3: Annual averaged Niño 3.4 (green bars) and Niño 3.0 (blue bars) sea surface temperature (SST) anomaly data (˚C; black line) and visually assessed luminescence index data from modern coral cores from the Palm Islands, Great Barrier Reef, Australia.

This page is intentionally left blank

Chapter 5

High resolution geochemical analysis of massive *Porites* corals from the Wet Tropics, Great Barrier Reef; rare earth elements and yttrium as indicators of terrigenous input

Leonard, N.D.[1,2], Welsh, K.J.[2], Nguyen, A.D.[1,2], Sadler, J.[2], Pandolfi, J.M.[3], Clark, T.R.[1,2], Zhao, J-x.[1,2], Webb, G.E.[2]

[1]Radiogenic Isotope Facility, School of Earth Sciences, The University of Queensland, Brisbane, Qld 4072, Australia

[2]School of Earth Sciences, The University of Queensland, Brisbane, Qld 4072, Australia

[3]Centre for Marine Science, Australian Research Council Centre of Excellence for Coral Reef Studies, School of Biological Sciences, The University of Queensland, Brisbane, Qld 4072, Australia

***Corresponding author: Nicole Leonard; email: nicole.leonard@uqconnect.edu.au**

Keywords: rare earth elements, yttrium, coral, Great Barrier Reef, climate, geochemical proxies

Target Journal: Geochimica et Cosmochimica Acta

Abstract

Increased sediment supply due to catchment modification and subsequent decreasing water quality in developed coastal regions is affecting coral reefs globally. Yet obtaining water quality baselines beyond instrumental monitoring and prior to anthropogenic influence is problematic. Massive, annually banded *Porites* corals offer the potential to reconstruct both spatial water quality gradients and water quality changes through time, by use of the geochemical proxies that are incorporated into the skeletal matrix. The rare earth elements (REEs) offer potential as tracers of river discharge and water quality in coastal waters, as ~90% of REEs are terrestrially derived. Here we present the results of ~monthly resolved REE, yttrium (Y) and barium (Ba) concentrations from four massive *Porites* corals collected across a known water quality gradient in the Wet Tropics, Great Barrier Reef, Australia. Results show that sub-annual REE time series patterns were comparable between the corals despite having significantly different total concentrations. Annual peaks in total REE concentrations also reflect regional rainfall and river discharge. Spatial interpolation models of average Y/Ho molar ratios reflect the cross shelf water quality gradient, whereas REE and Y spatial interpolations better reflect local (reef) scale difference in water quality. The results from this study demonstrate that high resolution REE and Y analysis of *Porites* corals offer great potential for assessing water quality gradients in palaeoenvironmental reconstructions, and for assessing sub-annual to annual rainfall and river discharge beyond instrumental monitoring.

Introduction

Recognised as an international World Heritage Area, the Great Barrier Reef (GBR) is the largest contiguous coral reef system in the world (Hughes et al., 2015). However, increasing anthropogenic pressure (sedimentation, over fishing, coastal development) combined with global climate change (e.g. increasing temperatures and coral bleaching) has resulted in a significant decline in coral cover in recent decades (Pandolfi et al., 2003, Hughes et al., 2015). Understanding both climatic and environmental conditions that effected coral reef growth and reef ecology in the recent geological past is thus invaluable to improving predictions of future response (Pandolfi, 2015). Turbidity and fluvial sediment delivery to the GBR following European settlement has been cited as a major control on reef health and community composition, especially at inshore locations (Fabricius, 2005, Smith et al., 2005, Roff et al., 2013), yet deriving water quality baselines prior to instrumental monitoring is challenging (De'ath and Fabricius, 2010). Long lived, annually banded massive corals provide a unique opportunity for high resolution reconstruction of past environmental and climatic conditions by use of both luminescent lines (Isdale et al., 1998, Lough et al., 1998, Lough et al., 2014, Rodriguez-Ramirez et al., 2014) and geochemical proxies that are incorporated into the skeletal matrix during coral growth (Shen and Sanford, 1990, Fallon and McCulloch, 2002, Fallon et al., 2003, McCulloch et al., 2003, Correge, 2006, Lewis et al., 2007, Prouty et al., 2010, Lewis et al., 2012, Walther et al., 2013, Saha et al., 2016). Visible under ultra violet (UV) light, luminescence bands in massive *Porites* corals have been shown to be robust indicators of river discharge at near shore locations on the GBR (Isdale, 1984, Isdale et al., 1998, Lough et al., 2002, Lough, 2011a), thereby serving as a tool for quantifying river flow beyond instrumental records (Lough et al., 2015). Subsequently, luminescence records also have been used to reconstruct longer term climatic drivers of Australian rainfall such as the El Niño Southern Oscillation (ENSO) (e.g. Hendy et al., 2003, Lough et al., 2014) and the Pacific decadal oscillation (PDO) (Rodriguez-Ramirez et al., 2014). Yet, luminescent bands offer no interpretation of ambient seawater conditions, including sediment loads, derived from high discharge/rainfall events. Consequently, trace elements and isotopic signatures incorporated into the skeletal lattice during coral growth are commonly used to reconstruct past seawater conditions, however, for geochemical proxies to be used reliably in palaeoenvironmental reconstructions it is first necessary to demonstrate homogeneity of geochemical signals at local to regional scales in modern corals that align with instrumental data (Prouty et al., 2008).

The most commonly reported proxy for riverine sediment input onto the GBR is Barium (Ba), which is desorbed from fine suspended sediments at low salinities in the estuarine mixing zone, and therefore acts as a dissolved tracer of flood plumes reaching reefs (McCulloch et al., 2003, Sinclair and McCulloch, 2004, Lewis et al., 2007, Jupiter et al., 2008, Lewis et al., 2012). An estimated 5-10 fold increase in fluvial sediment delivery to the GBR since European settlement was inferred from Ba/Ca baseline levels in the Burdekin River region (McCulloch et al., 2003) and peaks in Ba/Ca have been found to correspond generally well with instrumental records of high rainfall/river flow events (Sinclair and McCulloch, 2004, Wyndham et al., 2004, Walther et al., 2013). However, a 250 year coral record from Havannah Island, GBR showed that Ba/Ca did not peak with luminescent bands prior to European settlement, only matching well with luminescence and known flood events after anthropogenic influence increased (McCulloch et al., 2003). Peaks in Ba/Ca decoupled from river discharge events also have been reported from elsewhere on the GBR (Sinclair, 2005, Jupiter et al., 2008), with corals in close proximity to each other (<100m) displaying high variability (Lewis et al., 2012). Although the exact cause of Ba anomalies is still undetermined, biological mediation in the water column (Sinclair, 2005, Lewis et al., 2007, Elliot et al., 2009), release of Ba from hyper-saline mangrove zones during dry seasons or sub-marine ground water seeps have all been proposed (Alibert et al., 2003).

In contrast with Ba, Yttrium (Y) which is not biologically mediated, has been shown to be a more conservative proxy for fine suspended sediments across water quality gradients at annular or longer timescales (Alibert et al., 2003, Jupiter et al., 2008, Lewis et al., 2012), but is seemingly less reliable at sub-annual resolution (Prouty et al., 2010, Moyer, 2012). In the Palm Islands region (GBR), average coral Y concentrations were found to be six times higher at inshore versus mid-shelf sites (Alibert et al., 2003) and positive correlations in annual mean Y/Ca values and luminescent band intensity were also reported in the Whitsundays, yet inter-annual Y/Ca was not significantly correlated with either river discharge or luminescence (Lewis et al., 2012). The rare earth elements (REEs) offer potential as a proxy for reconstructing rainfall/flood events and turbidity as, in coastal waters, ~90% are derived from suspended and dissolved riverine input (Dubinin, 2004). Yet, compared with Ba and Y, high resolution records of REEs in corals are relatively few (Sholkovitz and Shen, 1995, Naqvi et al., 1996, Fallon and McCulloch, 2002, Akagi et al., 2004, Nguyen et al., 2013), and only two records of REEs in corals from the GBR are currently available (Wyndham et al., 2004, Jupiter, 2008).

In marine geochemistry relative shale normalised (subscript SN) patterns of REE or REEs and Yttrium (REY_{SN}) can be more informative than measurements of absolute concentrations (Quinn et al., 2004). Normalisation of the REYs against a terrestrial input value (e.g., an upper crust proxy such as a shale) allows for comparison in relation to both terrigenous and expected coastal seawater REY behaviour. The larger ionic radii of the light rare earth elements (LREEs) means that in the estuarine mixing zone these elements are preferentially adsorbed onto Fe-organic and salt-enriched colloids (Hoyle et al., 1984, Elderfield et al., 1990) with preferential association with larger particles in seawater, compared with ~ 70% of HREEs with particles < 0.4µm (Hoyle et al., 1984). The resultant pattern of shale normalised REYs for coastal sea water is therefore identified by LREE depletion, a superchondritic Y/Ho ratio and negative Ce anomaly as a result of the oxidation of Ce3+ to insoluble Ce4+ and subsequent removal from the water column by particulate scavenging (Elderfield and Greaves, 1982, Hoyle et al., 1984, Elderfield et al., 1990, Sholkovitz et al., 1994). Although Y and Ho are considered a geochemical pair due to near identical ionic radii (Lawrence et al., 2006), Ho is scavenged twice as fast as Y in the estuarine mixing zone at relatively low salinities [5.5‰ (Nozaki et al., 1997, Lawrence and Kamber, 2006)] therefore, lower Y/Ho ratio values are indicative of fresh water intrusion (i.e. fluvial plumes).

To further investigate the utility of REEs in high resolution palaeoclimatic and broad scale palaeoenvironmental reconstructions we present the results of ~monthly resolved REE, Y and Ba concentration data obtained from four modern *Porites* sp. coral cores collected across a known water quality gradient in the Wet Tropics region of the GBR.

Materials and Methods

Location and environmental setting

The Frankland Islands and Sudbury Cay are located in the Wet Tropics region of the GBR, Australia (Fig. 1). The Frankland Islands group consists of five continental islands (High, Russell, Normanby, Mabel and Round Island), which support fringing reefs to the leeward and windward. These islands are all within ~10 km of the coast, and are influenced by the Russell and Mulgrave Rivers, which discharge into the GBR lagoon via the Mutchero Inlet. Flood plume frequency analysis derived from satellite imagery demonstrates that plumes are typically advected north by the predominant south-easterly trade winds. Consequently, High Island is influenced more often by river discharge events than Russell Island, although both

sites are impacted by river flood plumes annually. On the mid-shelf at Sudbury Cay (located ~ 32 km north east of the Russell-Mulgrave River system) flood plumes are estimated to reach this site only once every 4 – 6 years (Fig. 1; Devlin et al., 2001).

Annual rainfall is seasonal with more than 60% falling in the austral summer (December – March) with a rainfall to run off conversion of ~60% (Connolly et al., 2007). The lower coastal catchment areas of both the Russell and Mulgrave rivers have been modified to accommodate predominantly sugar-cane, with grazing, fruit crops and other minor horticultural activities also within the region (Furnas, 2003, Connolly et al., 2007). Within the catchments, the lowland tributaries of the Russell River are significantly degraded due to the removal of riparian vegetation leading to bank destabilisation, and subsequently, higher sediment loads than the Mulgrave River (Arthington et al., 2007).

Coral core collection, treatment and sampling

Coral cores were collected live in November 2012 using a pneumatic drill on SCUBA at ~5 m depth on the leeward side of Russell (FRI 12.1, FRI 12.3) and High (HI 12.1) islands and within the lagoon at Sudbury Cay (SUD 12.1; Fig. 1). Cores were rinsed in fresh water and air dried before transportation. Cores were cut along the growth axis into 6 mm thick slabs at the School of Earth and Environment, University of Western Australia. Sections were ultra-sonicated three times in Milli-Q water for 15 minutes and dried in an oven at 60˚C. Core sections were X-rayed at St Vincent's hospital, Brisbane, to determine growth axis and chronology based on density band counting. Coral slabs also were viewed under ultra violet light to allow visualisation of luminescent bands in the corals.

Based on river discharge data from the Department of Natural Resources and Mines (https://www.dnrm.qld.gov.au/water/water-monitoring-and-data) for the Russell (Station Number - 111101D), Mulgrave (111007A) and South Johnstone rivers (112101B), as well as daily rainfall data from Deeral (Station 031021; http://www.bom.gov.au/climate/data/), periods of substantially low and high rainfall/river discharge were selected for analysis. The 2001-2003 period was identified as having the lowest river runoff, with increased discharge recorded for the 2004-2006 period. To capture the entire record spanning ~2000-2006, 5 – 10 cm sections of each coral were selected with at least 1 year of overlap between the cores. One annual band from the base of coral FRI 12.1 (~1950) was also sampled to allow for comparison with modern values. Approximately 5 mg of aragonite was milled across the coral cores at ~1 mm increments following sub-annular bands along the primary growth axis

using a hand held Dremel drill with a flexible shaft extension and 1 mm diamond tip bit. To eliminate sample cross-contamination the coral cores were cleaned with compressed air between each sample and a new drill bit was used between every sample.

Geochemical procedures

Approximately 2 mg of each powdered sample was weighed on a five digit scale and transferred to ultra-cleaned 5 ml Teflon tubes. Samples were dissolved in ~4.5 ml (weighed) of 2% HNO_3 containing 6 ppb concentrations of internal standards of ^{6}Li, ^{45}Sc, ^{103}Rh, ^{115}In, ^{187}Re, ^{207}Bi and ^{235}U to achieve a final sample dilution factor of ~2500. Stock solutions of certified standards W2a-1, BIR-1 and BHVO-2 were weighed and diluted using the same internal standard solution to a final dilution factor of ~5000. The coral standard Jcp-1 (Okai et al., 2002) was similarly prepared to a final dilution factor of ~2500. All samples and standards were ultra-sonicated for 30 minutes to ensure complete digestion and homogenisation of the solutions, after which they were centrifuged at 3500 rpm for 15 minutes immediately prior to measurement on a Thermo X-series Quadrupole Inductively Coupled-Mass Spectrometer (ICP-MS) at the Radiogenic Isotope Facility, The University of Queensland. Samples were run over four batches of ~100 samples each, with one-half of FRI 12.3 samples run in batch 1 and the other half in batch 4 to check for trace element matching. Elemental count rates were corrected for any internal and external drifts and oxide interferences. The corrected elemental count rates were then used to calibrate against the W2a-1 standard to calculate elemental concentrations, except for Ca, Mg, Ba, U and Sr, which were calibrated using the Jcp-1 standard.

Apparent distribution coefficients

The concentration of REEs in coral is governed by the distribution coefficient for each element incorporated into the aragonite lattice compared with seawater, and relative to calcium [Ca] given by the equation:

$$D_{REE} = \frac{(REE/Ca)_{coral}}{(REE/Ca)_{seawater}}$$

Where Ca seawater = 0.01 mol/kg and Ca REE = 10 mol/kg (Sholkovitz and Shen, 1995, Webb and Kamber, 2000). Although no seawater was collected as part of the present study, an apparent distribution coefficient was calculated from previously published seawater values from the Wet Tropics region. For calculations of D_{REEs}, sea water REE ($REE_{(sw)}$) values

from Yongala Reef were used for SUD 12.1, and $REE_{(sw)}$ values from High Island were used for FRI 12.1, FRI 12.3 and HI 12.1 (Wyndham et al., 2004; Supp. Tbl. 4). $REE_{(sw)}$ values from High Island (the most turbid site with higher $REE_{(sw)}$) were chosen as the seawater samples were collected in October 2002, which was a period of considerable drought in the region. Reduced run-off for this period would likely lead to an under-representation of the average REE concentrations under "normal" rainfall climatology and therefore over-estimate the apparent D_{REE} in the corals if the Frankland Islands $REE_{(SW)}$ values were used. Concentrations for seawater Tb, Tm and Lu were not reported for seawater in the Frankland Islands or Yongala Reef so these were interpolated using a mixing line derived from Mud of Queensland (MUQ; Kamber et al., 2005), High Island, Frankland Island and Yongala Reef near neighbour values (Wyndham et al., 2004).

Geochemical analysis

Based on *in situ* sea surface temperature (SST) data from the Frankland Islands and Arlington Reef (Australian Institute of Marine Science), annual cycles of geochemical data were defined using the peaks and troughs of the Sr/Ca signal (measured simultaneously) with the coldest months assigned to July – August (highest Sr/Ca) and the warmest months assigned to January - February. Distinct patterns of ΣREE enabled further sub-annual refinement of the chronology of the cores. For the overlapping time period (2001-2002), ΣREE, Y, and Ba concentrations in the four coral colonies were compared by analysis of variance in Excel (ANOVA- with unequal variance). Pairwise t-tests with Bonferroni adjustments were then used to determine differences in the mean concentrations between each core for ΣREE, Y and Ba.

Rare earth element and Y (REY) data were normalised using Mud of Queensland (MuQ; shale normalised-REY_{SN}) values of Kamber et al. (2005) to examine general REY_{SN} patterns between cores, and for selected points of interest (peaks, troughs, anomalous points) based on time series data of the ΣREE signal.

Water quality gradients were reconstructed using a kriging spatial interpolation in PAST statistical package using Mud of Queensland [MuQ; (Kamber et al., 2005)] as point source values (i.e. Russell-Mulgrave River) and the average concentration data for ΣREE, ΣREY and Y/Ho mass ratio for each core plotted in latitudinal-longitudinal space.

Results

Core chronology and growth characteristics

X-ray positive images showed clear annual density bands in all the cores, although the rates of linear extension and tissue thickness of each colony was variable (Supp. Tbl. 1). As trace elements can be incorporated through the depth of the living tissue layer both extension rate and tissue thickness can affect sub-annual geochemical signals in corals (Taylor et al., 1995, Nothdurft et al., 2007). Therefore the ratio of tissue thickness relative to linear extension was used to determine an approximate month equivalent by which geochemical signals may be offset from a causative discharge event. Average linear extension was highest in FRI 12.3 (2.10 ± 0.19 cmyr^{-1}) compared to FRI 12.1 (1.59 ± 0.21 cmyr^{-1}), HI 12.1 (1.66 ± 0.23 cmyr^{-1}) and SUD 12.1 (1.18 ± 0.15 cmyr^{-1}). Colony FRI 12.3 also had the lowest average tissue thickness/linear extension ratio (0.29), resulting in an approximated possible offset the geochemical signal of - 3months. Core FRI 12.1 displayed the highest possible offset of almost 7 months due to the relative thick living tissue layer (0.9 cm) compared to the average linear extension in this coral.

Viewed under UV light, the annual luminescence bands in the three inshore corals were visibly well matched (Supp. Fig. 1), with a distinct double band observed in the three corals in 2000, which relates well to two major discharge events in the Mulgrave River (February and April). This double band event was not as clear in SUD 12.1, but still detectable. Luminescence intensity was relatively weak in all the corals for 2001-2003, which agrees well with lower overall discharge in the region for the same period. The coherency between the luminescent bands confirms the annual chronology based on density band counting, and the relative intensity of the luminescent bands compared with discharge data supports previous evidence that visual inspection of luminescent bands is a reliable indicator of relative river run-off volume (Hendy et al., 2003, Lough, 2011b).

Apparent distribution coefficients

The seawater REE concentrations derived from near neighbour values for Tb, Tm and Lu, although slightly lower (Tbl. 1; Tb -0.082, Tm -0.068 and Lu -0.062), compare well with Coral Sea sea-surface values (Zhang and Nozaki, 1996) and are therefore considered applicable for apparent D_{REE} calculations. Mean apparent average D_{REE} for all elements are relatively flat across the series for all four cores (Fig. 2) and are within the range of

previously reported values for corals [~1-4; (Sholkovitz and Shen, 1995, Akagi et al., 2004). The most uniform D_{REEs} across the REE series was for coral FRI 12.3 with average apparent D_{REE} of 1.38 ± 0.27 (standard deviation). High Island D_{REEs} were slightly higher and more variable with an average across the series of 2.03 ± 0.42, with FRI 12.1 and SUD 12.1 having the highest deviations across the series (2.26 ± 0.54 and 1.45 ± 0.58 respectively).

Geochemical time series

Combined coral core time series spanned ~1999-2006, with an overlap between the four cores in 2001-2002. Concentrations of ΣREE, Y and Ba were highly variable within the cores at sub-annular - annular scales, but co-varied coherently in cores FRI 12.3 and HI 12.1 (Fig. 3). On the mid-shelf (SUD 12.1), ΣREE and Y co-varied throughout the time series, however Ba peaks and troughs did not align with ΣREE, Y or the geochemical signals from the other cores (Fig. 3). Scaled annual to sub-annual ΣREE concentrations for cores HI 12.1, FRI 12.3 and SUD 12.1 demonstrate coherent patterns of peaks and troughs that are generally well aligned with regional rainfall (Fig. 4).

Core FRI 12.1 showed coherency with discharge for only part of the record (~April 1999 – February 2002) with two anomalously high peaks in ΣREEs (~250 ppb compared to an average of ~126 ppb) occurring in ~September 2000 and ~July 2001 (Supp. Fig. 2). These peaks were not associated with luminescent bands, and higher Nd_{SN}/Yb_{SN} ratios (0.63 and 0.75 compared to an average of 0.33) demonstrate that have decreased LREE depletion. Smaller positive peaks in ΣREE concentrations are observed in SUD 12.1 in ~October 2000 and August 2001, however no comparable peaks were observed in cores HI 12.1 and FRI 12.3. Although the peaks in colony FRI 12.1 broadly align with moderately high rainfall and a maximum daily discharge of ~5800 ML/day in August 2000 and ~5000 ML/day in June 2001, the lack of notable geochemical peaks in the other inshore corals suggests the peaks in coral FRI 12.1 are not directly related to a specific run-off event, and are more likely the result of localised resuspension of sediments. This core was subsequently removed from further time-series discussions however, as resuspension of sediments at inshore coral reefs is a significant contributor to turbidity regimes (Browne et al., 2013) it was included in the water quality spatial analysis (see Supp. 2 and Water Quality Gradient for further discussion).

Variance of geochemical concentrations

Unequal variance ANOVA for the overlapping time period 2001-2002 for ΣREE , Y , and Ba concentrations indicated a significant difference between the cores (F= 60.92, 24.71 and 320.16, respectively; p = <0.001; Supp. Tbl. 1). Pairwise t-tests with Bonferroni adjustments (95% confidence interval) revealed that all cores contained significantly different mean ΣREE concentrations from each other (p = <0.05; Supp. Table 2A) however, no significant difference was found for Y between cores FRI 12.3 and HI 12.1 (p = 4.51) or SUD 12.1 and FRI 12.3 (p = 0.43), and only cores FRI 12.3 and HI 12.1 showed a significant difference in Ba (p = <0.05; Supp. Tbl. 2B and 2C). Summary statistics for 2001-2002 demonstrate that the maximum ΣREE concentrations in coral FRI 12.1 are 2.5 and 4.2 times higher than HI 12.1 and FRI 12.3, respectively, whilst the mid-shelf coral (SUD 12.1) contained between 2-8 times lower concentrations of ΣREE than the inshore corals (Supp. Tbl. 3).

Average ΣREE concentrations are comparable to previously reported coral values from the GBR (Supp. Tbl. 4), however, elevated concentrations were observed in colony FRI 12.1, mainly due to the two previously identified anomalous “winter” peaks.

REY_{SN} patterns in the Frankland Island cores generally display patterns reflecting those expected for coastal sea water, with a progressive enrichment of HREE relative to LREE across the series and notably lower Ce normalised values compared to La and Pr. Some exceptions to these trends were less pronounced negative Ce normalised values for corals FRI 12.1 and SUD 12.1, with intermittent periods of positive Ce and Eu normalised anomalies in SUD 12.1 (Fig. 4b).

Discussion

The use of both luminescence bands and geochemical proxies in corals to extend environmental and climatic records beyond modern instrumentation is becoming common-place (e.g., Saha et al., 2016). However, heterogeneity in geochemical Ba/Ca between corals and decoupling of signals from both river discharge data and luminescent bands is ubiquitous (McCulloch et al., 2003, Sinclair, 2005, Lewis et al., 2012). Until these anomalies are fully understood, and new possible proxies are developed, the use of geochemical signals for robust high-resolution water quality reconstructions is limited. Here we compare the results of ~ monthly resolution ΣREE, Y, and Ba signals in massive *Porites* corals to instrumental

records of river discharge, rainfall and flood plume frequency across a known water quality gradient in the Wet Tropics region of the GBR.

Apparent distribution coefficients

The uniformity of incorporation of REEs across the series into the coral skeleton (i.e. distribution coefficients; D_{REE}) is an important consideration prior to their use in interpreting ambient seawater conditions (Sholkovitz and Shen, 1995, Webb and Kamber, 2000, Akagi et al., 2004). Mean apparent D_{REE} calculated from seawater values from High Island (inshore) and Yongala Reef (mid-shelf) were generally consistent across the series, ranging between 1-3, which is in agreement with previous values reported from High Island, but lower than those reported previously for Frankland Island (~ 3 - 4; Wyndham et al., 2004). The difference in apparent D_{REE} at Frankland Island is most likely due to the collection time of Frankland Island seawater by Wyndham et al. (2004) in a drought period (October 2002) which would likely underrepresent normal climatology REE concentrations. Variation in apparent D_{REE} values reflects the variability in water quality experienced by the corals through time.

The variability in apparent D_{REE} in core FRI 12.1 mainly affects the degree of LREE depletion, suggesting that this site is more influenced by LREE-rich runoff. High variability in LREEs has also been observed in *Porites* corals obtained from coastal Japan (Akagi et al., 2004) and the Indian Ocean, with the latter attributed to monsoon driven increases in terrestrially derived LREEs (Naqvi et al., 1996). Comparatively, HI 12.1 showed the most variability in the HREE, suggesting dissolved phase processes are dominant at this site. Variability in SUD 12.1 D_{REES} was extremely high for Ce and Eu, which was unexpected as this site is most removed from fluvial influence. This may be an artefact of the low concentrations of REEs in this coral, detrital contamination (Wyndham et al., 2004), surface redox chemistry (De Carlo et al., 1997, Bau and Koschinsky, 2009, Bau et al., 2014) or biological control (Alibert et al., 2003). Positive Ce anomalies (Ce/Ce*;Table 1) in some years at Sudbury Reef follow peaks in manganese (~1 month lag, not shown) and may be related to the release of Ce via dissolution of Mn oxides by photo-reduction (Alibert et al., 2003). Nevertheless, given the temporal and spatial variability of REES in both corals and seawater, the apparent D_{REE} for the four cores are comparable to each other and to previously reported values from the GBR (Wyndham et al., 2004), Bermuda (Sholkovitz and Shen,

1995) and Japan (Akagi et al., 2004) indicating that the REEs in the Frankland Island corals are representative of ambient local seawater concentrations.

Geochemical time series

Total REE concentrations in the Frankland Islands region showed high variability both spatially and temporally similar to previous observations from inshore corals on the GBR (Wyndham et al., 2004). For the overlapping period of 2001-2002 ΣREE concentrations were significantly different between all four sites (Supp. Tbl. 2), however scaled annual to sub-annual time series of ΣREEs in cores FRI 12.3, HI 12.1 and SUD 12.1 co-vary coherently and appear to be related to rainfall (Fig. 4) and river discharge (Fig. 3) indicating these corals are reliably recording variations in seawater REE concentrations. Colony FRI 12.1 showed only limited covariance with the other cores, with two anonymously high peaks in ΣREE concentrations occurring in austral autumn-winter and has therefore been removed from further time series – discharge comparisons (see Supp. 2 for further discussion). Monthly resolution sampling of this core for ~1950 however, showed lower ΣREE concentrations (53-80 ppb) compared to the 1999-2002 period (78 -248 ppb), demonstrating that ΣREE might indicate changes to sediment delivery to the GBR following European settlement and coastal development (Supp. Fig. 2).

High Island (HI 12.1), which experiences more frequent flood plumes (Devlin et al., 2001) and higher turbidity (Fabricius et al., 2013), displayed higher average concentrations of ΣREE than FRI 12.3 and SUD 12.1 across the time series (85 > 55 >16 ppb respectively; Table 2). Peak ΣREE concentrations in HI 12.1 were as much as twice as high as those observed co-occurring in FRI 12.3 (132 ppb versus 84 ppb respectively) and four times higher than the mid-shelf coral SUD 12.1 (31 ppb). Average Nd_{SN}/Yb_{SN} ratios for the High Island coral also demonstrate increased depletion of LREEs relative to other inshore sites (HI 12.1 = 0.2 < FRI 12.3 = 0.26 < FRI 12.1 = 0.33; Table 2). The overall higher ΣREE concentration but lower LREE proportions suggests that the turbidity at this site is composed of both particulate and dissolved fractions that are relatively persistent throughout the year. Across the time series, average inshore ΣREE concentrations are 2.5 to 7.5 higher at inshore locations than at the mid-shelf (Tbl. 2). This difference is greater than the ΣREE gradient reported between Round Top and Keswick Islands in southern-central GBR [~ 2 times] (Jupiter, 2008). The average ΣREE concentration of 50 ppb for FRI 12.3 is similar to the reported values from Round Top Island [53 ppb, 5 km offshore (Jupiter, 2008)], however,

both FRI 12.1 (~ 10 km offshore) and HI 12.1 (~6 km offshore) have significantly higher average ΣREE concentration values (126 ppb and 80 ppb respectively). Average ΣREE values for SUD 12.1 (17ppb) are only moderately lower than those reported for Keswick Island [~25 ppb; (Jupiter, 2008)] with both sites being similar distances from the coast (32 km).

The most coherent ΣREE signal (i.e. well defined peaks and troughs) was obtained from core FRI 12.3 which, although inshore, is located slightly south of the predominant plume direction and is therefore less affected by minor river discharge events (Fig. 1; Devlin et al., 2001). The clearer geochemical signal in coral FRI 12.3 is also likely due to the comparatively low tissue thickness/extension ratio in this coral compared to the other colonies (Supp. Tbl. 1). Although the majority of element incorporation is predicted to occur at the precipitating surface of the coral, trace elements can be incorporated to secondary skeletal deposits throughout the depth of the living tissues layer (Taylor et al., 1995). In the Frankland Islands corals, this is seen as increases in ΣREE concentrations appearing to precede maximum discharge events (Fig. 3). Alternatively, initial increases in ΣREE concentrations in the corals may be recording transportation of sediment derived from early season rainfall events not associated with high river discharge. The covariance of the scaled ΣREE signals for FRI 12.3, HI 12.1 and SUD 12.1 and rainfall data (Fig. 4) indicates this is the most likely scenario, suggesting that even when discharge events are moderate, substantial sediment delivery still occurs to these reefs. The seasonally earlier and smaller discharge events may represent initial increased erosion following dryer months when mobilisation of fine topsoils is more prevalent. These results suggest that ΣREEs incorporated into inshore corals offer seemingly greater potential for use in rainfall reconstruction than in quantifying river discharge.

Annual time series of Ba and Y co-varied with ΣREE in cores HI 12.1 and FRI 12.3, however sub-annual alignment was poor between all cores (Fig. 3). At the mid-shelf location (SUD 12.1) Ba peaks occur largely in the early Austral spring, and are not aligned with river discharge or rainfall. These results are comparable to Ba/Ca patterns reported for Davies Reef, a similar mid-shelf site, for which biological processes were suggested to be dominant (Alibert et al., 2003). A lack of correlation in sub-annual Ba and Y time-series signals between inshore *Porites* have also been reported in the Whitsunday Islands (Lewis et al., 2012), with Ba/Ca peaks commonly decoupled from discharge (Sinclair, 2005, Lewis et al., 2012). Although the source of anomalous peaks has been ascribed to upwelling in shelf edge

regions (Walther et al., 2013), the cause at inshore and mid-shelf sites is still ambiguous. Notably, the most reliable relationships previously reported for Ba and river discharge are in corals under the influence of the Burdekin River in the Dry Tropics (Alibert et al., 2003, McCulloch et al., 2003, Sinclair, 2005). Satellite image observations of flood events have shown that in the Burdekin catchment, where cattle grazing is dominant, plumes contain higher levels of inorganic sediments compared to catchments in which sugarcane is grown, in which dissolved and particulate organics are generally higher (Schroeder et al., 2012). Barium concentrations in coastal waters, therefore, appear to be not only biologically mediated, but also largely dependent on regional scale hydrology (e.g. Dry Tropics versus Wet Tropics; Devlin et al., 2012), catchment geology and land use.

REY_{SN} patterns

REY_{SN} for the inshore Frankland Islands corals largely reflect that expected of coastal seawater, and average REY_{SN} values for FRI 12.3 and HI 12.1 are indistinguishable from values previously reported by Wyndham et al. (2004) for the same sites (Fig. 5). Average REY_{SN} patterns for FRI 12.1 however show highly variable depletion of LREEs (Nd_{SN}/Yb_{SN} = 0.18 – 0.75; TBL. 2) and generally reduced negative Ce anomaly, similar to patterns in corals from Vietnam after port dredging activities (Nguyen et al., 2013) further validating our hypothesis that localised sediment resuspension is occurring at this site. The average REY_{SN} pattern at Sudbury Reef (mid-shelf - SUD 12.1) is characterised by lower overall REY values, a reduced Ce anomaly, extremely positive Y values (relative to Ho) and an unexpected positive Eu anomaly. The relatively constant apparent distribution co-efficient for Eu for SUD 12.1 (2.25 ± 0.46) is within the range calculated for other inshore corals (1.4 - 2.5) suggesting that this anomaly is not an artefact of the low concentrations in this coral and warrants further investigation.

Comparison of REY_{SN} of wet versus dry periods (Fig 6.) shows notable differences with higher ΣREE in wet versus dry periods. At High Island there is also increased fractionation of HREE across the series in wet versus dry years. The higher MUQ normalised HREE patterns observed at High Island compared with both FRI 12.3 and SUD 12.1 for wet years supports previous observations of flood plume dispersal in this region (Devlin et al., 2001) which are driven north by the predominant south-easterly winds. This is reflected in the local coral community structure, whereby High Island has the lowest juvenile coral recruitment and the lowest density of coral cover within the Frankland Islands group (Smith et al., 2005).

Water quality gradient; ΣREE, ΣREY and Y/Ho

Given the clear distinctions between total ΣREE concentrations between sites in the Frankland Islands, spatial interpolations were applied to average ΣREE, ΣREY and Y/Ho values to assess whether coral cores could reliably reconstruct both broad scale and local water quality patterns The spatial interpolation model of Y/Ho produced a simple water quality gradient (Fig.7) with inshore Y/Ho ratios not differentiating well at local scales, but predicting well the expected inshore-offshore gradient. Whilst the Y/Ho ratios for the inshore corals (minimum 69-74; maximum 108-125) fall close to that of near surface marine values [~40 -140;(Zhang and Nozaki, 1996, Nozaki et al., 1997, Zhang and Nozaki, 1998, Alibo and Nozaki, 1999)] and are similar to previous coral records from the inshore GBR [67.3;(Jupiter, 2008)] and coastal Vietnam [52 -112; (Nguyen et al., 2013)], significantly higher Y/Ho ratios were observed at Sudbury Cay (>300; Tbl. 2). High Y/Ho ratios have also been observed by Jupiter et al. (2008) at a GBR mid-shelf site (140), and calculated ratios from Heron Reef (southern GBR) corals range from 300 – 1200 (Webb and Kamber, 2000). The super-chondritic ratios are driven by extremely low Ho values (0.2) recorded in the corals at both Sudbury Cay and Heron Reef, and supports previous observations of the persistence of Y in the soluble phase of sea water compared to REEs (Nozaki et al., 1997, Zhang and Nozaki, 1998). Although beyond the scope of this study, future work is recommended to determine the discrepancies between sea water Y/Ho ratios and mid-shelf corals. Nevertheless, spatial interpolation of Y/Ho offers potential for reconstructing palaeo-water quality gradients in regions where local hydrodynamics are not complex, or where palaeo-cross shelf water quality gradients are required for ecological evaluations.

Compared to patterns of turbidity derived from *in situ* data (Fabricius et al., 2013) and flood plume frequency analysis (Devlin et al., 2001) the ΣREE spatial interpolation model (Fig. 7b) underestimated turbidity at High Island relative to NW Russell Island (FRI 12.1), whereas the ΣREY model (Fig 7c) better reflects both instrumental turbidity data and flood plume frequency reconstructions (Devlin et al., 2001, Schaffelke et al., 2008, Fabricius et al., 2013). This suggests that Y desorbed from particulates in the estuarine mixing zone effectively traces the extent of discharge plumes due to the strong solution complexation of Y (and to a lesser extent HREEs) with carbonate ions (dissolved) compared with LREE covalent complexation to particulates in sea water (Zhang and Nozaki, 1996, Quinn et al., 2004). The higher ΣREE concentrations in core FRI 12.1 than HI 12.1 was unexpected, as nearby *in situ* monitoring of these Islands for the period 2007 – 2010 indicates higher mean and maximum

turbidity at High Island (0.95 and ~7 Nephelometric Turbidity Units [NTU] respectively) compared with Russell Island (0.65 and ~2 NTU; Schaffelke et al., 2008, Fabricius et al., 2013). Flood plume frequency mapping of Russell-Mulgrave River discharge events also indicates that High Island experiences more frequent flood plumes than Russell Island (Devlin et al., 2001). As the *in situ* data logger for the 2007-2010 monitoring period was located closer to FRI 12.3 (~80m) than to FRI 12.1 (~350m), the difference in ΣREE concentrations in coral FRI 12.1 may be due to sub-reef scale differences in turbidity. A mean ~monthly record of turbidity obtained in 2000 indicated a higher NTU value (1.3 NTU) for the NW of Russell Island (i.e. closer to core FRI 12.1) than values observed at sites on High Island reef (0.8 - 1.2 NTU) for the same period (Macdonald et al., 2013) suggesting the peaks observed in FRI 12.1 are likely reflecting localised resuspension at this site. Increased localised resuspension of sediments at FRI 12.1 could be due to either tidal current attenuation through the inter-reef passage, (Fig. 1) or to the coral's close proximity (<30 m) to a permanent mooring buoy, which may cause intermittent disturbance of sediments. Regardless of the cause for higher turbidity at FRI 12.1, the ΣREY spatial interpolation provides an effective tool for reconstructing more complex palaeo-water quality gradients to assess past reef growth histories. These results suggest that spatial interpolation of REYs in non-traditional (non- massive) samples obtained from reef cores (Sadler et al., 2014) could potentially be used for point-time change, as well as spatial analysis of palaeo-water quality gradients to assess ecological heterogeneity.

Conclusions

The extensive coral reefs of the Great Barrier Reef (GBR) grow in widely divergent environments, with inshore reefs subjected to significantly higher terrigenoclastic input from rivers, as well as resuspension of coastal sediment, compared to the mid-shelf and outer reefs. The unique behaviours of the REEs and Y in coastal mixing zones suggests the potential for their use in reconstructing palaeo-climatic and environmental conditions that have controlled reef growth. Although further work needs to be undertaken to fully understand both the temporal and spatial variability of REYs at sub-annual timescales, the comparable distribution coefficients for the Frankland Islands to previously reported values on the GBR and elsewhere suggests that corals can be used successfully to interpret changes in REY systematics in coastal seawater. The primary aim of this study was to identify potential uses

for REY geochemistry in coastal locations for use in palaeo-research. A summary of our results is as follows:

1. ΣREE concentration is a better indicator of regional rainfall than river discharge, as early season (smaller) peaks are likely associated more efficient removal of top soils following dry periods.
2. Scaled ΣREE time series data matched well between the cores at annual to sub-annual resolution irrespective of significant differences in total ΣREE concentrations between sites, thus offering potential for sub-annular to annual resolution rainfall and river discharge reconstructions
3. ΣREE concentrations have the potential to track changes in sediment delivery to the GBR since European settlement, with higher ΣREE observed in 1999-2002 (78 – 250 ppb in dry and wet years) than in 1950 (53-79 ppb).
4. Spatial interpolation models of Y/Ho serve as indicator for cross shelf sediment delivery, however ΣREY models better predict known turbidity and flood plume patterns in regions of more complex oceanography. Applying a similar approach to corals obtained from reef matrix cores would allow for interpretation of ecological data in the context of relative turbidity between sites, transitions through cores or for interpretation of absolute time periods.
5. Corals with the largest linear extension rate and lowest tissue thickness/extension ratios are best suited to geochemical analysis. To fully understand geochemical signals in fossil corals, determination of the tissue thickness (by measuring the last deposited dissepiment) is necessary prior to interpretation (Barnes and Lough, 1992).

References

Akagi, T., Hashimoto, Y., F-F, F., Tsuno, H., Tao, H. & Nakano, Y. 2004. Variation of the distribution coefficients of rare earth elements in modern coral-lattices: species and site dependencies 1 1 Associate editor: R. H. Bryne. *Geochimica et Cosmochimica Acta* **68,** 2265-2273.

Alibert, C., Kinsley, L., Fallon, S. J., Mcculloch, M. T., Berkelmans, R. & Mcallister, F. 2003. Source of trace element variability in Great Barrier Reef corals affected by the Burdekin flood plumes. *Geochimica et Cosmochimica Acta* **67,** 231-246.

Alibo, D. S. & Nozaki, Y. 1999. Rare earth elements in seawater: particle association, shale-normalization, and Ce oxidation. *Geochimica et Cosmochimica Acta* **63,** 363-372.

Arthington, A. H., Connolly, N. M. & Pearson, R. G. 2007. Introduction: the Catchment to Reef Program and Stream Ecosystem Health Monitoring. *In:* Arthington, A. H. & Pearson, R. G. (eds.) *Biological Indicators of Ecosystem Health in Wet Tropics Streams. Final Report Task 3 Catchment to Reef Program Cooperative Research Centre for Rainforest Ecology & Management and Cooperative Research Centre for the Great Barrier Reef World Heritage Area.*

Barnes, D. J. & Lough, J. M. 1992. Systematic variations in the depth of skeleton occupied by coral tissue in massive colonies of Porites from the Great barrier reef. *Journal of experimental marine biology and ecology* **159,** 113-128.

Bau, M. & Koschinsky, A. 2009. Oxidative scavenging of cerium on hydrous Fe oxide: Evidence from the distribution of rare earth elements and yttrium between Fe oxides and Mn oxides in hydrogenetic ferromanganese crusts. *Geochemical Journal* **43,** 37-47.

Bau, M., Schmidt, K., Koschinsky, A., Hein, J., Kuhn, T. & Usui, A. 2014. Discriminating between different genetic types of marine ferro-manganese crusts and nodules based on rare earth elements and yttrium. *Chemical Geology* **381,** 1-9.

Browne, N. K., Smithers, S. G. & Perry, C. T. 2013. Spatial and temporal variations in turbidity on two inshore turbid reefs on the Great Barrier Reef, Australia. *Coral Reefs* **32,** 195-210.

Connolly, N. M., Pearson, B., Loong, D., Maughan, M. & Pearson, R. G. 2007. Hydrology. Geomorphology and Water Quality of Four Wet Tropics Streams with Contrasting Land-use Management. *In:* Arthington, A. H. & Pearson, R. G. (eds.) *Biological Indicators of Ecosystem Health in Wet Tropics Streams. Final Report Task 3 Catchment to Reef Research Program Cooperative Research Centre for Rainforest Ecology and Management and Cooperative Research Centre for the Great Barrier Reef World Heritage Area.*

Correge, T. 2006. Sea surface temperature and salinity reconstruction from coral geochemical tracers. *Palaeogeography, Palaeoclimatology, Palaeoecology* **232,** 408-428.

De'ath, G. & Fabricius, K. 2010. Water quality as a regional driver of coral biodiversity and macroalgae on the Great Barrier Reef. *Ecological Applications* **20,** 840-850.

De Carlo, E. H., Wen, X.-Y. & Irving, M. 1997. The Influence of Redox Reactions on the Uptake of Dissolved Ce by Suspended Fe and Mn Oxide Particles. *Aquatic Geochemistry* **3,** 357-389.

Devlin, M., Waterhouse, J., Taylor, J. & Brodie, J. E. 2001. Flood plumes in the Great Barrier Reef : spatial and temporal patterns in composition and distribution. Townsville: Great Barrier Reef Marine Park Authority.

Devlin, M. J., Mckinna, L. W., Álvarez-Romero, J. G., Petus, C., Abott, B., Harkness, P. & Brodie, J. 2012. Mapping the pollutants in surface riverine flood plume waters in the Great Barrier Reef, Australia. *Marine Pollution Bulletin* **65,** 224-235.

Dubinin, A. V. 2004. Geochemistry of Rare Earth Elements in the Ocean. *Lithology and Mineral Resources* **39,** 289-289.

Elderfield, H. & Greaves, M. J. 1982. The rare earth elements in seawater. *Nature* **296,** 214-219.

Elderfield, H., Upstill-Goddard, R. & Sholkovitz, E. R. 1990. The rare earth elements in rivers, estuaries, and coastal seas and their significance to the composition of ocean waters. *Geochimica et Cosmochimica Acta* **54,** 971-991.

Elliot, M., Welsh, K., Chilcott, C., Mcculloch, M., Chappell, J. & Ayling, B. 2009. Profiles of trace elements and stable isotopes derived from giant long-lived Tridacna gigas bivalves: Potential

applications in paleoclimate studies. *Palaeogeography, Palaeoclimatology, Palaeoecology* **280,** 132-142.
Fabricius, K. E. 2005. Effects of terrestrial runoff on the ecology of corals and coral reefs: review and synthesis. *Marine Pollution Bulletin* **50,** 125-146.
Fabricius, K. E., De'ath, G., Humphrey, C., Zagorskis, I. & Schaffelke, B. 2013. Intra-annual variation in turbidity in response to terrestrial runoff on near-shore coral reefs of the Great Barrier Reef. *Estuarine, Coastal and Shelf Science* **116,** 57-65.
Fallon, S., Wyndham, T., Hendy, E., Lough, J. & Barnes, D. 2003. Coral record of increased sediment flux to the inner Great Barrier Reef since European settlement. *Nature* **421,** 727-730.
Fallon, S. J. & Mcculloch, M. T. 2002. Porites corals as recorders of mining and environmental impacts: Misima Island, Papua New Guinea. *Geochimica et Cosmochimica Acta* **66,** 45-62.
Furnas, M. 2003. *Catchments and corals: terrestrial runoff to the Great Barrier Reef,* Townsville, Qld, Australian Institute of Marine Science.
Hendy, E. J., Gagan, M. K. & Lough, J. 2003. Chronological control of coral records using luminescent lines and evidence for non-stationary ENSO teleconnections in northeast Australia. *The Holocene* **13,** 187-199.
Hoyle, J., Elderfield, H., Gledhill, A. & Greaves, M. 1984. The behaviour of the rare earth elements during mixing of river and sea waters. *Geochimica et Cosmochimica Acta* **48,** 143-149.
Hughes, T. P., Day, J. C. & Brodie, J. 2015. Securing the future of the Great Barrier Reef. *Nature Climate Change* **5,** 508-511.
Isdale, P. 1984. Fluorescent bands in massive corals record centuries of coastal rainfall. *Nature* **310,** 578-579.
Isdale, P. J., Stewart, B. J., Tickle, K. S. & Lough, J. M. 1998. Palaeohydrological variation in a tropical river catchment: a reconstruction using fluorescent bands in corals of the Great Barrier Reef, Australia. *The Holocene* **8,** 1-8.
Jupiter, S. Year. Coral rare earth element tracers of terrestrial exposure in nearshore corals of the Great Barrier Reef. *In:* Proceedings of the 11th International Coral Reef Symposium, 7-11th July 2008 Ft. Lauderdale, Florida.
Jupiter, S., Roff, G., Marion, G., Henderson, M., Schrameyer, V., Mcculloch, M. & Hoegh-Guldberg, O. 2008. Linkages between coral assemblages and coral proxies of terrestrial exposure along a cross-shelf gradient on the southern Great Barrier Reef. *Coral Reefs* **27,** 887-903.
Kamber, B. S., Greig, A. & Collerson, K. D. 2005. A new estimate for the composition of weathered young upper continental crust from alluvial sediments, Queensland, Australia. *Geochimica et Cosmochimica Acta* **69,** 1041-1058.
Lawrence, M. G., Jupiter, S. D. & Kamber, B. S. 2006. Aquatic geochemistry of the rare earth elements and yttrium in the Pioneer River catchment, Australia. *Marine & Freshwater Research* **57,** 725-736.
Lawrence, M. G. & Kamber, B. S. 2006. The behaviour of the rare earth elements during estuarine mixing-revisited. *Marine Chemistry* **100,** 147-161.
Lewis, S. E., Brodie, J. E., Mcculloch, M. T., Mallela, J., Jupiter, S. D., Stuart Williams, H., Lough, J. M. & Matson, E. G. 2012. An assessment of an environmental gradient using coral geochemical records, Whitsunday Islands, Great Barrier Reef, Australia. *Marine Pollution Bulletin* **65,** 306-319.
Lewis, S. E., Shields, G. A., Kamber, B. S. & Lough, J. M. 2007. A multi-trace element coral record of land-use changes in the Burdekin River catchment, NE Australia. *Paleogeography, Paleoclimatology, Paleoecology* **246,** 471-487.
Lough, J., Barnes, D. & Mcallister, F. 2002. Luminescent lines in corals from the Great Barrier Reef provide spatial and temporal records of reefs affected by land runoff. *Coral Reefs* **21,** 333-343.
Lough, J. M. 2011a. Great Barrier Reef coral luminescence reveals rainfall variability over northeastern Australia since the 17th century. *Paleoceanography* **26**.
Lough, J. M. 2011b. Measured coral luminescence as a freshwater proxy: comparison with visual indices and a potential age artefact. *Coral Reefs* **30,** 169-182.
Lough, J. M., Lewis, S. E. & Cantin, N. E. 2015. Freshwater impacts in the central Great Barrier Reef: 1648–2011. *Coral Reefs* **34,** 739-751.

Lough, J. M., Llewellyn, L. E., Lewis, S. E., Turney, C. S. M., Palmer, J. G., Cook, C. G. & Hogg, A. G. 2014. Evidence for suppressed mid-Holocene northeastern Australian monsoon variability from coral luminescence. *Paleoceanography* **29,** 581-594.

Lough, J. M., Stewart, B. J., Isdale, P. J. & Tickle, K. S. 1998. Palaeohydrological variation in a tropical river catchment: a reconstruction using fluorescent bands in corals of the Great Barrier Reef, Australia. *The Holocene* **8,** 1-8.

Macdonald, R. K., Ridd, P. V., Whinney, J. C., Larcombe, P. & Neil, D. T. 2013. Towards environmental management of water turbidity within open coastal waters of the Great Barrier Reef. *Marine Pollution Bulletin* **74,** 82-94.

Mcculloch, M., Fallon, S., Wyndham, T., Hendy, E., Lough, J. & Barnes, D. 2003. Coral record of increased sediment flux to the inner Great Barrier Reef since European settlement. *Nature* **421,** 727-730.

Moyer, R. P. 2012. A multiproxy record of terrestrial inputs to the coastal ocean using minor and trace elements (Ba/Ca, Mn/Ca, Y/Ca) and carbon isotopes (C, Δ C) in a nearshore coral from Puerto Rico. *Paleoceanography* **27**.

Naqvi, S. a. S., Nagender Nath, B. & Balaram, V. 1996. Signatures of rare-earth elements in banded corals of Kalpeni atoll - Lakshadweep archipelago in response to monsoonal variations. *Indian Journal of Marine Sciences* **25,** 1-4.

Nguyen, A. D., Zhao, J. X., Feng, Y. X., Hu, W. P., Yu, K. F., Gasparon, M., Pham, T. B. & Clark, T. R. 2013. Impact of recent coastal development and human activities on Nha Trang Bay, Vietnam: evidence from a Porites lutea geochemical record. *Coral Reefs***,** 1-13.

Nothdurft, L. D., Webb, G. E., Bostrom, T. & Rintoul, L. 2007. Calcite-filled borings in the most recently deposited skeleton in live-collected Porites (Scleractinia): Implications for trace element archives. *Geochimica et Cosmochimica Acta* **71,** 5423-5438.

Nozaki, Y., Zhang, J. & Amakawa, H. 1997. The fractionation between Y and Ho in the marine environment. *Earth and Planetary Science Letters* **148,** 329-340.

Okai, T., Suzuki, A., Kawahata, H., Terashima, S. & Imai, N. 2002. Preparation of a New Geological Survey of Japan Geochemical Reference Material: Coral JCp-1. *Geostandards Newsletter* **26,** 95-99.

Pandolfi, J. M. 2015. Incorporating Uncertainty in Predicting the Future Response of Coral Reefs to Climate Change. *Annual Review of Ecology, Evolution, and Systematics* **46,** 281-303.

Pandolfi, J. M., Bradbury, R. H., Sala, E., Hughes, T. P., Bjorndal, K. A., Cooke, R. G., Mcardle, D., Mcclenachan, L., Newman, M. J. H., Paredes, G., Warner, R. R. & Jackson, J. B. C. 2003. Global Trajectories of the Long-Term Decline of Coral Reef Ecosystems. *Science* **301,** 955-958.

Prouty, N. G., Field, M. E., Stock, J. D., Jupiter, S. D. & Mcculloch, M. 2010. Coral Ba/Ca records of sediment input to the fringing reef of the southshore of Moloka'i, Hawai'i over the last several decades. *Marine Pollution Bulletin* **60,** 1822-1835.

Prouty, N. G., Hughen, K. A. & Carilli, J. 2008. Geochemical signature of land-based activities in Caribbean coral surface samples. *Coral Reefs* **27,** 727-742.

Quinn, K. A., Byrne, R. H. & Schijf, J. 2004. Comparative Scavenging of Yttrium and the Rare Earth Elements in Seawater: Competitive Influences of Solution and Surface Chemistry. *Aquatic Geochemistry* **10,** 59-80.

Rodriguez-Ramirez, A., Grove, C. A., Zinke, J., Pandolfi, J. M. & Zhao, J.-X. 2014. Coral Luminescence Identifies the Pacific Decadal Oscillation as a Primary Driver of River Runoff Variability Impacting the Southern Great Barrier Reef. *PloS one* **9,** e84305.

Roff, G., Clark, T. R., Reymond, C. E., Zhao, J.-X., Feng, Y., Mccook, L. J., Done, T. J. & Pandolfi, J. M. 2013. Palaeoecological evidence of a historical collapse of corals at Pelorus Island, inshore Great Barrier Reef, following European settlement. *Proceedings. Biological sciences / The Royal Society* **280**.

Sadler, J., Webb, G. E., Nothdurft, L. D. & Dechnik, B. 2014. Geochemistry-based coral palaeoclimate studies and the potential of 'non-traditional' (non-massive Porites) corals: Recent developments and future progression. *Earth Science Reviews* **139,** 291-316.

Saha, N., Webb, G. E. & Zhao, J.-X. 2016. Coral skeletal geochemistry as a monitor of inshore water quality. *Science of The Total Environment* **566–567,** 652-684.

Schaffelke, B., Mcallister, F. & Furnas, M. 2008. Reef Water Quality Protection Programme; 3.7.2 Ext b: Marine flood plume monitoring. *Water Quality and Ecosystem Monitoring Programme.* Final ed. Townsville: Australian Institute of Marine Science.

Schroeder, T., Devlin, M. J., Brando, V. E., Dekker, A. G., Brodie, J. E., Clementson, L. A. & Mckinna, L. 2012. Inter-annual variability of wet season freshwater plume extent into the Great Barrier Reef lagoon based on satellite coastal ocean colour observations. *Marine Pollution Bulletin* **65,** 210-223.

Shen, G. T. & Sanford, C. L. 1990. Trace element indicators of climate variability in reef-building corals. *Global ecological consequences of the 1982-83 El Nino-Southern Oscillation,* 255-283.

Sholkovitz, E. & Shen, G. T. 1995. The incorporation of rare earth elements in modern coral. *Geochimica et Cosmochimica Acta* **59,** 2749-2756.

Sholkovitz, E. R., Landing, W. M. & Lewis, B. L. 1994. Ocean particle chemistry: The fractionation of rare earth elements between suspended particles and seawater. *Geochimica et Cosmochimica Acta* **58,** 1567-1579.

Sinclair, D. J. 2005. Non-river flood barium signals in the skeletons of corals from coastal Queensland, Australia. *Earth and Planetary Science Letters* **237,** 354-369.

Sinclair, D. J. & Mcculloch, M. T. 2004. Corals record low mobile barium concentrations in the Burdekin River during the 1974 flood: evidence for limited Ba supply to rivers? *Palaeogeography, Palaeoclimatology, Palaeoecology* **214,** 155-174.

Smith, L., Devlin, M., Haynes, D. & Gilmour, J. 2005. A demographic approach to monitoring the health of coral reefs. *Marine Pollution Bulletin* **51,** 399-407.

Taylor, R. B., Barnes, D. J. & Lough, J. M. 1995. On the inclusion of trace materials into massive coral skeletons. 1. Materials occurring in the environment in short pulses. *Journal of experimental marine biology and ecology* **185,** 255-278.

Walther, B. D., Kingsford, M. J. & Mcculloch, M. T. 2013. Environmental Records from Great Barrier Reef Corals: Inshore versus Offshore Drivers. *PloS one* **8,** e77091.

Webb, G. E. & Kamber, B. S. 2000. Rare earth elements in Holocene reefal microbialites: a new shallow seawater proxy. *Geochimica et Cosmochimica Acta* **64,** 1557-1565.

Wyndham, T., Mcculloch, M., Fallon, S. & Alibert, C. 2004. High-resolution coral records of rare earth elements in coastal seawater: biogeochemical cycling and a new environmental proxy. *Geochimica et Cosmochimica Acta* **68,** 2067-2080.

Zhang, J. & Nozaki, Y. 1996. Rare earth elements and yttrium in seawater: ICP-MS determinations in the East Caroline, Coral Sea, and South Fiji basins of the western South Pacific Ocean. *Geochimica et Cosmochimica Acta* **60,** 4631-4644.

Zhang, J. & Nozaki, Y. 1998. Behavior of rare earth elements in seawater at the ocean margin: a study along the slopes of the Sagami and Nankai troughs near Japan. *Geochimica et Cosmochimica Acta* **62,** 1307-1317.

Table 1: Average rare earth element (REE) and Y concentration data (ppb) from the Frankland Islands, Great Barrier Reef (GBR-this study) and previously published REY data from corals on the GBR [Wyndham (2004), Webb and Kamber (2000) and Jupiter (2008)] , Bermuda [Sholkovitz and Shen (1995)] an sea water from Frankland Island, High Island (inshore) and Yongala Reef (mid-shelf) GBR. (NB. Bold and italicised seawater values for Tb, Tm and Lu are interpolated.)

Location	La	Ce	Pr	Nd	Sm	Eu	Gd	Tb	Dy	Y	Ho	Er	Tm	Yb	Lu	
DL*	*2.6*	*3.9*	*1.0*	*1.2*	*0.5*	*0.5*	*0.3*	*0.6*	*0.9*	*1.3*	*0.6*	*1.2*	*0.6*	*0.8*	*1.1*	
RSD (%) **	*2.6*	*1.9*	*1.1*	*1.0*	*1.3*	*1.3*	*1.2*	*1.5*	*0.9*	*3.2*	*1.0*	*0.8*	*0.8*	*1.0*	*1.3*	
Coral																**Reference**
Russell Island (FRI 12.1)	25.71	32.93	4.90	18.69	4.22	1.16	5.25	0.85	5.62	118.04	1.39	4.39	0.77	5.65	0.96	*This study*
Russel Island (FRI 12.3)	12.08	12.21	2.16	8.80	2.18	0.67	3.36	0.56	3.91	88.58	0.96	3.40	0.49	3.34	0.58	*This study*
High Island (HI 12.1)	19.48	16.19	3.36	13.69	3.25	1.07	5.08	0.85	6.12	129.50	1.56	5.32	0.90	6.86	1.20	*This study*
Sudbury Cay (SUD 12.1)	3.19	4.68	*0.54*	2.27	0.57	*0.38*	0.90	*0.15*	1.11	89.21	*0.29*	1.01	*0.18*	1.30	*0.23*	*This study*
Frankland Island	15	11	2.9	11.7	2.8		4.1		4		1	3.1		3.5		*Wyndham (2004)*
High Island	17.2	13.7	3.5	14.9	3.7		5.2		6.1		1.5	5.1		6.5		*Wyndham (2004)*
Pandora Reef	29.8	14		22.3	5.3	1.5	7.6					7.8		9.6		*Wyndham (2004)*
Havannah Reef	27.5	17.4		19.1	4.8	1.6	6.5					6.5		7.6		*Wyndham (2004)*
Davies Reef	1.5	1.4		1.9	0.79							0.9		1		*Wyndham (2004)*
Heron Island	15.3	15	1.9	9.1	1.5	1.4	2.5	0.3	2.2	122	0.4	1.3		2	0.2	*Webb and Kamber (2000)*
Heron Island	5.3	8.7	0.8	4.6		0.6	1.2	0.2	1.5	121	0.1	1.3		1.1	0.2	*Webb and Kamber (2000)*
Heron Island	9.1	15.3	1.1	9.3		0.5	2.1	0.3	0.9	180	0.2	2.6		3.8	0.2	*Webb and Kamber (2000)*
Round Top Island	26.84	19.62	5.21	22.38	5.02	1.49	7.29	1.19	8.65	138.62	2.07	6.15	0.94	6.07	0.99	*Jupiter (2008)*
Keswick Island	5.05	4.93	1.09	4.76	1.35	0.37	2.08	0.33	2.82	82.62	0.58	2.00	0.36	2.68	0.05	*(Jupiter 2008)*
Bermuda	19	60.8		30.6	9.76	1.85	13.1		10.8			8.84		8.12	1.26	*Sholkovitz and Shen (1995)*
Bermuda	17.3	27.5		22.7	6.87	0.9	9.71		7.66			6.51		6.21	0.92	*Sholkovitz and Shen (1995)*
Bermuda	13.3	20.8		19.2	5.42	1.2	8.42		8.39			7.3		6.95	1.01	*Sholkovitz and Shen (1995)*
Bermuda (Porites *sp*.)	25.8	43.1		33.2	10.2	1.74			10.4			7.78		5.93	0.85	*Sholkovitz and Shen (1995)*
Bermuda	12.7	17.4		18.4	5.96	1.25			9.74			8.79		7.31	1.01	*Sholkovitz and Shen (1995)*
Tarawa	7.17	17.8		13.8	3.89		6.42		5.18			4.41		2.52	0.34	*Sholkovitz and Shen (1995)*
Tarawa	12.1	24.2		20.5	7.41		9.84		5.45			6.19		2.76	0.38	*Sholkovitz and Shen (1995)*
Seawater																
Frankland Island (Oct 2002)	3.6	2.9	0.71	3.2	0.84	0.22	1.2	***0.19***	1.6		0.4	1.2	***0.18***	1.1	***0.17***	*Wyndham (2004)*
High Island (Oct 2002)	8.9	9.7	1.7	7.6	1.8	0.47	2.7	***0.42***	3.4		0.87	2.8	***0.42***	2.6	***0.39***	*Wyndham (2004)*
Yongala Reef (Feb 2001)	2.4	1.7	0.5	2.3	0.59	0.17	0.88	***0.14***	1.1		0.29	0.8	***0.12***	0.7	***0.11***	*Wyndham (2004)*

Table 2: Summary of selected geochemical data from ~monthly resolution sampling of *Porites* coral cores from the Wet Tropics, Great Barrier Reef, Australia. Y/Ho is molar ratio, total rare earth elements (ΣREE) and Yttrium (Y; ppb), Barium (Ba; ppm) and Y/Ho as molar ratios. Cerium anomaly (Ce/Ce*) was calculated using the equation [Ce_N/Pr_N * (Pr_N/Nd_N)], where element concentrations were normalised (N) using the values of Mud of Queensland (MUQ; Kamber et al. 2005). Nd_N/Yb_N are MUQ normalised ratios, where lower ratio values represent a relative depletion of light REE (LREE) compared to heavy REE (HREE).

Sample		Σ REE (2001-2002)	Y/Ho	Y	Ba	Ce/Ce*	ΣREE (all years)	Nd_N/Yb_N
	DL*			*1.3*	*0.05*			
	RSD%**			*3.23*	*0.74*			
FRI 12.1	Min	78.55	69.7	81.47	2.52	0.64	73.57	0.18
	Max	247.74	126.0	166.33	5.60	2.10	247.74	0.75
	Average	126.32	88.6	121.01	3.79	0.89	112.49	0.33
HI 12.1	Min	66.99	74.7	108.81	3.44	0.44	56.37	0.16
	Max	97.10	88.5	159.08	5.54	0.73	132.06	0.26
	Average	78.98	82.6	123.00	4.47	0.54	84.92	0.20
FRI 12.3	Min	40.94	82.6	82.04	2.23	0.47	36.79	0.19
	Max	59.23	108.4	106.16	5.08	0.61	84.58	0.35
	Average	49.91	97.3	94.25	3.33	0.54	54.72	0.26
SUD 12.1	Min	11.31	212.8	78.98	2.07	0.75	10.40	0.12
	Max	31.92	383.7	104.79	4.66	1.23	31.92	0.36
	Average	16.99	311.0	87.97	3.62	0.94	16.81	0.18

*DL (Detection Limit) = 3 * the standard deviation of the blank (background)

** RSD % (Relative Standard Deviation) = standard deviation/average*100 (1σ)

Figures

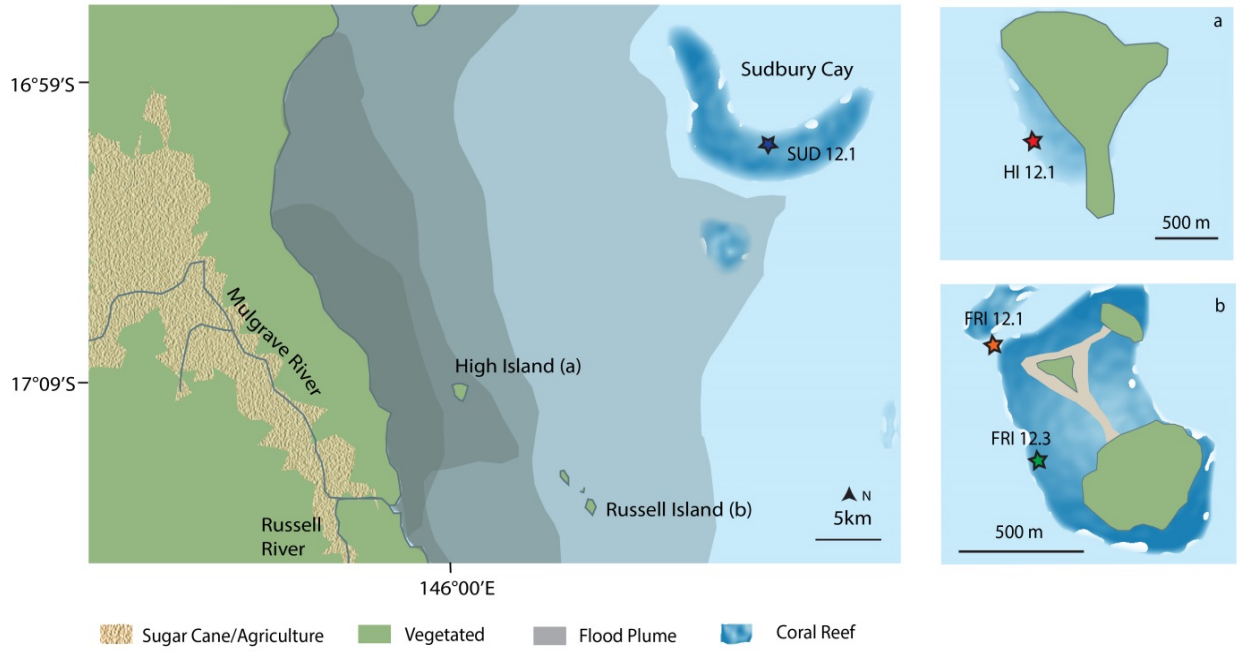

Figure 1: Frankland Islands region, Wet Tropics, Great Barrier Reef, Australia. Grey shading indicates flood plume frequency distribution (Devlin et al. 2001), stars indicates locations of *Porites* sp. coral cores at Sudbury Cay (blue) and inset a) High Island (red) and b) Russell Island (green and orange).

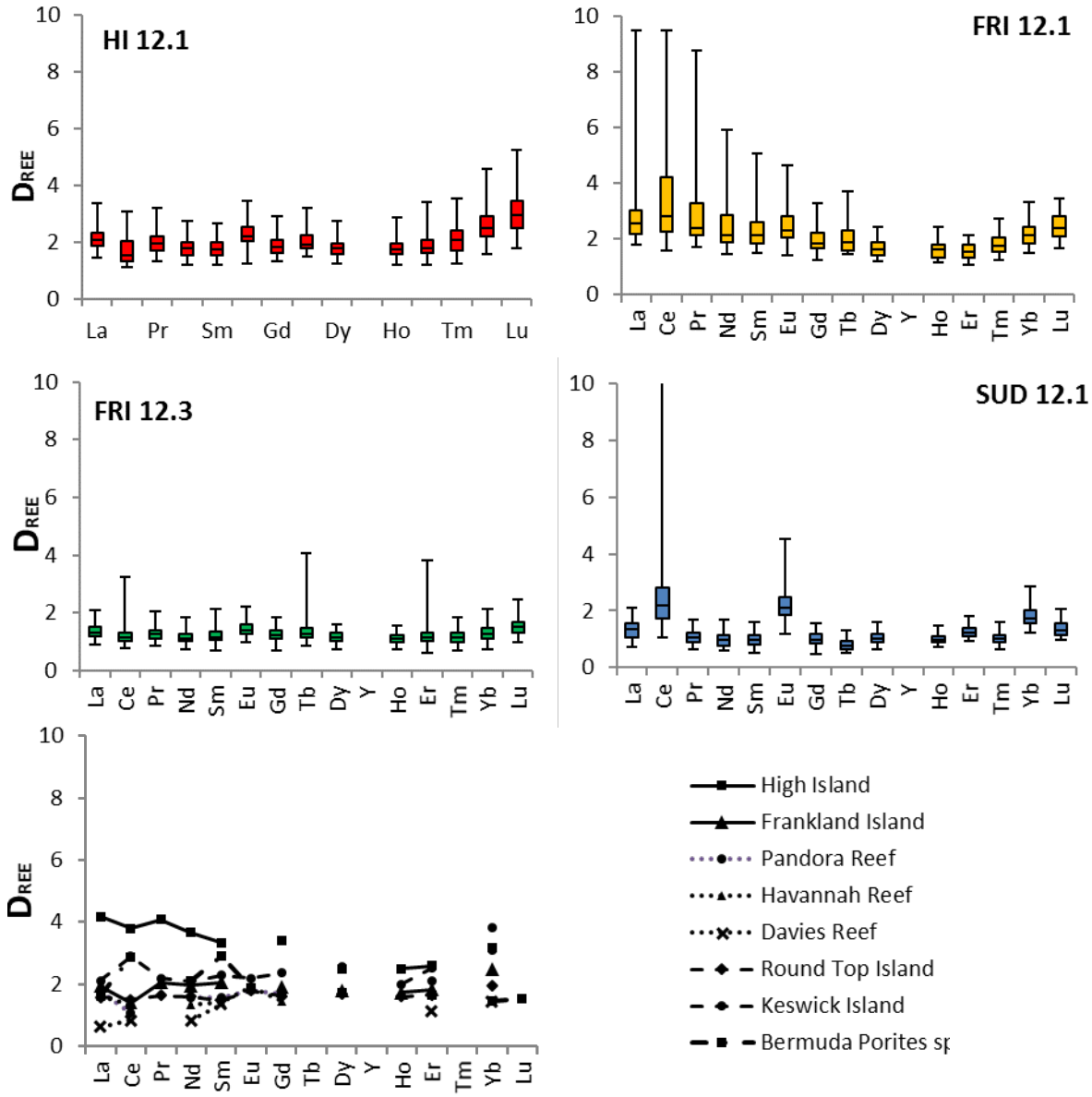

Figure 2: Quartile plots of apparent distribution coefficients (D_{REE}) for four Porites *sp.* corals (HI 12.1, FRI 12.3, FRI 12.1, SUD 12.1) from the Wet Tropics, Great Barrier Reef (GBR), Australia compared to previously reported average D_{REE} for Porites *sp.* corals from the GBR - High and Frankland Islands, Pandora, Havannah and Davies Reefs (Wyndham et al. 2004), Round Top and Keswick Islands (Jupiter 2008) and Bermuda (Sholkovitz and Shen 1995).

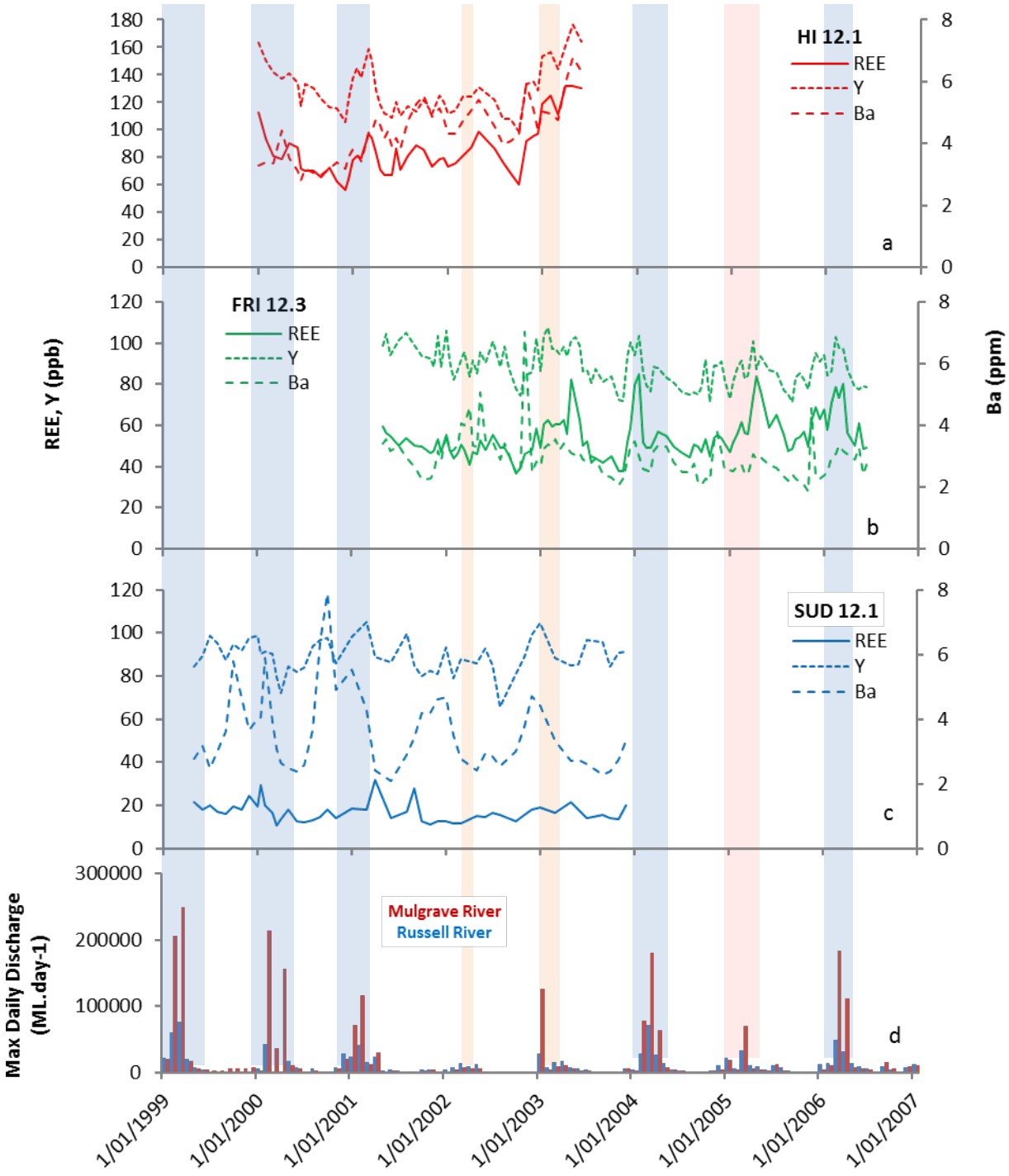

Figure 3: Geochemical time series data for *Porites* corals from the Wet Tropics, Great Barrier Reef, Australia; a) High Island (HI 12.1); (b) Russell Island (FRI 12.3) and (c); Sudbury Cay (SUD 12.1). Maximum daily river discharge (ML.day^{-1}) for the Russell and Mulgrave Rivers are also shown (d). Blue and red vertical bars represent high and moderate discharge events respectively.

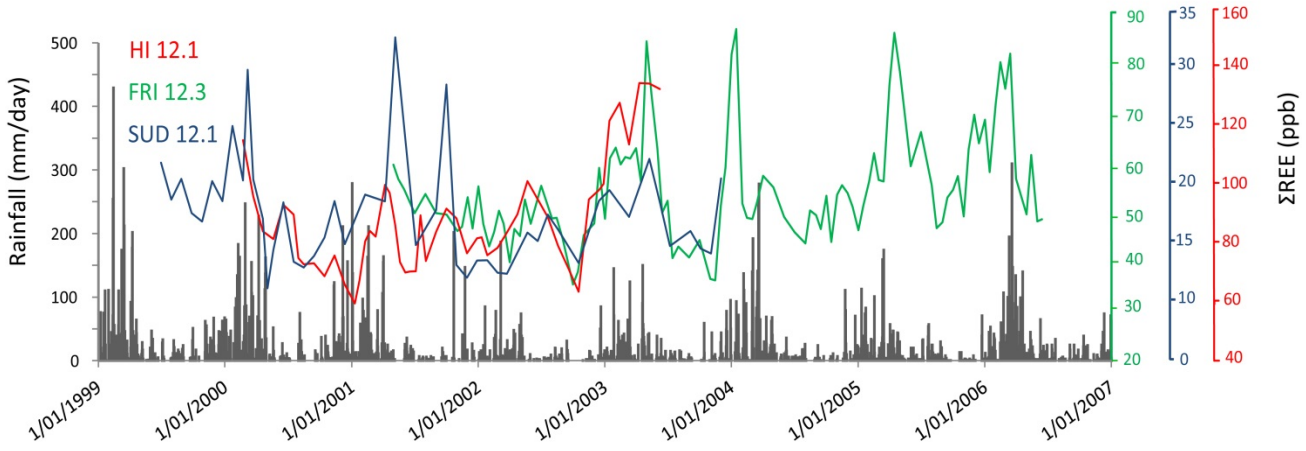

Figure 4: Scaled geochemical time series data for *Porites* corals from the Wet Tropics, Great Barrier Reef, Australia; High Island (HI 12.1; red), Russell Island (FRI 12.3; green) and Sudbury Cay (SUD 12.1; blue); and daily rainfall (mm.day^{-1}) for Deeral Station 031021 (grey).

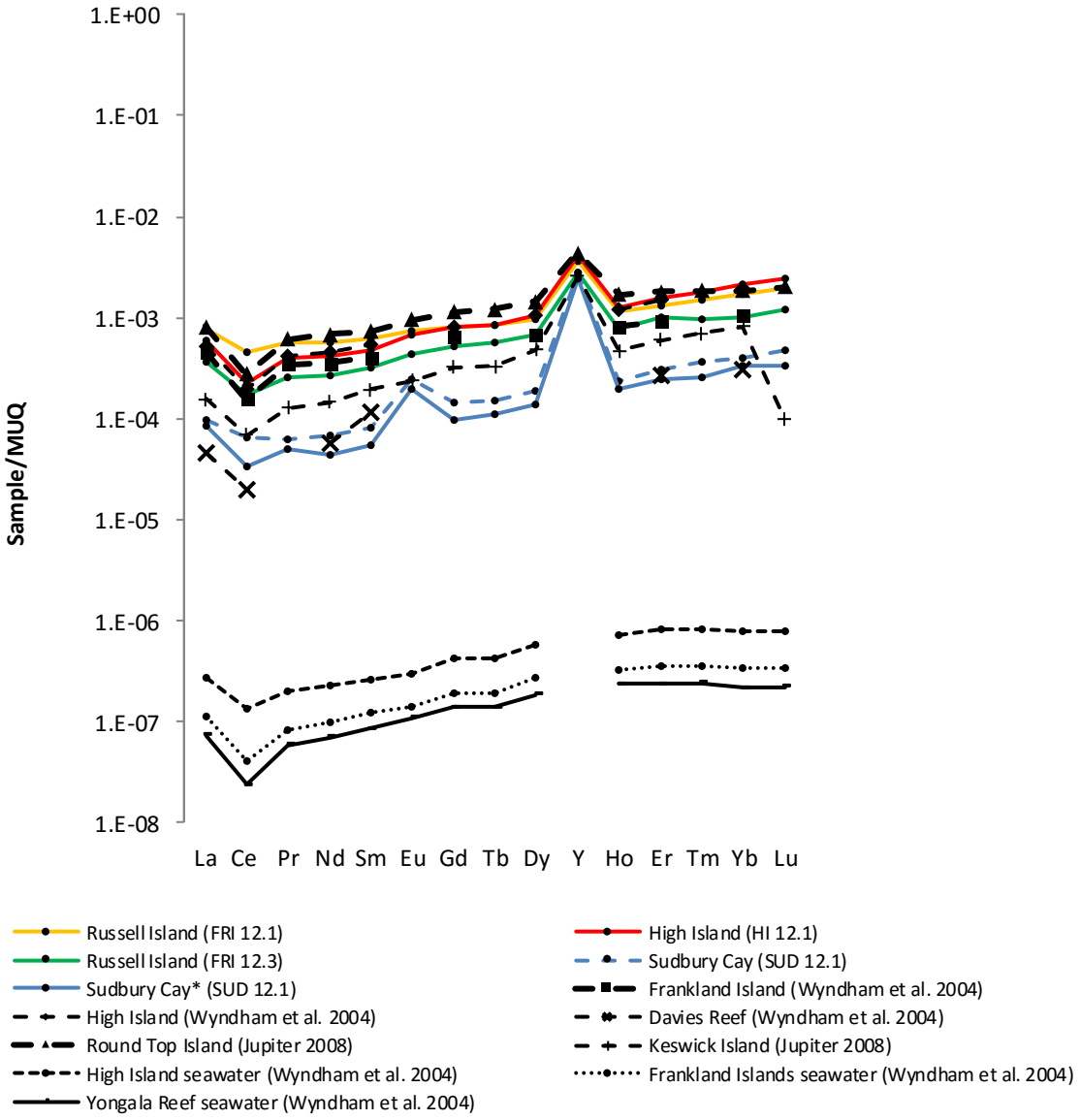

Figure 5: Average Mud of Queensland [MUQ; Kamber et al. 2005) normalised REE and Yttrium (REY) data from four *Porites* corals from the Wet Tropics, Great Barrier Reef (GBR), compared with previously reported coral and sea water data from the GBR.

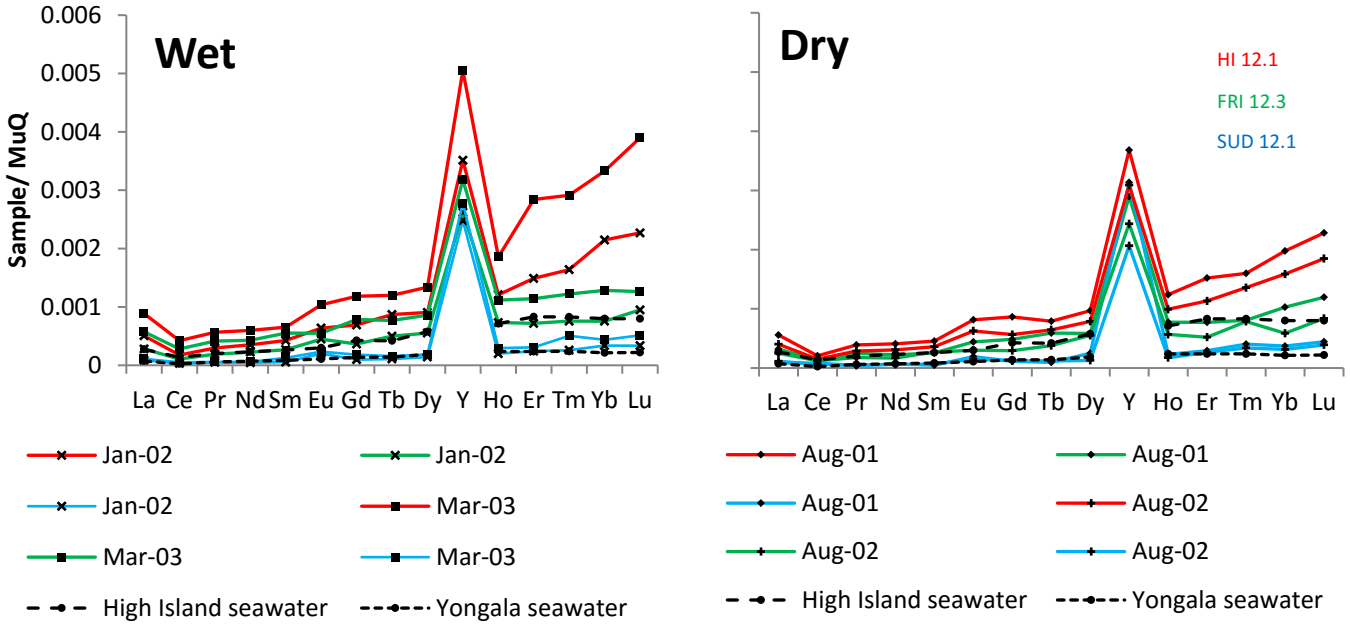

Figure 6: Mud of Queensland (MUQ; Kamber et al. 2005) normalised rare earth element and Yttrium (REY) composition of Porites *sp*. corals from the Wet Tropics, Great Barrier Reef, Australia for wet (high rainfall/high discharge) and dry periods for High Island (HI 12.1 – red), Russell Island (FRI 12.3 – green) and Sudbury Cay (SUD 12.1 – blue). Also shown are High Island and Yongala Reef sea water values [x1000] (Wyndham et al. 2004).

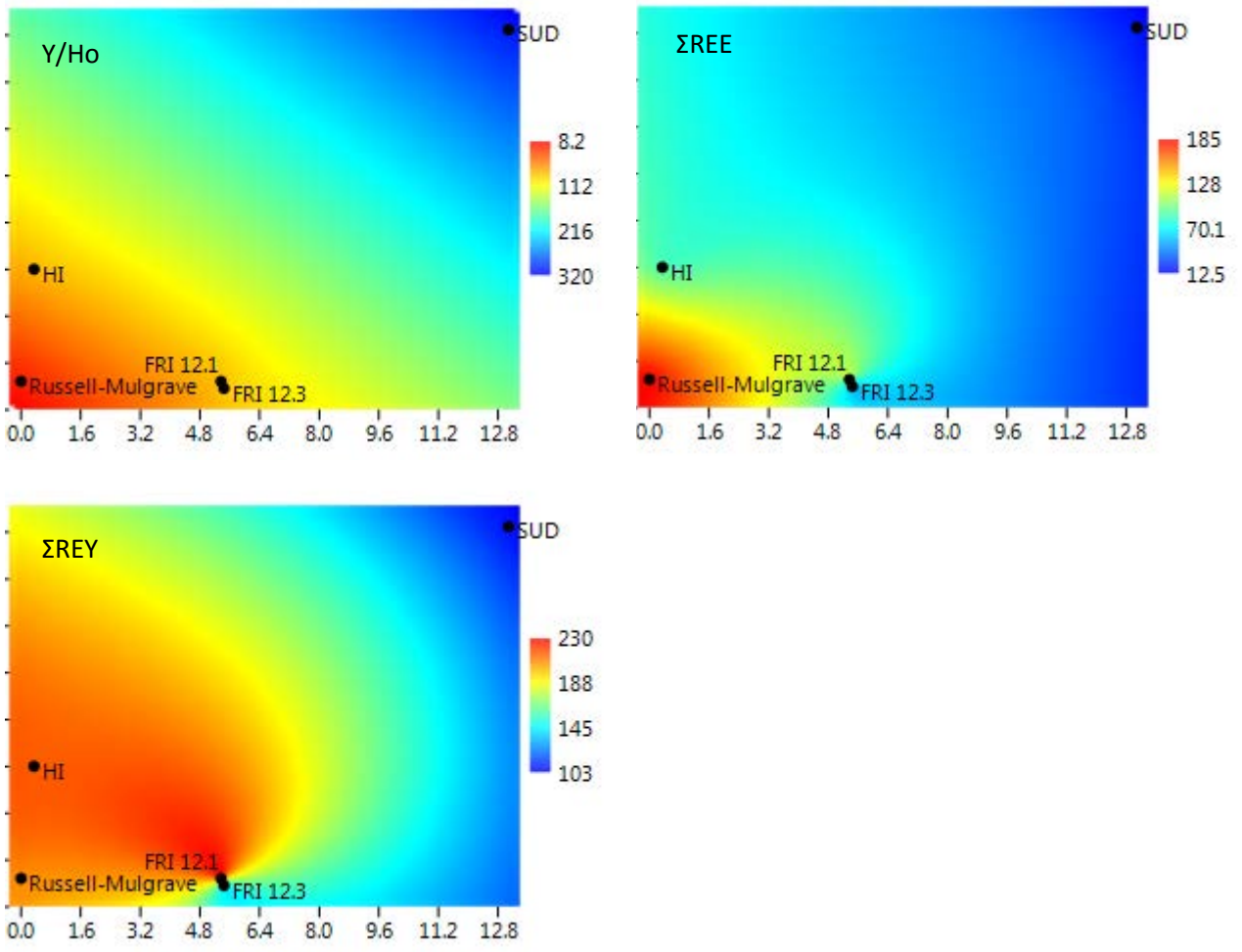

Figure 7: Gridded spatial interpolation of average monthly resolution geochemical data from Porites *sp.* coral cores in the Wet Tropics, Great Barrier Reef, Australia; a) Yttrium/Holmium (Y/Ho) molar ratio; (b) Total rare earth elements (ΣREE – ppb) and ; c) total rare earth elements and Y (REY – ppb)

Supplementary

Supplementary 1: Growth Characteristics

Supplementary Table 1: Measured tissue thickness and annual linear extension of four Porites *sp*. corals from the Frankland Islands, Great Barrier Reef. The average ratio is defined as the tissue thickness/average linear extension. Month equivalent values were calculated by multiplying the ratio by 12 (months).

	FRI 12.1	HI 12.1	FRI 12.3	SUD 12.1
Tissue Thickness (cm)	0.9	0.5	0.6	0.5
Linear extension *(cmyr^{-1})	1.7	1.8	2.3	1.2
	1.6	1.7	2	1.4
	2	2	2.3	1.3
	1.6	1.5	2	1.4
	1.8	1.5	2	1
	1.3	1.2	1.7	1
	1.6	2	2.3	1.1
	1.5	1.7	2	1.3
	1.6	1.7	2.2	1.2
	1.5	1.5	2.2	1
	1.7	1.7		1
	1.2			1.2
Average (cmyr^{-1})	1.59	1.66	2.10	1.18
Standard Deviation (cm)	0.21	0.23	0.19	0.15
Ratio (average)	0.57	0.30	0.29	0.43
~Month equivalent	6.8	3.6	3.4	5.1

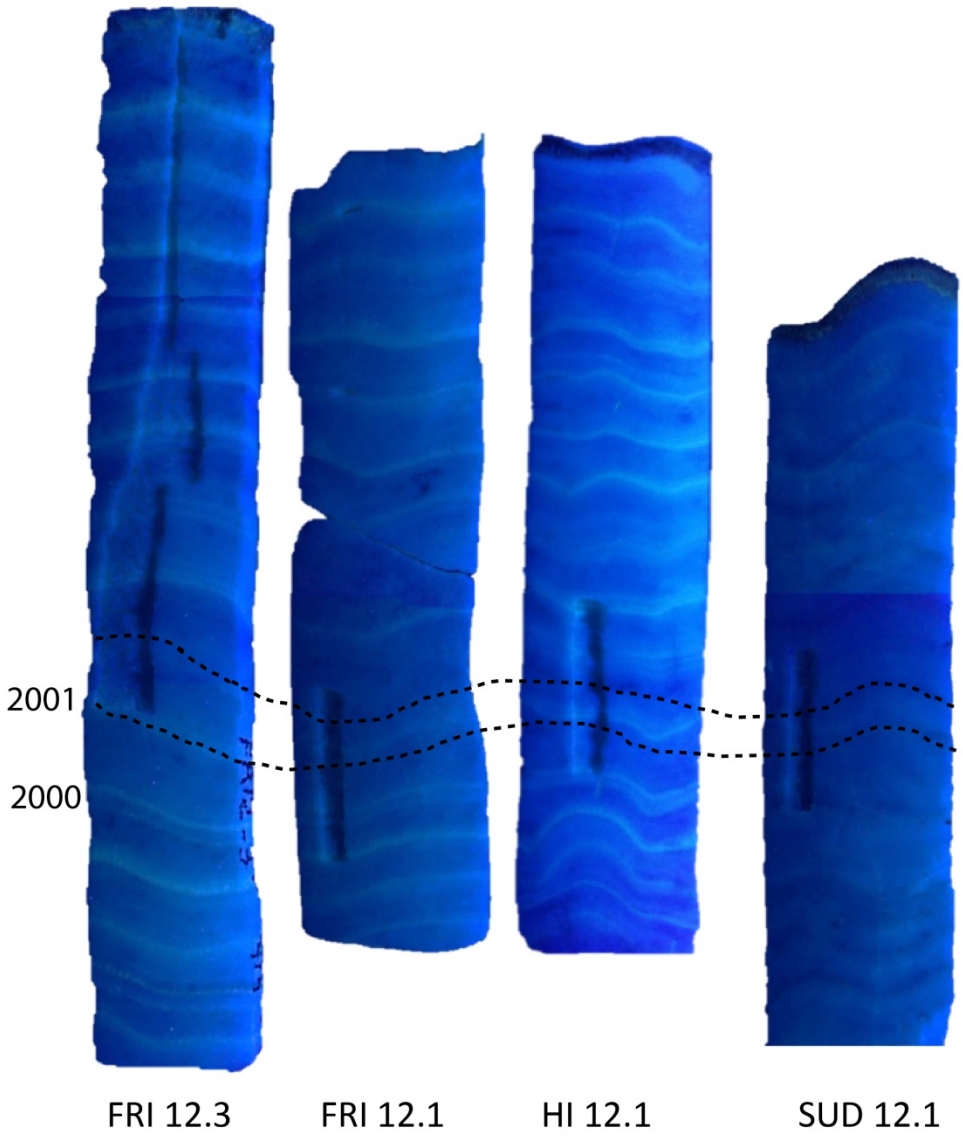

Supplementary Figure 1: Scaled and digitally enhanced photographs of coral luminescent bands in four *Porites* sp. corals from the Wet Tropics, Great Barrier Reef, Australia. Dashed lines represent overlapping period of 2001-2002 used for geochemical comparisons (see main text).

Supplementary 2: Coral FRI 12.1

Coral FRI 12.1 from the NW side of Russell Island shows two anomalous peaks (~250 ppb) which are approximately twice the baseline values for this coral (Supp. Fig. 2). These peaks do not correspond to any similarly high peaks in the other corals, or with UV luminescence, and occur almost coevally with the lowest annual SST (highest Sr/Ca). Although moderately high discharge events were observed in the instrumental record at this time, increased in Nd/Yb ratios (i.e. colloidal association) and a lack of observable peaks in the other inshore corals suggests that localised resuspension may be the primary driver. Mud of Queensland (Kamber et al., 2005) normalised REY patterns are notably different compared to the wet and dry phase REY trends from the other inshore corals, with a shale-like pattern characterised by no negative Ce anomaly and little depletion of LREEs. Similar REY patterns, although of much higher concentrations, were attributed to resuspension following dredging activities in Vietnam by Nguyen et al. (2013). The location of this coral at an inter-reef passage, and close to a permanent mooring buoy, likely results in localised resuspension of sediments at this site. The larger tissue thickness of this colony compared to the other cores from the region (0.9 cm compared to ~0.5cm; Supp. Tbl. 1) also supports the notion that this coral has increased exposure to both organic and inorganic nutrient sources (Barnes and Lough, 1992).

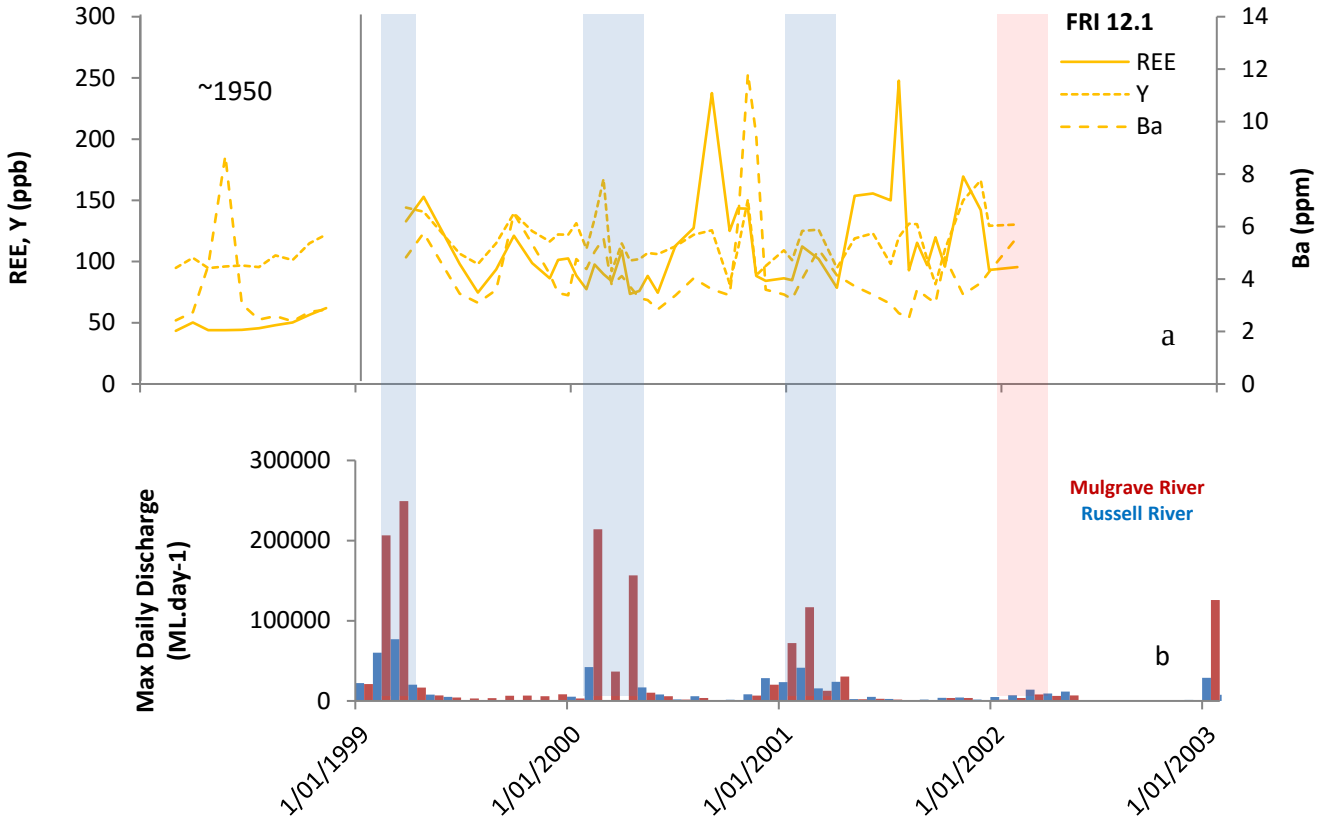

Supplementary Figure 2: (a) Geochemical time series data for *Porites* coral from Russell Island (FRI 12.1) from the Wet Tropics, Great Barrier Reef, Australia and; (b) Maximum daily river discharge (ML.day^{-1}) for the Russell and Mulgrave Rivers. Blue and red vertical bars represent high and moderate discharge events respectively.

Supplementary 3: Geochemical statistics

Supplementary Table 2: Single Factor Analysis of Variance (ANOVA) of geochemical data from four coral cores from the Frankland Islands, Great Barrier Reef for the period 2001-2002; FRI 12.1 AND FRI 12.3 from Russell Island and HI 12.1 from High Island (inshore) and SUD 12.1 from Sudbury Cay (mid-shelf). A) Total rare earth elements (ΣREE); B) total Yttrium (Y); and C) total Barium (Ba).

A: ΣREE

SUMMARY

Groups	*Count*	*Sum*	*Average*	*Variance*
FRI 12.1	16	2021.134	126.3209	1813.32
HI 12.1	19	1500.695	78.98397	78.72337
FRI 12.3	20	995.4418	49.77209	20.21776
SUD 12.1	10	169.8788	16.98788	51.84102

ANOVA

Source of Variation	*SS*	*df*	*MS*	*F*	*P-value*	*F crit*
Between Groups	88282.98	3	29427.66	60.91748	2.46E-18	2.755481
Within Groups	29467.52	61	483.0741			
Total	117750.5	64				

B: Yttrium

SUMMARY

Groups	*Count*	*Sum*	*Average*	*Variance*
FRI 12.1	16	1936.179	121.0112	437.3454
HI 12.1	19	2336.937	122.9967	217.383
FRI 12.3	20	1883.547	94.17733	54.12034
SUD 12.1	10	879.7391	87.97391	76.26461

ANOVA

Source of Variation	*SS*	*df*	*MS*	*F*	*P-value*	*F crit*
Between Groups	14809.39	3	4936.464	24.70714	1.38E-10	2.755481
Within Groups	12187.74	61	199.7991			
Total	26997.14	64				

C: Barium

SUMMARY

Groups	*Count*	*Sum*	*Average*	*Variance*
FRI 12.1	16	60630.01	3789.375	731852.1
HI 12.1	19	84.74543	4.460286	0.298068
FRI 12.3	20	64.85241	3.242621	0.350854
SUD 12.1	10	36.22231	3.622231	0.834916

ANOVA

Source of Variation	*SS*	*df*	*MS*	*F*	*P-value*	*F crit*
Between Groups	1.73E+08	3	57616525	320.1559	2.87E-37	2.755481
Within Groups	10977801	61	179963.9			
Total	1.84E+08	64				

Supplementary Table 3: Pairwise t-tests of geochemical data from four coral cores from the Frankland Islands, Great Barrier Reef for the period 2001-2002. FRI 12.1 AND FRI 12.3 from Russel Island and HI 12.1 from High Island (inshore) and SUD 12.1 from Sudbury Cay (mid-shelf). A) Total rare earth elements (ΣREE); B) total Yttrium (Y); and C) total Barium (Ba). Significant Bonferroni adjusted differences (95% confidence) are in bold.

A: t-Test: Two-Sample Assuming Unequal Variances: ΣREE

	FRI 12.1	*HI 12.1*		*FRI 12.1*	*FRI 12.3*
Mean	126.3209	78.98397	Mean	126.3209	49.77209
Variance	1813.32	78.72337	Variance	1813.32	20.21776
Observations	16	19	Observations	16	20
Hypothesized Mean Difference	0		Hypothesized Mean Difference	0	
df	16		df	15	
t Stat	4.367426		t Stat	7.158676	
P(T<=t) one-tail	0.000239		P(T<=t) one-tail	1.64E-06	
t Critical one-tail	1.745884		t Critical one-tail	1.75305	
P(T<=t) two-tail	0.000479		P(T<=t) two-tail	3.29E-06	
t Critical two-tail	2.119905		t Critical two-tail	2.13145	
Bonferroni	**0.002871**		Bonferroni	**1.97E-05**	

	FRI 12.1	*SUD 12.1*		*HI 12.1*	*FRI 12.3*
Mean	126.3209	16.98788	Mean	78.98397	49.77209
Variance	1813.32	51.84102	Variance	78.72337	20.21776
Observations	16	10	Observations	19	20
Hypothesized Mean Difference	0		Hypothesized Mean Difference	0	
df	16		df	26	
t Stat	10.04296		t Stat	12.86701	
P(T<=t) one-tail	1.29E-08		P(T<=t) one-tail	4.4E-13	
t Critical one-tail	1.745884		t Critical one-tail	1.705618	
P(T<=t) two-tail	2.59E-08		P(T<=t) two-tail	8.8E-13	
t Critical two-tail	2.119905		t Critical two-tail	2.055529	
Bonferroni	**1.55E-07**		Bonferroni	**5.28E-12**	

	SUD 12.1	*FRI 12.3*		*HI 12.1*	*SUD 12.1*
Mean	16.98788	49.77209	Mean	78.98397	16.98788
Variance	51.84102	20.21776	Variance	78.72337	51.84102
Observations	10	20	Observations	19	10
Hypothesized Mean Difference	0		Hypothesized Mean Difference	0	
df	13		df	22	
t Stat	-13.1718		t Stat	20.2994	
P(T<=t) one-tail	3.39E-09		P(T<=t) one-tail	4.88E-16	
t Critical one-tail	1.770933		t Critical one-tail	1.717144	
P(T<=t) two-tail	6.78E-09		P(T<=t) two-tail	9.76E-16	
t Critical two-tail	2.160369		t Critical two-tail	2.073873	
Bonferroni	**4.07E-08**		Bonferroni	**5.86E-15**	

B: t-Test: Two-Sample Assuming Unequal Variances: Yttrium

	FRI 12.1	*HI 12.1*		*FRI 12.1*	*FRI 12.3*
Mean	121.0112	122.9967	Mean	121.0112	94.17733
Variance	437.3454	217.383	Variance	437.3454	54.12034
Observations	16	19	Observations	16	20
Hypothesized Mean Difference	0		Hypothesized Mean Difference	0	
df	26		df	18	
t Stat	-0.31886		t Stat	4.895897	
P(T<=t) one-tail	0.376192		P(T<=t) one-tail	5.82E-05	
t Critical one-tail	1.705618		t Critical one-tail	1.734064	
P(T<=t) two-tail	0.752383		P(T<=t) two-tail	0.000116	
t Critical two-tail	2.055529		t Critical two-tail	2.100922	
Bonferroni	4.5143		Bonferroni	**0.000698**	

	FRI 12.1	*SUD 12.1*		*HI 12.1*	*FRI 12.3*
Mean	121.0112	87.97391	Mean	122.9967	94.17733
Variance	437.3454	76.26461	Variance	217.383	54.12034
Observations	16	10	Observations	19	20
Hypothesized Mean Difference	0		Hypothesized Mean Difference	0	
df	22		df	26	
t Stat	5.587467		t Stat	7.662115	
P(T<=t) one-tail	6.43E-06		P(T<=t) one-tail	1.97E-08	
t Critical one-tail	1.717144		t Critical one-tail	1.705618	
P(T<=t) two-tail	1.29E-05		P(T<=t) two-tail	3.93E-08	
t Critical two-tail	2.073873		t Critical two-tail	2.055529	
Bonferroni	**7.72E-05**		Bonferroni	**2.36E-07**	

	SUD 12.1	*FRI 12.3*		*HI 12.1*	*SUD 12.1*
Mean	87.97391	94.17733	Mean	122.9967	87.97391
Variance	76.26461	54.12034	Variance	217.383	76.26461
Observations	10	20	Observations	19	10
Hypothesized Mean Difference	0		Hypothesized Mean Difference	0	
df	16		df	26	
t Stat	-1.92987		t Stat	8.020506	
P(T<=t) one-tail	0.035774		P(T<=t) one-tail	8.43E-09	
t Critical one-tail	1.745884		t Critical one-tail	1.705618	
P(T<=t) two-tail	0.071547		P(T<=t) two-tail	1.69E-08	
t Critical two-tail	2.119905		t Critical two-tail	2.055529	
Bonferroni	0.429283		Bonferroni	**1.01E-07**	

C: t-Test: Two-Sample Assuming Unequal Variances: Ba

	FRI 12.1	*HI 12.1*		*FRI 12.1*	*FRI 12.3*
Mean	3.789375	4.460286	Mean	3.789375	3.242621
Variance	0.731852	0.298068	Variance	0.731852	0.350854
Observations	16	19	Observations	16	20
Hypothesized Mean Difference	0		Hypothesized Mean Difference	0	
df	25		df	26	
t Stat	-2.70695		t Stat	2.173439	
P(T<=t) one-tail	0.006031		P(T<=t) one-tail	0.019521	
t Critical one-tail	1.708141		t Critical one-tail	1.705618	
P(T<=t) two-tail	0.012063		P(T<=t) two-tail	0.039043	
t Critical two-tail	2.059539		t Critical two-tail	2.055529	
Bonferroni	0.072376		Bonferroni	0.234257	

	FRI 12.1	*SUD 12.1*		*HI 12.1*	*FRI 12.3*
Mean	3.789375	3.622231	Mean	4.460286	3.242621
Variance	0.731852	0.834916	Variance	0.298068	0.350854
Observations	16	10	Observations	19	20
Hypothesized Mean Difference	0		Hypothesized Mean Difference	0	
df	18		df	37	
t Stat	0.46495		t Stat	6.67974	
P(T<=t) one-tail	0.323771		P(T<=t) one-tail	3.8E-08	
t Critical one-tail	1.734064		t Critical one-tail	1.687094	
P(T<=t) two-tail	0.647543		P(T<=t) two-tail	7.6E-08	
t Critical two-tail	2.100922		t Critical two-tail	2.026192	
Bonferroni	3.885255		Bonferroni	**4.56E-07**	

	SUD 12.1	*FRI 12.3*		*HI 12.1*	*SUD 12.1*
Mean	3.622231	3.242621	Mean	4.460286	3.622231
Variance	0.834916	0.350854	Variance	0.298068	0.834916
Observations	10	20	Observations	19	10
Hypothesized Mean Difference	0		Hypothesized Mean Difference	0	
df	13		df	12	
t Stat	1.194273		t Stat	2.661104	
P(T<=t) one-tail	0.126854		P(T<=t) one-tail	0.010375	
t Critical one-tail	1.770933		t Critical one-tail	1.782288	
P(T<=t) two-tail	0.253707		P(T<=t) two-tail	0.020749	
t Critical two-tail	2.160369		t Critical two-tail	2.178813	
Bonferroni	1.522244		Bonferroni	0.124494	

This page is intentionally left blank

Chapter 6

Conclusions and future directions

Conclusions

The Great Barrier Reef (GBR) is the largest coral reef system in the world, with over 2900 reefs and 900 coral cays and islands. Many of the inshore reefs on the GBR demonstrate similar patterns of reef growth history, initiating around 8500 yBP following inundation of the shallow Pleistocene shelf during the post glacial marine transgression, and accreting rapidly in a either a "catch up" or "keep up" mode of growth until ~5500 yBP (Neumann and Macintyre, 1985, Kleypas and Hopley, 1992, Smithers et al., 2006, Perry and Smithers, 2011). Yet after 5500 cal. yr. BP the growth history of the GBR becomes convoluted, with a significant reduction in reef flat progradation from 5500 to 4800 cal. yr. BP (Smithers et al., 2006) and significant reef "turn-off" after 4600 yBP (Perry and Smithers, 2011). Three possible drivers of the mid-Holocene "turn-off" have been suggested being; a) a slowly regressing sea level following the mid-Holocene highstand resulting in emergence of reef flats; b) reef flat senescence limiting accretion potential; and c) conditions marginal to reef growth caused by changes in climatic conditions (Perry and Smithers, 2011). The primary aim of this thesis, therefore, was to investigate the possible environmental and/or climatic mechanisms responsible for the mid-Holocene reef hiatus on the Great Barrier Reef.

Holocene sea level

Whether eustatic sea level oscillated throughout the Holocene or if ocean volumes remained constant following the post glacial marine transgression has been a contentious issue for decades. Evidence from the Australian East Coast (AEC) has given support to both hypotheses however palaeo-sea level reconstructions have often been restricted by chronologies with large age errors making interpretations at sub-centennial scales problematic.

In **Chapter 2** three emergent sub-fossil reef flats from the inshore Keppel Islands, Great Barrier Reef (GBR), Australia, were used to examine whether, by using a single type of sea level indicator (coral microatolls) in conjunction with high precision U-Th dating, sub-centennial sea level variability could be reliably detected. Elevation surveys and U-Th dates

from the coral microatolls (n=32) and reef flat coral colonies (n=10) provided evidence in support of an oscillating relative sea level (RSL) regression following a mid-Holocene highstand. Results demonstrate that RSL was as least 0.75 m above present from ~6,500 – 5,500 yBP but then a rapid lowering of RSL of at least 0.4 m occurred from 5,500 – 5,300 yBP. RSL returned to higher levels following this lowstand, before a 2,000 year hiatus in reef flat corals after 4,600 yBP. A second RSL lowering event of ~0.3 m from ~2,800 –1,600 yr. BP was also detected. This is the first evidence of RSL instability in the mid-Holocene from the southern GBR, and contributes significantly to the sea level database for the Australian east coast.

To determine whether the RSL oscillations detected in the southern GBR was a local scale response, or if RSL oscillated coherently elsewhere on the GBR **Chapter 3** focussed on reconstructing RSL across a large latitudinal range on the GBR (11˚S – 20˚S). Elevation surveys and high precision U-Th dates of 94 microatolls from eight separate reefs provided further evidence in support of a RSL oscillation at 5500 yBP, in agreement with the data from the Keppel Islands. Additionally, a second oscillation of ~-0.3m at 4600 yBP was also detected in this study. The synchronicity of the negative sea level oscillations with previously documented periods reduced reef accretion and reef "turn-off" suggests that sea level instability was likely the primary driver of the mid-Holocene hiatus on the GBR. The timing of the sea level oscillations on the GBR were also shown to coincide with SL oscillations reported elsewhere in the Indo-Pacific suggesting a eustatic contribution to SL instability in the Holocene. Furthermore, these SL oscillations were shown to correspond with periods of reduced ENSO activity (Gliganic et al., 2014), rapid cooling events (Hodell et al., 2001, Moros et al., 2009) and global glacier advances (Mayewski et al., 2004). It is therefore proposed Holocene SL oscillations are likely the result of ocean-atmosphere climatic perturbations affecting SSTs and sensitive mountain ice-cap and non-polar icesheet water storage balances in both the northern and southern hemispheres. These climate signals may have been emphasized on the GBR due to the response of the ENSO system, however, high resolution (sub-centennial) climate records for the southern hemisphere are notably limited (Wanner et al., 2015). Therefore, the second part of this thesis investigated new possible techniques for acquiring palaeo-climatic and –environmental data from massive *Porites* corals, with a focus on reconstructing rainfall and associated sediment delivery to the GBR which, on the GBR, is largely modulated by ENSO.

Coral luminescence and ENSO

Luminescent lines in corals are commonly used to assess river flow beyond the instrumental record on the GBR and to reconstruct rainfall frequency with links to driving climatic mechanisms such as ENSO and the Pacific Decadal Oscillation (PDO; Isdale et al., 1998, Lough et al., 2002, Lough, 2007, Lough, 2011, Lough et al., 2014, Rodriguez-Ramirez et al., 2014). In **Chapter 4** the utility of rapid visual assessment of ultraviolet (UV) luminescent bands in massive Porites *sp.* coral cores was tested by applying continuous wavelet transforms (CWT) to a previously published modern luminescent index record from Great Palm Island (Hendy et al., 2003) and sea surface temperature (SST) data from the Niño 3 region for the same period (i.e. an indicator of ENSO). Applying CWTs allows for time series data to be viewed in time-frequency space, thereby allowing for detection of ENSO frequency through time. The transformed modern coral luminescence record matched well with the Niño 3 SST ENSO signal, so was therefore considered a viable tool for use in palaeoclimate reconstructions. Continuous wavelet transforms were applied to luminescence index data of three massive *Porites* corals U-Th dated to 5200 yBP, 4900 yBP and 4300 yBP. Results from luminescence signals suggest less intense ENSO events during the mid-Holocene with a reduction in ENSO frequency in the 2-7 year band after 5200 y BP. Limited linear extension rates in the fossil corals ($<10 mm yr^{-1}$) compared to modern values (~15mmyr-1) also suggest SSTs were cooler than present between 5200 - 4300 yBP.

Reliable reconstructions of past environmental conditions on the GBR have previously been hampered by the effects of biological mediation of the geochemical signals found in massive corals. To date, the behaviour of rare earth elements (REEs) and REE and Yttrium (REY) at sub-annual scales is relatively unknown, with few high resolution studies of REEs conducted on corals (Sholkovitz and Shen, 1995, Naqvi et al., 1996, Fallon and McCulloch, 2002, Akagi et al., 2004), and only two records from the GBR (Wyndham et al., 2004, Jupiter, 2008). In **Chapter 5** results from ~monthly resolved REE data obtained from four live collected *Porites* sp. coral cores from a the Frankland Islands region, Wet Tropics, GBR are presented. The location of the live coral cores across a known water quality gradient was reflected in the total REE (ΣREE) concentrations of the corals, and spatial interpolation of the data reconstructed broad cross shelf (Y/Ho) and locally relevant (ΣREY) water quality gradients well. Total REE concentrations were also shown to potentially track changes in sediment delivery to the GBR since European settlement and potentially throughout the Holocene, with higher ΣREE observed in 1999-2002 (78 – 250 ppb in dry and wet years) than in 1950 (53-79

ppb). Time series of ΣREE showed better potential as an indicator of regional rainfall than for discharge as the potential erosivity of top soils after dry periods (i.e. Queensland winter) increased delivery of sediment regardless of river discharge magnitude.

Future research directions

With the future of corals reefs uncertain due to a changing climate and increasing anthropogenic pressure, understanding what caused reef "turn-off" events in the geological past is imperative to improving future management strategies. Results presented within this thesis (**Chapters 2 and 3**) strongly suggest that an oscillatory mode of RSL regression following the mid-Holocene highstand was the primary cause of the hiatus in reef growth observed on the GBR after 5500 y BP. The late Holocene RSL is still however tenuous, as relatively few samples were dated for this period. Future research should focus on establishing RSL for the late Holocene to understand the driver of reef re-initiation in the last 2800 years on the GBR.

In support of previous work this research has demonstrated that coral microatolls are reliable indicators of RSL variability and that U-Th ages can be constrained to sub-centennial accuracies, and therefore should be targeted more intensively in future research. Reconstructing SL for the wider Indo-Pacific region using microatolls would allow for evaluation of regional scale response to rapid climate shifts throughout the Holocene, enabling improvements to future projections in response to changing global climate.

Continuous wavelet analysis of modern coral luminescent index data shows great potential for use in the fossil coral record for reconstructing ENSO on the GBR. This fast and economic method not only has the potential to be applied to cores obtained from dredged coral material, but also to significant fragments of *Porites* material recovered during reef matrix coring efforts where misalignment along the major growth axis limits their utility in geochemical studies. The increased number of records potentially available via this method would allow for progressive expansion of ENSO "windows". Future work should concentrate on utilising corals previously rejected for geochemical analysis, and to cores obtained from numerous reef matrix coring expeditions across the GBR to expand the current record of ENSO variance throughout the Holocene.

Chapter 5 of this thesis demonstrated that ΣREE concentrations in corals have the potential to reconstruct water quality changes and water quality gradients across the GBR throughout

the Holocene. Future research should be focussed on at least annually resolved concentrations of REE and REYs both across the continental shelf and within distinct time periods within reef matrix cores to further elucidate environmental conditions on the GBR that led to the mid-Holocene reef hiatus. Furthermore, longer sub-annular records of REEs in modern corals should be analysed and compared to rainfall and river discharge events to better understand the high resolution variability of REYs incorporated into coral skeletons.

Overall, this thesis has demonstrated a tangible link between relative sea level oscillations in the mid-Holocene to the previously recognised reef "turn-off' or hiatus on the GBR, suggesting that relatively minor (<0.5m) oscillations in RSL can have an extremely detrimental effect on reef growth. However, results from the Keppel Islands suggest that if RSL rises in line with future projections there is the potential for re-colonization of currently emerged fossil reef substrates if environmental and climatic conditions are suitable for coral growth. The use of continuous wavelet transforms to visually assessed luminescence time series indices in long-lived corals has also been presented as a novel, rapid and cost efficient technique to determine past climatic variations in the strength and frequency of ENSO on the GBR. Luminescence records from the central GBR indicate reduced ENSO activity on the GBR between ~5200 and 4300 yBP, thus making ENSO an unlikely mechanism for reef decline in the mid-Holocene. This thesis has also demonstrated that REYs incorporated into coral skeletons show potential in reconstructing palaeo-water quality gradients and temporal changes in water quality throughout the Holocene, allowing for interpretations of environmental conditions on the GBR leading up to the mid-Holocene hiatus, and to changes to sediment delivery following European settlement. Understanding coral reef response to variations in environmental and climatic conditions in the geological past is imperative to better predicting response potential under future climate change scenarios.

References

Akagi, T., Hashimoto, Y., F-F, F., Tsuno, H., Tao, H. & Nakano, Y. 2004. Variation of the distribution coefficients of rare earth elements in modern coral-lattices: species and site dependencies 1 1 Associate editor: R. H. Bryne. *Geochimica et Cosmochimica Acta* **68,** 2265-2273.

Fallon, S. J. & Mcculloch, M. T. 2002. Porites corals as recorders of mining and environmental impacts: Misima Island, Papua New Guinea. *Geochimica et Cosmochimica Acta* **66,** 45-62.

Gliganic, L. A., Cohen, T. J., May, J.-H., Jansen, J. D., Nanson, G. C., Dosseto, A., Larsen, J. R., Aubert, M., Stockholms, U., Naturvetenskapliga, F. & Institutionen För Naturgeografi Och, K. 2014. Late-Holocene climatic variability indicated by three natural archives in arid southern Australia. *The Holocene* **24,** 104-117.

Hendy, E. J., Gagan, M. K. & Lough, J. 2003. Chronological control of coral records using luminescent lines and evidence for non-stationary ENSO teleconnections in northeast Australia. *The Holocene* **13,** 187-199.

Hodell, D. A., Kanfoush, S. L., Shemesh, A., Crosta, X., Charles, C. D. & Guilderson, T. P. 2001. Abrupt Cooling of Antarctic Surface Waters and Sea Ice Expansion in the South Atlantic Sector of the Southern Ocean at 5000 cal yr B.P. *Quaternary Research* **56,** 191-198.

Isdale, P. J., Stewart, B. J., Tickle, K. S. & Lough, J. M. 1998. Palaeohydrological variation in a tropical river catchment: a reconstruction using fluorescent bands in corals of the Great Barrier Reef, Australia. *The Holocene* **8,** 1-8.

Jupiter, S. Year. Coral rare earth element tracers of terrestrial exposure in nearshore corals of the Great Barrier Reef. *In:* Proceedings of the 11th International Coral Reef Symposium, 7-11th July 2008 Ft. Lauderdale, Florida.

Kleypas, J. A. & Hopley, D. Year. Reef Development Across a Broad Continental Shelf, Southern Great Barrier Reef, Australia. *In:* Richmond, R. H., ed. Seventh International Coral Reef Symposium, 1992 Guam. University of Guam Press, 1129-1141.

Lough, J., Barnes, D. & Mcallister, F. 2002. Luminescent lines in corals from the Great Barrier Reef provide spatial and temporal records of reefs affected by land runoff. *Coral Reefs* **21,** 333-343.

Lough, J. M. 2007. Tropical river flow and rainfall reconstructions from coral luminescence: Great Barrier Reef, Australia. *Paleoceanography* **22**.

Lough, J. M. 2011. Measured coral luminescence as a freshwater proxy: comparison with visual indices and a potential age artefact. *Coral Reefs* **30,** 169-182.

Lough, J. M., Llewellyn, L. E., Lewis, S. E., Turney, C. S. M., Palmer, J. G., Cook, C. G. & Hogg, A. G. 2014. Evidence for suppressed mid-Holocene northeastern Australian monsoon variability from coral luminescence. *Paleoceanography* **29,** 581-594.

Mayewski, P. A., Holmgren, K., Lee-Thorp, J., Rosqvist, G., Rack, F., Staubwasser, M., Schneider, R. R., Steig, E. J., Rohling, E. E., Curt Stager, J., Karlén, W., Maasch, K. A., David Meeker, L., Meyerson, E. A., Gasse, F. & Van Kreveld, S. 2004. Holocene climate variability. *Quaternary Research* **62,** 243-255.

Moros, M., De Deckker, P., Jansen, E., Perner, K. & Telford, R. J. 2009. Holocene climate variability in the Southern Ocean recorded in a deep-sea sediment core off South Australia. *Quaternary Science Reviews* **28,** 1932-1940.

Naqvi, S. a. S., Nagender Nath, B. & Balaram, V. 1996. Signatures of rare-earth elements in banded corals of Kalpeni atoll - Lakshadweep archipelago in response to monsoonal variations. *Indian Journal of Marine Sciences* **25,** 1-4.

Neumann, A. C. & Macintyre, I. G. Year. Reef response to sea level rise: keep-up, catch up or give-up. *In:* Proc. 5th Int Coral Reef Congr, 1985 Tahiti. 105-110.

Perry, C. & Smithers, S. 2011. Cycles of coral reef 'turn-on', rapid growth and 'turn-off' over the past 8500 years: a context for understanding modern ecological states and trajectories. *Global Change Biology* **17,** 76-86.

Rodriguez-Ramirez, A., Grove, C. A., Zinke, J., Pandolfi, J. M. & Zhao, J.-X. 2014. Coral Luminescence Identifies the Pacific Decadal Oscillation as a Primary Driver of River Runoff Variability Impacting the Southern Great Barrier Reef. *PloS one* **9,** e84305.

Sholkovitz, E. & Shen, G. T. 1995. The incorporation of rare earth elements in modern coral. *Geochimica et Cosmochimica Acta* **59,** 2749-2756.

Smithers, S. G., Hopley, D. & Parnell, K. E. 2006. Fringing and Nearshore Coral Reefs of the Great Barrier Reef: Episodic Holocene Development and Future Prospects. *Journal of Coastal Research,* 175-187.

Wanner, H., Mercolli, L., Grosjean, M. & Ritz, S. P. 2015. Holocene climate variability and change; a data-based review. *Journal of the Geological Society* **172,** 254-263.

Wyndham, T., Mcculloch, M., Fallon, S. & Alibert, C. 2004. High-resolution coral records of rare earth elements in coastal seawater: biogeochemical cycling and a new environmental proxy. *Geochimica et Cosmochimica Acta* **68,** 2067-2080.